Functional Analysis of MicroRNAs as Regulators of Membrane Trafficking

Dissertation

submitted to the

Combined Faculties for the Natural Sciences and for the Mathematics

of the Ruperto-Carola University of Heidelberg, Germany

for the degree of

Doctor of Natural Sciences

Written and presented by:
MSc in Genetics Andrius Serva
Born in Joniškis, Lithuania
Oral-examination: 08.02.2012

Dissertation referees:
Prof. Dr. Roland Eils
Dr. Vytautė Starkuvienė-Erfle

DECLARATION

I, Andrius Serva, confirm that the work presented in this thesis is my own. Where information has been derived from other sources, I confirm that this has been indicated in the thesis.

TABLE OF CONTENTS

PUBLICATIONS ARISING FROM THIS THESIS

Andrius Serva, Christoph Claas and Vytaute Starkuviene. A Potential of microRNAs for High Content Screening. [review] Journal of Nucleic Acids, 2011; 2011:870903.

Andrius Serva, Bettina Knapp, Christoph Claas, Petr Matula, Nathalie Harder, Urte Neniskyte, Lars Kaderali, Karl Rohr, Roland Eils, Holger Erfle and Vytaute Starkuviene. *miR-17* family regulates endocytosis of degradable cargo. (under submission).

Ursula Rost, Andrius Serva, Bettina Knapp, Lars Kaderali, Pascal Pucholt, Vytaute Starkuviene and Ursula Kummer. Reliability of gene expression profiling data used for the development of computational miRNA target prediction algorithms. (in preparation).

ACKNOWLEDGEMENTS

I would like to thank Dr. Vytautė Starkuvienė-Erfle for granting me the opportunity to work in her group at BioQuant, University of Heidelberg. I am grateful for scientific supervising, support and fruitful discussions during this interesting and challenging project.

I would like to thank Prof. Dr. Roland Eils for being the first supervisor of my PhD studies. I would like to thank him and Prof. Dr. Ursula Kummer for being my TAC committee members, for their fruitful discussions and interest in my project. I would also like to thank PD. Dr. Stefan Wiemann for joining my doctoral examination committee.

I am grateful to my lab colleagues Sanchary Roy, Tautvydas Lisauskas, Anastasia Eskova, Dr. Christoph Claas and Yueh-Tso Tsai for making the lab such an enjoyable place to work. Many thanks go to Susanne Reusing for being always understanding and very much helpful.

Further, I gratefully acknowledge Bettina Knapp for her immense help and advice in statistical data analysis. I thank Nina Beil, Jürgen Beneke, Dr. Jürgen Reymann and Dr. Holger Erfle for their immediate assistance in the pre-miR library screening.

I sincerely thank my friends Alex, Lavanya, Saravanan, Fabio and Ilaria for adventurous trips and great time we have spent together. My special thanks goes to Andrius, Mindaugas, Upe, Gintaras and Donatas for being my best mates “in fortune and misfortune” ever and for their great support wherever they are!

I am very much grateful to my parents and lovely sisters for providing me the opportunity to study far away from home, giving me everything I ever needed, for making my visits back home so warm, for their care and continued support.

Finally, my biggest thanks goes to Lucia for her enormous support and constant encouragement during my studies. Thanks her for making my life colourful!

ABBREVIATIONS

Ago1-4 – Argonaute 1-4 proteins
ANC - anti-miR negative control
Anti-miR – syntetic single-stranded RNA molecule to inhibit miRNA
"AllStars" – siRNA negative control
CCV – clathrin-coated vesicle
CDS – protein coding sequence
CME – clathrin-mediated endocytosis
ConA - lectin Concanavalin A
COPI – coat protein complex I
COPII – coat protein complex II
DiI-LDL – 3,3'-dioctadecylindocarboncyanine-labelled LDL
EEA1 – early endosome antigen 1
ER – endoplasmic reticulum
ERES – ER exit site
ERGIC – ER-Golgi intermediate compartment
GAP - GTPase-activating protein
GDF – GDI dissociation factor
GDI – GDP dissociation inhibitor
GEF – guanine nucleotide exchange factor
GM – growth medium
HPCD – 2-hydroxypropyl-β-cyclodextrin
IM – imaging medium
IRES – internal ribosome entry site
LDL – low-density lipoprotein
miRNA - microRNA
miRISC – miRNA-induced silencing complex
miRLC – miRISC loading complex
MTC – multisubunit tethering complexes
PM – plasma membrane
PNC - pre-miR negative control
Pre-miR – synthetic double-stranded RNA molecule to mimic miRNA
Pre-miRNA – precursor miRNA
Pri-miRNA – primary miRNA transcript
qRT-PCR – quantitative real-time PCR
RNAi – RNA interference
SD – standard deviation
SM – starvation medium
SNARE – soluble NSF attachment protein receptor
SVM - support vector machine
TF – transcription factor
TGN – *trans*-Golgi network
TM – transfection medium
ts-O45-G - temperature-sensitive glycoprotein mutant of vesicular stomatitis virus tagged with yellow fluorescent protein

1. SUMMARY

MicroRNAs (miRNAs) are a large family of small noncoding RNAs that extensively regulate gene expression in animals, plants and protozoa. The first miRNA was identified in the early 1990s, but it took almost a decade until miRNAs were recognized as key post-transcriptional regulators of gene expression. Despite the rapidly growing list of miRNA-regulated physiological and pathological processes, intracellular membrane trafficking has attracted little interest from scientific miRNA community. Membrane trafficking defines a complex network of pathways, including biosynthetic trafficking and endocytosis that are indispensable for normal cellular functions. Previous studies have analyzed a few miRNAs involved in insulin secretion, however, no systematic investigation of miRNAs as important regulators of membrane trafficking has been performed.

The overall aim of this study was to identify miRNAs and their biologically relevant target genes involved in the regulation of membrane trafficking. As tools to modulate miRNA functions, we used synthetic miRNA mimics (pre-miRs) and inhibitors (anti-miRs) to enhance (gain-of-function) and to suppress (loss-of-function) the activity of cellular miRNAs, respectively. As proof of principle, we demonstrated that increased activity of *miR-17* family miRNAs accelerates the biosynthetic cargo protein (ts-O45-G) transport and reduces the cellular internalization of DiI-LDL ligand.

Taking the advantage of available technological platforms, we designed a gain-of-function large-scale screening to identify miRNAs that affect biosynthetic ts-O45-G transport rate. We showed that 44 out of 470 tested miRNAs induced significant changes in cargo trafficking. Using image analysis platform, we further identified eight miRNAs (*miR-30b, -382, -432, -517a, -517b, -517c, -637* and *-765*) that also showed significant effects on Golgi complex integrity. Importantly, the majority of identified miRNAs are not endogenously expressed in HeLa cells, indicating the need for validation studies in other experimental systems.

To identify functionally relevant target genes, we selected *miR-17* and *miR-517a* and performed genome-wide transcriptome analysis 12h, 24h and 48h after transfection with the respective pre-miRs. We identified *TBC1D2* and *LDLR* genes as novel functional *miR-17* targets and confirmed that they exert the *miR-17*-mediated regulation of endocytosis. Further studies are needed to identify target genes responsible for the *miR-17*-governed acceleration of ts-O45-G to the plasma membrane. In case of *miR-517a*, we found a set of target genes with functions in

membrane trafficking system, however, their functional interplay with *miR-517a* remains to be confirmed.

Bioinformatics analysis of transcriptome profiling data confirmed that the presence of miRNA seed binding site in the 3´UTRs of human mRNAs is an important determinant for functional miRNA:mRNA interaction. Additionally, we demonstrated that the sets of transcripts downregulated at early time points after transfection with pre-miRs have substantially higher fractions of transcripts with miRNA binding sites in their 3´UTRs compared to the transcripts downregulated at late time points. We believe that these findings could contribute to the development of more accurate miRNA target prediction tool, also allowing identification of nonconserved miRNA targets.

In conclusion, we have established an experimental platform that consists of (i) a functional screening module to identify miRNAs that affect membrane trafficking, (ii) a microarray module to identify miRNA target genes, (iii) a statistics and bioinformatics module for data analysis and integration and (iv) a target validation module to validate functional links between targets and miRNAs. Using this platform, we identified numerous miRNAs with novel functions in membrane trafficking system. Moreover, we identified and confirmed *TBC1D2* and *LDLR* genes as novel functional targets of *miR-17*.

2. ZUSAMMENFASSUNG

MicroRNAs (miRNAs) sind eine große Familie kleiner nichtcodierender RNAs, die weitgehend die Genexpression in Tieren, Pflanzen und Protozoen regulieren. Die erste miRNA wurde in den frühen 1990ern identifiziert, aber es dauerte beinahe ein Jahrzehnt bis die miRNAs als Schlüssel-posttranskriptionale Regulatoren der Genexpression begriffen wurden. Trotz der schnell wachsenden Liste von miRNA-regulierten physiologischen und pathologischen Prozesse hat der intrazelluläre Membrantransport wenig Interesse bei der wissenschaftlichen miRNA Gemeinschaft geweckt. Membrantransport definiert ein komplexes Netzwerk von Bahnen, die den biosynthetischen Transport und Endocytose beinhalten, die unentbehrlich für normale zelluläre Funktionen sind. Frühere Studien haben einige miRNAs analysiert, die an der Insulin-Sekretion beteiligt waren, jedoch wurde keine systematische Erforschung von miRNAs als wichtige Regulatoren von Membrantransport durchgeführt.

Das allgemeine Ziel dieser Studie war es, miRNAs und ihre biologisch relevanten Zielgene, die in der Regulation des Membrantransports involviert sind, zu identifizieren. Als Werkzeuge zur Modellierung der miRNA-Funktionen verwendeten wir synthetische miRNA mimics (pre-miRs) und Inhibitoren (anti-miRs), um die Aktivität der zellulären miRNAs zu erhöhen (Anstieg der Funktion) oder entsprechend abzuschalten (Verlust der Funktion). Als Beweis zeigten wir, daß die erweiterte Aktivität der *miR-17* Familie mRNAs den biosynthetischen Cargo-Protein (ts-O45-G) Transport beschleunigt und die zelluläre Internalisierung von Dil-LDL Liganden reduziert.

Indem wir den Vorteil einer verfügbaren Technologieplattform nutzten, entwickelten wir ein gain-of function Hochdurchsatzscreen, um miRNAs zu identifizieren, die eine Auswirkung auf die biosynthetische ts-O45-G-Transportrate haben. Wir zeigten, daß 44 von 470 getesteten miRNAs signifikante Veränderungen im Cargotransport induzierten. Durch Nutzung der Bildanalyse-Plattform identifizierten wir weitere acht miRNAs (*miR-30b*, *-382*, *-432*, *-517a*, *-517b*, *-517c*, *-637*, -und *-765*) die auch signifikante Effekte auf die Golgikomplexintegrität zeigten. Es ist wichtig, daß die Mehrheit der identifizierten miRNAs, die nicht endogen in Hela-Zellen exprimiert werden, die Notwendigkeit für Validierungsstudien in anderen experimentellen Systemen zeigen.

Um funktionell relevante Zielgene zu identifizieren, selektierten wir *miR-17* und *miR-517a* und führten eine genomweite Transkriptionsanalyse 12h, 24h und 48h nach Transfektion mit den entsprechenden pre-miRs durch. Wir identifizierten TBC1D2- und LDLR-Gene als neue

funktionelle *miR-17* targets und bestärkten, daß sie die *miR-17* -herbeigeführte Regulation der Endozytose gebrauchen. Weitere Studien sind notwendig, um Zielgene zu identifizieren, die verantwortlich sind für die *miR-17*-beeinflußte Beschleunigung von ts-O45-G zur Plamamembran. Im Fall von *miR-517a* fanden wir ein Set von Zielgenen mit Funktionen im Membrantransportsystem, jedoch bleibt ihre funktionelle Wechselwirkung mit *miR-517a* zu bestätigen.

Bioinformatikanalyse von Transkriptionsprofildaten bekräftigten, daß die Anwesendheit von miRNA "seed"-Bindungstellen an den 3´UTRs von humanen mRNAs eine wichtige Determinante für miRNA:mRNA funktionelle Interaktion ist. Zusätzlich zeigten wir, daß die Sets von Transkripten, die zu frühen Zeitpunkten nach Transfektion mit pre-miRs substanziell höhere Fraktionen von Transkripten mit miRNA-Bindungsstellen in ihren 3´UTRs aufweisen, verglichen mit den Transkripten, die zu späteren Zeitpunkten runterreguliert wurden. Wir glauben, daß diese Ergebnisse zur Entwicklung von genaueren miRNA Vorhersagetools beitragen könnten, auch könnte es die Identifizierung von unkonservierten miRNA-Targets erlauben.

Zum Abschluß etablierten wir eine experimentelle Plattform, die aus einem funktionellen Screening-Modul besteht, um miRNAs zu identifizieren, die eine Auswirkung auf den Memrantransport haben, ein microarray-Modul zur Identifizierung von miRNA Targetgenen, ein statistisches und Bioinformatik-Modul zur Datenanalyse und Integration, ein Target-Modul zur Validierung eines funktionellen Links zwischen Targets und miRNAs zu erzielen. Mittels dieser Plattform identifizierten wir eine Anzahl von miRNAs mit neuen Funktionen im Membrantransportsystem. Außerdem identifizierten und bestätigten wir TBC1D2 und LDLR-Gene als neue funktionelle Targets von *miR-17*.

3. INTRODUCTION

3.1. miRNAs and their discovery

MicroRNAs (miRNAs) are a family of small ~21-nucleotide-long noncoding single-stranded endogenous RNA molecules that regulate gene expression post-transcriptionally by base-pairing to target mRNAs. Bioinformatics and experimental approaches have revealed that ~30-75% of human protein-coding genes can be potentially targeted by miRNAs (Baek *et al*, 2008; Bartel, 2009; Friedman *et al*, 2009; Lewis *et al*, 2005; Selbach *et al*, 2008). Originally recognized as regulators of fundamental processes at cellular and organism level, including development (Bernstein *et al*, 2003; Lee *et al*, 1993; Olsen & Ambros, 1999), cell proliferation (Johnson *et al*, 2007), differentiation (Chen *et al*, 2004) and apoptosis (Brennecke *et al*, 2003; Chan *et al*, 2005; Cimmino *et al*, 2005), miRNAs have now been demonstrated to modulate cholesterol metabolism (Krutzfeldt *et al*, 2005), stress response (Huang *et al*, 2009), neuronal plasticity (Schratt *et al*, 2006; Siegel *et al*, 2009) and immune response (Xiao & Rajewsky, 2009). Furthermore, aberrant miRNA expression has been linked to various diseases, such as diabetes (Guay *et al*, 2011), cancer (Croce, 2009; Lynam-Lennon *et al*, 2009), hepatitis C (Jopling *et al*, 2005) and mental disorders (Xu *et al*, 2010).

Historically, the first hint about miRNAs as novel regulatory genes in *C. elegans* was published by Chalfie and colleagues in 1981 (Chalfie *et al*, 1981). However, only in 1993 Ambros, Lee and Feinbaum discovered that *lin-14* gene is regulated by a short 22-nt RNA encoded by the *lin-4* gene in *C. elegans*. The *lin-4* miRNA sequence was found to be partially complementary to the multiple sequences in the 3´untranslated region (3´UTR) of the *lin-14* mRNA (Lee *et al*, 1993). The second miRNA *let-7*, which inhibits the expression of *lin-41*, *lin-14*, *lin-28*, *lin-42* and *daf-12* genes during development of *C. elegans*, was characterized by Ruvkun and colleagues 7 years later (Reinhart *et al*, 2000). Although originally thought to be a genetic oddity of nematodes, *let-7* and some other *C. elegans* miRNAs were soon shown to be conserved in other metazoans including human (Pasquinelli *et al*, 2000). Finally, in 2001, miRNAs burst on the stage with three landmark articles published in a single issue of *Science*, reporting the discovery of over a hundred novel miRNAs in nematodes, flies and mammals (Lagos-Quintana *et al*, 2001; Lau *et al*, 2001; Lee & Ambros, 2001). These papers introduced the term “microRNA” to refer to a family of small non-coding RNAs with similar genomic features.

During the following years, thousands of miRNAs have been and are still being characterized in almost all studied organisms, ranging from viruses (Cai *et al*, 2006) and green algae (Molnar *et al*, 2007) to complex animal species (Lagos-Quintana *et al*, 2001). To date, there are 21 643 mature miRNAs identified in 168 species including 1 527 miRNAs found in human genome annotated in miRBase 18 release (http://www.mirbase.org/). miRNAs are located in diverse regions of the genome including both protein-coding and non-coding transcription units. Computational analysis revealed 55 and 51 distinct miRNA clusters encoding approximately 46% and 47% of known by that time human and mouse miRNAs, respectively (Griffiths-Jones *et al*, 2008; Yuan *et al*, 2009). Analysis of the primary miRNA transcripts (pri-miRNAs) indicated that clusters can contain from 2 to 46 tandemly encoded miRNA hairpins (Baskerville & Bartel, 2005; Bortolin-Cavaille *et al*, 2009). By mapping miRNA genomic coordinates to genomic position of all annotated human genes, Hinske and colleagues demonstrated that 42.6% miRNAs are located within intronic regions, 5.3% within exonic regions and the remaining 52.1% are intergenic miRNAs. Interestingly, genomic distribution of miRNAs in other surveyed species with well-annotated protein-coding genes is very similar to the one in humans (Hinske *et al*, 2010).

3.2. Biological functions of animal miRNAs

Many fundamental biological processes were shown to be regulated by miRNAs. The first evidence of miRNA involvement in regulation of developmental timing came from studies of *lin-4* gene mutantion in *C. elegans* (Lee *et al*, 1993). As identified later, *lin-4* encodes a miRNA that is partially complementary to seven motifs in the 3´UTR of the transcription factor *lin-14* messenger RNA. *lin-4* miRNA (ortholog of mammalian *miR-125*) binds to *lin-14* mRNA and controls the developmental transition from the L1 to L2 larval stage by promoting *lin-14* mRNA degradation. Loss-of-function mutation in *lin-4* miRNA results in the repeated cell division and failed differentiation (Bagga *et al*, 2005; Lee *et al*, 1993; Wightman *et al*, 1993). Other four members of *let-7* family (*let-7*, *miR-48*, *miR-84* and *miR-241*) were shown to control the developmental transition from the L2 to the L3 stage by regulation of the transcription factors HBL-1 and DAF-2 (Abbott *et al*, 2005; Hammell *et al*, 2009; Li *et al*, 2005). The terminal transition from the L4 larval stage to the adult nematode is conferred by upregulation of the *let-7* miRNA in the L4 stage, which downregulates LIN-41 and thereby upregulates the transcription factor LIN-29 (Reinhart *et al*, 2000; Rougvie & Ambros, 1995). Considering that both *lin-4* and *let-7* miRNA families are broadly conserved, they might have similar functions in other

organisms. Consistent with this notion, Pasquinelli and colleagues discovered that *let-7* expression is temporally regulated during development in different animal species (Pasquinelli *et al*, 2000). Moreover, the evolutionary conserved roles for temporally regulated miRNAs, particularly the *let-7* family, have been confirmed during terminal differentiation of fly wing imaginal discs and proliferation of mammalian stem cells during both normal development and cancer (reviewed in Nimmo & Slack, 2009; Tennessen & Thummel, 2008).

The loss of *lin-4* and the *let-7* miRNA function causes clear cell differentiation defects associated with cell proliferation. In addition to numerous studies investigating the biological roles of miRNAs in organogenesis in nematodes (Johnston & Hobert, 2003), flies (Lai *et al*, 2005) and zebrafish (Giraldez *et al*, 2005), an elaborate knockout work of *miR-17-92* cluster in mice revealed that deletion of this cluster leads to neonatal lethality. Furthermore, deletion of this cluster impairs normal development of heart, lungs and B cells. The proapoptotic *Bim* gene was identified as target of the cluster and likely partially responsible for the phenotypes caused by knockout of *miR-17-92*. Authors also showed that concomitant deletion of *miR-17-92* and paralogue *miR-106b-25* cluster causes more severe cardiac defects, increased apoptosis and embryonic death by midgestation, indicating functional cooperation between related miRNA clusters (Ventura *et al*, 2008).

Since genetic loss-of-function mutations are unavailable for most of miRNAs, *dicer* knockout mutants have been particularly useful models for studying miRNA functions during embryogenesis and early development. Observations that depletion of Dicer by RNAi in *C. elegans* leads to developmental phenotypes reminiscent of the *lin-4* and *let-7* mutants (Grishok *et al*, 2001) clearly indicate a crucial role of miRNAs in early animal development. Moreover, loss of Dicer also causes developmental arrest in zebrafish (Giraldez *et al*, 2005) and depletion of stem cells in mice (Bernstein *et al*, 2003).

Functional studies have demonstrated that miRNAs are involved in the regulation of almost every investigated cellular process. In most cases, however, these findings come from the examination of pathological samples. Thus, our understanding, regarding the physiologic functions of most of the identified miRNAs, remains very fragmented. A number of previous studies have revealed the high degree of similarity between dysregulation of developmental processes and malignant transformation. Importantly, a set of miRNAs have been implicated in both pathological conditions. Aberrant miRNA expression profiles have been detected in most tumors examined (Hayashita *et al*, 2005; Volinia *et al*, 2006). These findings have highlighted the potential of miRNA profiling in cancer diagnosis, progressions and outcome (Jay *et al*, 2007; Lu

et al, 2005). In this context, the definition of oncogenes and tumor suppressors has been expanded from the protein-coding genes to include miRNAs (Garzon *et al*, 2006; Wu *et al*, 2007).

Due to particular focus of this project on *miR-17-92* cluster, recent advances in understanding the role of this cluster in tumorigenesis will be reviewed in the next section.

3.2.1. *miR-17-92* cluster and cancer

One of the best-characterized polycistronic miRNA cluster, *miR-17-92*, resides in the *C13orf25* gene locus on chromosome 13 and gives rise to six mature miRNAs: *miR-17*, *miR-18*, *miR-19a*, *miR-20a*, *miR-19b* and *miR-92a* (Ota *et al*, 2004; Tanzer & Stadler, 2004). The six miRNAs can be grouped into three distinct seed families according to their seed sequences: the *miR-17* seed family (*miR-17* and *miR-20a*), the *miR-18* seed family (*miR-18a*), the *miR-19* family (*miR-19a* and *miR-19b*) and the *miR-92* family (*miR-92a*). Other paralogous miRNAs encoded by *miR-106a-363* and *miR-106b-25* clusters can also be grouped into these families. Most likely, paralogous *miR-106a-363* and *miR-106b-25* clusters originated via a series of duplications and deletions of *C13orf25* locus during early vertebrate evolution (Tanzer & Stadler, 2004; Ventura *et al*, 2008).

The high-level amplification of 13q31-q32, a locus of *miR-17-92*, has been observed in several hematopoietic malignancies and solid tumors, including lung carcinoma, Burkitt's lymphoma, follicular lymphoma, diffuse large B-cell lymphoma, glioma, bladder cancer, squamous-cell carcinoma of the head and neck, liposarcoma and colon carcinomas, just to mention a few (Ota *et al*, 2004; Volinia *et al*, 2006). Some of the first functional data indicating the oncogenic activity of *miR-17-92* cluster came from a mouse B-cell lymphoma model, in which overexpression of truncated *miR-17-92* cluster (lacking *miR-92a*) functionally cooperates with *c-MYC* oncogene to accelerate the progression of malignant lymphomas (He *et al*, 2005). Dysregulated expression of *c-MYC* due to mutation or amplification is one of the most common abnormalities in human cancers (Cole & McMahon, 1999). As low degree of apoptosis was observed in tumors resulting from combined *c-MYC* and truncated *miR-17-92* expression, the cluster inhibits apoptotic factors induced by c-MYC oncoprotein. This collaboration leads to highly malignant, disseminated B-cell lymphomas. Inspired by these findings, authors coined the term "oncomiR", with *miR-17-92* being *oncomiR-1*, to denote miRNAs with a role in tumorigenesis (He *et al*, 2005). The anti-apoptotic effects of *miR-17-92* cluster can be at least

partially explained by inhibition of pro-apoptotic *BIM* and *PTEN* expression. An elegant study of functional dissection of the individual miRNA in B-cell lymphoma model revealed that *miR-19a* and *miR-19b* are essential and sufficient to recapitulate the oncogenic activity of the entire cluster through repression of apoptosis by inhibiting *PTEN* (Mu *et al*, 2009). Consistent with results observed in a mouse B-cell lymphoma model, upregulation of *BIM* and *PTEN* most likely contributes to the increased apoptosis rate during pro-B to pre-B transition in miR-17-92 deficient animals during both fetal and adult B-cell development (Ventura *et al*, 2008; Xiao *et al*, 2008).

The direct interaction between *miR-17-92* and c-MYC was initially underlined by the finding that c-MYC binds directly to the genomic locus of *miR-17-92* and induces its transcription (O'Donnell *et al*, 2005). At the same time, it has been shown that E2F transcription factors, E2F1, E2F2 and E2F3, are negatively regulated by *miR-17* and *miR-20a*. Despite the fact that the 3´UTRs of all three transcription factors contain *miR-17*/*miR-20a* binding sites, the downregulation of E2F1 protein level is stronger than for the other two (O'Donnell *et al*, 2005; Sylvestre *et al*, 2007). E2Fs are essential factors in the regulation of the cell cycle and, in particular E2F1, can induce apoptosis in response to DNA damage (Lin *et al*, 2001). Since c-MYC and E2Fs have been demonstrated to activate each other transcriptionally, O'Donnell *et al.* uncovered a tighly controlled and unusually structured network in which c-MYC activates the transcription of E2Fs while simultaneously limits their translation via induction of *miR-17* and *miR-20a* (**Fig. I.3**) (O'Donnell *et al*, 2005; Sylvestre *et al*, 2007). Furthermore, E2F transcription factors also activate the transcription of *miR-17-92* cluster, with E2F3 being the major transcription activator of the cluster as demonstrated by chromatin immunoprecipitation (Woods *et al*, 2007). Taken all these evidences together, a complex interaction network of c-MYC, E2Fs and the *miR-17-92* cluster is proposed; *miR-17-92* exerts its oncogenic activity by shifting the E2F transcriptional balance away from the pro-apoptotic E2F1 toward the proliferative E2F3 transcriptional network, thereby assisting the DNA-damaged cells to avoid the programmed cell death (**Fig. I.3**).

Apart from E2Fs, BIM and PTEN, the oncogenic activity of the *miR-17-92* cluster was attributed to the downregulation of tumor suppressors such as Retinoblastoma-like protein 2 (RBL2) (Lu *et al*, 2007) or cyclin-dependent kinase inhibitor (CDKN1A, also known as p21) (Fontana *et al*, 2008). Moreover, Cloonan and colleagues discovered that *miR-17* inhibits the expression of mitogen-activated kinase JNK2, which results in an increased cyclin D1 expression and cell cycle progression (Cloonan *et al*, 2008). Whereas *miR-17*, *miR-20a* and *miR-19a*/*b* are important regulators of proliferation and apoptosis of transformed cells, *miR-18a* induces tumor

neovascularization via downregulation of anti-angiogenic proteins such as connective tissue growth factor (CTGF) and trombospondin-1 (TSP1) (**Fig. I.3**) (Dews *et al*, 2006). Recent data from breast cancer cell lines showed that *miR-19* also downregulates expression of the tissue factor (TF) which is recognized as an important regulator of tumor angiogenesis and metastasis (Zhang *et al*, 2011).

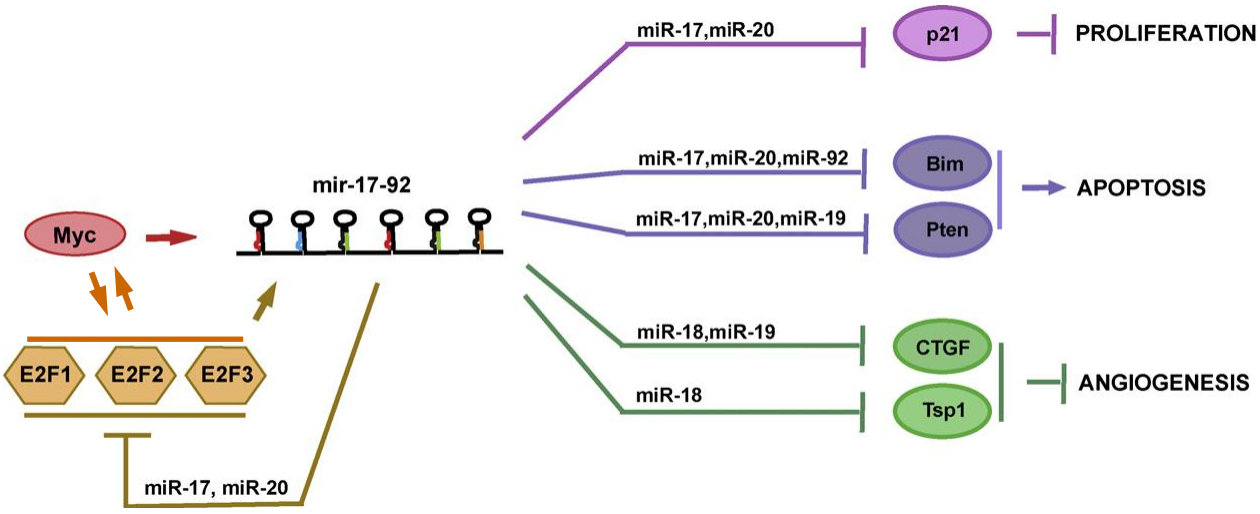

Fig. I.3: The interactions among c-MYC, E2Fs and the *miR-17-92* cluster. Depending on both cell type and physiological context, *miR-17-92* can promote proliferation, inhibit apoptosis and increase neoangiogenesis through the post-transcriptional inhibition of a number of target mRNAs. Modified from (Olive *et al*, 2010).

In contrast to the above cited studies, accumulating evidences indicate that the *miR-17-92* cluster also acts as a tumor suppressor in some circumstances. Loss of heterozygosity of *miR-17-92* correlates with multiple tumor progression, including breast cancer, nasopharyngeal carcinoma, retinoblastoma, hepatocellular carcinoma and squamous cell carcinoma of the larynx (reviewed in Coller *et al*, 2007). *miR-17* exerts its tumor-suppressive activity by limiting the expression of Nuclear receptor coactivator 3 (NCOA3), which in turn activates the PI3K/Akt signaling pathway resulting in increased expression levels of downstream targets like cyclin D1 (Hossain *et al*, 2006). Cyclin D1 is a key regulator of the G1-S phase transition. Importantly, overexpression of this oncoprotein is observed in ~50% of human breast cancers (Fu *et al*, 2004). Consistently, Yu and colleagues (Yu *et al*, 2008) demonstrated that *miR-17* and *miR-20a* repress cyclin D1 expression and identified a novel cyclin D1-miRNA regulatory feedback loop. They showed that the cyclin D1 binds to the regulatory region of *miR-17-92* promoter and induces the cluster transcription.

In summary, a central role of *miR-17-92* in control of proliferative signals and thereby tumorigenesis is emphasized by the fact that at least four key regulatory proteins (c-MYC, E2F3, AML1 and cyclin D1) converge on the cluster promoter region to create important regulatory feedback loops (Fontana *et al*, 2007; Yu *et al*, 2008; O'Donnell *et al*, 2005; Sylvestre *et al*, 2007). The findings that *miR-17-92* cluster acts both as oncogene and tumor suppressor is likely dependent on the cell type, the expression pattern and/or the levels of the target mRNAs (Cloonan *et al*, 2008).

3.2.2. miRNAs and membrane trafficking

Much of the progress in understanding the essential roles of miRNAs in homeostatic processes such as development, cell proliferation and death has been made over the last decade. However, our knowledge of how miRNAs might regulate exocytic and endocytic machineries in eukaryotic cells is limited to only a few reports showing the effects of some miRNAs on regulated insulin secretion (Lovis *et al*, 2008; Plaisance *et al*, 2006; Poy *et al*, 2004). Despite the specific control mechanisms that are essential for a strict regulation of induced cargo secretion, the core exocytic machinery of both constitutive and regulated secretion pathways is conserved. The first evidence that miRNAs are actively involved in the regulation of secretory cargo trafficking came from a report on *miR-375* function in the murine pancreatic β-cell line MIN6. The authors demonstrated that pancreatic islet-specific *miR-375* effectively inhibits glucose-stimulated insulin secretion through downregulation of myotrophin (MTPN) protein level (Poy *et al*, 2004). The functions of MTPN have not been investigated in β-cells, but it has been shown that this protein is implicated in vesicle transport and neurotransmitter catecholamine release in neurons (Yamakuni *et al*, 2002). It is possible that MTPN causes changes in the actin network by interacting with the actin-capping protein CAPZ, thereby influencing secretory granule docking and fusion (Taoka *et al*, 2003). Recently, Li and colleagues confirmed *Mtpn* as a physiological target of *miR-375* and showed that it acts as an anti-apoptotic gene in β-cell lipoapoptosis, suggesting that *miR-375* could regulate both function and viability of pancreatic β-cells (Li *et al*, 2010).

In addition to *miR-375*, other miRNAs, including *miR-124a* and *miR-96* have been identified to modulate the expression of several other proteins involved in insulin exocytosis in MIN6 β-cells. Among them, only RAB27A seems to be directly targeted by *miR-124a*, whereas dysregulation of SNAP-25, RAB3A, synapsin-1A and NOC2 is potentially caused by secondary

miR-124a-mediated mechanisms such as regulation of transcription factors (Baroukh *et al*, 2007; Lovis *et al*, 2008). The effects of *miR-96* on insulin exocytosis are mediated through increased mRNA and protein levels of granuphilin and decreased level of NOC2 (Lovis *et al*, 2008). Granuphilin is RAB3A and RAB27A effector protein which is associated with insulin secretory granules and negatively regulates their docking to the plasma membrane (Coppola *et al*, 2002; Yi *et al*, 2002). In contrast, NOC2 positively regulates insulin secretion by inhibiting Gi/o signaling (Matsumoto *et al*, 2004). Moreover, it was shown that another miRNA, *miR-9*, downregulates the expression of granuphilin targeting directly its transcription factor ONECUT-2 (Plaisance *et al*, 2006).

Taken together, these findings in murine cells provide a strong basis for speculation that miRNAs can also actively regulate vesicle transport pathways in human cells.

3.3. Principles of miRNA-mRNA interactions: an overview

Once incorporated into miRISC, the miRNA brings the complex to its target messenger RNAs by interacting with complementary binding sites, which can be present in multiple copies (Park *et al*, 2009; Tian *et al*, 2010). An individual miRNA can regulate expression of hundreds of transcripts and, as a consequence, level of multiple proteins (Baek *et al*, 2008; Lewis *et al*, 2005; Selbach *et al*, 2008). On the other hand, multiple miRNAs can repress expression of an individual target mRNA (Du *et al*, 2009; le Sage *et al*, 2007; Lewis *et al*, 2005; Wu *et al*, 2010). Animal miRNAs preferentially bind to the 3´UTRs of transcripts (Grimson *et al*, 2007), while the majority of plant miRNA binding sites are located in the protein-coding sequences (CDS) (Rhoades *et al*, 2002). However, recent experimental evidences prove the existence of a new class of animal miRNA targets that contain binding sites in their 5´UTRs (Lee *et al*, 2009; Lytle *et al*, 2007; Orom *et al*, 2008) or within the CDS (Elcheva *et al*, 2009). Although animal miRNA binding sites in the CDS were demonstrated to be less potent than the 3´UTR binding sequences (Baek *et al*, 2008; Selbach *et al*, 2008), both types of sites act synergistically when present in the same transcript (Fang & Rajewsky, 2011).

miRNAs interact with their targets via Watson-Crick base pairing. Target identification by animal miRNAs is achieved mainly through complementarity to the 5´-proximal so called "seed" sequence. The minimal size of the seed sequence sufficient to trigger target silencing has been subject to ongoing debate. Grimson and colleagues have initially classified experimentally identified miRNA binding sites into four distinct groups. These groups include 6mer (miRNA

positions 2-7), 7mer-m8 (positions 2-8), 7mer-A1 (positions 1-7 and adenosine is located across position 1 of the miRNA) and 8mer (miRNA nucleotides 1-8 and adenosine is located across position 1 of the miRNA). Importantly, comparison of 11 experimental data sets revealed that a majority (75%) of the downregulated mRNAs possesses sequences complementary to the 7mer-m8 type seed region of examined miRNAs (Grimson *et al*, 2007). Of course, there is an exception to every rule: functional miRNA:target interactions containing mismatches or bulges in the seed region, such as *Lin-41* mRNA and *let-7* miRNA pair in *C. elegans*, have also been identified (Didiano & Hobert, 2006; Vella *et al*, 2004).

In contrast to animal miRNAs, most of the plant miRNAs form complementary or nearly complementary hybrids with target mRNAs. It allows Ago proteins to cleave target mRNA between the nucleotides paired at positions 10 and 11 of the interacting miRNA (Llave *et al*, 2002), in a manner similar to siRNA-directed cleavage. The cleavage products are degraded by the exosome and the 5´-3´ exonuclease XRN4 (Souret *et al*, 2004). Animal miRNAs inhibit target mRNA expression either by repressing protein translation and/or by inducing deadenylation and subsequent degradation (reviewed in Huntzinger & Izaurralde, 2011). However, recently several groups have reported that miRNAs are capable of activating rather than inhibiting target expression under certain conditions (Orom *et al*, 2008; Vasudevan *et al*, 2007; Vasudevan *et al*, 2008). In summary, transcriptome analyses confirmed that target mRNA degradation by endonucleolytic cleavage is a prominent mechanism of miRNA-mediated gene silencing in plants (Schwab *et al*, 2005), while exonucleolytic degradation is a dominant way promoting decay of animal miRNA targeted mRNAs (discussed in details below).

The most relevant aspects concerning animal miRNA-mediated degradation, translational repression and some examples of translational target mRNA activation are discussed in details in the following sections.

3.3.1. miRNA-mediated target degradation

A number of previous observations supports the idea that animal miRNA-mediated gene silencing is frequently accomplished by target mRNA degradation. These observations come from a series of transcriptome studies showing that the abundance of dozens of validated or predicted miRNA targets inversely correlates with the level of miRNA (Baek *et al*, 2008; Giraldez *et al*, 2006; Guo *et al*, 2010; Hendrickson *et al*, 2009; Lim *et al*, 2005; Selbach *et al*, 2008). Moreover, combining ribosome profiling with mRNA microarray data revealed that at

least 84% of decreased protein production can be attributable to decreased mRNA levels rather than to reduced translational efficiency (Guo *et al*, 2010). Hence, although initially miRNAs were considered to repress protein translation with modest or no effect on mRNA level (Olsen & Ambros, 1999; Wightman *et al*, 1993), genome-wide studies proved that mRNA degradation is a widespread mode of miRNA action in animal cells.

Although animal miRNAs can generally direct mRNA cleavage catalyzed by AGO2 (Yekta *et al*, 2004), they rarely do so due to the fact that the majority of miRNA-target pairs are only partially complementary or contain bulges, which inhibits the slicer activity of Ago2. miRNA-mediated destabilization of mRNA is predominantly initiated through deadenylation, which promotes de-capping followed by exonucleolytic decay (Behm-Ansmant *et al*, 2006; Eulalio *et al*, 2008; Piao *et al*, 2010). Deadenylation is performed by CAF1-CCR4-NOT deadenylase complex recruited to repressed mRNAs via interaction with GW182, a component of miRISC, while the de-capping complex DCP1-DCP2 is required for the removal of the cap structure (Behm-Ansmant *et al*, 2006). The importance of mRNA degradation factors in miRNA-based target destabilization has been demonstrated by depletion of components of the CAF1-CCR4-NOT and the DCP1-DCP2 complexes. For example, knockdown of DCP1 and DCP2 prevents mRNA degradation, but results in an accumulation of deadenylated, translational repressed targets (Behm-Ansmant *et al*, 2006). Following deadenylation, repressed mRNAs are rapidly degraded either from their 3´ ends by the exosome, or after subsequent de-capping, by the cytoplasmic 5´-3´ exonuclease XRN1 (reviewed in Parker & Song, 2004).

3.3.2. miRNA-mediated translational repression

Translational inhibition can be defined as a phenomenon when the decrease in protein expression exceeds the level of mRNA degradation. Translation can be generally divided into initiation, elongation and termination. Initiation is the most common target for translational regulation of eukaryotic genes. Briefly, initiation starts with the assembly of eukaryotic translation initiation factor 4F (eIF4F, which is comprised of eIF4E, eIF4G and eIF4A subunits) on 5´-terminal m^7G cap of the mRNA. This assembly is followed by mRNA circularization induced by eIF4G subunit interaction with the polyadenylate-binding protein C1 (PABPC1, also known as PABP1) and subsequent formation of the active 80S ribosome (reviewed in Kapp & Lorsch, 2004).

miRNA-mediated translational repression in animals has been proposed to occur via inhibition of translation initiation. However, early observations in *C. elegans* (Olsen & Ambros, 1999; Seggerson *et al*, 2002) together with more recent experiments in mammalian cells (Nottrott *et al*, 2006; Petersen *et al*, 2006) demonstrated that miRNA-targeted mRNAs possess the same polysomal profile as non-repressed messages. Contrary to the concept of miRNA-mediated repression, these polysomes are sensitive to various translational inhibitors suggesting that they are actively engaged in translation (Nottrott *et al*, 2006; Petersen *et al*, 2006). Due to divergent experimental data, different models for miRNA-guided translational repression were proposed: (i) co-translational degradation of nascent polypeptide chain, (ii) inhibition of translation elongation and (iii) translation termination due to miRNA-induced drop off of ribosomes prematurely. The model of co-transcriptional peptide degradation was proposed by Nottrott and colleagues (Nottrott *et al*, 2006), however, no further model validation by other laboratories was reported. Initially proposed by Petersen and colleagues (Petersen *et al*, 2006), the premature translation termination model characterized by miRNA-mediated dissociation of ribosomes was supported by the finding that translation, initiated through an internal ribosome entry site (IRES), is still susceptible to miRNA-guided repression (Lytle *et al*, 2007).

In contrast to these observations, other studies concluded that miRNAs inhibit translation at the initiation step. Pillai and colleagues (Pillai *et al*, 2005) showed that miRISC-bound mRNAs do not co-sediment with polysomes in sucrose sedimentation gradient, but shift towards lighter fractions. In addition to that, messenger RNAs containing IRES were immune to repression by miRNAs (Pillai *et al*, 2005). A series of experiments in cell-free extracts of rabbit reticulocytes, *Drosophila* and mammalian cell lines also showed that m^7G structure is required for repression, further supporting the model that miRNA-mediated translational inhibition occurs at the initiation step (Thermann & Hentze, 2007; Wakiyama *et al*, 2007; Wang *et al*, 2006). The observation that molecular tethering of human Ago proteins to the 3'UTR of the reporter mRNA still suppressed translation (Pillai *et al*, 2004) promped researchers to investigate how miRISC proteins interact with translational machinery. The early work of Kiriakidou and colleagues proposed that mammalian AGO2 binds to m^7G cap directly via its MC domain and in this way prevents translation initiation by competing with eIF4E subunit (Kiriakidou *et al*, 2007). However, follow-up structure modeling (Kinch & Grishin, 2009) and other experimental studies (Eulalio *et al*, 2008) disproved the proposed model. Instead, the mutation of two phenylalanines predicted to mediate cap binding was shown to actually abolish the AGO1 interaction with both GW182 and miRNAs in *D. melanogaster* (Eulalio *et al*, 2008). These findings suggested that GW182, a

cellular factor known to be essential for miRNA-mediated repression, not only promotes deadenylation of miRISC-bound target mRNA but also interferes with protein translation.

In summary, these evidences suggest that miRNA-mediated translational repression, besides target degradation, occurs predominantly at the initiation step.

3.3.3. Translational activation by miRNAs

Several reports indicating that miRNAs can enhance rather than repress expression of specific mRNAs under certain conditions further expand the functional repertoire of these small RNAs. Vasudevan and colleagues reported that AGO2-*miR-369-3* complex stimulates *TNFα* mRNA translation in quiescent cells arrested in G0/G1 phase (Vasudevan *et al*, 2007). More recently, the same laboratory found that *xlmiR-16* (*Xenopus laevis miR-16*) is required for upregulated expression of cell cycle regulator Myt1 kinase in prophase I-arrested immature *X. laevis* oocytes (Mortensen *et al*, 2011). It should also be noted that AGO association with Fragile X Related Protein (FRX1) was required for translational activation in both studies.

Further examples of miRNA-mediated translational activation involve *miR-10a* and *miR-122*. *miR-10a* was reported to bind to the 5´UTR immediately downstream of the regulatory 5´TOP motif located in mRNAs encoding ribosomal proteins and to enhance their translation under amino acid starvation conditions. Furthermore, authors speculate that *miR-10a* might positively regulate global protein synthesis via stimulation of ribosomal protein expression and potentially affect processes of cellular transformation (Orom *et al*, 2008). Liver-specific *miR-122* was shown to stimulate replication of Hepatitis C virus (HCV) RNA in hepatoma cells by binding to it's 5´UTR (Jopling *et al*, 2005). Recent findings suggest that miR-122 might also enhance HCV RNA translation (Henke *et al*, 2008). However, additional experiments are required to elucidate whether this function is AGO- or GW182-dependent and does not occur due to any conformational changes of HCV RNA that facilitates ribosome loading.

3.4. miRNA biogenesis

The biogenesis pathway in animals consists of a series of several biochemical steps that process pri-miRNAs into biologically active, mature miRNAs (**Fig. I.1**). The miRNA genes are initially transcribed by RNA polymerase II (Lee *et al*, 2004). It has been proposed that the largest human miRNA gene cluster *C19MC* encoding 59 miRNAs is exclusively transcribed by RNA

polymerase III (Borchert *et al*, 2006). However, a recent study revealed that most likely *C19MC* is also transcribed by RNA polymerase II (Bortolin-Cavaille *et al*, 2009). Similar to other protein-coding mRNAs, primary transcripts of intergenic human miRNAs are 3´ polyadenylated and bear a 5´ terminal 7-methyl guanylate cap (Cai *et al*, 2004). The majority of primary transcipts are from 3 to 4 kb in length (Saini *et al*, 2007). The conventional miRNA biogenesis pathway is characterized by two sequential cleavage reactions mediated by RNase III family enzymes. The first endonucleolytic reaction occurs in the nucleus where pri-miRNAs are recognized and cleaved by a multi-protein complex, called microprocessor, liberating ~70-nt long stem-loop structured precursor-miRNAs (pre-miRNAs). The two essential components of the minimal microprocessor complex are RNase III enzyme Drosha and the double-stranded RNA binding protein DiGeorge critical region 8 (DGCR8, also known as Pasha in *D. melanogaster* and *C. elegans*) (Denli *et al*, 2004). The larger microprocessor complex contains many accessory proteins such as heterogeneous nuclear ribonucleoproteins (hnRNPs), DEAD-box helicases p68 and p72 and Ewing's sarcoma proteins (Gregory *et al*, 2004). The two double-stranded RNA-binding domains of DGCR8/Pasha stably interact with the pri-miRNAs and determine the precise cleavage site (Han *et al*, 2006), whereas RNase domains cleave the 5´ and 3´ arms of the pri-miRNA hairpin structure (Han *et al*, 2004).

After nuclear processing, the 2-nt 3´overhang of pre-miRNA is recognized by exportin-5 in complex with GTP-bound Ran cofactor and the pre-miRNA hairpin is exported from the nucleus (Yi *et al*, 2003).

In the cytoplasm, pre-miRNAs are further processed by a second RNase III enzyme Dicer. Dicer cleaves off the terminal loop by cutting both strands of the pre-miRNAs, leaving a transient, roughly 20-nt long, miRNA/miRNA* duplex with 2-nt overhangs at each 3´ end. Overall hairpin length and loop size influence the efficiency of Dicer processing, and the imperfect nature of the miRNA/miRNA* pairing also affects cleavage (Park *et al*, 2011). Similar to Drosha, Dicer is a member of a multi-protein complex, called miRNA RISC loading complex (miRLC), which additionally contains other double-stranded RNA binding proteins, Tar RNA binding protein (TRBP, Chendrimada *et al*, 2005), protein activator of PKR (PACT, Lee *et al*, 2006) and Argonaute-2 (Ago2, Gregory *et al*, 2005). In contrast to Drosha-DGCR8 complex, TRBP and PACT are not essential for Dicer activity, however, they facilitate the cleavage of terminal loop, stabilize Dicer protein and recruit Ago2 to the miRLC (Chendrimada *et al*, 2005; Gregory *et al*, 2005; Lee *et al*, 2006). Noteworthy, the exported pre-miRNA hairpin binds already

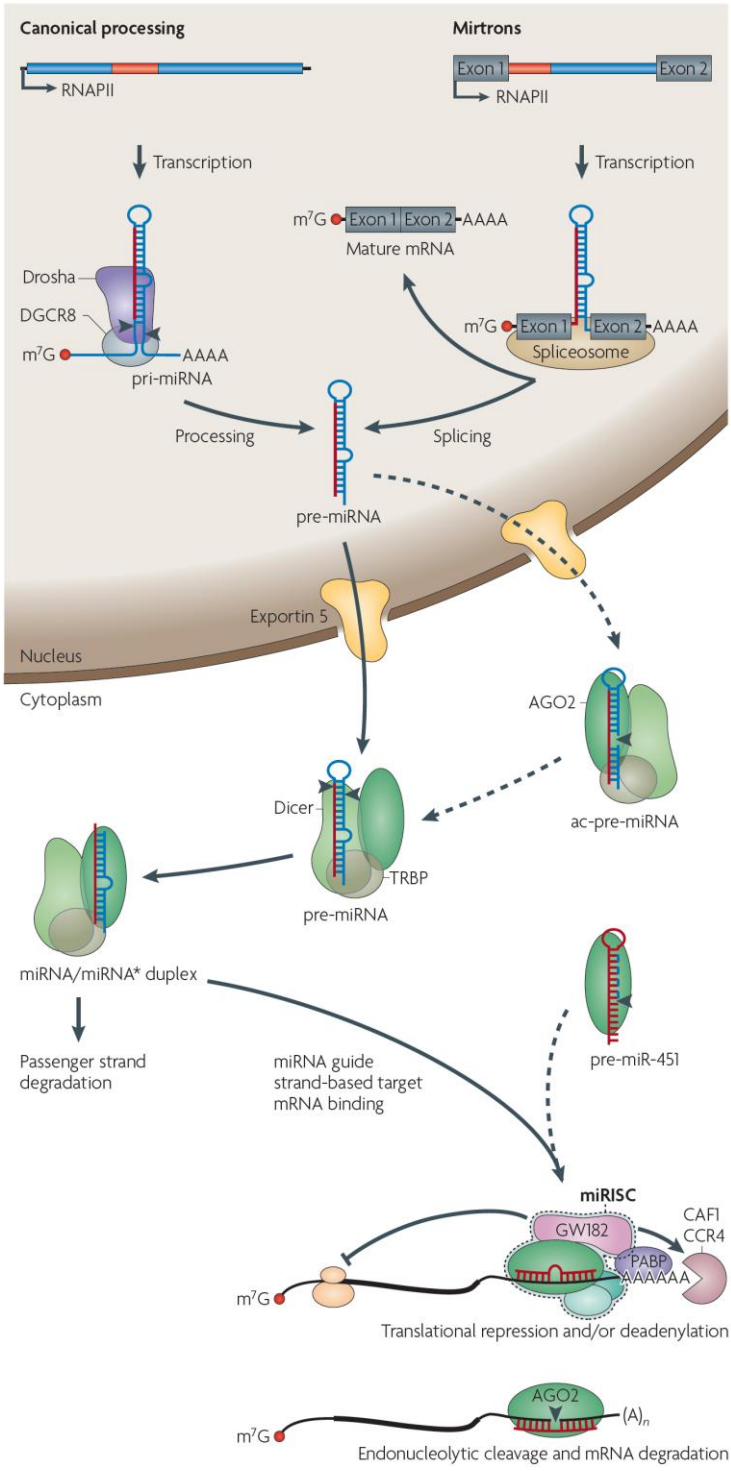

Fig. I.1: Animal miRNA biogenesis and effect on target mRNAs. miRNA genes are transcribed to generate primary miRNA (pri-miRNA) molecules that fold into hairpin structures. After excision from pri-miRNAs by the microprocessor complex (Drosha-DGCR8), a hairpin (pre-mRNA) is exported to the cytoplasm and further processed by the Dicer-TRBP complex to yield a miRNA/miRNA* duplex. Following processing, the miRNA duplex liberates the mature miRNA to assemble into a miRISC comprised of core Ago proteins and other auxiliary proteins. The incorporated miRNA guides miRISC to the target mRNAs and inhibit protein synthesis by either repressing translation or promoting mRNA deadenylation followed by decay. Alternative miRNA biogenesis pathways such as of mirtrons, ac-pre-miRNA and pre-miR-451 are also depicted. Adapted from (Krol *et al*, 2010).

preassembled miRLC in the cytoplasm (Gregory *et al*, 2005). The formation of miRLC is an ATP-independent process (Maniataki & Mourelatos, 2005).

Following cleavage, Dicer and interacting proteins TRBP or PACT dissociate from the miRLC initiating the transition of the miRLC into the active miRISC. This transition is further continued by the immediate separation of the miRNA/miRNA* duplex into the functional

mRNA-targeting mature miRNA strand (guide strand), which is complementary to the target mRNA, and the miRNA* strand (passenger strand). It was assumed that miRNA* is usually degraded, however, recent studies have demonstrated that passenger strands are not always by-products and a substantial cohort of miRNA* species are functionally active (Chiang *et al*, 2010; Yang *et al*, 2011). Although many helicases such as p68, p72, RNA helicase A, Mov10 (Gregory *et al*, 2004; Meister *et al*, 2005) have been attributed to the miRNA biogenesis, a common enzyme responsible for miRNA/miRNA* unwinding has not been identified yet. In some cases, specific helicases are found in complex with distinct miRNAs such as let-7 (Salzman *et al*, 2007), on the other hand, the formation of active miRISC in the absence of ATP suggests that helicases might be generally dispensable (Maniataki & Mourelatos, 2005).

As mentioned, the miRNA/miRNA* duplex can be a source of two different mature miRNAs. However, the thermodynamic stability of the miRNA duplex 5´ ends determines which strand is preferentially incorporated into miRISC; usually, the retained is the one that has less stable base pair at its 5´ end in the duplex (Khvorova *et al*, 2003). In addition to the processing of miRNA precursor molecules, Drosha and Dicer also have a significant impact on miRNA loading into miRISC. Notably, cleavage of some precursor miRNAs by these enzymes is not very accurate and results in miRNA variants with heterogenic termini. Hence, cleavage heterogeneity can result into different 5´ end stability and, consequently, alter active miRNA strand selection (Carthew & Sontheimer, 2009).

The mammalian Ago/miRNA complex is associated with a number of different proteins such as Gemin3, Gemin4, Mov10, Imp8 and GW182 (Meister *et al*, 2005; Weinmann *et al*, 2009). In addition, studies in human, worms and flies indicate that the minimal Ago/miRNA/GW182 complex is sufficient for miRNA-mediated gene silencing (Ding & Grosshans, 2009; Eulalio *et al*, 2008; Liu *et al*, 2005) (**Fig. I.1**).

3.4.1. Alternative miRNA biogenesis pathways

In addition to the well-defined conventional miRNA biogenesis pathway that governs the maturation of most miRNAs in animals, several alternative maturation pathways were identified that do not generally require Drosha or Dicer cleavage. The most prominent alternative mechanism uses splicing machinery and the lariat-debranching enzyme to generate pre-miRNA hairpins, thereby bypassing the initial Drosha cut. Such short-hairpin introns are known as mitrons; although they were initially thought to exist only in flies and nematodes (Okamura *et al*,

2007; Ruby *et al*, 2007), Berezikov and colleagues identified them also in mammals (Berezikov *et al*, 2007). In contrast to the canonically processed intronic miRNAs, mitrons are located within very short introns and the ends of the hairpin are determined by the splice sites of such introns. Following RNA refolding, mitrons are subjected to exportin-5-Ran-mediated transport to the cytoplasm where they are further processed by Dicer (Okamura *et al*, 2007; Ruby *et al*, 2007).

Most recently, a Dicer-independent biogenesis pathway of blood-specific *miR-451* has been identified (Cheloufi *et al*, 2010; Cifuentes *et al*, 2010). *pre-miR-451*, which has shorter stem part compared to other pre-miRNAs, is cleaved by AGO2 RNase H-like endonuclease activity. The 3´ end of functional *miR-451* is generated by exonucleolytic trimming by a cellular nuclease independently of Dicer (Cheloufi *et al*, 2010; Cifuentes *et al*, 2010). In addition to its central role in miRNA-mediated gene repression, AGO2 has been reported to cleave some, but not all, pre-miRNAs to an additional processing intermediate called AGO2-cleaved pre-miRNA or ac-pre-miRNA (Diederichs & Haber, 2007). AGO2 nicks the prospective passenger miRNA strand 12 nucleotides from its 3´ end before Dicer cleavage, however, the physiological functions of this intermediate remain unknown (Diederichs & Haber, 2007). The alternative miRNA maturation pathways are depicted in **Figure I.1**.

3.4.2. Regulation of miRNA biogenesis

miRNA biogenesis can be controlled by the regulation of miRNA gene transcription and post-transcriptional processing. The similar features of intergenic miRNA and mRNA promoters and the common DNA binding factors required for the transcription of both indicate that transcription of miRNA genes is regulated by similar mechanisms to those of protein-coding genes (Corcoran *et al*, 2009). For example, the proto-oncogene *c-MYC* is a transcription factor, which regulates 10 to 15% of human genes, modulates transcription of the *miR-17-92* cluster (He *et al*, 2005) through binding to E-boxes within its promoter (O'Donnell *et al*, 2005). On the contrary, expression of several tumor suppressor miRNA genes, including the *miR-15a*, *-29*, *-34* and *let-7* families, is inhibited by the same c-MYC transcription factor (Chang *et al*, 2008). Another example of regulated miRNA gene transcription is the tumor suppressor *miR-34a* which expression is increased by p53 in response to genotoxic stress (Raver-Shapira *et al*, 2007).

Additionally, regulation of miRNA gene transcription is a major level of control responsible for spatiotemporal expression of miRNAs as well as the same rule is valid for tissue- or development-specific expression of protein-coding genes. The orchestrated spatiotemporal

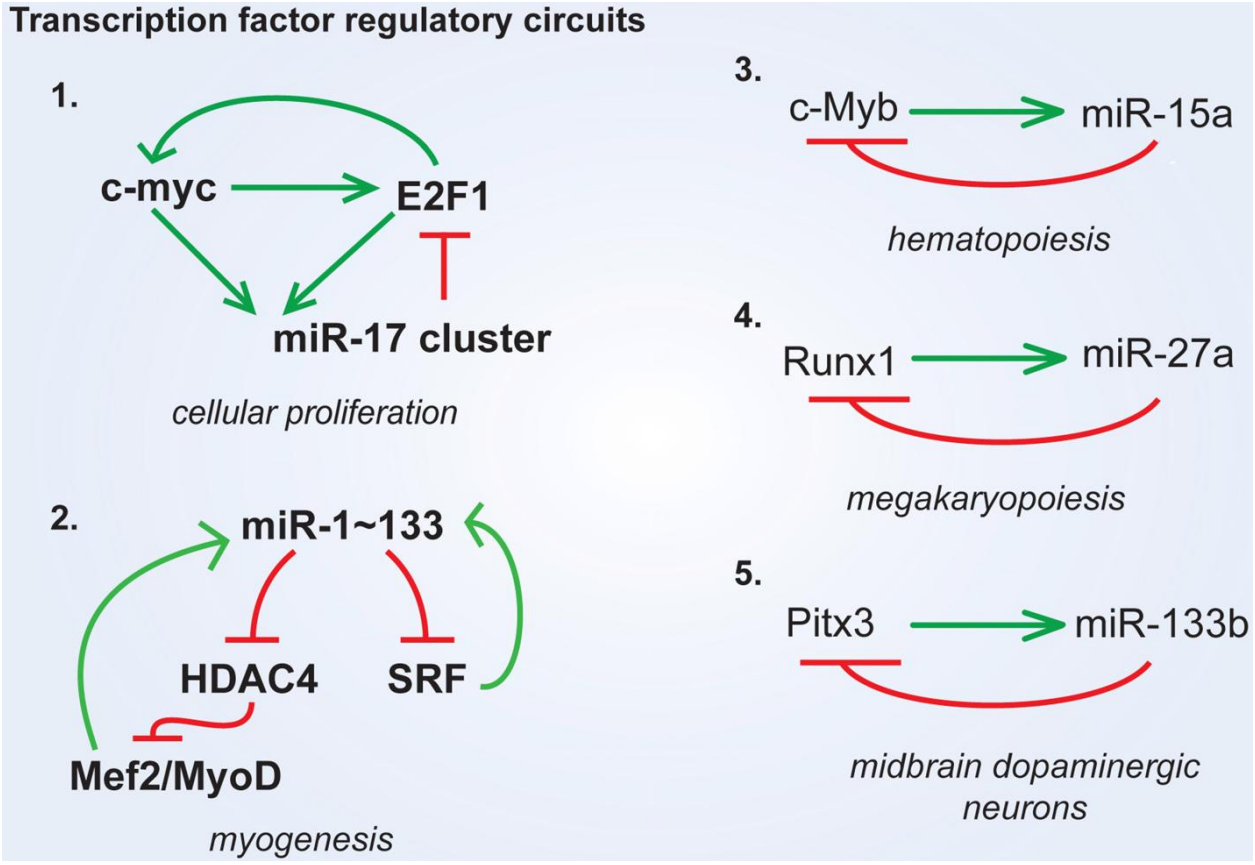

Fig. I.2: Transcription factor – miRNA regulatory circuits. (**1**) Expression of *miR-17-92* cluster is positively regulated by both c-Myc and E2F1 transription factors, whereas *miR-17* inhibits translation of the important cell cycle regulator E2F1. Consistent with activation of proto-oncogenic c-Myc, this feed-back circuit is often found deregulated in tumors. (**2**) Transcription of several myocyte-specific miRNAs, including *miR-1* and *miR-133*, is upregulated by MEF2, MyoD and SRF during myogenesis. (**3-5**) A number of single-negative miRNA autoregulatory loops with transcription factors have been described in differentiating hematopoietic progenitor cells (c-Myb-*miR-15a*, Runx1-*miR-27a*) or dopaminergic neurons (Pitx3-*miR-133b*). Adapted from (Davis & Hata, 2009).

expression of miRNAs with mRNAs is exemplified in **Figure I.2** and is also discussed in details in recent reviews (Davis & Hata, 2009; Schanen & Li, 2011).

Post-transcriptional processing of miRNA consists of many maturation steps and each stage of biogenesis provides a broad spectrum of regulatory options to generate individual miRNA differently. Some of the major options are: (i) editing of pri- or pre-miRNAs by adenosine deaminases (ADARs) that catalyze the A-to-I transition in double stranded RNA and thereby block further processing of edited sequences by Drosha (Yang *et al*, 2006) or Dicer (Kawahara *et al*, 2007); (ii) positive regulation of Drosha activity by RNA helicases p68 and p72 (Fukuda *et al*, 2007) and p68-interacting SMAD proteins (Davis *et al*, 2010; Hata & Davis, 2011); (iii) competition of Lin-28 and Dicer for interaction with *let-7* family pre-miRNAs

(Lightfoot *et al*, 2011; Rybak *et al*, 2008) and (iv) inhibition of Dicer activity by other yet-unknown factors (Obernosterer *et al*, 2006). Although recent studies have provided deeper insights into regulation of miRNA biogenesis (Davis & Hata, 2009; Krol *et al*, 2010; Siomi & Siomi, 2010; Suzuki & Miyazono, 2010), this topic is not the focus of the project, therefore, it is not discussed in details here.

3.5. High-content screening approaches for studying miRNA functions

Despite the recent rapid accumulation of experimental data and the emergence of functional models, the complexity of miRNA-based regulation is still far from being well understood. In particular, there is a lack of comprehensive knowledge concerning which cellular processes are regulated by which miRNAs or how temporal and spatial interactions between miRNAs and their targets occur. In this regard, results from large-scale functional analyses have immense potential to address these questions.

The established infrastructure for siRNA/shRNA screenings (robotics for large-scale sample preparation, automated data acquisition and analysis, data storage capacities) can easily be applied for high-throughput studies of miRNA function. As for siRNA library screenings, lipid-based transfection is most commonly used to achieve a transient overexpression (Lam *et al*, 2010) or inhibition (Cheng *et al*, 2005) of miRNAs in cell culture. The advantages of the solid-phase reverse transfection method, in combination with an automated liquid handling system, have been also applied in miRNA screenings by several groups with a high success rate (Ovcharenko *et al*, 2007; Whittaker *et al*, 2010). Several miRNA screenings have been completed under conditions of miRNA stable overexpression achieved by transduction with retroviral vectors encoding specific miRNAs (Huang *et al*, 2008; le Sage *et al*, 2007; Nagel *et al*, 2009; Voorhoeve *et al*, 2006).

A number of miRNA library screenings have been completed during the last 5 years (reviewed in Serva *et al*, 2011). Two major groups of biological processes have been investigated so far, namely, (i) cell viability, proliferation and apoptosis, and (ii) gene expression and/or activity regulation. Many miRNAs that regulate cell proliferation and apoptosis has been identified by using high-throughput approaches (Lam *et al*, 2010; Voorhoeve *et al*, 2006; Whittaker *et al*, 2010) since Cheng and colleagues (Cheng *et al*, 2005) reported the first large-scale screen to identify mammalian miRNAs involved in these processes. In 2007, Ovcharenko and colleagues (Ovcharenko *et al*, 2007) performed a screening of 187 miRNAs in order to

capture the modulators of TRAIL-induced apoptotic pathway. miRNAs regulating expression of BCL-2 family protein MCL1 were identified by screening a library of 810 human miRNAs for their ability to sensitize cancer cells to ABT-263, an inhibitor of BCL-2 family members (Lam *et al*, 2010). As a result, 10 miRNAs were shown to bind directly to the 3´UTR of *MCL1* mRNA and thereby inhibit protein expression. These examples demonstrate the potency of large-scale screenings in identifying miRNAs that regulate proliferation or modulate sensitivity to chemotherapeutic agents, and this knowledge contributes to the development of novel miRNA-based anti-cancer therapeutics. The feasibility of proliferation-focused miRNA screenings has been significantly improved by the development of quantification methods from straightforward cell counting (Cheng *et al*, 2005) to recording of electrical impedance over 96 hours (Cole *et al*, 2008).

miRNAs that regulate the expression of gene of interest are usually identified in so-called "target-based" screenings. In the most cases, luciferase or fluorescent protein reporters bearing 3´UTR of gene of interest are employed and the intensity of the detected signal is used to quantify gene expression level upon modulation of miRNAs (Nagel *et al*, 2009; Park *et al*, 2009; Tian *et al*, 2010; Wu *et al*, 2010). For instance, using a functional genetic approach with stable expression of individual miRNAs, *miR-221* and *miR-222* were identified to specifically regulate expression of tumour suppressor $p27^{Kip1}$ (le Sage *et al*, 2007).

Apart from two major groups of processes mentioned above, the repertoire of cellular processes analysed by miRNA functional screenings is expanding rapidly (reviewed in Serva *et al*, 2011). Conducting miRNA library screenings in appropriate cellular contexts, for instance, screening for miRNAs regulating steroidogenesis in ovarian cells (Sirotkin *et al*, 2009) or screening for miRNAs regulating lipid droplet formation in hepatocytes (Whittaker *et al*, 2010), ensures acquisition of physiologically relevant information.

There are virtually no reasons why the read-out strategies in miRNA screenings should be different from the ones established in siRNA-based screenings. Nevertheless, fluorescence microscopy-based approaches are considered to be highly advantageous over biochemical techniques in large-scale miRNA screenings. Features that make fluorescence microscopy ideal to analyse regulatory potential of miRNAs include (i) rapid collection of large amount of data, (ii) feasibility of phenotype multiplexing, (iii) possibility to acquire quantitative data on a single cell and/or population levels and (iv) detection of subtle phenotypes (Pepperkok & Ellenberg, 2006; Sacher *et al*, 2008). The pioneers in applying this approach for functional miRNA investigation were Sirotkin and colleagues (Sirotkin *et al*, 2010), who performed a fluorescence

microscopy-based miRNA screening in order to identify miRNAs regulating cell proliferation and apoptosis. Primary human ovarian cells were transfected with synthetic miRNA mimics and immufluorescence of proliferating cell nuclear antigen (PCNA) and Cyclin-B1 were used to determine miRNA effects on cell proliferation. Immunofluorescence of BAX was used to estimate apoptosis rate. Additionally, Whittaker and colleagues (Whittaker *et al*, 2010) demonstrated that the sensitivity of fluorescence microscopy technique in measuring lipid dropled formation in hepatocytes upon overexpression of miRNAs is a high as of laborious biochemical assay. Using an automated image acquisition platform combined with image analysis software, authors identified 11 out of 327 screened miRNAs as the most potent regulators of intracellular lipid content.

3.6. Membrane trafficking in mammalian cells

Eukaryotic cells have a highly evolved membrane trafficking organization. The evolution of eukaryotic cells introduced a major challenge to traffic a vast array of different cargoes (for example, hormones, matrix and serum proteins, digestive enzymes, antibodies and growth factors) between distinct membranous organelles in a specific and regulated manner. Moreover, membrane trafficking is involved in controlling size, shape and molecular composition of most cellular organelles. Functionally, membrane trafficking routes are broadly divided into the biosynthetic pathway responsible for the transport of cargoes synthesized in the endoplasmic reticulum (ER) to the cell surface, or to other endomembrane organelle, and the endocytic pathway. The latter is responsible for the internalization of compounds from the extracellular space to be utilized for cellular metabolism. Both biosynthetic transport and endocytosis are multistep processes involving cargo selection and vesicle formation at the donor membrane, vesicle transport, tethering and fusion with the target membrane. To carry out so many diverse tasks, membrane trafficking system relies on an array of membranous organelles, including the ER, the Golgi complex, different types of endosomes, lysosomes, the plasma membrane and secretory granules in specialized secretory cells (**Fig. I.4)**. In addition to structural components, different cargo trafficking processes are coordinated by a sophisticated regulatory machinery that is estimated to comprise thousands of proteins (Gilchrist *et al*, 2006).

3.6.1 Biosynthetic membrane trafficking

The biosynthetic transport of membrane and secretory proteins initiates at their site synthesis, the ER, whose environment is especially suited to facilitate the proper folding of newly synthesized proteins and the initial steps of their N-linked glycosylation (Ellgaard & Helenius, 2003). While some of the proteins are able to fold into their native structures during co-translational insertion into the ER, others require more assistance from a complex folding machinery that includes chaperones and other folding enzymes (Kleizen & Braakman, 2004). Folding is essential for protein transport to the Golgi complex, and if this step can not be completed, misfolded proteins are retained in the ER and are degraded by the ER-associated degradation machinery (Sitia & Braakman, 2003). After folding, post-translational modifications and quality control, mature proteins enter ER exit sites (ERES), where they are sorted into budding vesicles interacting directly with components of the coat protein complex II (COPII) or indirectly through interactions with specific cargo receptors such as the lectin ERGIC53 (Kuehn *et al*, 1998; Schrag *et al*, 2003).

Sequential polymerization of COPII subcomplexes (Sec23–Sec24 and Sec13p–Sec31p) causes the membrane curvature required for the formation of the vesicle and potentially induces the subsequent scission of the budding COPII-coated vesicles from the ER (Barlowe, 2002; Stephens, 2003). COPII vesicles rapidly uncoat and fuse to form the ER-Golgi intermediate compartment (ERGIC). From there, coat protein complex I (COPI)-coated vesicular carriers are transported towards the *cis*-Golgi complex along microtubules by the dynein motor protein (Appenzeller-Herzog & Hauri, 2006; Bannykh *et al*, 1998). From ERGIC, ER resident proteins that participate in the formation of anterograde carriers are recycled back to the ER by COPI-mediated retrograde transport (Scales *et al*, 1997).

Once in the Golgi complex, cargo proteins migrate through the multiple stacks of this organelle, to emerge at the trans-Golgi network (TGN). The Golgi complex is a highly dynamic organelle comprising from three to eight cisternae. Fuctionally, the Golgi complex is devided in *cis*-Golgi, medial-Golgi and TGN, each part containing different resident enzymes that act at early, intermediate and late steps of secretory cargo processing, respectively (Rabouille *et al*, 1995). Although several models have been proposed for intra-Golgi cargo transport, COPI-mediated transport appears to play a central role in Golgi function (Glick & Nakano, 2009). However, the directionality of COPI-dependent transport remains an open question; while several groups have reported that COPI vesicles are responsible for the anterograde intra-Golgi

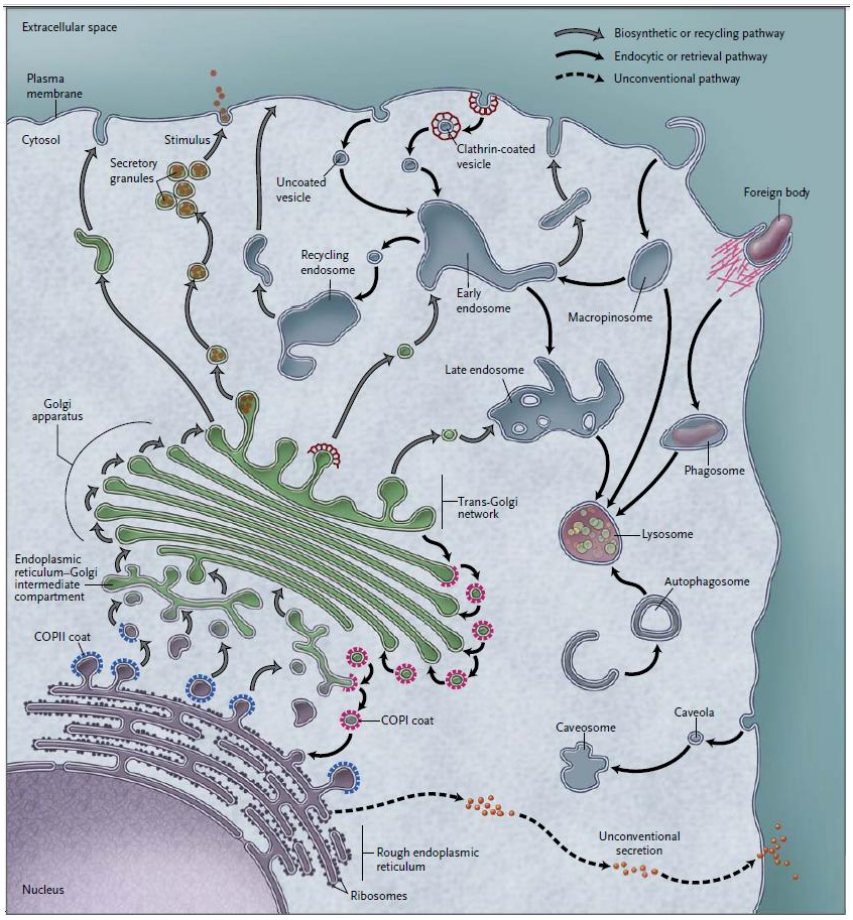

Fig. I.4: Biosynthetic and endocytic membrane trafficking pathways in mammalian cells. The transport of newly synthesized secretory proteins as well as proteins that reside in membrane trafficking system starts from the ER, where they are packaged into COPII-coated carriers that fuse to form the ER-Golgi intermediate compartment (ERGIC). In the Golgi apparatus, the cargoes enter the cis-Golgi network, move through the Golgi stack, and are sorted at the trans-Golgi network (TGN). COPI-mediated retrograde transport recycles Golgi resident proteins from upstream compartments as well as ER proteins from the ERGIC and Golgi complex. From TGN, different types of carriers transport sorted cargoes to various final destinations. Most plasma membrane proteins and extracellular cargoes are internalized through clathrin-dependent or -independent endocytosis. The endocytic vesicles fuse with each other to form the early endosomes from where cargoes can be transferred to the lysosomes via the late endosomes or to the TGN, or recycled back to the plasma membrane. Macropinocytosis and phagocytosis pathways for the uptake of large extracellular fluid volumes and solid particles, respectively, are shown. Adapted from (De Matteis & Luini, 2011)

movement of cargo (Orci *et al*, 1997; Rothman, 1994), others failed to detect secretory cargo in COPI vesicles (Martinez-Menarguez *et al*, 2001), suggesting that these vesicles are not involved in anterograde cargo transport. Similarly, conflicting data comes from studies about anterograde transport of resident Golgi glycosylation enzymes (Cosson *et al*, 2002; Martinez-Menarguez *et al*, 2001), indicating that new methods might be necessary to resolve these controversies.

After passing through the medial-Golgi complex, different cargoes are sorted in the TGN and packaged in specialized carriers for delivery to their respective destinations. For instance, clathrin-coated vesicles (CCVs) transport certain cargoes from the TGN to endosomes. Most lysosomal enzymes contain a mannose-6-phosphate tag and are sorted by mannose-6-phosphate receptor (M6PR) into CCVs that deliver cargo to the late endosomes (Braulke & Bonifacino, 2009; Hille-Rehfeld, 1995). Many secretory proteins are loaded into large pleiomorphic carriers and delivered to the plasma membrane by a variety of routes (Bossard *et al*, 2007). Apart from secretory proteins that utilize the constitutive biosynthetic pathway, certain specialized cells sort specific cargoes (hormones, neurotransmitters) into secretory granules that accumulate in the cytoplasm until their secretion is triggered by physiological signals (Burgoyne & Morgan, 2003). In addition to serving as cargo sorting and exit site of the Golgi, the TGN is also central to the recycling pathway of various endosomal and plasma membrane proteins. This can be illustrated by the fact that many of these proteins are found in both endosomes and TGN (Pavelka *et al*, 1998; Shen *et al*, 2006). Thus, the TGN represents the interface between the biosynthetic and endocytic pathways.

3.6.1 Endocytic membrane trafficking

The endocytic pathway is comprised of various vesicular organelles, including early/sorting endosomes, recycling endosomes, multivesucular bodies, late endosomes and lysosomes. Similarly to post-Golgi biosynthetic trafficking, endocytosis includes several distinct pathways. Besides clathrin-mediated endocytosis (CME), which accounts for a large proportion of endocytic events, an array of clathrin-independent pathways has been identified. These pathways include caveolin1-dependent endocytosis, ARF6-dependent endocytosis, flotillin-dependent endocytosis, macropinocytosis, phagocytosis and trans-endocytosis (Doherty & McMahon, 2009). Although a list of cargoes that have been shown to undergo clathrin-independent endocytosis is rapidly expanding (Kirkham & Parton, 2005), molecular mechanisms and physiological functions of CME is the best-understood.

CCV formation occurs through five stages: initiation, cargo selection, coat assembly, scission and uncoating. Clathrin coats are made up of clathrin triskelia that do not possess any affinity for biological membranes. Therefore, many transmembrane receptors and their ligands are packaged into CCVs only in complex with adaptor proteins, such as AP2, and cargo-specific accessory proteins, such as AP180 and epsin. Noteworthy, specific adaptor complexes are

required for CCV formation at the TGN and at the plasma membrane (Traub, 2005). There are six different adaptor complexes in mammals (AP-1-6), however, AP-2 is a core adaptor for the formation of CCVs at the plasma membrane (Ohno, 2006). The uptake of the best-characterized clathrin-dependent cargoes, such as transferrin, epidermal growth factor and low-density lipoprotein has been shown to require AP-2 (Boucrot *et al*, 2010; Huang *et al*, 2004). AP-2 and other accessory proteins are recruited at sites of the plasma membrane, which are destined to be internalized, by the putative nucleation module (Henne *et al*, 2010; Stimpson *et al*, 2009). Once at the plasma membrane, these proteins bind to the cytoplasmic tails of transmembrane cargo molecules and subsequently initiate clathrin coat assembly by recruiting clathrin triskelia directly from the cytosol. Following the formation of CCV, the membrane scission GTPase dynamin twists around the connective neck and mediates membrane fission releasing the vesicle from the donor plasma membrane (Sweitzer & Hinshaw, 1998). After pinching off from the plasma membrane, CCVs are uncoated by the ATPase heat shock cognate 70 (HSC70) and its cofactor, auxilin (Schlossman *et al*, 1984; Ungewickell *et al*, 1995), and naked vesicles generally fuse to the RAB5-positive early endosomes (Nielsen *et al*, 1999).

Similar to the TGN, endosomes represent a major sorting compartment in mammalian cells. Sorting of internalized material within the endosomal system is complex, involving ligands being released from their receptors for degradation in the lysosomes and recycling of receptors to the plasma membrane (Maxfield & McGraw, 2004). Endocytosed membrane proteins, including the epidermal growth factor receptor, that are tagged for degradation by ubiquitylation are collected in multivesicular bodies, also referred to as a form of late endosomes, through the action of ESCRT-I, -II and –III complexes (Felder *et al*, 1990; Katzmann *et al*, 2002). The formation of late endosomes from early endosomes requires the conversion from a RAB5-positive compartment into a RAB7-positive compartment, a process regulated by the SAND-1-CCZ-1 complex (Kinchen & Ravichandran, 2010; Poteryaev *et al*, 2010).

Besides previously mentioned biosynthetic cargo trafficking pathways between the TGN and the endosomal system, there are at least two main retrograde transport routes between these membranous compartments. The pathway between the early endosomes and the TGN is used by, for example, Shiga toxin to reach the Golgi complex and the ER (Mallard *et al*, 1998), and cargo receptor TGN38, which is transported to the TGN before recycling back to the plasma membrane (Chapman & Munro, 1994). The second endosome-to-TGN pathway implicates late endosomes. This route is involved in the retrograde transport of, for example, furin (Mallet & Maxfield, 1999) and M6PR (Hille-Rehfeld, 1995). Thus, the endosomal system is a sophisticated and

dynamic network through which different cargoes and resident proteins are transported following diverse anterograde and retrograde pathways.

3.7. Core regulatory proteins in membrane trafficking

Many regulatory and structural proteins that are involved in the membrane trafficking process have been characterized: adaptor proteins for specific cargo sequestration, proteins responsible for vesicle budding and scission, motor proteins that transport vesicular carriers along cytoskeletal components and the vesicle coat proteins. However, the molecular mechanisms by which the membrane trafficking is coordinated to maintain both the fidelity and the efficiency of the cargo transport remains a significant focus of research. GTPases of the Ras superfamily have come to the frontline as key regulatory factors that play a critical role in membrane trafficking. These GTPases are classified into five families: Ras, Rho, Rab, Arf and Ran. Members of Rab and Arf families are of particular importance as they, in complexes with numerous effector proteins, participate in the regulation of almost all vesicular transport steps in eukaryotic cells, starting from the vesicle formation, trafficking to and fusion with target membranes (Donaldson & Jackson, 2011; Stenmark, 2009). GTPases are small monomeric GTP-binding proteins that cycle between the cytoplasmic GDP-bound inactive and the membrane-associated GTP-bound active forms providing a major mechanism to regulate assembly and disassembly of functional membrane domains in the biosynthetic and endocytic membrane trafficking pathways. The activation and inactivation of Rab and Arf GTPases are controlled by guanine nucleotide exchange factors (GEFs) and GTPase-activating proteins (GAPs), respectively. GDP dissociation inhibitors (GDIs) represents the third type of regulators specific to Rabs (Bernards, 2003; Jackson & Casanova, 2000; Matsui *et al*, 1990; Randazzo & Hirsch, 2004).

Besides GTPases, heterogeneous tethering factors and highly conserved SNAP receptors (SNAREs) have been show to drive tethering of vesicular carrier to and fusion with acceptor membranes as well as to contribute specificity of membrane trafficking.

3.7.1. Arf GTPases

The small ADP-ribosylation factor (Arf) GTPases are major regulators of vesicle biogenesis process. The Arf family consists of Sar1, ARF1-6, Arf-like (Arl) and Arf-related (Arp) proteins. Sar1 GTPase plays central role in COPII coat assembly and cargo selection at

ERES and thereby is an essential protein for ER-to-Golgi transport (Nakano & Muramatsu, 1989). After activation by GEF Sec12, Sar1 inserts into ER membrane and recruits a heterodimeric Sec23/24 complex, which is a part of COPII coatomer (Bielli *et al*, 2005; Hicke *et al*, 1992; Nakano *et al*, 1988). Subsequently recruited Sec13/31 complex forms a structural cage around the budding vesicle acting as a scaffold for the outer layer subunits of the COPII coat (Stagg *et al*, 2006).

While Sar1 regulates COPII coat assembly at ER, the Arf GTPases control biogenesis of COPI and clathrin coats at the Golgi, endosomes and plasma membrane (D'Souza-Schorey & Chavrier, 2006). Based on sequence homology, the six mammalian Arfs can be divided into three classes (Kahn *et al*, 2006). Class I Arf proteins (ARF1, ARF2 and ARF3) control the assembly of different types of vesicle coat complexes onto budding vesicles along the biosynthetic pathway. Class II Arf proteins (ARF4 and ARF5) are thought to play a role in early Golgi transport, whereas ARF6, the sole member of class III, is involved in the regulation of endosomal membrane trafficking and actin cytoskeleton remodelling at the cell periphery (Bonifacino & Glick, 2004; Claude *et al*, 1999; D'Souza-Schorey *et al*, 1995; Radhakrishna *et al*, 1996). All Arfs and Arls, but not Sar1, are co-translationally myristoylated at the second Gly residue of the N-terminus and this modification is required for membrane binding as well as for biological activity. In contrast to Rab GTPases, ARFs require activation by specific GEFs prior to membrane binding via the myristoyl group and associated N-terminal amphipathic helix (Antonny *et al*, 1997). Activated ARFs recruit cargo sorting proteins, coat proteins, lipid-modifying enzymes and other effector molecules that affect cargo packaging and coated vesicle maturation (Gillingham & Munro, 2007). For example, GTP-bound ARF1 interacts with cytosolic β-COP and ε-COP subunits and recruits them to the Golgi complex promoting cargo sorting into and formation of COPI-coated carriers (Lippincott-Schwartz *et al*, 1998; Zhao *et al*, 1997; Zhao *et al*, 1999). It has been shown that ARF1 binds to membrin, a mammalian ER-Golgi SNARE located on COPI-coated vesicles (Honda *et al*, 2005). Moreover, ARF1 also interacts with GS15 and YKT6 SNAREs involved in retrograde membrane trafficking (Lee *et al*, 2005), suggesting that interplays between the GTPase and tethering factors might function on ARF1 targeting to Golgi complex and on vesicle tethering at Golgi. ARF1 also regulates the formation of CCV at the TGN and endosomal compartments through the recruitment of AP-1, AP-3 and AP-4 complexes (Boehm *et al*, 2001; Ooi *et al*, 1998; Stamnes & Rothman, 1993), as well as Golgi-localized γ-ear-containing ARF-binding (GGA) proteins (Shiba *et al*, 2003). These

examples illustrate that ARF1 is an important regulator of both anterograde and retrograde cargo trafficking.

As mentioned previously, ARF6 GTPase plays a distinct role in endocytic membrane trafficking. ARF6 has been shown to recruit and activate type I phosphatidylinositol-4-phosphate 5-kinase (PIP5K) (Krauss *et al*, 2003), leading to increased levels of phosphatidylinositol 4,5-biphosphate ($PI(4,5)P_2$) at the cell periphery. It is well known that $PI(4,5)P_2$ regulates clathrin-mediated endocytosis (Haucke, 2005; Wenk & De Camilli, 2004) and cooperates with ARF6 to translocate AP-2 complex to the membrane (Paleotti *et al*, 2005), pointing towards a major role for ARF6 in AP-2/clathrin coat assembly. Moreover, $PI(4,5)P_2$ regulates actin polymerization (Miki *et al*, 1996), mediating ARF6 function in the cytoskeleton remodelling. ARF6 also participates in at least one clathrin-independent pathway responsible for the endocytosis of cargoes including IL2Rβ, CD59, MHC class I and carboxypeptidase E (Arnaoutova *et al*, 2003; Donaldson, 2003)

3.7.2. Rab GTPases

Rabs are compartment-specific GTPases that play a crucial role in regulating each of the five major steps in membrane trafficking: vesicle budding, uncoating, delivery to their destination compartment, tethering and fusion with the target membrane (**Fig. I.5**). Rab GTPases constitute the largest family of the Ras superfamily with 11 genes identified in yeast and almost 70 in humans (Pereira-Leal & Seabra, 2001). While some of the Rabs are tissue-specific, many are ubiquitously expressed (Miaczynska & Zerial, 2002 and references therein). Rab proteins are reversibly associated with the surfaces of distinct membranous compartments by hydrophobic geranylgeranyl groups that are attached to one or, in most cases, two Cys residues in CAAX box at the C-terminus (Andres *et al*, 1993; Desnoyers *et al*, 1996). Following prenylation, GDI binds modified Rabs and assists their targeting to the relevant membranous compartments. Additionally, GDI can act as a Rab recycling factor. If the Rab fails to encounter its effectors or after the delivery of vesicle to its destination, GDI can detach GTPase from the membrane and deliver it to another compartment; here the Rab-GDI complex is recognized and dissociated by membrane-associated GDI displacement factors (GDFs). Although Rab targeting to the membrane is not yet fully understood, GDFs have been proposed to be at the apex of a hierarchy that defines membrane identity through the recruitment of specific Rab-GDI (Sivars *et al*, 2003; Soldati *et al*, 1994; Ullrich *et al*, 1994) (**Fig. I.5**).

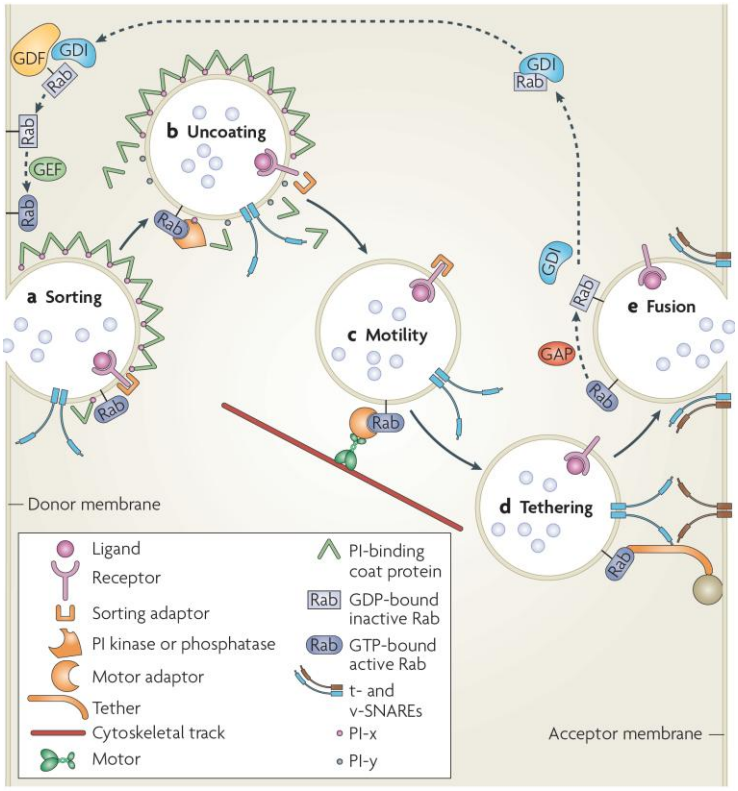

Fig. I.5: Functions of Rab GTPases in membrane trafficking. (a) An active GTP-bound Rab activates a sorting adaptor to sort a cargo into a vesicle, which is subsequently coated with cargo-specific coat complexes. **(b)** Rabs recruit phosphoinositide (PI) kinases or phosphatases that may alter PI compositions and thereby lead to vesicle uncoating. **(c)** Rabs mediate vesicle transport along actin- or microtubule-based cytoskeletal structures by interacting with motor adaptors, such as RAB11FIP2, or by binding directly to motors, such as kinesin KIF20A. **(d)** Rabs control vesicle tethering by recruiting tethering factors, such as SNAREs, which induce vesicle fusion with the target membrane. **(e)** Following membrane fusion and cargo release, Rabs are converted into the inactive state through hydrolysis of GTP and, in complex with GDI, recycled back to the donor membrane, where they can be reactivated by specific GEFs for another cycle of vesicle transport. Adapted from (Stenmark, 2009).

Once inserted into the membrane, Rabs are activated by specific GEFs. Following activation, Rabs recruit or activate distinct sets of effector proteins, including cargo sorting adaptors, kinases, phosphatases, motor proteins or their adaptors and tethering factors (**Fig. I.5**). The best example of Rabs involved in cargo selection and vesicle formation process is RAB9, which regulates membrane trafficking between late endosomes and the TGN (Lombardi *et al*, 1993). Diaz and Pfeffer identified TIP47 protein that binds to the cytoplasmic tail of mannose-6-phosphate receptors (M6PRs) and is required for their recycling from late endosomes back to the Golgi (Diaz & Pfeffer, 1998). TIP47 also binds RAB9 and this interaction increases the affinity

of TIP47 for M6PRs, which leads to enrichment of the M6PRs within the budding vesicle (Carroll *et al*, 2001). In contrast to previously described ARF6-mediated clathrin coat formation on budding vesicle, RAB5 regulates clathrin-coated vesicle uncoating after fission from the donor membrane. Uncoating can be activated in two ways: (i) RAB5 induces displacement of μ2 kinase from AP-2 and (ii) RAB5 accelerates $PI(4,5)P_2$ turnover through the recruitment of effectors such as PI phosphatases (Semerdjieva *et al*, 2008; Shin *et al*, 2005). Rabs also recruit effector proteins that are necessary for vesicle transport along actin- or microtubule-based cytoskeletal structures (**Fig. I.5**). For example, RAB11 efector RAB11FIP2 acts as adaptor for RAB11-positive recycling endosomes to bind myosin Vb motor (Hales *et al*, 2002). Some kinesins can directly interact with active Rabs; for instance, KIF20A binds to the Golgi-localized RAB6 (Echard *et al*, 1998). Several examples of Rab functions in vesicle tethering are described in the following section. The exact role of Rabs in vesicular carrier fusion with the target membrane is less understood; however, it is known that Rab-effector complexes interact with SNAREs and might affect their activity membrane fusion (Collins *et al*, 2005; Subramanian *et al*, 2004).

After delivery of the cargo-loaded vesicle to the acceptor membrane, Rab is deactivated through GTP hydrolysis to GDP, which is not only accomplished by the intrinsic GTPase activity of the Rab, but also accelerated by GAPs (Bernards, 2003). More than 40 different GAPs are present in humans and mice. Most of them share a conserved TBC1 (Tre-2/Cdc16/Bub2) domain (Fukuda, 2011; Strom *et al*, 1993). Importantly, GEFs and GAPs as well as Rab effectors are thought to restrict either spatial or temporal activity of Rabs and thereby, in combination with GDFs, they might assist in establishing Rab-specific compartment identity (Pfeffer, 2005; Rink *et al*, 2005). This compartment identity is an essential prerequisite to ensure the fidelity of the entire membrane trafficking system.

3.7.3. Tethering factors and SNAREs

One of the fundamental issues in vesicular transport is how a given cargo carrier is able to bind and fuse to its specific acceptor membrane. Eukaryotic cells have developed an elaborate system that involves Rab GTPases, tethering factors and SNAREs. While GTP-bound Rabs activate tethering factors that are required for the initial vesicle binding, the subsequent membrane fusion is determined by membrane-embedded SNARE proteins. Tethers are thought to bridge membranes binding both to Rabs and SNAREs, and thus prepare membranes for fusion. In contrast to highly conserved SNAREs, tethering factors are much more conserved and are

divided into two broad groups: coiled-coil filamentous tethering proteins and multisubunit tethering complexes (MTCs). Coiled-coil tethers form long, rod-like complexes spanning up to 200nm distances and bridging vesicle and target membranes. Most of the tethers belonging to the first group are integral membrane proteins of Golgi complex and, therefore, are termed golgins. One of the best-studied golgins is p115. It is important for the clustering of COPII-coated vesicles as well as the docking of COPI- and COPII-coated carriers to the *cis*-Golgi network (Moyer *et al*, 2001; Weide *et al*, 2001). In order to perform these functions, p115 interacts with a number of Golgi SNAREs, including syntaxin-5, membrin, GOS-28 and BET1 (Shorter *et al*, 2002), and other golgins, such as GM130 and giantin (Nakamura *et al*, 1997b; Nelson *et al*, 1998). Apart from being predominantly located at the cis-Golgi, p115 is also recruited to COPII vesicles by GTP-bound RAB1 (Allan *et al*, 2000). The functional relevance of p115 in biosynthetic membrane trafficking is exemplified by the finding that siRNA-based RNAi of p115 leads to Golgi complex fragmentation and blocks VSV-G transport to the plasma membrane (Puthenveedu & Linstedt, 2004). Another well-characterized coiled-coil tether early endosomal antigen 1 (EEA1) is recruited by active RAB5 and together with SNAREs, such as syntaxin-13, participates in homotypic fusion of early endosomes (Christoforidis *et al*, 1999; McBride *et al*, 1999).

Currently, there are at least nine different MTCs that act throughout the membrane trafficking system and at the plasma membrane in eukaryotic cells (Brocker *et al*, 2010). Similarly to coiled-coil tethering factors, MTCs bridge the recognition of vesicles via specific Rabs and SNARE-mediated membrane fusion processes. The Dsl1p MTC is located at the ER and regulates retrograde Golgi-ER transport by tethering COPI-coated vesicles (Andag *et al*, 2001). The COG complex is responsible for COPI-mediated intra-Golgi transport and maintenance of Golgi structure (Oka *et al*, 2004; Ungar *et al*, 2002). The TGN-associated GARP complex cooperates with RAB6 in tethering vesicles derived from both early and late endosomes to the TGN (Siniossoglou & Pelham, 2001). Secretory cargo-loaded vesicles are tethered to the plasma membrane by the octameric exocyst complex (Wiederkehr *et al*, 2004). Two MTCs operate sequentially between endosomes and lysosomes. The CORVET is required for tethering of TGN-derived vesicles to endosomes and one of the complex subunits (Vps8) interacts with RAB5 as its effector (Chen & Stevens, 1996; Markgraf *et al*, 2009). Vps39 subunit of the HOPS complex has been proposed to act as GEF for RAB7 during early-to-late endosome maturation (Rink *et al*, 2005), however, this model was disproved by recent findings that RAB7 is activated by the RAB5-recruited SAND-1-CCZ-1 complex (Kinchen & Ravichandran, 2010; Poteryaev *et*

al, 2010). Nevertheless, the HOPS complex is implicated in several fusion events at the late endosome and the vacuole, including the fusion of multivesicular bodies, Golgi-derived AP-3-positive vesicles and the homotypic fusion of vacuoles (Nakamura *et al*, 1997a). The TRAPP is found in three forms (I, II, III) and has been described as a multisubunit GEF for yeast Rabs Ypt1 (a homolog of human RAB1 GTPases) and Ypt31/32. (Jones *et al*, 2000). Apart from acting as GEFs, TRAPP complexes also promote vesicle tethering. The best example is the TRAPPI complex, which tethers ER-derived vesicles to the cis-Golgi by binding to COPII coat subunit Sec23 (Cai *et al*, 2007). Due to their oligomeric composition of different proteins (3 – 10 subunits), MTCs, in particular TRAPPI-III, can carry out additional regulatory functions at different organelles (Brocker *et al*, 2010).

The final step of vesicle trafficking is its fusion with the acceptor membrane driven by SNARE proteins. There are 36 SNAREs identified in humans. SNAREs are functionally classified into v- and t-SNAREs, because they reside on opposing membrane, usually on a transport vesicle and a target membrane, respectively (Jahn & Scheller, 2006). t-SNAREs form oligomeric complexes to acquire specificity for different v-SNAREs (Parlati *et al*, 2002). Following tethering, SNAREs from opposing membranes generates *trans*-SNARE complexes or SNAREpins, which bring two bilayers into close proximity and induce membrane fusion (Weber *et al*, 1998). A functional t-SNARE complex provides the template for v-SNARE binding and is a prerequisite for SNAREpin assembly. The assembly of SNAREpin is also regulated by so-called SM (Sec1/Munc1) proteins. SM proteins directly interact with v- and t-SNARE complexes at different transport steps and thereby stimulate specific membrane fusion and confer additional specificity to membrane trafficking (Peng & Gallwitz, 2002; Shen *et al*, 2007). Moreover, distinct SM proteins can augment the SNAREpin-mediated membrane fusion process (Scott *et al*, 2004). After fusion, the *trans*-SNARE complexes are often referred to as *cis*-SNARE pairs because they reside in a single lipid bilayer (Jahn & Scheller, 2006). The *cis*-SNARES are dissociated and recycled to different membranous compartments by cytosolic SNAP and NSF proteins for another round of cargo transport (Block *et al*, 1988).

Membrane trafficking is a highly coordinated multistep process involving the formation of vesicular carriers loaded with defined sets of cargo, their transport between compartments and the fusion with the target membranes. The fidelity of membrane trafficking relies on an array of regulatory proteins and on their interactions with effector molecules. Despite the fact that different groups of regulatory proteins can regulate the same steps of membrane traffic, their

successive roles in this process can be discerned. While Arf GTPases are the central regulators of vesicle biogenesis, Rab GTPases play crucial roles in defining membrane identity, which is essential for specific cargo selection, vesicle transport and targeting to the correct cellular compartment. Finally, tethering factors and SNAREs are responsible for vesicular carrier docking to and fusion with the specific target membranes. Recent recognition of miRNAs as important regulators of virtually all investigated physiological and pathological processes suggests that these RNA molecules can potentially constitute the additional level of membrane trafficking regulation. Indeed, this notion has been supported by recent finding that *miR-92a* regulates the expression of RAB14, which is involved in surfactant secretion in lung cells (Gou *et al*, 2008; Kanzaki *et al*, 2011).

4. OBJECTIVES

The overall goal of this study was to identify miRNAs and their biologically relevant target genes involved in the regulation of membrane trafficking. Considering the evidence to date, miRNAs seem to be responsible for fine regulation of numerous target genes. We envisage that miRNAs act as novel adaptive regulators of membrane trafficking, providing robustness to this complex cellular process. Previous studies have analyzed a few miRNAs involved in insulin secretion, however, no systematic investigation of miRNAs as regulators of membrane trafficking has been performed.

For this reason, the following aims of this study were proposed:

1. To apply quantitative approaches for detection of miRNA-mediated changes in biosynthetic trafficking and endocytosis;
2. To identify miRNAs involved in the regulation of membrane trafficking;
3. To identify and validate novel functionally relevant targets that exert miRNA-mediated regulation of membrane trafficking.

To implement proposed aims, the following approaches were applied:

Aim 1. miRNA-mediated changes in biosynthetic trafficking efficiency were evaluated using a fluorescence intensity-based ts-O45-G protein transport assay. A quantitative fluorescence intensity-based DiI-LDL internalization assay was applied for quantification of endocytosis efficiency. Synthetic miRNA mimics (pre-miRs) and miRNA inhibitors were used to modulate the activity of endogenous miRNAs.

Aim 2. In order to identify miRNAs involved in the regulation of biosynthetic cargo trafficking, large-scale functional screening of Pre-miR^{TM} miRNA Precursor Library was performed. Hit miRNAs were confirmed in small-scale ts-O45-G transport assay and further investigated for their effects on the Golgi complex integrity.

Aim 3. In order to identify membrane trafficking-related miRNA targets, genome-wide mRNA expression profiling in combination with bioinformatics analysis was conducted. Functional relevance of potential targets was confirmed by siRNA-based RNAi. Novel miRNA targets were validated by luciferase reporter assay, qRT-PCR and western blot approaches.

5. MATERIALS AND METHODS

5.1. Materials

5.1.1. siRNAs, miRNAs and miRNA library

siRNAs targeting human *α-COP* (SI00351491 and SI04157419), *TBC1D2* (SI02807518 and SI04239494), *ASAP2* (SI00360619 and SI04151784), *M6PR* (SI00626052 and SI03069920), *LDLR* (SI00011186 and SI03024525) and non-silencing control siRNA "All Stars" (SI03650318) were purchased from Qiagen. Cy3-labeled siRNA targeting *INCENP* (28431) was purchased from Ambion.

Synthetic double-stranded RNA molecules mimicking human endogenous miRNAs (pre-miRs) and single-stranded inhibitors for endogenous miRNAs (anti-miRs) were purchased from Ambion; *miR-17* (products PM12412 and AM12412), *miR-18a* (PM12973 and AM12973), *miR-19a* (PM10649 and AM10649), *miR-20a* (PM10057 and AM10057), *miR-20b* (PM10975 and AM10975), *miR-92a* (PM10916 and AM10916), *miR-93* (PM10951 and AM10951), *miR-320a* (PM11621 and AM11621) and negative control pre-miR (PNC) and anti-miR (ANC) (AM17120 and AM17011). Synthetic DNA/LNA anti-miR for *miR-20b* (410133-00) and DNA/LNA anti-miR negative control (199004-00) were from Exiqon. miRZip-20b expression plasmid (MZIP20b-PA-1) and plasmid expressing control miRZIP (MZIP000-PA-1) were purchased from System Biosciences. Large-scale pre-miR library (Pre-miR^{TM} miRNA Precursor Library – Human v3, 4385830) of 470 human miRNAs based on Sanger miRBase v9.2 was purchased from Ambion. List of the miRNAs included in the library is in **Appendix I**.

5.1.2. Luciferase reporter plasmids

A panel of dual-luciferase reporter plasmids was prepared and used in this project to measure human miRNA activity and miRNA regulatory effect on target gene expression:

1. psiCheck^{TM}-2-miR-17
2. psiCheck^{TM}-2-miR-20a
3. psiCheck^{TM}-2-miR-92a
4. psiCheck^{TM}-2-miR-320a

5. psiCheck™-2-TBC1D2-3´UTR

6. psiCheck™-2-TBC1D2-3´UTR-mut

7. psiCheck™-2-TBC1D2-3´UTR-mut

8. psiCheck™-2-LDLR-3´UTR

A luciferase reporter vector psiCheck™-2 (Promega, a generous gift from Dr. D. Grimm, BioQuant, University of Heidelberg) was used to generate dual-luciferase reporters. In order to measure the activity of miRNAs, DNA fragments encoding single completely complementary miRNA-binding site for specific miRNAs were cloned into XhoI- and NotI-digested psiCheck™-2 vector immediately downstream of the top codon of *Renilla* luciferase gene (no.1 throught no.4 plasmids). The DNA fragments were obtained by annealing two synthetic oligonucleotides. The sequences of oligonucleotides used to generate human miRNA-specific reporters are as follows:

1. For *miR-17* binding site in psiCheck™-2-miR-17 plasmid:
   FWD 5′-TCGAGCTACCTGCACTGTAAGCACTTTGTCTAGAGC-3′
   REV 5′-GGCCGCTCTAGACAAAGTGCTTACAGTGCAGGTAGC-3′

2. For *miR-20a* binding site in psiCheck™-2-miR-20a plasmid:
   FWD 5′-TCGAGCTACCTGCACTATAAGCACTTTATCTAGAGC-3′
   REV 5′-GGCCGCTCTAGATAAAGTGCTTATAGTGCAGGTAGC-3′

3. For *miR-92a* in psiCheck™-2-miR-92a plasmid:
   FWD 5′-TCGAGACAGGCCGGGACAAGTGCAATATCTAGAGC-3′
   REV 5′-GGCCGCTCTAGATATTGCACTTGTCCCGGCCTGTC-3′

4. For *miR-320a* in psiCheck™-2-miR-320a plasmid:
   FWD 5′-TCGAGTCGCCCTCTCAACCCAGCTTTTTCTAGAGC-3′
   REV 5′-GGCCGCTCTAGAAAAAGCTGGGTTGAGAGGGCGAC-3′

For plasmids to measure *miR-17* regulatory effect on target gene expression, the 352-bp and 2534-bp full-length *TBC1D2* and *LDLR* 3´UTRs, respectively, were PCR-amplified from the genomic DNA of HeLa cells. The primer sequences used for PCR are as follows:

5. For *TBC1D2*-3´UTR:
FWD 5′-ATACTCGAGCTTGGCCACCTCCCCTCCCCAC-3′
REV 5′-ATAGCGGCCGCTGAATGATTTCCACCATTTACA-3′

6. For *LDLR*-3´UTR:
FWD 5′-ATACTCGAGACATCTGCCTGGAGTCCCGTCC-3′
REV 5′-GCGGCGGCCGCTTTAGACAAATTGGTTCATTTA-3′

PCR products were cleaved with XhoI and NotI restriction endonucleases and cloned into XhoI- and NotI-digested psiCheck™-2 vector immediately downstream of the top codon of *Renilla* luciferase gene. The resulting plasmids were entitled psiCheck-2-TBC1D2-3´UTR and psiCheck-2-LDLR-3´UTR. To mutate or delete a predicted *miR-17* binding site in the 3´UTR of *TBC1D2* mRNA, psiCheck-2-TBC1D2-3´UTR was used as a template plasmid for Phusion site-directed mutagenesis kit (Finnzymes). The following 5´-phosphorylated primers were used:

7. For psiCheck™-2-TBC1D2-3´UTR-mut:
FWD 5′-Pho-CCTCTTCCACAGTCGTGAAACGCATGTAAACAA-3′
REV 5′-Pho-TGACGAAAGGGTGGCATCCCTGGGTAAGTA-3′

8. For psiCheck™-2-TBC1D2-3´UTR-mut:
FWD 5′-Pho-GCATGTAAACAAGCAAGAGCACTGC-3′
REV 5′-Pho-GACGAAAGGGTGGCATCCCTGGGTA-3′

5.1.3 Antibodies and other reagents

The mouse monoclonal anti-ts-O45-G antibody recognizing the extracellular epitope of ts-O45-G protein was a generous gift from Prof. M.D. K. Simons (MPI-CBG, Germany). Polyclonal rabbit anti-TBC1D2 antibody was a kind gift from Dr. V. Braga (Imperial College London, UK). Polyclonal rabbit anti-LDLR antibody was purchased from Cayman Chemicals. Monoclonal mouse anti-GM130 (clone 35/GM130) was purchased from BD Transduction Laboratories. Alexa647 conjugate of lectin Concanavalin A was from Invitrogen. Secondary anti-mouse and anti-rabbit IgG HRP-conjugated antibodies were purchased from R&D Systems. Secondary goat Alexa647/Cy3-conjugated anti-mouse IgG antibody was purchased from Invitrogen. Transfection reagent Lipofectamine™ 2000 was purchased from Invitrogen.

qRT-PCR TaqMan® miRNA expression assays (ID 002308 for *miR-17*, ID 000580 for *miR-20a*, ID 000430 for *miR-92a*, ID 002277 for *miR-320a* and ID 001093 for endogenous control small nuclear *RNU6B* RNA) were purchased from Applied Biosystems. qRT-PCR TaqMan® mRNA expression assays (ID Hs00917985_m1 for *TBC1D2*, ID Hs00181192_m1 for *LDLR* and ID Hs99999905_m1 for endogenous control *GAPDH* mRNAs) were also purchased from Applied Biosystems. Dil-LDL was purchased from Invitrogen.

5.2. Methods

5.2.1. Cell culture and media

Human epithelial carcinoma cells (HeLa) and HIV-infectible HeLa-CD4 (Clavel & Charneau, 1994) cells were cultured in Growth Medium (GM) consisting of Dulbecco's Modified Eagle Medium (DMEM, Invitrogen) supplemented with 10% (v/v) fetal calf serum (PAA Laboratories), 2mM L-glutamine (Invitrogen), 50µg/ml streptomycin and 50U/ml penicillin (Invitrogen). HeLa and HeLa-CD4 cells were cultured in 10cm culture dishes and split on a regular basis every three days to maintain optimal growth conditions. For splitting, cells were washed with pre-warmed phosphate-buffered saline (PBS) solution to remove traces of GM and incubated in 1ml 0.25% trypsin-EDTA (Invitrogen) solution for 5min at 37°C. Cells were then resuspended in fresh GM and 1/8 part of cell suspension plated in culture dishes. Unless otherwise indicated, cells were maintained at 37°C in a humidified atmosphere with 5% CO_2.

Starvation Medium (SM) consisting of DMEM supplemented with 2mM L-glutamine, 50µg/ml streptomycin and 50U/ml penicillin and Imaging Medium (IM, pH 7.4) consisting of Modified Eagle Medium without phenol red (MEM, Invitrogen) supplemented with 30mM HEPES and 0.5g/l sodium bicarbonate were used for DiI-LDL internalization experiments. Transfection Medium (TM) consisting of DMEM supplemented with 10% (v/v) fetal calf serum and 2mM L-glutamine was used for tranfection with pre-miRs, anti-miRs and siRNAs.

5.2.2 Transfection with pre-miRs, anti-miRs and siRNAs

Transfection of HeLa cells with pre-miRs, anti-miRs or siRNAs was performed either by means of the liquid-phase direct transfection or solid-phase reverse transfection. For both types of transfection, the Lipofectamine™ 2000 was used as transfection reagent. While all small-scale experiments described in this work were based on liquid-phase transfection, a large-scale screening of a human pre-miR library was performed by using reverse transfection approach described elsewhere (Erfle *et al*, 2007; Erfle *et al*, 2008). For reverse transfection, 5µl of the respective pre-miR or siRNA 30µM stock solution was mixed with 4.75µl OptiMEM I + GlutaMAX I (Invitrogen)/0.4M sucrose (USB) solution and 1.75µl Lipofectamine™ 2000. This mixture was incubated for 30min at room temperature. Next, 7.25µl of a 0.08% (w/v) gelatin

(Sigma-Aldrich) solution containing 3.5 x 10^{-4}% (v/v) human fibronectin (Sigma-Aldrich) was added reaching a total volume of 18.75µl. Finally, transfection solution was diluted in 450µl of MilliQ water and 25µl of this solution was transferred into each well of 96-well µ-plates (Ibidi). The plates were dried for 2.5h in the Speed Vac. In this way, a pre-miR library of 470 pre-miRs was distributed over 10 different layouts of 96-well µ-plates replicated 18 times, with a final amount of 8pmol of respective pre-miR or siRNA per well. Three wells containing siRNA against human *α-COP* were distributed over each layout and used as positive control for reverse transfection efficiency. Additionally, five wells with PNC were distributed over each layout and used as negative control in ts-O45-G-based library screening.

In case of liquid-phase transfection with pre-miRs, anti-miRs and siRNAs, Lipofectamine™ 2000 was used according to the manufacture's instructions. The solutions of respective oligonucleotide/OptiMEM I + GlutaMAX I/Lipofectamine 2000 were applied to cells growing in TM. Unless otherwise indicated, pre-miRs, anti-miRs and siRNAs were transfected at final concentration of 50nM.

5.2.3. Total DNA and RNA isolation

Total DNA from HeLa cell culture was purified by DNeasy® Blood & Tissue Kit (Qiagen) according to the manufacturer's recommendations.

Total RNA was isolated using *mir*Vana™ miRNA Isolation Kit (Ambion) according to the manufacturer's instructions. The kit is designed to purify total RNA including very small RNA species, such as miRNAs. Briefly, HeLa cells were washed 2 – 3 times with ice-cold PBS and lysed in Lysis/Binding Solution. Lysates were collected, mixed with 1/10 volume of miRNA Homogenate Additive and incubated for 10min on ice. Next, the equal volume of acid phenol:chloroform solution was added to lysates, followed by centrifugation for 5 min at maximum speed. The upper aqueous phase was collected and mixed with 1.25 volumes of 100% ethanol. The lysate/ethanol mixtures were filtered through Filter Cartridge by centrifugation, followed by one washing step with miRNA Wash Solution 1 and two washing steps with Wash Solution 2/3. The Filter Cartridges were transferred into fresh collection tubes and total RNA recovered in 100µL of pre-heated (95°C) nuclease-free water.

All buffers, washing solutions and filter cartridges required for total DNA and RNA extraction were provided in isolation kits.

5.2.4. Biosynthetic ts-O45-G trafficking assay

To evaluate effects of miRNAs on the biosynthetic trafficking, well-described ts-O45-G transport assay (Starkuviene & Pepperkok, 2007) was applied. In order to screen pre-miR library of 470 miRNAs, 5.5 x 10^3 of actively growing HeLa cells in 250µl/TM were plated into prepared 96-well µ-plates with pre-miRs. For small-scale assays, cells were seeded on 8-well µ-slides (7 x 10^3/well) and transfected either with pre-miRs or anti-miRs or respective control oligonucleotides at a final concentration of 50nM on the next day. Next, cells were incubated with recombinant adenovirus encoding ts-O45-G-YFP (hereafter, ts-O45-G) 42h after transfection. After 45min incubation at 37°C, cells were washed and incubated for 6h at 39.5°C in a humidified atmosphere with 5% CO_2. The synchronized release of ts-O45-G from ER was achieved by moving cells to a permissive temperature, 32°C, in the presence of 100µg/ml cycloheximide (Sigma-Aldrich). One hour later, cells were fixed with 3% paraformaldehyde and plasma membrane-traversed ts-O45-G was immunostained with a primary mouse anti-ts-O45-G antibody, followed by immunostaining with a secondary Alexa647-conjugated goat anti-mouse IgG antibody. Nuclei were stained with 0.3µg/ml Hoechst 33342. Images were acquired by Scanˆ R Acquisition module (Olympus) on IX81 motorized inverted fluorescence microscope (Olympus) using 10x UplanSApo objective (NA 0.4); 20 images/well or 36 images/well were acquired from 96-well µ-plates or 8-well µ-slides, respectively. The total fluorescence intensity of single cell-associated plasma membrane (PM)-incorporated fraction of ts-O45-G (Alexa647 channel) and the total fluorescence intensity of expressed ts-O45-G (YFP channel) were measured by means of the image analysis software Scanˆ R Analysis module (Olympus), and extracted data were further analyzed as described in "Statistical data analysis".

Depending on the experimental format, 7 500 – 10 000 cells were analyzed for each transfected RNA molecule.

5.2.5. DiI-LDL internalization assay

For analysis of cellular uptake of fluorescently labeled low-density lipoprotein (3,3'-dioctadecylindocarboncyanine-labelled LDL, DiI-LDL, Invitrogen), HeLa cells were seeded on 8-well µ-slides (Ibidi) in GM (1x10^4 cells/well). The next day, cells were transfected with pre-miRs or anti-miRs, or siRNAs at a final concentration of 50nM. Transfected cells were cultured in GM for 24h and medium was then exchanged for SM supplemented with 0.2% (w/v) bovine

serum albumin (BSA) for additional 24h. DiI-LDL internalization assay was carried out as described elsewhere (Gilbert *et al*, 2009). Briefly, 48h after transfection, cells were exposed for 45min at 37°C to 10mg/ml 2-hydroxy-β-cyclodextrin (HPCD, Sigma-Aldrich) and 0.2% (w/v) BSA added to SM, followed by washing with ice-cold IM supplemented with 0.2% (w/v) BSA. Next, cells were labeled with 50µg/ml Dil-LDL for 30min at 4°C and Dil-LDL internalization was stimulated for 20min at 37°C. Cells were washed with ice-cold acidic IM (pH 3.5) for 1min in order to strip off residual DiI-LDL on plasma membrane. Cells were fixed in 3% paraformaldehyde for 20min on ice. Nuclei were stained with 0.3µg/ml Hoechst 33342 and 49 images/well were acquired as described in "Biosynthetic ts-O45-G trafficking assay". The total fluorescence intensity of single cell-associated DiI-LDL was measured by means of the image analysis software Scanˆ R Analysis module (Olympus), and extracted data were further analyzed as described in "Statistical data analysis". On average, 8 700 cells were analyzed for each transfected RNA molecule.

5.2.6. Dual-luciferase reporter assay

The day before transfection, Hela cells were seeded into 24-well plates (4 x 10^4 cells/well). The next day, cells were co-transfected with 10ng of the respective luciferase reporter vector and either with pre-miRs or anti-miRs at a final concentration of 50nM. Dual-luciferase reporter assay (Promega) was performed 24h after transfection following the manufacturer's protocol with minor changes. Briefly, before lysis, cells were washed once with ice-cold PBS and 100µl of 1x Passive Lysis Buffer was applied per well. The plates were mounted on a rocking platform for 15min rocking at room temperature to complete cell lysis. Later, lysates were collected and stored at -20°C. Before luciferase activity measurement, lysates were thawed on ice, centrifuged briefly to pellet cell debris and 5µl of lysates were transferred into a white 96-well plate (Greiner Bio-One). The read-out of luminescence signal was performed with a Glomax 96-microplate luminometer (Promega) equipped with two injectors and primed with LARII and Stop&Glo® reagents. The activity of firefly luciferase was initiated by automatically injecting 25µl of LARII and luminescence acquired for 10s. After, the luminescence of firely luciferase was quenched by injecting 25µl of Stop&Glo® reagent, which also initiated *Renilla* luciferase activity. Luminescence of *Renilla* luciferase was measured for another 10s. Luminescence intensity of *Renilla* luciferase depends on the protein expression level, which is regulated by intracellular miRNAs. In order to determine the effect of miRNAs on reporter protein expression,

luminescence intensity of *Renilla* luciferase was normalized to the intensity of firefly luciferase used as internal transfection control.

5.2.7. qRT-PCR mRNA and miRNA expression assays

qRT-PCR TaqMan® miRNA expression assays specific for each miRNA of interest were performed as previously described (Chen *et al*, 2005). Briefly, Hela cells were seeded in 24-well plates. The next day cells were transfected with either pre-miRs or anti-miRs at a final concentration of 50nM, or mock-transfected (only Lipofectamine 2000). Total RNA was isolated 24h, 48h and 72h after transfection. TaqMan® miRNA assays were used to reverse transcribe 15ng of total RNA. Each 15µl reverse transcription reaction mix contained 50nM miRNA-specific stem-loop Reverse Transcription primer, 100 mM dNTPs, 1x Reverse Transcription buffer, 0.25 U/µl RNase Inhibitor and 3.33 U/µl of MultiScribe™ Reverse Transcriptase and nuclease-free water. The reaction mixes were kept on ice for 5 min, then incubated in the MJ Mini thermocycler (Bio-Rad) at 16°C for 30 min, at 42°C for 30 min, at 85°C for 5 min and finally were held at 4°C. qRT-PCR reactions were carried out in 96-well ABgene® PCR Plates (Thermo Fisher Scientific) using the Real Time PCR 7500 system (Applied Biosystems). Each 20µl reaction mix contained 1.33 µl of cDNA beforehand diluted 1:10, 1x TaqMan® Universal Master Mix, 1 µl of TaqMan® miRNA assay mix containing TaqMan® primer, forward and reverse primers and nuclease-free water. The $2^{-\Delta\Delta CT}$ method for miRNA expression quantification was applied as described elsewhere (Livak & Schmittgen, 2001) using expression level of *RNU6B* RNA as a reference for normalization.

For qRT-PCR of *TBC1D2* and *LDLR* mRNAs, HeLa cells were transfected with pre-miR-17, siRNAs targeting *TBC1D2* and *LDLR*, or with respective controls at final concentration of 50nM in 24-well plates. Total RNA was extracted at 12h, 24h and 48h after transfection. Total RNA (500ng) was reverse transcribed to cDNA using TaqMan® Reverse Transcription Reagents (Applied Biosystems) with random hexamers. The qRT-PCR of *TBC1D2* and *LDLR* mRNAs was carried out in the Applied Biosystems StepOnePlus Real-Time PCR system (Applied Biosystems) using 65ng of cDNAs with the respective TaqMan® mRNA assay in accordance with the manufacturer's protocol. Relative expression level of *TBC1D2* and *LDLR* mRNAs was calculated by applying $2^{-\Delta\Delta CT}$ method and using expression level of *GAPDH* mRNA as a reference for normalization.

Expression profiling experiments for each miRNA and mRNA were performed with two-three biological samples, two replicates of reverse transcription reaction per sample and two replicates of real-time PCR per reverse transcription reaction.

5.2.8. Western blotting

For human TBC1D2 and LDLR western blot analysis, HeLa cells were transfected with pre-miR-17, siRNAs against *TBC1D2* or *LDLR* and appropriate negative controls in 24-well plates. Forty-eight hours post-transfection, cells for TBC1D2 protein analysis were lysed in 30µl of pre-heated (95°C) Laemmli lysis buffer (Laemmli, 1970) supplemented with 10mM DTT and proteins separated on 8% SDS-PAGE gels. Cells for LDLR protein analysis were lysed in 100µl lysis buffer (2.9% glycerol, 0.66mM DTT, 1% SDS, 20.8mM Tris-HCl, pH6.8, 1mM PMSF, 0.0025% Bromophenol Blue) and proteins were separated on 7% SDS-PAGE gels. Before electrophoresis, all lysates were treated with benzonase nuclease (Sigma-Aldrich) in order to degrade nucleic acids. Proteins were blotted on PVDF Immobilon-P membranes (Millipore) and non-specific antibody binding was blocked with 5% non-fat milk in TBS buffer. Blots were probed with primary anti-TBC1D2 or anti-LDLR antibodies in TBS-0.1% Tween-20 solution overnight at 4°C to detect TBC1D2 and LDLR proteins, respectively. In order to detect tubulin-α, blots were probed with anti-tubulin antibody in TBS-0.1 % Tween-20 solution for 1h at room temperature. Next, all blots were probed with secondary HRP-conjugated antibodies in TBS-0.1% Tween-20 solution for 1h at room temperature and chemiluminescence signals were detected using the enhanced chemiluminescence (ECL) reagents (GE Healthcare). Protein-specific chemiluminescence signals were acquired by a Chemiluminescence Detection System (Intas) and quantified by means of the ImageJ software (NIH, Abramoff *et al*, 2004). The total chemiluminescence intensity of TBC1D2-specific bands was normalized to the tubulin-α-specific chemiluminescence intensity and the LDLR-specific signal was normalized to the signal of cross-reacting band of the anti-LDLR antibody used (~63kDa).

5.2.9. mRNA microarray analysis

For mRNA expression profiling upon transfection with pre-miR-17, in HeLa-CD4 cells were plated in 24-well plates at a density of 4×10^4 cells/well. The following day, cells were transfected with pre-miR-17 or PNC at a final concentration of 50nM.

For mRNA expression profiling upon transfection with pre-miR-517a, HeLa cells were seeded in 12-well plates at different densities depending on the incubation period: 6 x 10^4 for 12h and 24h, 3 x 10^4 for 48h experiments. The next day, cells were transfected with pre-miR-517a or PNC at a final concentration of 50nM.

Total RNA of two biological replicates of each experimental condition was isolated 12h, 24h and 48h after transfection as described in "Biosynthetic ts-O45-G trafficking assay" and submitted for expression profiling at the Microarray Core Facility at German Cancer Research Center (DKFZ, Heidelberg). Briefly, the quality of total RNA was checked by gel analysis on the Agilent 2100 Bioanalyzer (Agilent Technologies) and estimated by calculating the 28S/18S ratio of ribosomal RNAs by RIN algorithm (Schroeder *et al*, 2006). Only samples with RIN index value greater than 8.5 were selected for further expression profiling. Next, 250ng of total RNA was used for complementary DNA (cDNA) synthesis, followed by an amplification/labeling step (*in vitro* transcription) in order to synthesize biotin-labeled complementary RNA (cRNA) using the MessageAmp II aRNA Amplification kit (Ambion) in accordance with the manufacturer's protocol. The cRNA was column-purified by using the TotalPrep RNA Amplification Kit and quality was controlled using the RNA Nano Chip Assay on Agilent 2100 Bioanalyzer.

Human Sentrix-8 BeadChip® arrays (Illumina) and HumanHT-12 v4 BeadChip® arrays (Illumina) were used for hybridization of biotin-labeled cRNA samples obtained from *miR-17* and *miR-517a* experiments, respectively. Hybridization was carried out in GEX-HCB buffer (Illumina) at a concentration of 100ng cRNA/µl for 20h at 58°C. Spike-in controls for low, medium and highly abundant mRNAs as well as mismatch control and biotinylation control oligonucleotides were added. The arrays were scanned on Beadstation array scanner (Illumina). Data extraction was done for all beads individually. Differentially regulated genes were defined by further analysis as described in "Statistical data analysis".

5.2.10. miRNA microarray analysis

HeLa cells were plated at a density of 4 x 10^4 cells/well in 12-well plates. The cells were treated under three different conditions: (I) cells were incubated for 49h at 37°C in a humidified atmosphere with 5% CO_2; (II) cells were incubated for 42h at 37°C and then moved for another 7h at 39.5°C; (III) cells were incubated for 42h at 37°C, then transduced with recombinant adenoviral vector, which encodes ts-O45-G protein as described in "Biosynthetic ts-O45-G trafficking assay", and incubated for another 6h at 39.5°C. Independently to the type of treatment,

the total RNA was isolated 49h after cell seeding and samples were submitted for miRNA expression profiling at the Genomics Core Facility at European Molecular Biology Laboratory (EMBL, Heidelberg). The total RNA samples were processed and hybridized on the glass slide formatted with 8 high definition human miRNA microarrays (Agilent) following the manufacturer's protocol. Arrays were based on Sanger miRBase v14.0. The steady-state expressed miRNAs in HeLa cells under condition (I) and miRNAs affected by temperature change or viral transduction under conditions (II) and (III), respectively, were defined by further analysis as described in "Statistical data analysis". Due to the limited number of 8 miRNA microarrays per glass slide, four biological replicates of samples treated under condition (I) and two biological replicates of each condition (II) and condition (III) were used for miRNA expression profiling.

5.2.11. Automated classification of nuclei in apoptosis and proliferation assay

Effects of miRNAs on cell proliferation were determined by applying automated image analysis of cell nuclei in collaboration with Dr. Nathalie Harder (Biomedical Computer Vision group, Dr. Karl Rohr). The following steps were used: (i) segmentation of cell nuclei, (ii) gray value normalization, (iii) feature extraction and (iv) nuclei classification. To segment cell nuclei in apoptosis, mitosis, or interphase, a gradient based thresholding approach was extended for the segmentation of cell nuclei as described previously (Matula *et al*, 2009). In this approach, bright sides of edges of all objects were detected by taking connected sets of pixels (connected components) with negative Laplacian that contained pixels with high gradient magnitude. Each connected component was morphologically closed with a small 3x3 pixel structuring element and the holes in the components were filled. In order to correctly segment apoptotic cell nuclei, an additional step was introduced, in which small connected components within a short distance were combined into one component. Each component was treated as a cell nucleus in later steps. Since the images of different experiments had highly differing gray value ranges, normalization of the gray values was performed before feature extraction. For nuclei normalization, characteristics of the gray value distribution of the foreground pixels (histogram of the nuclues pixels), such as the location and the width of the maximum peak, were determined for each experiment. Next, the mean of the extracted histogram characteristics over all experiments and the parameters to transform each individual distribution to this mean distribution was determined. These parameters were used to shift and scale the gray values of all images into a common gray

value range. After normalization, a set of 354 features were extracted for each cell nucleus. The feature set contained features, such as size, shape, mean and standard deviation (SD) of gray values, texture-related features (for example, Haralick texture features and wavelet features) and moment-based features (for example, Zernike moments). Based on the extracted features, cell nuclei were classified into four classes, namely, (i) interphase, (ii) mitosis, (iii) apoptosis and (iv) artefacts (e.g., clusters of nuclei, background artefacts). Weighted support vector machines (SVMs) with a radial basis function kernel were used for classification. Furthermore, for training of the classifier, a set of 577 manually annotated samples were taken from six different experiments. Before applying the classifier to unseen data, the performance of the classifier was tested by using four-fold cross validation on the training set. More details on the feature extraction and classification steps can be found in work of Harder and colleagues (Harder *et al*, 2008). As a final result, the percentage of nuclei per class for each experiment was determined.

5.2.12. Automated quantification of Golgi complex integrity

Effects of miRNAs on the integrity of the Golgi complex were determined by an automated image analysis approach developed in collaboration with Jan-Philip Bergeest (Biomedical Computer Vision group, Dr. Karl Rohr). HeLa cells were transfected with either pre-miRs or siRNA against *α-COP*, or non-targeting siRNA on 8-well µ-slides ($7x10^3$ cells/well) and incubated for 48h. After incubation, cells were fixed with 3% paraformaldehyde, permeabilized with PBS-0.1% Triton X-100 solution. The Golgi complex was immunostained with a primary mouse anti-GM130 antibody, followed by immunostaining with a secondary Cy3-conjugated goat anti-mouse antibody. Additional staining of cellular glycoproteins with an Alexa647-conjugated lectin Concanavalin A (ConA) was used to determine cell regions. Finally, nuclei were stained with 0.3µg/ml Hoechst 33342 and 20 images/well of three fluorescence channels were acquired by Scanˆ R Acquisition module (Olympus) on IX81 motorized inverted fluorescence microscope (Olympus) using 20x UplanSApo objective (NA 0.75). Next, microscopic images were segmented in three steps: (i) segmentation of cell nuclei based on Hoechst 33342 channel, (ii) segmentation of cell regions based on ConA-Alexa647 channel and (iii) Golgi segmentation based on GM130-Cy3 channel. First, in order to segment cell nuclei, an edge-based segmentation approach was used as previously described (Matula *et al*, 2009). Apoptotic cells were identified as decribed above and removed from further analysis. Second, cell regions were segmented on a basis of ConA immunostaining applying a seeded watershed

transform, where the segmented cell nuclei were used as seeds. The resulting watershed basins were referred to as influence zones for each cell nuclei. Then, region growing was performed in each influence zone, starting from the pixels at the edge of cell nucleus. All pixels with intensities within a certain range and with a connection to the edge of nucleus were included as cell region (Matula *et al*, 2009). Third, noise artifacts in images of GM130-Cy3 channel were reduced by applying a morphological top-hat transform (Soille, 2004) and Golgi complex was segmented by using the triangle thresholding approach within each segmented cell region (Zack *et al*, 1977). Each resulting connected region was considered as a separate Golgi fragment. Next, the Golgi complex was quantified in terms of (i) number of Golgi fragments, (ii) size of fragments, (iii) distance between the Golgi fragment center and the center of the nucleus and (iv) immunofluorescence intensity of GM130 protein. The maximum distance of Golgi fragment from the nucleus was considered as the distance between the center of the outermost Golgi fragment and the center of nucleus in each cell. The average fluorescence intensity of GM130 protein was calculated as ratio of the total GM130 fluorescence intensity to the total size (pixels) of Golgi complex in each cell. All features were extracted on a cell-by-cell basis and averaged for all cells transfected with individual pre-miRs or siRNAs. The image analysis approach was implemented in MATLAB (Mathworks, USA) using the DIPImage Toolbox (Delft University of Technology, Netherlands) and the Image Processing Toolbox (Mathworks, USA).

5.2.13. Statistical data analysis

a.) Statistical data analysis of biosynthetic ts-O45-G trafficking assay

ts-O45-G transport assay was performed either on 8-well µ-slides or in 96-well µ-plates and 36 or 20 images/well were acquired, respectively. The image quality was visually inspected for the quality control and total intensity thresholds were defined for each experiment separately. Specifically, the cells with the highest total intensity of expressed ts-O45-G (~7.5% of analyzed cells) and cells that were not transduced with the adenoviral vector (~5% of analyzed cells) were removed from further analysis. ts-O45-G transport rate in a single cell was estimated by the ratio of the total grey values of PM-incorporated to the total grey values of the total amount of expressed protein. Next, the mean of ts-O45-G transport rates for each experimental sample was calculated over all cells in the corresponding images. The R programming language (http://cran.r-project.org/) and the "RNAither" (Rieber *et al*, 2009) package from Bioconductor

(http://www.bioconductor.org/) were used for normalization of experimental data. For normalization of experiments carried out on 8-well µ-slides, the mean of the transport rate in the negative controls (control siRNA, PNC or ANC) was subtracted from the mean of the transport rate in each experimental sample and variance was adjusted by dividing by the standard transport rate deviation of the negative controls as defined by the equation (1):

$$\text{Equation (1)} \quad \text{norm}(x) = \frac{x(i) - \mu(\text{ctl})}{\sigma(\text{ctl})}$$

where x is the mean of ts-O45-G transport rate in experimental sample, i is the well of experimental sample, and µ(ctl) and σ(ctl) are the mean and the standard deviation of ts-O45-G transport rate in cells transfected with respective negative controls on the µ-slide, respectively. The thresholds of +/- 2 SDs of the normalized ts-O45-G transport rate compared to the mean transport rate in negative control-transfected cells were used to define effector miRNAs in ts-O45-G transport assay performed on 8-well µ-slides.

Since the screening of pre-miR library was carried out in 96-well µ-plates, *Z*-score normalization was used to identify hit miRNAs as defined by the equation (2):

$$\text{Equation (2)} \quad Z = \frac{x(i) - \mu(\text{plate})}{\sigma(\text{plate})}$$

where x is the mean of ts-O45-G transport rate in experimental sample, i is the well of experimental sample, and µ(plate) and σ(plate) are the mean and the standard deviation of overall ts-O45-G transport rate in the experimental µ-plate, respectively. The thresholds of +/- 1.5 of the *Z*-score-normalized trafficking rate were used to identify hit miRNAs in the pre-miR library screening.

Finally, positive values indicate acceleration of ts-O45-G transport rate and negative values represent inhibition of ts-O45-G transport rate.

b.) Statistical data analysis of DiI-LDL internalization assay

DiI-LDL internalization assay was performed on 8-well µ-slides and 49 images/well were acquired. Similar to ts-O45-G trafficking assay, the total grey values of internalized DiI-LDL fluorescence intensity in single cells were taken for calculations and the efficiency of ligand uptake was normalized to the respective negative controls as defined by the equation (1). Consequently, positive values indicate increased amount of internalized DiI-LDL and negative values represent reduced amount of internalized DiI-LDL compared to negative control samples.

The thresholds of +/- 1 SD of normalized intracellular DiI-LDL amount compared to the mean internalized amount in negative control-transfected cells were used to identify the effector miRNAs in DiI-LDL assay.

c.) Statistical data analysis of mRNA microarrays

Data analysis of Illumina mRNA microarrays was accomplished by normalization of the averaged signals of all specific probe replicates using the quantile normalization algorithm without background substraction. Analysis was performed by means of the Chipster analysis platform v1.4.7 (http://chipster.csc.fi/). Expression level fold change (log_2) of the respective transcript was defined as difference between the normalized mean intensity of the respective probes from samples transfected with pre-miR-17 or pre-miR-517a and negative control samples. The statistical significance of expression level fold changes was estimated by calculating a p-value using empiricalBayes method (a modification of t-test) and Benjamini-Hochberg multiple testing correction method. Next, the log_2 expression fold changes were transformed to linear expression fold changes and cutoff values of +/- 1.5 corresponding to an adjusted p-value ≤ 0.05 (in case of pre-miR-517a, p-value ≤ 0.01) were applied to identify significantly deregulated transcripts.

d.) Statistical data analysis of miRNA microarrays

Data analysis of Agilent miRNA microarrays was achieved by normalization of the averaged signals of all miRNA-specific probe replicates using the median normalization algorithm after background substraction. The background signal of each microarray was determined by averaging the intensities of "Negative control" probes distributed over the microarray. Median-normalized intensities of miRNAs from samples treated under condition (i) were used to determine the steady-state expression levels of individual miRNAs. Fold changes of individual miRNA expression levels under different experimental conditions were defined as normalized intensity ratios between samples prepared under conditions (I) and (II), and samples prepared under conditions (I) and (III). The statistical significance was estimated by using empiricalBayes method and Benjamini-Hochberg multiple testing correction method.

e.) Statistical significance

Statistical data significance of ts-O45-G transport, DiI-LDL uptake, qRT-PCR, luciferase reporter assays and western blot analyses was tested using a two-tailed Student's t-test. p-values lower than 0.05 were considered as significant.

5.2.14. Bioinformatics analysis

Human 3´UTRs, 5´UTRs and protein coding sequences (CDS) based on RefSeq database were obtained from UCSC Genome Browser (http://genome.ucsc.edu/). If multiple RefSeq identifiers were mapped to a single Entrez Gene ID present in the mRNA microarray data, the RefSeq with the longest 3´UTR was used for further analysis. Next, the 3´UTRs, 5´UTRs and CDS of *miR-17*- and *miR-517a*-affected mRNAs were searched for 5´-GCACUUU-3´ and 5´-UGCACGA-3´ heptamers, respectively. These heptamers are reverse complementary to the defined seed sequences (miRNA positions 2-8) of investigated miRNAs. The overall frequency of potential miRNA binding sites (heptamers) in human transcriptome was referred to as background rate and determined by searching all obtained transcript sequences for the presence of the indicated heptamers.

Transcriptome-wide enrichment analysis for nucleotide motifs of mRNA expression data upon transfection with pre-miR-17 or pre-miR-517a was performed with Sylamer algorithm (http://www.ebi.ac.uk/enright/sylamer/).

miRNA target predictions were queried in three web-based prediction tools: (i) MicroCosm Targets v5, which uses miRanda algorithm to identify potential miRNA binding sites (http://www.ebi.ac.uk/enright-srv/microcosm/htdocs/targets/v5/info.html), (ii) Diana-microT v3.0 (http://diana.cslab.ece.ntua.gr/microT/) and (iii) TargetScanHuman release 5.2 (http://www.targetscan.org/vert_50/). Predictions were queried using default parameters (for TargetScanHuman only conserved miRNA binding sites were used).

Membrane trafficking-related genes that are directly annotated to the Gene Ontology terms of "Protein transport" (GO:0015031), "Endocytosis" (GO:0006897) and "Protein secretion" (GO:0009306) were queried in two databases: (i) Ensembl (http://www.ensembl.org/biomart/) and (ii) AmiGO (http://amigo.geneontology.org/).

6. RESULTS

6.1. Proof of principle: application of pre-miRs and anti-miRs for membrane trafficking assays

Gain-of-function (overexpression) and/or loss-of-function (inhibition) approaches are two the most often used methods to elucidate the regulatory miRNA mechanisms of gene expression. Much of the progress in investigating miRNA functions has been gained from loss-of-function studies with synthetic miRNA antisense RNA oligonucleotides (hereafter, anti-miRs). Anti-miRs sterically block the mature miRNA and sequester it from participating in miRISC-associated inhibition of target mRNAs. RNA molecules that mimics mature miRNA (hereafter, pre-miRs) have been widely used to achieve *de novo* or to increase the expression of specific miRNAs (Borgdorff *et al*, 2010; Cheng *et al*, 2005; Davis *et al*, 2006; Davis *et al*, 2009; Lam *et al*, 2010).

Chemical modifications are necessary to protect synthetic anti-miRs and pre-miRs from serum and intracellular nucleases when administrated to animals or cell cultures. Other properties of chemically modified RNA molecules include enhanced hybridization affinity for the target miRNA (in case of anti-miRs) or mRNA (in case of pre-miRs) and improved activation of RNase H or other proteins involved in the miRNA-mediated regulation (Esau, 2008). Moreover, specific modifications contribute to enhanced tissue and cellular uptake (Krutzfeldt *et al*, 2005). The potency of anti-miRs containing different chemical modifications was recently investigated in HeLa cells by Lennox and Behlke (Lennox & Behlke, 2010).

Considering that various chemical modifications might confer substantially different functional features to oligonucleotides, we performed a set of proof of principle experiments to evaluate transfection efficiency, activity and stability of pre-miRs and anti-miRs used in this project. Noteworthy, the exact chemical modifications and structural characteristics of pre-miRs and anti-miRs are undisclosed (patent pending products of Ambion), further highlighting the need for proof of principle experiments.

6.1.1. Transfection efficiency of synthetic pre-miRs and anti-miRs

In order to determine the optimal transfection conditions for synthetic pre-miRs and anti-miRs, four widely used adherent cell lines (HeLa, HeLa-CD4, A549 and NIH 3T3) were

transfected with Cy3-labeled negative controls of pre-miRs (PNC) and anti-miRs (ANC). Two different transfection approaches were tested: the liquid-phase direct transfection and the solid-phase reverse transfection. The latter strategy, in combination with automated multi-channel fluorescence microscopy, is more suitable for large-scale high-throughput studies as well as it effectively shortens the duration of cellular assays (Erfle *et al*, 2007). To evaluate the efficiency of liquid-phase direct transfection, different cell lines were transfected with Cy3-labeled PNC or ANC at a final concentration of 50nM. Lipofectamine 2000 was used as a transfection reagent. More than 80% of cells were transfected in all tested cell lines 24h after transfection and no significant difference was observed between PNC and ANC transfection efficiency.

Delivery of PNC and ANC by solid-phase reverse transfection was evaluated in 96-well µ-plates and 384-spot cell arrays. In this set of experiments, 8pmol of PNC or ANC were used per well or spot (Erfle *et al*, 2008). Transfection efficiency was examined in four cell lines and found to be comparable to that of direct transfection.

In conclusion, it was showed that synthetic pre-miRs and anti-miRs can be delivered efficiently into four adherent cell lines using Lipofectamine 2000 as a transfection reagent. Furthermore, delivery of pre-miRs and anti-miRs can be achieved using either liquid-phase or solid-phase reverse transfection approaches.

Transfection experiments were performed by the master student U. Neniškytė (previous member of Screening of Cellular Networks laboratory); therefore, results are not visually presented in this thesis.

6.1.2. Functionality tests of pre-miRs and anti-miRs

To investigate whether transfected pre-miRs and anti-miRs can effectively increase or decrease intracellular levels of specific miRNAs, respectively, we conducted quantitative real-time PCR (qRT-PCR) and luciferase reporter assays. For these experiments, we selected three human miRNAs encoded by extensively studied polycistronic *miR-17-92* cluster, namely *miR-17*, *miR-20a* and *miR-92a* (Tanzer & Stadler, 2004), and unrelated *miR-320a*. In line with previously published data (Chen *et al*, 2008), our microarray-based miRNA profiling results, which are discussed later (**Appendix II**), confirmed that all four selected miRNAs are expressed in HeLa cells. To examine the potency of pre-miRs and anti-miRs to modulate the expression levels of the selected miRNAs, respective pre-miRs and anti-miRs were transfected into HeLa cells. Levels of mature miRNAs were assayed by qRT-PCR 24h, 48h and 72h after transfection. Relative miRNA

expression changes were calculated by using a critical threshold (C(T)) method, also known as $2^{-\Delta\Delta CT}$ (Livak & Schmittgen, 2001). Expression level of abundant small nuclear *U6B* RNA (*RNU6B*) was used as a reference for normalization throughout the experiments. We detected significantly increased levels of all tested miRNAs (2.7- to 6-fold, $\log_2$) in the cells transfected with respective pre-miRs compared to the mock-transfected cells (**Fig. R.1 A**). Importantly, very similar results were obtained up to 72h after transfection (**Fig. R.1 B**), indicating a high degree of pre-miR resistance to serum and intracellular nucleases.

Quantification of miRNA expression in the cells transfected with anti-miRs showed no significant changes in *miR-17*, *miR-20a* and *miR-320a* levels. Anti-miR-92a was an exception: we observed nearly 3-fold ($\log_2$) reduction of *miR-92a* in the cells transfected with anti-miR-92a compared to the mock-transfected cells (**Fig. R.1 A**). This data is somewhat in contrast to previously published results showing an effective target miRNA degradation induced by anti-miRs (Davis *et al*, 2006; Esau *et al*, 2006; Krutzfeldt *et al*, 2007). On the other hand, anti-miRs containing specific chemical modifications can sequester target miRNA into a stable complex and inhibit its activity without detectable degradation (Davis *et al*, 2009; Elmen *et al*, 2008). Moreover, some high affinity chemical modifications, which stabilize the anti-miR:miRNA duplex, can significantly interfere with miRNA detection by qRT-PCR methods (Davis et al., 2009). Taken together, profiling of miRNA expression is not a reliable method to evaluate the extent of miRNA inhibition by anti-miRs used in this study.

In order to directly evaluate functional potency of pre- and anti-miRs, we applied a dual-luciferase reporter assay, which has been successfully used to measure miRNA activity in cell cultures (Davis *et al*, 2006; Lennox & Behlke, 2010). The assay is based on the expression of luciferase gene cloned into psiCHECK^{TM}-2 vector (Promega), which was used as a template to generate specific reporter constructs for *miR-17*, *miR-20a*, *miR-92a* and *miR-320a*. Each construct contained a single perfect complementary binding site for miRNA of interest in the 3´UTR of the *Renilla* luciferase gene. Firefly luciferase gene cloned in the same vector was used as an internal transfection efficiency reporter. The miRNA-specific luciferase reporter constructs were co-transfected with respective pre-miRs or anti-miRs into HeLa cells. Cells were lysed 24h post-transfection and assayed for *Renilla* and firefly luciferase activities. In accordance with the data obtained by miRNA qRT-PCR, miRNA overexpression by pre-miRs led to a significant downregulation of *Renilla* luciferase protein level compared to the cells co-transfected with reporter construct and PNC. Normalized decrease in luciferase level varied from 2- to 3-fold, depending on overexpressed miRNA (**Fig. R.1 C**). In contrast, inhibition of miRNAs by anti-

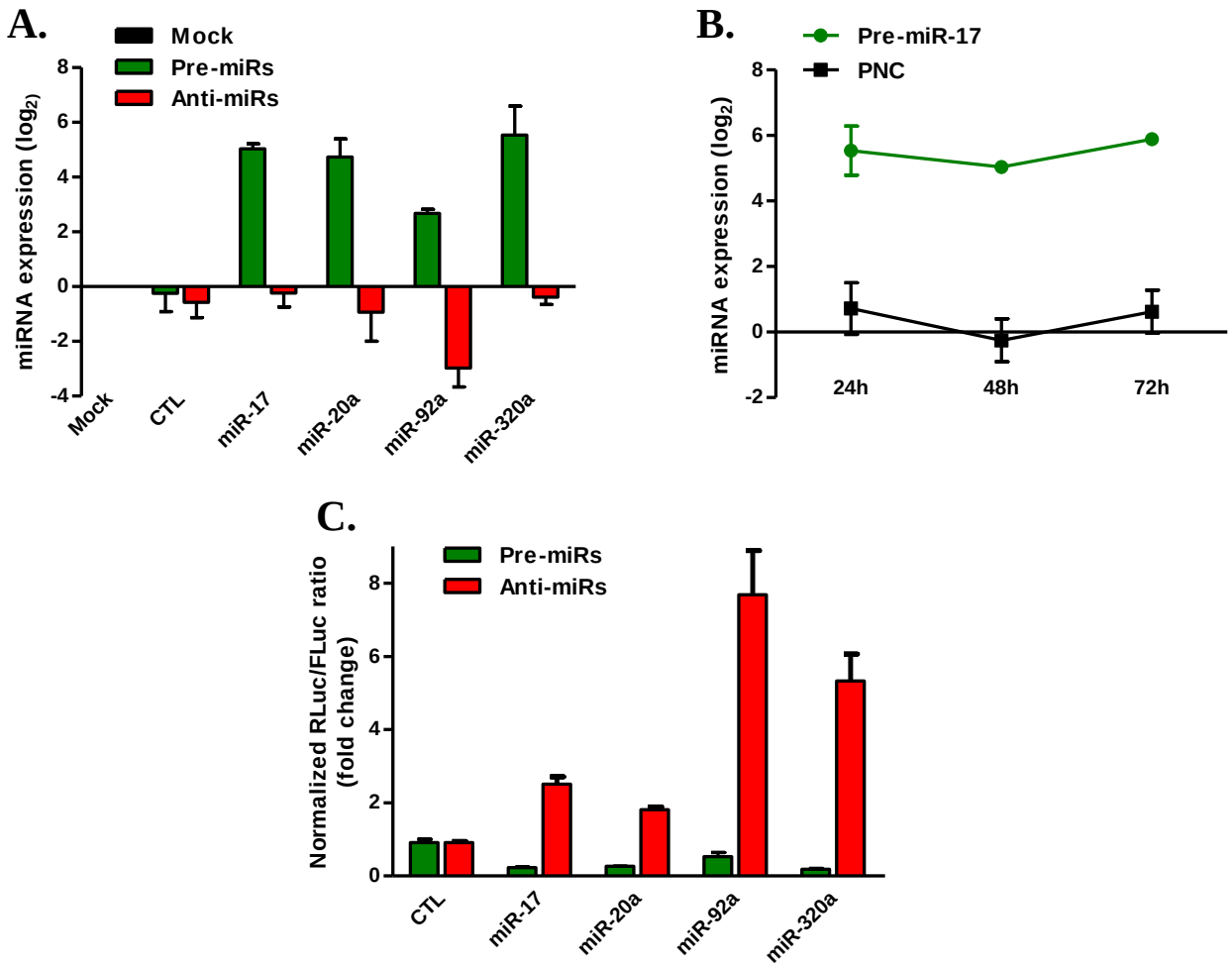

Figure R.1: Proof of principle: evaluation of functional potency of pre-miRs and anti-miRs. (A) Quantitative RT-PCR was used to quantify changes in the miRNA expression levels after transfection with pre- or anti-miRs. HeLa cells were transfected with the indicated pre- or anti-miRs and qRT-PCR was performed 48h after transfection. Expression levels of *miR-17*, *miR-20a*, *miR-92a*, and *miR-320a* in mock-transfected cells (only transfection reagent Lipofectamine 2000) were adjusted to 0 and used as a reference to normalize miRNA expression changes in the cells transfected with corresponding pre- or anti-miRs. CTL represents PNC or ANC. Results are shown as normalized expression mean values from 3 independent transfection experiments (n=3) ± S.E.M. **(B)** Representative time-course qRT-PCR experiment in the cells transfected with pre-miR-17 or PNC. Results are normalized and represented as in (A). **(C)** Dual luciferase reporter assay was performed in HeLa cells co-transfected with respective reporter constructs and pre- or anti-miRs. *Renilla* and firefly luciferase activities were measured 24h post-transfection. *Renilla* expression level was determined by *Renilla*/firefly luciferase activity ratio and normalized against the control cells (CTL) co-transfected with respective reporter construct and PNC or ANC. Results are shown as mean values of normalized *Renilla*/firefly luciferase ratios from three independent experiments (n = 3) ± S.E.M.

miRs resulted in a derepression of the *Renilla* luciferase mRNA and thereby a markedly upregulated luciferase protein expression. Notably, anti-miR-92a, which was the most effective

anti-miR in qRT-PCR, also was the most potent inhibitor in luciferase assay. It induced an 8-fold higher *Renilla* luciferase expression compared to ANC (**Fig. R.1 C**). To conclude, these results demonstrate that synthetic pre-miRs and anti-miRs are functionally potent, respectively, to enhance or to inhibit the activity of endogenous miRNAs in HeLa cells. Moreover, we show that these compounds, at least pre-miRs, are resistant to nuclease degradation up to 72h post-transfection.

6.1.3. Quantitative investigation of the biosynthetic membrane trafficking

To investigate whether miRNAs are actively involved in the regulation of biosynthetic membrane trafficking, we employed a well-described quantitative fluorescence intensity-based protein transport assay (Starkuviene *et al*, 2004; Starkuviene & Pepperkok, 2007). The key component of this assay is a fluorescent protein-tagged temperature-sensitive glycoprotein mutant of vesicular stomatitis virus (ts-O45-G). This ectopically expressed chimeric transmembrane protein remains in misfolded state at 39.5°C and, therefore, accumulates in the endoplasmic reticulum (ER) (Zilberstein *et al*, 1980). The synchronized release of ts-O45-G is achieved by moving cells to the permissive temperature of 32°C; the protein passes through the biosynthetic trafficking system and incorporates into the plasma membrane. ts-O45-G transport rate is estimated by the ratio between ts-O45-G specific fluorescence on the plasma membrane and the total amount of the expressed protein on a single cell basis (see Methods). An automated image acquisition and analysis, a similar approach to the one used by Starkuviene and Pepperkok (Starkuviene and Pepperkok 2007), enabled us to collect information from 8 000 – 10 000 cells for each experiment, ensuring the reliability of the data. We further applied an elaborate statistical data analysis that allowed normalizing and comparing data across different experiments. For this purpose, we used the R programming language and the "RNAither" package from Bioconductor (Rieber *et al*, 2009).

As mentioned in the introduction, human miRNAs encoded by one of the best-characterized *miR-17-92* cluster and its paralogous *miR-106a-363* and *miR-106b-25* clusters can be grouped into four separate miRNA families according to their seed sequences (**Fig. R.2 A**). We selected *miR-17*, *miR-18a*, *miR-19a* and *miR-92a* as representative members of each seed family and investigated whether overexpression or inhibition of each of them can have any effect on biosynthetic cargo trafficking. *miR-320a* was also used in this assay as miRNA unrelated to the paralogous clusters. We performed a ts-O45-G transport assay with five selected miRNAs in

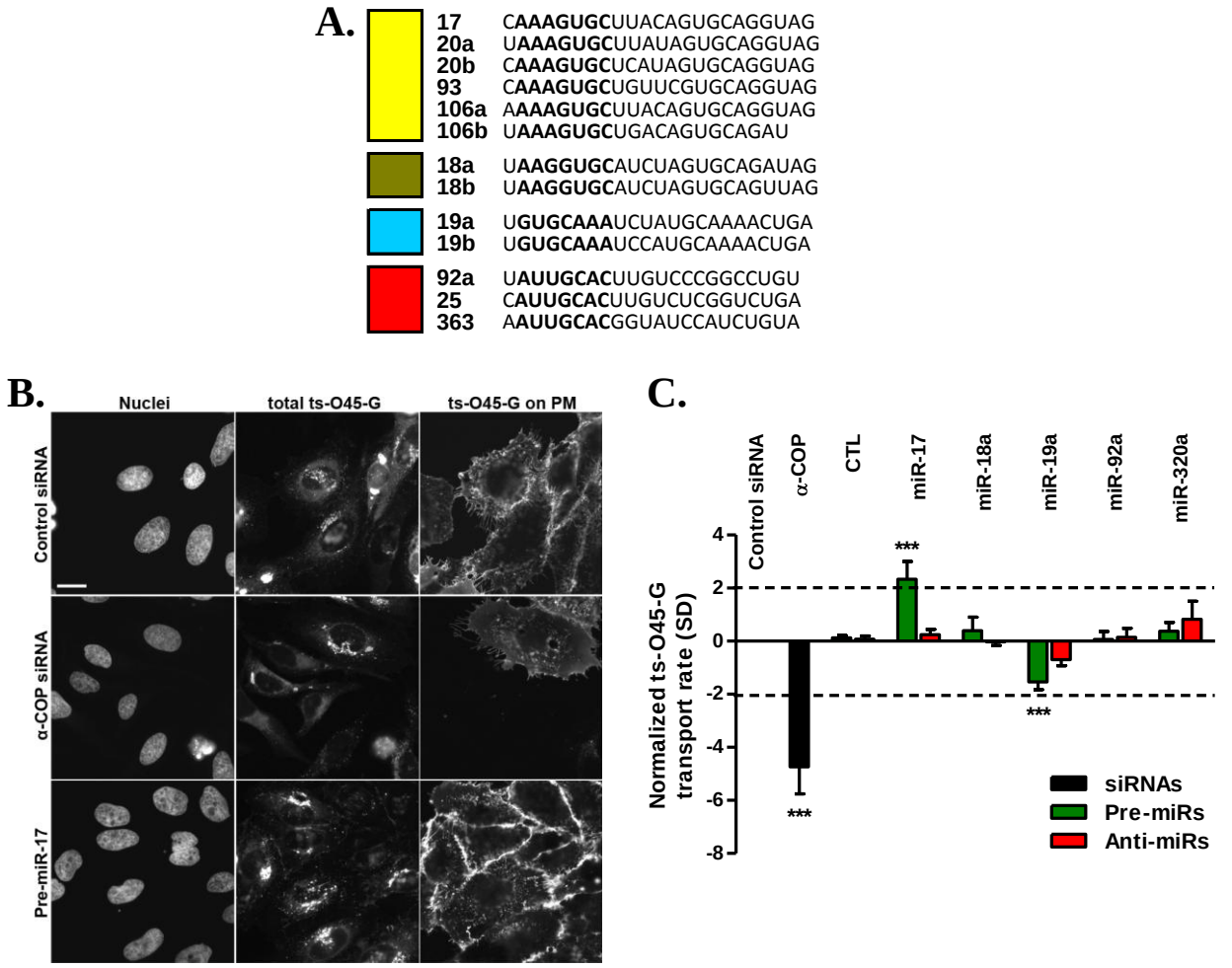

Figure R.2: Overexpression of *miR-17* induces significant changes in biosynthetic ts-O45-G trafficking in HeLa cells. (A) Sequence comparison of mature miRNAs encoded by the three paralogous clusters in mammals. miRNAs are grouped into four families according to their seed sequences (nucleotides 2-8). **(B)** Representative images of ts-O45-G transport assay in HeLa cells. While no changes in ts-O45-G secretion rate were obtained in cells transfected with control siRNA (upper row), knockdown of *α-COP* with specific siRNA resulted in a strong inhibition of cargo trafficking (middle row) 48h post-transfection. Importantly, transfection with pre-miR-17 significantly increased the fraction of PM-incorporated ts-O45-G (lower row). Scale bar represents 20 µm. (**C**) Quantification of fluorescence intensity-based ts-O45-G biosynthetic transport assay. HeLa cells were transfected with siRNAs, pre- and anti-miRs, and the respective controls on the 8-well µ-slides. After 48h, ts-O45-G transport assay was performed and quantified as described in Methods. The ts-O45-G transport rate was normalized against the control siRNA-transfected cells. CTL represents either PNC or ANC, dashed lines cutoff values. Results are shown as normalized ts-O45-G transport rate mean values from at least three independent experiments ($n \geq 3$) ± S.E.M. ***, $p<0.001$. PM, the plasma membrane.

HeLa and HeLa-CD4 cell lines on 8-well µ-slides. Respective pre-miRs and anti-miRs were introduced by liquid-phase direct transfection. Additionally, siRNA targeting *α-COP* mRNA was included as positive control in each µ-slide. α-COP is a subunit of the oligomeric COPI coatomer

complex that is essential for both anterograde and retrograde vesicular trafficking in the ER-Golgi segment (Gerich *et al*, 1995; Letourneur *et al*, 1994; Orcl *et al*, 1993). The results of our functional assay revealed that overexpression of *miR-17* significantly accelerated ts-O45-G transport in both HeLa (**Fig. R.2 B and C**) and HeLa-CD4 (data not shown) cells 48h after transfection, indicating that *miR-17* is an active regulator of biosynthetic trafficking. In contrast to *miR-17*, overexpression of *miR-19a* inhibited cargo trafficking compared to PNC; however, the effect of *miR-19b* was less pronounced than the one induced by *miR-17*. While overexpression of *miR-17* and *miR-19a* caused reproducible phenotypes of cargo trafficking, we could not observe any significant effect on cargo transport after inhibition of these miRNAs by anti-miRs (**Fig. R.2 C**). In line with previous studies (Erfle *et al*, 2004), knockdown of *α-COP* significantly compromised biosynthetic cargo trafficking. Importantly, data normalization showed that a strong inhibition of ts-O45-G transport in *α-COP* siRNA-transfected cells is represented by more than 4 standard deviations (SDs) from the mean of protein transport rate in control siRNA-transfected cells (**Fig. R.2 B and C**). Based on this observation, we set stringent thresholds at +/- 2 SDs from the mean of ts-O45-G transport rate observed for negative controls in order to identify miRNAs that induce biologically significant changes in biosynthetic cargo trafficking.

We further confirmed miRNA-mediated ts-O45-G transport phenotypes in reverse-transfected HeLa cells in 96-well plates. Consistent with the results obtained after liquid-phase transfection with pre-miRs, overexpression of *miR-17* resulted in more than 2 SDs increased transport rate of model cargo protein (data not shown).

These results indicate that miRNAs are active regulators of biosynthetic cargo trafficking in mammalian cells. Specifically, we showed that overexpression of *miR-17* significantly increases cargo trafficking rate and this effect is not specific to the single cell type since it was observed both in HeLa and HeLa-CD4 cell lines.

6.1.4. Quantitative investigation of the endocytosis

In order to measure miRNA-mediated effects on endocytosis, an opposite process of protein secretion, we employed a low-density lipoprotein (LDL) internalization assay. This assay is based on a fluorescently labeled LDL (DiI-LDL; LDL conjugated to 3,3'-dioctadecylindocarboncyanine) that is internalized into cells via clathrin-mediated endocytosis upon binding to the LDL receptor (LDLR). Following internalization, DiI-LDL distributes within endosomal compartments where the amount of internalized ligand molecules can be measured

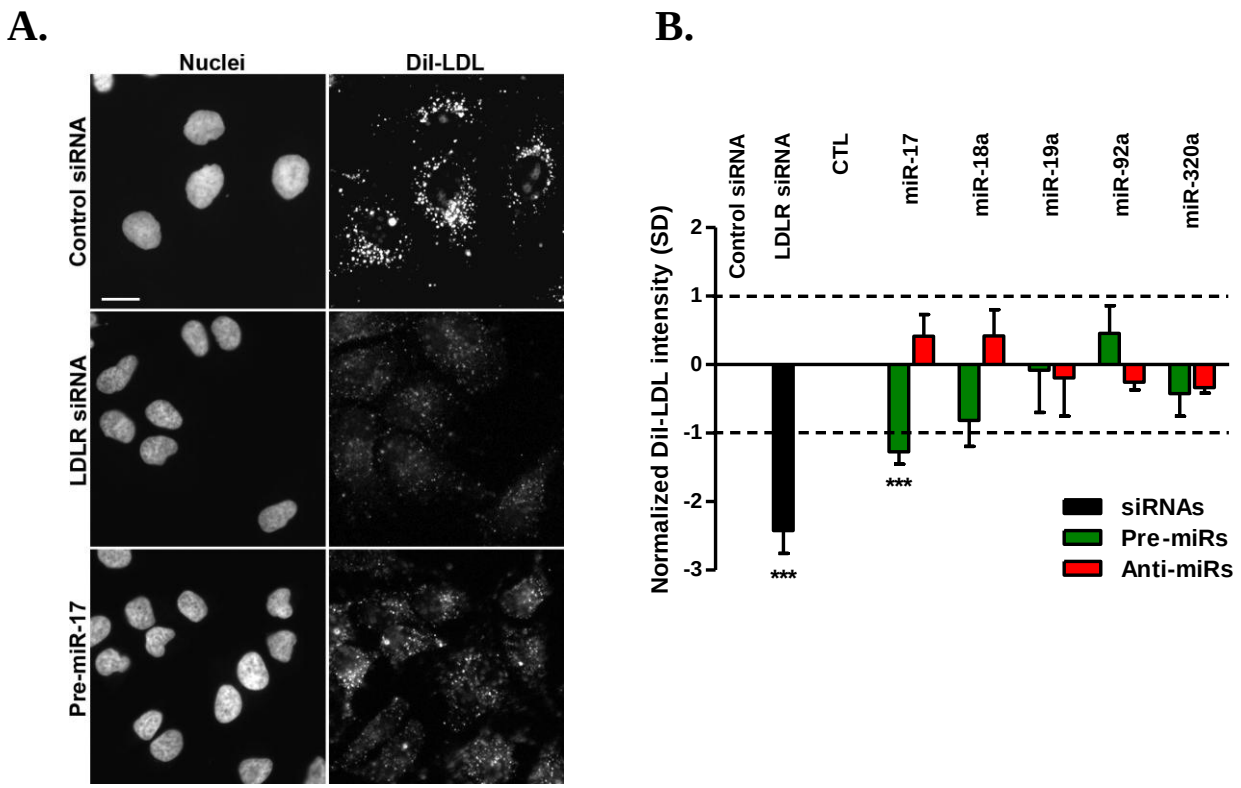

Figure R.3: Overexpression of *miR-17* leads to significantly reduced internalization of DiI-LDL in HeLa cells. (A) Representative images of DiI-LDL internalization assay in HeLa cells. In contrast to unaffected DiI-LDL uptake in control siRNA-transfected cells (upper row), ligand internalization was strongly reduced in *LDLR* siRNA- (middle row) and pre-miR-17-transfected cells (lower row). Scale bar represents 20 µm. **(B)** Quantification of internalized DiI-LDL fluorescence intensity in cells transfected with indicated siRNAs, pre-miRs and anti-miRs. Single cell-associated total intensity of DiI-LDL was measured and normalized to the respective controls (LDLR siRNA to control siRNA, pre-miRs to PNC and anti-miRs to ANC) as described in Methods. CTL represents either PNC or ANC, dashed lines cutoff values. Results are shown as normalized mean DiI-LDL intensity values from three to six independent experiments ($3 \leq n \leq 6$) ± S.E.M. ***, $p<0.001$.

quantifying their fluorescence intensity (Ghosh *et al*, 1994). To this end, we transfected HeLa cells with pre-miRs or anti-miRs for selected miRNAs by liquid-phase transfection on 8-well µ-slides. Since depletion of LDLR has been reported to compromise DiI-LDL internalization (Gilbert *et al*, 2009), siRNA targeting *LDLR* mRNA was chosen as a positive control. DiI-LDL internalization was stimulated 48h post-transfection and total single cell-associated fluorescence intensity was measured and quantified as described in Methods. The endocytosis assay revealed that overexpression of *miR-17* significantly reduced DiI-LDL uptake compared to PNC (**Fig. R.3**), indicating that this miRNA has also an active role in endocytosis regulation. Although we observed reduced DiI-LDL internalization in cells transfected with pre-miR-18 in separate experimental replicas, the overall result was not significant due to high data variability (**Fig. R.3**

B). Unfortunately, the inhibition of miRNAs with anti-miRs had no significant influence on cellular DiI-LDL uptake. In agreement with published data (Gilbert *et al*, 2009), knockdown of *LDLR* resulted in a strong reduction of internalized DiI-LDL (**Fig. R.3 B**). Importantly, data analysis showed that DiI-LDL amount in *LDLR* siRNA-transfected HeLa cells was reduced by more than 2 SDs from the mean of DiI-LDL fluorescence intensity in negative control siRNA-transfected cells (**Fig. R.3 B**). Based on this finding, we set cutoff values at +/- 1 SD from the mean of internalized ligand amount in negative controls in order to identify miRNAs that cause biologically significant changes in DiI-LDL uptake. Taken together, these experiments suggest that miRNAs are also potent regulators of endocytosis process with *miR-17* being involved in LDL internalization.

6.1.5. Members of the *miR-17* family regulate membrane trafficking

miRNAs with identical seed sequences are predicted to have a highly overlapping set of targets and, therefore, it is possible that they regulate the same biological processes (Bartel, 2009; Lewis *et al*, 2005; Sethupathy *et al*, 2006). Indeed, several experimental studies have supported this prediction on target gene (Doebele *et al*, 2010; O'Donnell *et al*, 2005; Uhlmann *et al*, 2010; Wu *et al*, 2010; Xu *et al*, 2007) or biological process (Borgdorff *et al*, 2010) level. Therefore, we hypothesized that other members of *miR-17* seed family also could be implicated in the regulation of biosynthetic ts-O45-G transport and DiI-LDL internalization. To address this hypothesis, we performed ts-O45-G transport and DiI-LDL uptake assays in HeLa cells transfected with pre-miRs or anti-miRs for other three *miR-17* family members, namely, *miR-20a*, *miR-20b* and *miR-93*. As seen in **Figure R.4 A**, individual overexpression of all three miRNAs resulted in a significantly accelerated ts-O45-G transport rate. Consistently, transfection with pre-miRs markedly reduced the amount of internalized DiI-LDL (**Fig. R.4. B**). Again, inhibition of these miRNAs did not induce phenotypic changes that significantly differ from the control ANC in any assay (**Fig. R.4**), indicating the systematic difficulties to obtain cellular phenotypes after miRNA inhibition under used experimental conditions.

Together with previously reported observations, our findings further support the hypothesis that miRNAs with the same seed sequence have redundant functions in regulating distinct biological processes. Moreover, we demonstrated that *miR-17* seed family members are novel regulators of biosynthetic cargo transport and endocytosis.

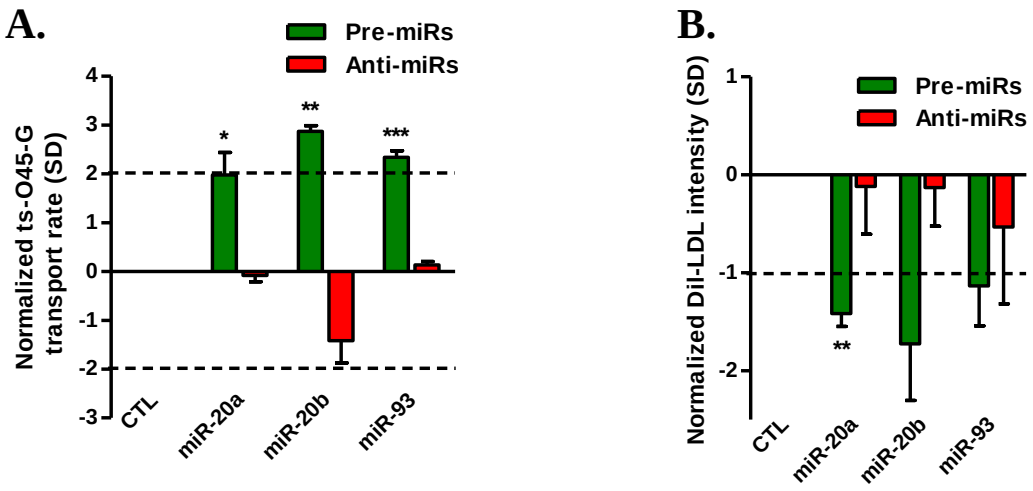

Figure R.4: *miR-17* seed family members regulate biosynthetic ts-O45-G transport and DiI-LDL uptake in HeLa cells. (A) Quantification of ts-O45-G transport assay in cells transfected with indicated pre-miRs and anti-miRs. **(B)** Quantification of DiI-LDL uptake assay 48h after transfection as in (A). CTL represents either PNC or ANC, dashed lines cutoff values. Both assays were quantified and normalized to the respective controls (pre-miRs to PNC and anti-miRs to ANC) as described in Methods. Results are represented as mean values of normalized ts-O45-G transport rates (A) or means of normalized DiI-LDL intensity values (B) from at least three independent experiments ($n \geq 3$) ± S.E.M. *, $p<0.05$; **, $p<0.01$; ***, $p<0.001$.

6.1.6. Overexpression of *miR-320a* inhibits cell proliferation

Numerous independent studies have demonstrated a role of miRNAs in cell proliferation and apoptosis (Cheng *et al*, 2005; Schaar *et al*, 2009). In accordance with the tumorigenic activity of the *miR-17-92* cluster, it has been extensively reported as an important regulator of cellular growth and apoptosis (Hayashita *et al*, 2005; He *et al*, 2005; Mu *et al*, 2009; O'Donnell *et al*, 2005). In is well known that membrane trafficking is ceased in mitotic (Misteli & Warren, 1995; Warren, 1993) and apoptotic cells (Nozawa *et al*, 2002). To examine whether miRNA-mediated changes in membrane trafficking are associated with altered cell proliferation or apoptosis, we set a microscopy-based nuclei classification assay. HeLa cells were transfected with pre-miRs or anti-miRs for *miR-17*, *miR-20a*, *miR-92a*, *miR-93* and *miR-320a*. PNC and ANC were included as negative controls; siRNA against the inner centromere protein (*INCENP*) mRNA was used as positive control. It has been shown that depletion of INCENP leads to abnormal spindle midzone/midbody formation during mitosis and thereby results in bi- and multinucleated arrested cells (Neumann *et al*, 2006; Zhu *et al*, 2005). For our assay, we stained nuclei with 0.3µg/ml

Hoechst 33342 and performed live cell imaging 48h after transfection. Having achieved the 96% accuracy of the automated nuclei segmentation (data not shown), we further classified nuclei into four distinct classes, namely, (i) interphase, (ii) mitosis, (iii) apoptosis and (iv) so called "artefacts" (for example, multinucleated cells, clusters of nuclei, background artefacts). Classification was accomplished by the extended approach described by Harder *et al* (Harder *et al*, 2008). By normalizing the nuclei intensity across the individual experiments, we achieved an accuracy of 97.6% for classifying interphase cells and 82% for classifying mitotic cells (**Fig. 5A**). The accuracy of the assay was demonstrated by the substantially reduced mitotic events in the *INCENP* siRNA-transfected cells (**Fig. 5B**). In line with previous observations (Schaar *et al*, 2009), classification of cell nuclei revealed that overexpression of *miR-320a* decreased the fraction of mitotic cells. Cell proliferation was also modestly decreased in response to overexpression of *miR-17*, *miR-20a* and *miR-93*, the effectors of ts-O45-G transport rate and cellular DiI-LDL internalization; however, difference from control cells was not significant (**Fig. 5B**). In contrast to recent studies (Tsuchida *et al*, 2011), modulation of *miR-92a* activity had no impact on proliferation, further supporting the context-dependent functions of *miR-17-92* cluster

A.

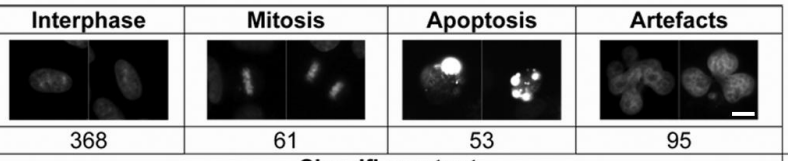

True class	Classifier output				Accuracy
	Interphase	Mitosis	Apoptosis	Artefacts	
Interphase	359	2	0	7	**97.6%**
Mitosis	2	50	9	0	**82.0%**
Apoptosis	1	3	44	5	**83.0%**
Artefacts	9	0	4	82	**86.3%**

B.

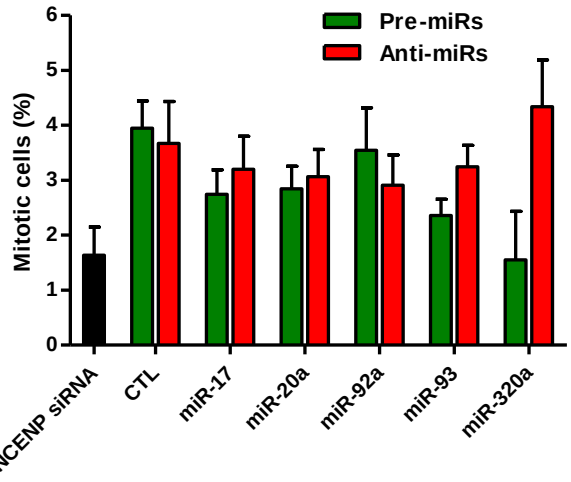

Figure R.5: Microscopy-based nuclei classification assay. (**A**) Representative images of four nuclei classes considered in the automated image analysis are represented in upper row. Confusion matrix for classification of nuclei using a weighted SVM classifier with fourfold cross-validation and accuracy of the results are given in lower row. (**B**) Quantification of HeLa cell proliferation 48h after transfection with indicated RNA molecules. CTL represents either PNC or ANC. Results are represented as mean values of percentage of mitotic cells from three independent experiments (n = 3) ± S.E.M.

(Cloonan *et al*, 2008; Hossain *et al*, 2006). Similar to our results from functional membrane trafficking assays, inhibition of miRNAs had no effect on cell proliferation (**Fig. 5B**). Despite accurate classification of apoptotic nuclei (**Fig. 5A**), we found quantification of apoptosis not reliable due to frequently observed loss of adherence of dying cells under the used experimental conditions. Unfortunately, we did not measure the effect of *miR-19a* which has been recently reported as a key compotent to exert the oncogenic activity of the cluster by promoting cell survival (Mu *et al*, 2009; Olive *et al*, 2009).

Altogether, automated nuclei analysis confirmed an anti-proliferative effect of *miR-320a*. These results also demonstrated that membrane trafficking phenotypes induced by overexpression of *miR-17* family members are direct effects, rather than consequence of altered cell proliferation.

6.1.7. Alternative approaches for inhibition of endogenous miRNAs

An approach that effectively inhibits miRNA activity is important for performing a comprehensive functional analysis of miRNAs. Multiple steps in miRNA biogenesis pathway can be targeted with antisense oligonucleotides that inhibit miRNA maturation and/or function. Nevertheless, one of the most straightforward methods for determining the function of a mature miRNA is to block its activity in miRNA-induced silencing complex (miRISC). Considering that turnover of mature miRNAs is relatively slow (Lee *et al*, 2003), this strategy gains an advantage over others for short-term studies. Consistently, many investigators have demonstrated an effective targeting of mature miRNAs with antisense oligonucleotides in a variety of cultured cells (Davis *et al*, 2006; Hutvagner *et al*, 2004; Meister *et al*, 2004).

To investigate further whether inhibition of miRNAs can cause significant phenotypic changes in membrane trafficking, we applied two alternative strategies for inhibition of endogenous *miR-20b* in HeLa cells. We selected *miR-20b* because its overexpression led to the most significant acceleration of ts-O45-G transport and reduction of internalized DiL-LDL amount compared to other investigated *miR-17* family members (**Fig. R.4**). The first alternative miRNA inhibition strategy is based on the single-stranded DNA oligonucleotides with locked nucleic acid (LNA) backbone modifications incorporated at specific positions. These antisense oligonucleotides, referred to as DNA/LNA anti-miRs, have increased resistance to nuclease degradation, higher affinity to target miRNA and are more potent in inhibiting miRNA activity in cell cultures compared to the classical 2´-O-methyl-modified anti-miRs (Davis *et al*, 2006; Orom

et al, 2006). The second alternative miRNA inhibition approach is based on the transient expression of shRNA from a lentiviral expression vector. The asymmetric shRNAs are recognized by the RNase III enzyme Dicer and processed to functional single-stranded anti-miRs, referred to as miRZips, which bind to endogenous miRNAs and inhibit their function. To measure the extent of *miR-20b* inhibition by these two different approaches, we co-transfected HeLa cells with either DNA/LNA anti-miR-20b or miRZip-20b expression vector and the reporter plasmid. The reporter plasmid contained luciferase gene with the perfect complementary *miR-20b* binding site in the 3´UTR as described previously for other miRNAs. A negative control DNA/LNA oligonucleotide and a miRZip expression vector encoding non-targeting shRNA were used as negative controls for DNA/LNA anti-miR-20b or miRZip-20b transfections, respectively. We tested different concentrations of DNA/LNA anti-miR-20b (range from 10nM to 50nM) and different amounts of miRZip-20b expression vector (range from 10ng to 900ng/well in 24-well plate). We found that DNA/LNA anti-miR-20b at 50nM concentration and 100ng/well of miRZip-20b construct induced the most pronounced effects in luciferase reporter assay (**Fig. R.6 A**). As expected, inhibition of *miR-20b* by both DNA/LNA anti-miR-20b and miRZip-20b resulted in an upregulated luciferase expression. Importantly, anti-miR-20b, containing the same chemical modifications as other anti-miRs previously tested in membrane trafficking assays, showed the strongest effect on the reporter gene expression (**Fig. R.6 A**).

To examine whether *miR-20b* inhibition by DNA/LNA anti-miR-20b leads to changes in biosynthetic trafficking, we transfected cells with DNA/LNA anti-miR-20b or control oligonucleotide and measured ts-O45-G transport rate 48h later. Similar to our previous findings (**Fig. R.4 A**), we did not observe biologically significant changes in cargo transport rate in the DNA/LNA anti-miR-20b-transfected cells compared to the control cells (**Fig. R.6 B**).

These results indicate that although different inhibition approaches are efficient in suppressing miRNA activity in luciferase reporter assay, they induce none to modest phenotypic effects in our functional membrane trafficking assays. Perfect complementarity between miRNA of interest and luciferase mRNA allows AGO2-mediated cleavage of reporter transcript. Thus, completely complementary miRNA binding sites increase sensitivity and dynamic range of the luciferase reporter assay (Esau, 2008; Yekta *et al*, 2004). However, this type of binding sites is less sensitive to other miRNAs containing the same seed sequence as the miRNA of interest but with different nucleotides in other positions. We showed that the specific inhibition of the miRNA by anti-miRs leads to a significant upregulation of the reporter gene expression. However, considering that miRNAs with the same seed sequence have a highly overlapping set

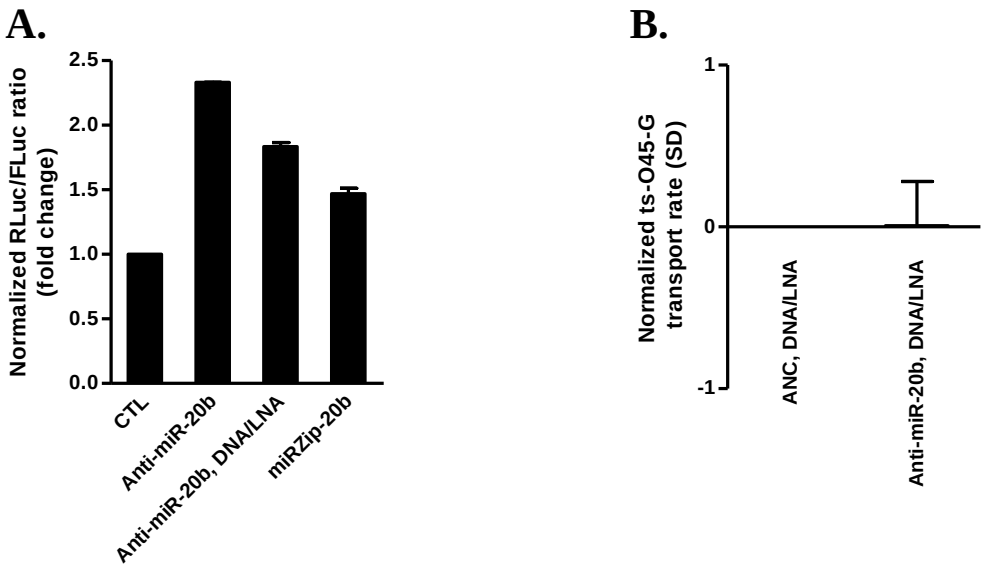

Figure R.6: Inhibition of *miR-20b* by alternative approaches (A) Luciferase reporter assay in HeLa cells co-transfected with *miR-20b* reporter construct and indicated anti-miRs (50nM final concentration) or miRZip expression vectors (100ng/well) in 24-well plates. *Renilla* and firefly luciferase activities were measured 24h post-transfection and their ratio normalized against the control cells. CTL represents cells co-transfected with *miR-20b* reporter construct and ANC or DNA/LNA negative control, or control miRZip expression vector. **(B)** Quantification of ts-O45-G transport assay in cells transfected with DNA/LNA anti-miR-20b or control oligonucleotides. The experiment was quantified and normalized to the control cells as described in Methods. Results are shown as mean values of normalized *Renilla*/firefly luciferase ratios (A) or normalized ts-O45-G transport rates (B) from three experiments (n = 3) ± S.E.M.

of targets, the less complementary natural target mRNAs remain suppressed by other seed family miRNAs. This would explain why anti-miRs are efficient in reporter assay, but have a poor performance in functional assays.

Conclusions: The results from previous experiments in our laboratory showed that synthetic pre-miR and anti-miR molecules can be efficiently introduced into different types of adherent cells by liquid-phase or solid-phase reverse transfection approaches using Lipofectamine 2000 as a transfection reagent. As proof of principle, we showed that pre-miRs and anti-miRs are efficient in enhancing or suppressing activity of cellular miRNAs, respectively, as determined by qRT-PCR and/or luciferase reporter assays. Moreover, we identified miRNAs of *miR-17* family as novel regulators of biosynthetic trafficking and endocytosis. We confirmed that overexpression of *miR-320a* suppresses cell proliferation. Despite the fact that efficient inhibition of individual miRNAs was achieved by different approaches, we could not observe

significant cellular phenotypes induced by suppression of investigated miRNAs. Therefore, the majority of the results in this project were obtained using gain-of-function miRNA approach.

6.2. Large-scale identification of miRNAs regulating biosynthetic cargo trafficking

Although significant progress has been made in understanding important regulatory roles of miRNAs in a wide range of biological processes (Bartel, 2009; Krol *et al*, 2010), the miRNA-mediated regulatory mechanisms of membrane trafficking have never been systematically investigated. Our understanding of the miRNA-mediated regulation of this cellular process is limited to a small number of reports on insulin secretion (Lovis *et al*, 2008; Plaisance *et al*, 2006; Poy *et al*, 2004) and to our findings on *miR-17* family miRNAs described earlier in this thesis. Application of high-content sample preparation technology (Erfle *et al*, 2008), in combination with automated image acquisition and analysis modules, has led to a number of successful genome-wide functional screenings of miRNAs (Serva *et al*, 2011). Having successfully completed proof of principle experiments and taking the advantage of available technological platforms, we next designed a gain-of-function large-scale screening to identify miRNAs involved in the regulation of biosynthetic ts-O45-G trafficking.

6.2.1. Functional screening identifies multiple miRNAs as potential regulators of biosynthetic trafficking

The primary screening of Pre-miR^{TM} miRNA Precursor Library (Ambion) of 470 human miRNAs annotated in miRBase v9.2 (**Appendix I**) was conducted in HeLa cells in 96-well plate experimental format. Pre-miRs were distributed across 10 different layouts of 96-well µ-plates and prepared for solid-phase reverse transfection as described in Methods. Additionally, each layout contained 3 wells with siRNAs against *α-COP* and 5 wells with PNC used as controls. Following library preparation, we seeded 5 500 cells per well. The cargo trafficking assay was performed 48h after cell seeding. Total plasma membrane-traversed ts-O45-G and overall expressed cargo protein fluorescence intensities were determined at single cell level from three independent experimental replicas. An average of 7 500 cells were analysed for each miRNA. Changes in biosynthetic ts-O45-G transport rate caused by overexpression of individual miRNAs were *Z*-score-normalized against the mean transport rate of the plate. Mean transport rate was computed over all wells in the plate except wells with *α-COP* siRNA and PNC. Then, *Z*-scores of

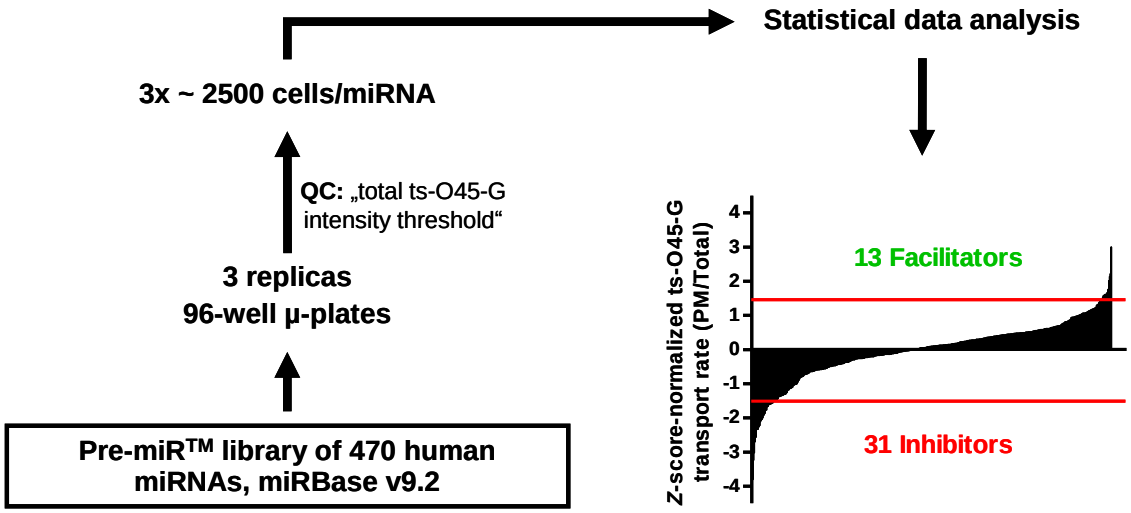

Figure R.7: Schematic representation of quantitative pre-miR library screening in order to identify miRNAs involved in regulation of biosynthetic trafficking. Of 470 tested miRNAs, 44 significantly affected transport rate of ts-O45-G protein under overexpression conditions.

Table 1: miRNAs that inhibited cargo transport.

Accession number in miRBase v9.2	miRNA ID	ts-O45-G transport		Cell growth	
		Z-score	S.E.M.	Fold change	S.E.M.
MIMAT0002888	miR-532	-4.14	0.61	0.70	0.05
MIMAT0002852	miR-517a	-3.70	0.76	0.88	0.05
MIMAT0003307	miR-637	-3.20	0.14	0.79	0.16
MIMAT0002857	miR-517b	-3.16	0.22	0.84	0.07
MIMAT0000074	miR-19b	-2.59	0.91	0.94	0.06
MIMAT0003330	miR-654	-2.54	0.79	0.80	0.20
MIMAT0000275	miR-218	-2.43	0.24	1.00	0.04
MIMAT0000267	miR-210	-2.42	0.28	1.18	0.07
MIMAT0003276	miR-608	-2.35	0.43	0.94	0.11
MIMAT0001636	miR-452*	-2.31	0.32	0.79	0.08
MIMAT0003317	miR-647	-2.15	0.12	0.56	0.09
MIMAT0003945	miR-765	-2.09	0.52	0.81	0.06
MIMAT0000423	miR-125b	-2.06	0.34	0.59	0.21
MIMAT0000710	miR-365	-2.04	0.07	0.98	0.10
MIMAT0000737	miR-382	-1.90	0.19	1.13	0.08
MIMAT0000773	miR-346	-1.89	0.30	1.03	0.11
MIMAT0002866	miR-517c	-1.86	0.48	0.94	0.05
MIMAT0003326	miR-663	-1.83	0.37	0.98	0.11
MIMAT0000259	miR-182	-1.73	0.12	1.16	0.03
MIMAT0000422	miR-124a	-1.71	0.18	1.01	0.33
MIMAT0000095	miR-96	-1.67	0.19	0.95	0.08
MIMAT0003272	miR-604	-1.67	0.97	0.83	0.06
MIMAT0000443	miR-125a	-1.66	0.12	0.79	0.37
MIMAT0003239	miR-574	-1.65	0.35	1.02	0.03
MIMAT0000420	miR-30b	-1.62	0.26	1.07	0.10
MIMAT0002173	miR-483	-1.62	0.57	1.00	0.05
MIMAT0002814	miR-432	-1.58	0.38	0.92	0.09
MIMAT0003216	miR-553	-1.55	0.33	0.43	0.08
MIMAT0001080	miR-196b	-1.55	0.53	0.81	0.12
MIMAT0000462	miR-206	-1.54	0.18	0.93	0.06
MIMAT0002174	miR-484	-1.54	0.27	0.88	0.03

Table 2: miRNAs that accelerated cargo transport.

Accession number in miRBase v9.2	miRNA ID	ts-O45-G transport		Cell growth	
		Z-score	S.E.M.	Fold change	S.E.M.
MIMAT0000676	miR-128b	3.06	0.11	0.72	0.14
MIMAT0000686	miR-34c	2.17	0.33	1.02	0.11
MIMAT0000681	miR-29c	2.07	0.10	0.95	0.02
MIMAT0000227	miR-197	2.01	0.25	0.94	0.07
MIMAT0000452	miR-154	1.81	0.18	0.88	0.08
MIMAT0000453	miR-154*	1.68	0.49	1.14	0.02
MIMAT0002805	miR-489	1.68	0.41	0.77	0.04
MIMAT0003263	miR-595	1.68	0.14	0.86	0.13
MIMAT0001413	miR-20b	1.65	0.22	0.96	0.13
MIMAT0004450	miR-297	1.62	1.02	1.19	0.06
MIMAT0000255	miR-34a	1.61	0.24	0.73	0.03
MIMAT0003299	miR-630	1.56	0.20	0.93	0.09
MIMAT0002804	miR-488	1.54	0.16	0.55	0.09

three replicas were averaged to a single value for each miRNA (**Fig. R.7**). Following data normalization, only miRNAs that accelerated or inhibited ts-O45-G transport rate by more than 1.5 *Z*-scores were considered as primary hit miRNAs. In total, our primary gain-of-function screen identified 44 miRNAs that significantly affected cargo transport rate, comprising about 10% of the library. Out of these, overexpression of 31 miRNAs inhibited (**Table 1**), whereas overexpression of other 13 miRNAs accelerated cargo trafficking rate (**Table 2**). Among the top inhibitory miRNAs we identified members of *miR-517* family (**Table 1**). Overexpression of *miR-34* family miRNAs, *miR-34c* and *miR-34a*, significantly accelerated ts-O45-G transport rate (**Table 2**). In strong agreement with the results of biosynthetic transport assay with *miR-17* family miRNAs (**Fig. R.4**), overexpression of *miR-20b* also significantly increased ts-O45-G transport rate (1.65 *Z*-scores) in library screening (**Table 2**). To our knowledge, no publications are available reporting on the interplay between our hit miRNAs and biosynthetic trafficking. This indicates the potency of our large-scale screening in identifying miRNAs with novel functions in the regulation of biosynthetic pathway.

Apart from quantification of ts-O45-G transport rate, image analysis on a cell-by-cell basis allowed us to estimate the changes in cell growth induced by miRNA overexpression (**Table 1 and 2**). Since this estimation was based on a total number of analyzed cells, we could not discern between miRNA-induced changes in apoptosis or proliferation rates. The total numbers of cells transfected with individual pre-miRs were normalized against the PNC, which was adjusted to 1, and the differences represented as fold changes in cell growth (**Table 1 and 2**). Similar to previous study where the same approach was applied for identification of miRNAs involved in cell growth (Cheng *et al*, 2005), we set fold change cutoff values at 0.8 and 1.2. miRNAs outside this range were considered as effectors of cell growth.

To confirm the results obtained from the large-scale screening, we performed a ts-O45-G transport assay with a representative set of the inhibitory miRNAs. For this purpose, we used a set of six pre-miRs from a different batch and introduced them by liquid-phase transfection into cells on 8-well µ-slides. Except for *miR-553*, we observed a strong correlation between the data from library screening and from the validation assay (**Fig. R.8**). Importantly, *miR-553* was one of the weakest ts-O45-G transport inhibitory hits as well as it was the strongest cell growth inhibitor among all screened miRNAs (**Table 1**). This suggests that *miR-553*-mediated inhibition of protein transport in the large-scale screening is likely a consequence of reduced cell growth, rather than specific effect on membrane trafficking. Noteworthy, the different extent of cargo transport inhibition between the screening and the validation assay might be due to different data

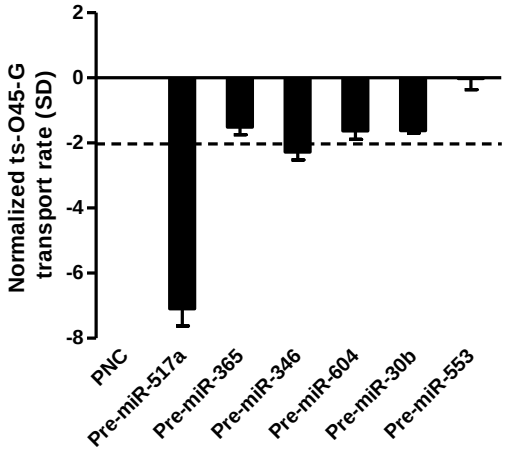

Figure R.8: Small-scale ts-O45-G transport assay validates primary miRNA hits. HeLa cells were liquid-phase transfeted with pre-miRs for six inhibitory miRNAs identified in library screening. The cargo trafficking assay was perfomed 48h post-transfection and the transport rate was normalized to PNC-transfected cells as described in Methods. Results are represented as mean values of normalized ts-O45-G transport rates from two independent experiments (n= 2) ± S.E.M.

normalization methods (normalization to plate mean was used for the data from the screening and normalization to PNC for the data from the validation assay). Together, these results validate the functional activity of pre-miRs of human Pre-miR^{TM} library and further demonstrate that our functional screening is an efficient strategy to identify miRNAs that regulate biosynthetic cargo trafficking.

6.2.2. Analysis of Golgi complex integrity confirms hit miRNAs

The Golgi complex is a highly dynamic organelle that serves as a major sorting and modification center of cellular proteins (Donaldson & Lippincott-Schwartz, 2000; Rodriguez-Boulan & Musch, 2005). Moreover, it regulates transport of cargo proteins via different membrane trafficking pathways (Bonifacino & Rojas, 2006; Pavelka *et al*, 2008). miRNAs can virtually affect any process or cellular structure involved in membrane trafficking system. Therefore, we next investigated whether miRNA-mediated phenotypes of ts-O45-G transport are associated with corresponding changes in the Golgi complex morphology. To this end, we developed a fully automated image analysis platform for quantification of the Golgi complex in single cells from microscopic images as described in Methods (**Fig. R.9**). The approach, which determines cell boundaries on a basis of nuclear location, nuclear size and lectin Concanavalin A distribution pattern, was designed to extract primary parameters of the Golgi complex. These parameters are as follow:

1. Number of Golgi fragments
2. Size of Golgi fragments
3. Distance of Golgi fragments from nuclear center
4. Fluorescence intensity of immunostained Golgi markers, such as GM130 protein

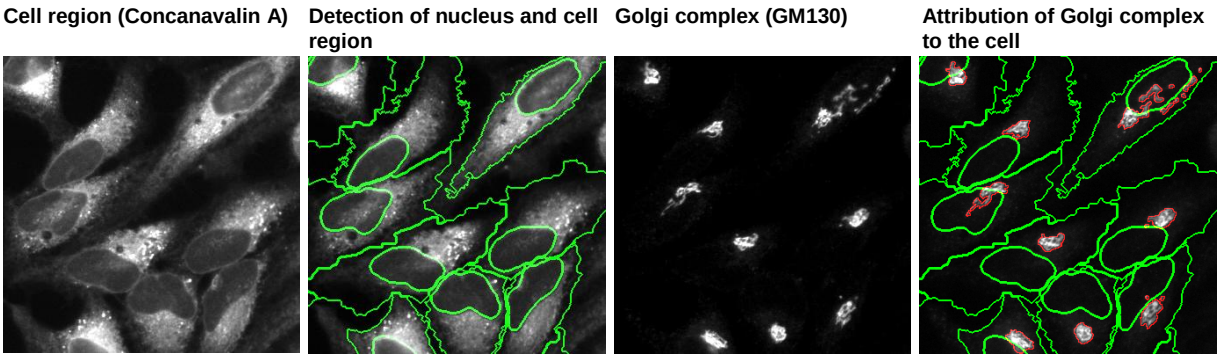

Figure R.9: Automated analysis of Golgi complex integrity. Simplified representation of automated image analysis process to quantify morphological changes in Golgi complex on a cell-by-cell basis. A detailed description of image segmentation and feature extraction steps is available in Methods.

In order to measure the effects of primary hit miRNAs (**Table 1 and 2**) on these Golgi complex parameters, we transfected cells with the respective pre-miRs. Transfection with siRNA against *α-COP* and non-targeting siRNA were used as positive and negative controls, respectively. To meet the temporal conditions of the large-scale miRNA screening, cells were fixed 48h after transfection. Following fixation, we immunostained cellular DNA, lectin Concanavalin A and *cis*-Golgi matrix protein GM130 for acquisition of microscopic images of nuclei, cell regions and Golgi complexes, respectively. In accordance with the functional screening data, the Golgi complex analysis revealed a markedly increased number of Golgi fragments in the cells transfected with pre-miRs of *miR-517* family members (**Fig. R.10 A and B**). Quantification of Golgi fragments showed more than 4-fold higher fragmentation in the pre-miR-517a or -517b, or -517c-transfected cells compared to the control cells, indicating that all three miRNAs have similar effect on Golgi structure. By applying cutoff values of 0.75 and 1.75 to the normalized numbers of Golgi fragments, we selected in total eight miRNAs whose overexpression significantly altered Golgi complex integrity (**Fig. R.10 B**). Whereas transfection with seven pre-miRs led to increased fragmentation, overexpression of *miR-382* induced condensation of Golgi complex (**Fig. R.10 A and B**). We focused further on these eight miRNAs to examine whether they cause other changes in the Golgi apparatus. Image analysis revealed that number of Golgi fragments negatively correlated with the average size of fragments (**Fig. R.10 C**) and positively correlated with the distribution area of the Golgi complex. The distribution area was defined by the distance between the outermost Golgi fragment and the nuclear center in each cell (**Fig. R.10 D**). To investigate whether overexpression of miRNAs can affect the level of Golgi protein GM130, we measured immunofluorescence intensity of this protein in the cells

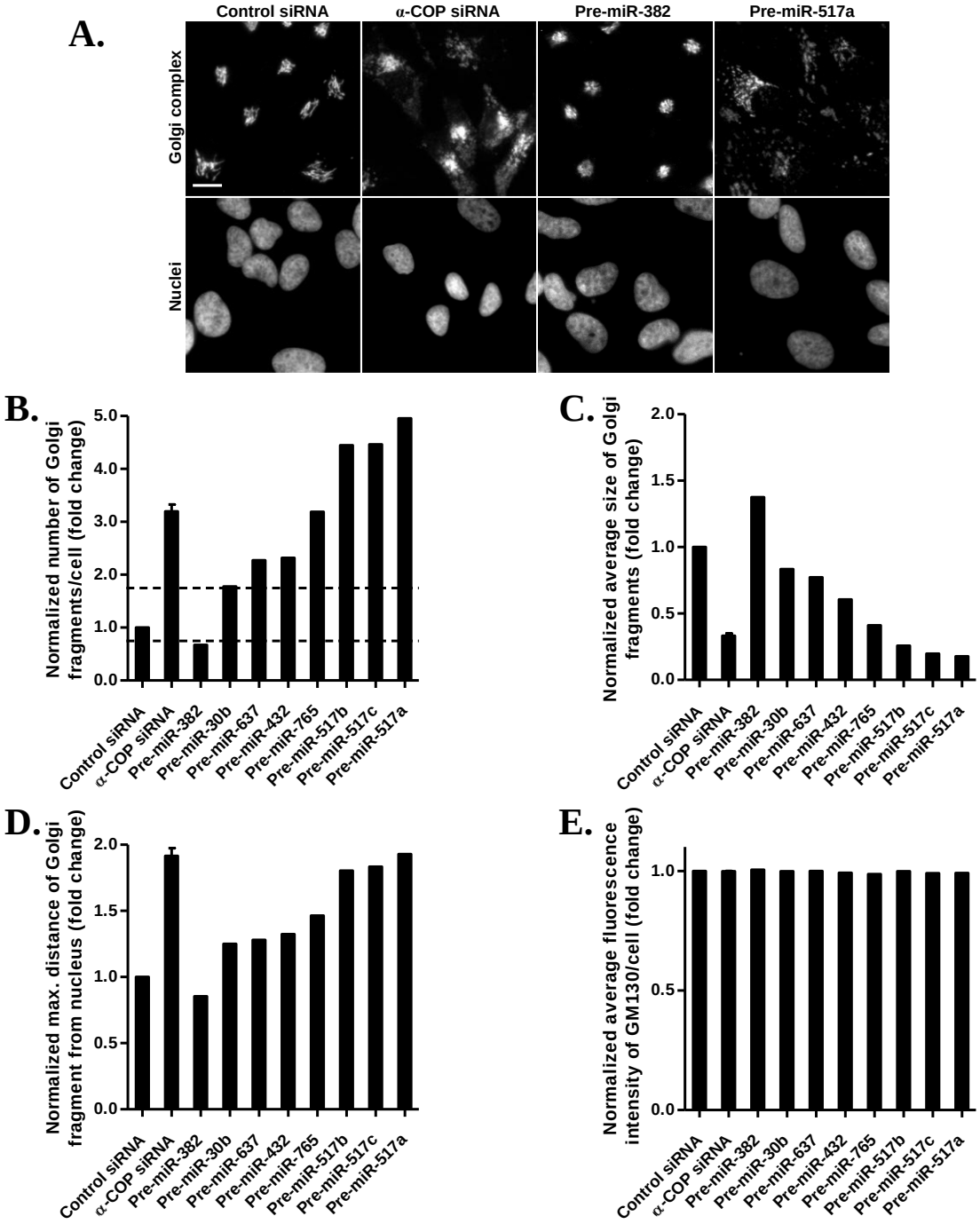

Figure R.10: Multi-parametric analysis of Golgi complex reveals phenotypic changes in Golgi complex induced by overexpression of miRNAs. (**A**) Representative images of Golgi complex. Two opposite effects of miRNA overexpression on Golgi morphology are shown; while transfection with pre-miR-382 leads to the condensation, delivery of pre-miR-517a significantly increases Golgi complex fragmentation. siRNA and *α-COP* siRNA was used positive control. Scale bar represents 20 μm. (**B-E**) Quantification of Golgi complex in the cells transfected with pre-miRs: (**B**) normalized number of Golgi fragments/cell, (**C**) normalized average size of Golgi fragments, (**D**) normalized maximum distance of Golgi fragment from the nucleus and (**E**) normalized average immunofluorescence intensity of GM130/cell. A detailed description of quantifications is available in Methods.

transfected with each of eight pre-miRs. As shown in **Fig. R.10 E**, overexpression of selected miRNAs did not alter GM130 protein level, independently of Golgi complex fragmentation.

By combining the results obtained from pre-miR library screening and the multi-parametric analysis of the Golgi complex, we identified eight miRNAs (*miR-382, -30b, -432, -637, -517a*/*b*/*c* and *-765*) as potential novel biosynthetic trafficking regulators that induce significant changes in the Golgi complex morphology. The eight miRNAs are easier to handle for the follow-up analysis compared to the 44 miRNAs that were identified as primary hits in the screening. Importantly, none of the miRNAs that accelerated ts-O45-G transport rate (**Table 2**) were identified as effectors in the Golgi complex integrity assay. This finding suggests that regulatory mechanisms of these miRNAs might converge on other cellular organelles and/or Golgi structure-independent processes in order to accelerate biosynthetic cargo trafficking.

Conclusions: To identify miRNAs involved in the regulation of biosynthetic trafficking, we screened 470 human miRNAs for their impact on ts-O45-G transport rate upon overexpression. We identified 44 miRNAs whose overexpression induce significant changes in cargo trafficking. Majority of arbitrarily selected inhibitory miRNAs (5 out of 6) were confirmed in a small-scale experimental format using pre-miRs from a different batch, demonstrating the reproducibility of large-scale screening data. Furthermore, comprehensive images analysis revealed that eight of identified hit miRNAs (*miR-30b, -382, -432, -517a, -517b, -517c, -637* and *-765*) cause significant changes in Golgi complex integrity.

6.3. Genome-wide identification of miRNAs expressed in HeLa cells

Large-scale experimental approaches have revealed that hundreds of miRNAs are expressed in highly tissue-specific patterns. Those approaches include sequencing of small RNA libraries (Landgraf *et al*, 2007) and microarray-based miRNA expression profiling (Baskerville & Bartel, 2005). Using purely computational methods to study the existing mRNA and miRNA expression data, Sood and colleagues have shown that tissue-specific miRNAs and their cognate targets are typically co-expressed in the same tissue; however, mRNAs are expressed at significantly lower levels compared to the tissues where the targeting miRNA is absent (Sood *et al*, 2006). Based on these observations, we hypothesized that introduction of miRNAs that are not endogenously expressed may result in stronger phenotypic effects compared to overexpression of endogenous miRNAs.

To test this hypothesis, we performed a microarray-based miRNA expression profiling to identify miRNAs that are endogenously expressed in HeLa cells. Total RNA was isolated from wild-type HeLa cells and hybridized to microarrays that contained probes for 887 human miRNAs annotated in the miRBase version 14. Microarray data were analysed as described in Methods. In this manner, we identified 113 mature miRNAs that were endogenously expressed at detectable levels (**Appendix II**). Next, we sought to compare miRNA expression data to

Table 3: Median-normalized linear expression levels of miRNAs that inhibited ts-O45-G transport in HeLa cells. miRNAs are listed according to their effect on cargo trafficking as in Table 1. "-" means that either miRNA was not detected by microarray and/or it did not cause any significant changes in Golgi complex morphology.

miRNA ID	Expression level	S.E.M.	Effect on Golgi complex morphology?
miR-532	-	-	-
miR-517a	-	-	Yes
miR-637	-	-	Yes
miR-517b	-	-	Yes
miR-19b	62.64	3.42	-
miR-654	-	-	-
miR-218	-	-	-
miR-210	-	-	-
miR-608	-	-	-
miR-452*	-	-	-
miR-647	-	-	-
miR-765	-	-	Yes
miR-125b	21.14	0.92	-
miR-365	7.90	0.87	-
miR-382	-	-	Yes
miR-346	-	-	-
miR-517c	-	-	Yes
miR-663	-	-	-
miR-182	-	-	-
miR-124a	-	-	-
miR-96	4.71	0.21	-
miR-604	-	-	-
miR-125a	-	-	-
miR-574	-	-	-
miR-30b	5.49	0.35	Yes
miR-483	-	-	-
miR-432	-	-	Yes
miR-553	-	-	-
miR-196b	1.64	0.07	-
miR-206	-	-	-
miR-484	-	-	-

Table 4: Expression levels of miRNAs that accelerated ts-O45-G transport rate in HeLa cells. miRNAs are listed according to their effect on cargo transport as in Table 2. "-" as in Table 3.

miRNA ID	Expression level	S.E.M.	Effect on Golgi complex morphology?
miR-128b	-	-	-
miR-34c	-	-	-
miR-29c	2.15	0.14	-
miR-197	1.41	0.06	-
miR-154	-	-	-
miR-154*	-	-	-
miR-489	-	-	-
miR-595	-	-	-
miR-20b	9.21	0.57	-
miR-297	-	-	-
miR-34a	9.06	0.49	-
miR-630	-	-	-
miR-488	-	-	-

the results of pre-miR library screening. Surprisingly, only six out of 31 miRNAs that inhibited ts-O45-G transport rate in the screening were expressed in HeLa cells (**Table 3**). Likewise, we found that only *miR-30b* was expressed endogenously of the eight miRNAs that induced significant changes in Golgi morphology (**Table 3**). In case of miRNAs that accelerated cargo transport, four out of 13 were expressed in HeLa cells (**Table 4**). Taken together, integrated data of miRNA microarray, pre-miR library screening and Golgi complex analyses indicate that the most robust cellular phenotypes are predominantly caused by miRNAs that are not endogenously expressed (**Table 3 and 4**).

To get the insight into miRNA expression dynamics under the experimental conditions used in pre-miR library screening, we measured miRNA expression levels in cells incubated for 7h at 39.5°C and either transduced or not with adenoviral vector, which encodes ts-O45-G protein. Experimental conditions are depicted in **Fig. R.11**. The analysis of miRNA expression profiles revealed a ~1.5-fold increase in global miRNA expression in HeLa cells incubated for 7h at 39.5°C (condition II) compared to the cells cultured at 37°C (condition I; data not shown). Upregulation of miRNA expression suggests the existence of temperature-dependent miRNA biogenesis and/or degradation mechanisms common to all miRNAs expressed in HeLa cells. Interestingly, Truettner and colleagues (Truettner *et al*, 2011) recently demonstrated that the expression of several rat miRNAs is significantly altered in hypothermia-treated brain. In plants, however, accumulation of miRNAs have been reported to be temperature-independent, whereas generation of endogenous anti-viral siRNAs is compromised at low temperature (Szittya *et al*, 2003). Similar to findings of Truettner and colleagues, we identified *miR-1290* and *miR-1308* which were upregulated more that other miRNAs (2.1-fold, $p<0.001$, and 2.8-fold, $p<0.001$,

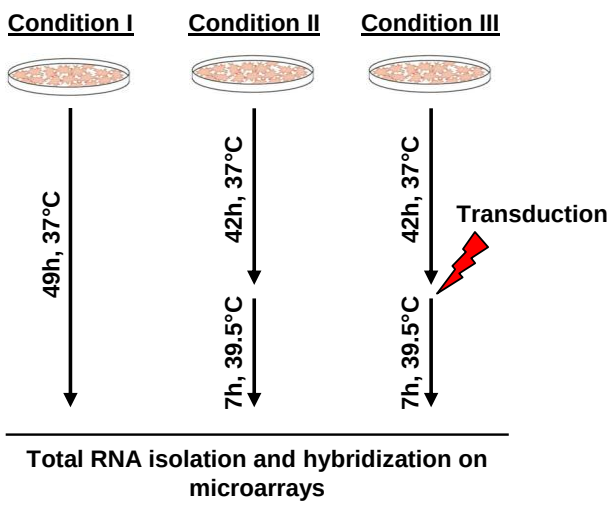

Figure R.11: Schematic representation of experimental conditions used in global miRNA expression analysis.

respesctively) in hyperthermia-treated cells, supporting a miRNA-specific response to temperature.

Next, we examined the effects of hyperthermia combined with adenoviral transduction on miRNA expression profiles (condition III). This condition exactly matched with the experimental settings used in pre-miR library screening. We compared miRNA profiles in control cells (condition I) with miRNA expression profiles in cells treated under condition III and observed a modest (~20%) increase in global miRNA expression in cells maintained under condition III (data not shown). While for the most of miRNAs this moderate increase was not statistically significant, *miR-1290* and *miR-1308* remained consistently upregulated (2-fold, $p<0.001$ and 3.1-fold, $p<0.001$, respectively).

Conclusions: Genome-wide miRNA analysis revealed 113 miRNAs that are expressed at detectable levels in HeLa cells. However, only few of them are identified as effectors in pre-miR library screening and Golgi complex analysis, supporting the hypothesis that the introduction of endogenously absent miRNAs predominantly leads to stronger cellular phenotypes compared to the overexpression of naturally transcribed miRNAs. Moreover, we demonstrated that the expression two poorly characterized miRNAs, *miR-1290* and *miR-1308*, is significantly upregulated by both hyperthermia (condition II) and hyperthermia combined with viral transduction (condition III). This highlights the need for follow-up functional studies in order to elucidate the roles of miRNAs in the adaptive cellular response to temperature changes and/or exposure to pathogens. Furthermore, future studies are required to discern the viral transduction-specific effects on the miRNA expression levels, which was not possible under the used experimental settings.

6.4. *miR-17* is a novel regulator of membrane trafficking

As described previously, *miR-17-92* cluster has been implicated in a diverse range of both physiological and pathological processes. However, to our knowledge, we provide the first experimental evidence indicating a functional interplay between members of the *miR-17* family and membrane trafficking system. *miR-17* family is composed of six miRNAs, namely, *miR-17*, *miR-20a*, *miR-20b*, *miR-93*, *miR-106a* and *miR-106b*, based on their identical seed sequence (Tanzer & Stadler, 2004). Results of our proof of principle experiments clearly showed that overexpression of four of these miRNAs leads to significantly accelerated ts-O45-G trafficking

rate (**Fig. R.2 and R.4 A**) and strongly inhibits internalization of DiI-LDL ligand (**Fig. R.3 and R.4 B**). Furthermore, we identified *miR-20b* as a hit miRNA in the pre-miR library screening (**Table 2**). Considering that miRNAs with the same seed sequences have been shown to affect almost identical sets of target genes (He *et al*, 2007), we selected *miR-17* as representative member of the miRNA family for further investigation.

6.4.1. Time-resolved gene expression profiling identifies potential targets of *miR-17*

Recent transcriptome and ribosome profiling studies revealed that miRNA-mediated decrease in protein expression can mainly be attributed to target mRNA degradation, rather than translational repression (Baek *et al*, 2008; Guo *et al*, 2010; Hendrickson *et al*, 2009). These observations led to the successful application of gene expression microarrays as a suitable tool for target identification of both endogenous and ectopically introduced miRNAs (Hanina *et al*, 2010; Selbach *et al*, 2008). Therefore, in order to identify potential *miR-17* targets which could be responsible for the observed membrane trafficking phenotypes, we performed time-resolved gene expression profiling in HeLa-CD4 cells transfected with pre-miR-17 or PNC. A time-resolved analysis was chosen to capture the temporal changes in gene expression profiles after transfection. For expression profiling we transfected HeLa-CD4 cells because they were initially used in proof of principle experiments with *miR-17*. Following total RNA isolation, gene expression profiles were anlysed on Illumina Human Sentrix-8 BeadChip® arrays containing specific probes for 25 456 annotated human transcripts. To select differently expressed genes, quantile-normalized probe intensities were compared between the pre-miR-17-tranfected and the control-transfected samples. Considering that overexpression of miRNAs in human cells causes only a modest downregulation of hundreds of transcripts (Baek *et al*, 2008; Lim *et al*, 2005; Selbach *et al*, 2008), we set a conservative expression change cutoff value of -1.5 to identify significantly downregulated genes. The cutoff value of 1.5 was applied to select upregulated genes. Using these thresholds, we identified 36 genes that were downregulated and 10 upregulated 12h after transfection; 44 genes that were downregulated and 18 upregulated 24h; and 44 genes that were downregulated and 35 upregulated 48h after transfection (**Appendix III**). Among downregulated genes, we found previously validated direct targets of *miR-17*. For example, TGF-beta receptor type-2 (*TGFBR2*; Tagawa *et al*, 2007; Volinia *et al*, 2006) was the most downregulated gene 12h and 24h after transfection (2.0-fold and 1.9-fold, respectively); Janus kinase 1 (*JAK1*; Doebele *et al*, 2010) and oligonucleotide/oligosaccharide-binding fold-

containing protein 2A (*OBFC2A*; Tan *et al*, 2009) were also significantly downregulated by overexpressed *miR-17* (**Appendix III**). Some of the known *miR-17* targets, such as *RUNX1* and *NCOA3*, were not affected in our experiment as *miR-17* has been shown to mediate their translational inhibition rather than destabilization of mRNAs (Fontana *et al*, 2007; Hossain *et al*, 2006). Importantly, almost 80% of genes downregulated 12h after transfection are predicted *miR-17* targets by at least one of the used miRNA target prediction algorithms (MicroCosm Targets v5, Diana-microT v3.0 and TargetScanHuman release 5.2) (**Appendix III**).

Among significantly downregulated genes, we found six with well-defined functions in membrane trafficking system (**Fig. R.12 A**). Surprisingly, in line with the results of DiI-LDL internalization assay, we identified *LDLR* as potentially direct targets of *miR-17*. Other downregulated membrane trafficking-related genes were as follow: *TBC1D2*, *M6PR*, *ASAP2*, *RAB32* and *NKD2*. Functionally, TBC1D2 and ASAP2 are GTPase-activating proteins (GAPs) for RAB7 GTPase (Frasa *et al*, 2010) and Arf GTPases (Andreev *et al*, 1999; Kondo *et al*, 2000),

A.

	TBC1D2	LDLR	M6PR	ASAP2	RAB32	NKD2
12h	-1.78			-1.56		
24h	-1.95		-1.53	-1.65	-1.51	
48h	-1.52	-1.64				-1.61

B.

	TBC1D2	LDLR	M6PR	ASAP2	RAB32	NKD2	miRNA seed sequence
miR-17	+	+	+	-	-	-	5'-AAAGUGC-3'
miR-20a	+	+	+	-	-	-	
miR-20b	+	+	+	-	-	-	
miR-93	+	+	+	-	-	-	
miR-106a	+	+	+	-	-	-	
miR-106b	+	+	+	-	-	-	
miR-18a	-	-	-	-	-	-	5'-AAGGUGC-3'
miR-18b	-	-	-	-	-	-	
miR-92a	-	-	-	-	-	-	5'-AUUGCAC-3'
miR-25	-	-	-	-	-	-	
miR-363	-	-	-	-	-	-	
miR-19a	-	+	+	+	-	-	5'-GUGCAAA-3'
miR-19b	-	+	+	+	-	-	

Figure R.12: Microarray-based identification of potential *miR-17* target genes. (A) Overexpression of *miR-17* significantly downregulated the expression of six genes that are known regulators of membrane trafficking system. Expression fold changes (linear scale) are given. Grey squares represent situations when the observed fold change was lower than the cutoff value of -1.5 **(B)** Computational prediction of *TBC1D2*, *LDLR*, *M6PR*, *ASAP2*, *RAB32* and *NKD2* genes as potential targets of miRNAs encoded by *miR-17-92*, *miR-106b-25* and *miR-106a-363* clusters. Prediction by at least one of three algorithms (MicroCosm Targets, Diana-microT and TargetScanHuman) was considered as valid. miRNAs are grouped according to their seed sequences.

respectively. Cation-independent mannose-6-phosphate receptor (M6PR) is involved in the transport of soluble hydrolases from the *trans*-Golgi to lysosomes (Stein *et al*, 1987). RAB32 GTPase is implicated in the trafficking of melanogenic enzymes from the *trans*-Golgi network to the premature melanosomes (Wasmeier *et al*, 2006). It is also required for mitochondrial fission (Alto *et al*, 2002). Naked cuticle homolog 2 protein (NKD2) mediates the delivery of TGF-α-loaded vesicles to the basolateral membrane in polarized MDCK cells (Li *et al*, 2007).

To investigate whether these genes can be direct targets of *miR-17*, we next performed a computational miRNA target prediction analysis using the three previously mentioned prediction algorithms. We found that *TBC1D2*, *LDLR* and *M6PR* are predicted *miR-17* targets by at least one of the prediction approaches (**Fig. R.12 B**). Additionally, we examined whether these genes are predicted targets for other miRNAs encoded by paralogous *miR-17-92*, *miR-106b-25* and *miR-106a-363* clusters. As anticipated, *TBC1D2*, *LDLR* and *M6PR* are predicted targets not only for *miR-17*, but also for other *miR-17* family members (**Fig. R.12 B**). Conversely, *TBC1D2*, *LDLR* and *M6PR* are not among potential targets of miRNAs belonging to *miR-18* or *miR-92* families. Importantly, prediction tools suggested *LDLR*, *M6PR* and *ASAP2* as potential targets of *miR-19* family miRNAs. Although modulation of *miR-19a* activity had no effect on Dil-LDL internalization, *miR-19a* overexpression significantly inhibited ts-O45-G transport in proof of principle experiments. Moreover, *miR-19b* was a strong inhibitor of cargo transport in pre-miR library screening. Taken together, all these findings provide a solid basis for follow-up studies to investigate the role of *miR-19* family in biosynthetic membrane trafficking.

Prediction algorithms indicated that *TBC1D2*, *LDLR* and *M6PR* mRNAs have one, four and three potential *miR-17* binding sites in their 3´UTRs, respectively (**Table 6**). We next searched for motifs complementary to the seed of *miR-17* in the selected mRNAs and uncovered one additional putative *miR-17* interaction site in the 3´UTR of *LDLR* and four sites in *ASAP2* mRNA: three in the coding sequence and one in the 3´UTR (**Table 6**). These binding sites were "overlooked" by all three prediction tools, most probably because algorithms explore only 3´UTRs of the transcripts and/or require particular site conservation features for the valid prediction of potential miRNA binding site (Alexiou *et al*, 2009).

In summary, integration of gene expression profiling, computational target prediction and mRNA sequence analyses provided us with four membrane trafficking-related genes that are potential direct targets of *miR-17* or other family members.

TBC1D1	3´UTR 247-255	5'	...CACCUCUUCCACAGAGCACUUUG...	3'
	miR-17	3'	GAUGGACGUGACAUUCGUGAAAC	5'
LDLR	3´UTR 815-821	5'	...UCCCGUGGUCUCCUUGCACUUUC...	3'
	miR-17	3'	GAUGGACGUGACAUUCGUGAAAC	5'
	3´UTR 1153-1159	5'	...ACGCCUGUAAUCCCAGCACUUUG...	3'
	miR-17	3'	GAUGGACGUGACAUUCGUGAAAC	5'
	3´UTR 1629-1635	5'	...ACGCCUGUAAUCCCAGCACUUUG...	3'
	miR-17	3'	GAUGGACGUGACAUUCGUGAAAC	5'
	3´UTR 2163-2169	5'	...UUUUUUGUUAUGUUUGCACUUUG...	3'
	miR-17	3'	GAUGGACGUGACAUUCGUGAAAC	5'
	3´UTR 2425-2430	5'	...UCUGGGAGAUGGGUGUCACUUUU...	3'
	miR-17	3'	GAUGGACGUGACAUUCGUGAAAC	5'
M6PR	3´UTR 3-9	5'	...UUGCACUUUA...	3'
	miR-17	3'	GAUGGACGUGACAUUCGUGAAAC	5'
	3´UTR 792-798	5'	...CCAGAAAAGGGAAGUCACUUUA...	3'
	miR-17	3'	GAUGGACGUGACAUUCGUGAAAC	5'
	3´UTR 899-905	5'	...AUUUCUAAACAUGUCGCACUUUC...	3'
	miR-17	3'	GAUGGACGUGACAUUCGUGAAAC	5'
ASAP2	CDS 327-334	5'	...ACAAAGGAGUUGACAGCACUUUU...	3'
	miR-17	3'	GAUGGACGUGACAUUCGUGAAAC	5'
	CDS 1126-1131	5'	...ACAUGACAGAACUUACCACUUUC...	3'
	miR-17	3'	GAUGGACGUGACAUUCGUGAAAC	5'
	CDS 3003-3009		CCCGGUGUCAUUUGUGCACUUUA...	3'
	miR-17	3'	GAUGGACGUGACAUUCGUGAAAC	5'
	3´UTR 1068-1073	5'	...AUACUCCCAAACAUCCCACUUUU...	3'
	miR-17	3'	GAUGGACGUGACAUUCGUGAAAC	5'

Table 6: Potential *miR-17* binding sites in *TBC1D2*, *LDLR*, *M6PR* and *ASAP2* mRNAs. *miR-17* binding sites identified by search of seed binding motifs are marked in grey, whereas others are predicted by one of the target prediction tools.

6.4.2. Analysis of potential *miR-17* targets as regulators of membrane trafficking

Having identified the potential *miR-17* binding sites in *TBC1D2*, *LDLR*, *M6PR* and *ASAP2* mRNAs, we further addressed the question whether or not these genes are functionally relevant to the *miR-17*-mediated membrane trafficking phenotypes. To this end, we performed DiI-LDL internalization and ts-O45-G transport assays following transfection with gene-specific siRNAs in order to mimic *miR-17* overexpression. We reasoned that, if *miR-17* induces trafficking phenotypes by downregulating these genes, the same effects should be at least partially reproduced by siRNA-mediated RNAi of biologically relevant targets. Functional assays were performed with two different siRNAs per gene, with a single siRNA used per well. Phenotypic effects caused by individual siRNAs were normalized to control siRNA and results of the most effective siRNA are presented.

As shown previously, knockdown of *LDLR* significantly reduced cellular DiI-LDL uptake. Moreover, we also observed a considerably reduced amount of internalized DiI-LDL in *TBC1D2* and *M6PR* siRNA-transfected cells (**Fig. R.13 A and B**), indicating that these genes are actively involved in cellular uptake, trafficking and/or degradation of DiI-LDL.

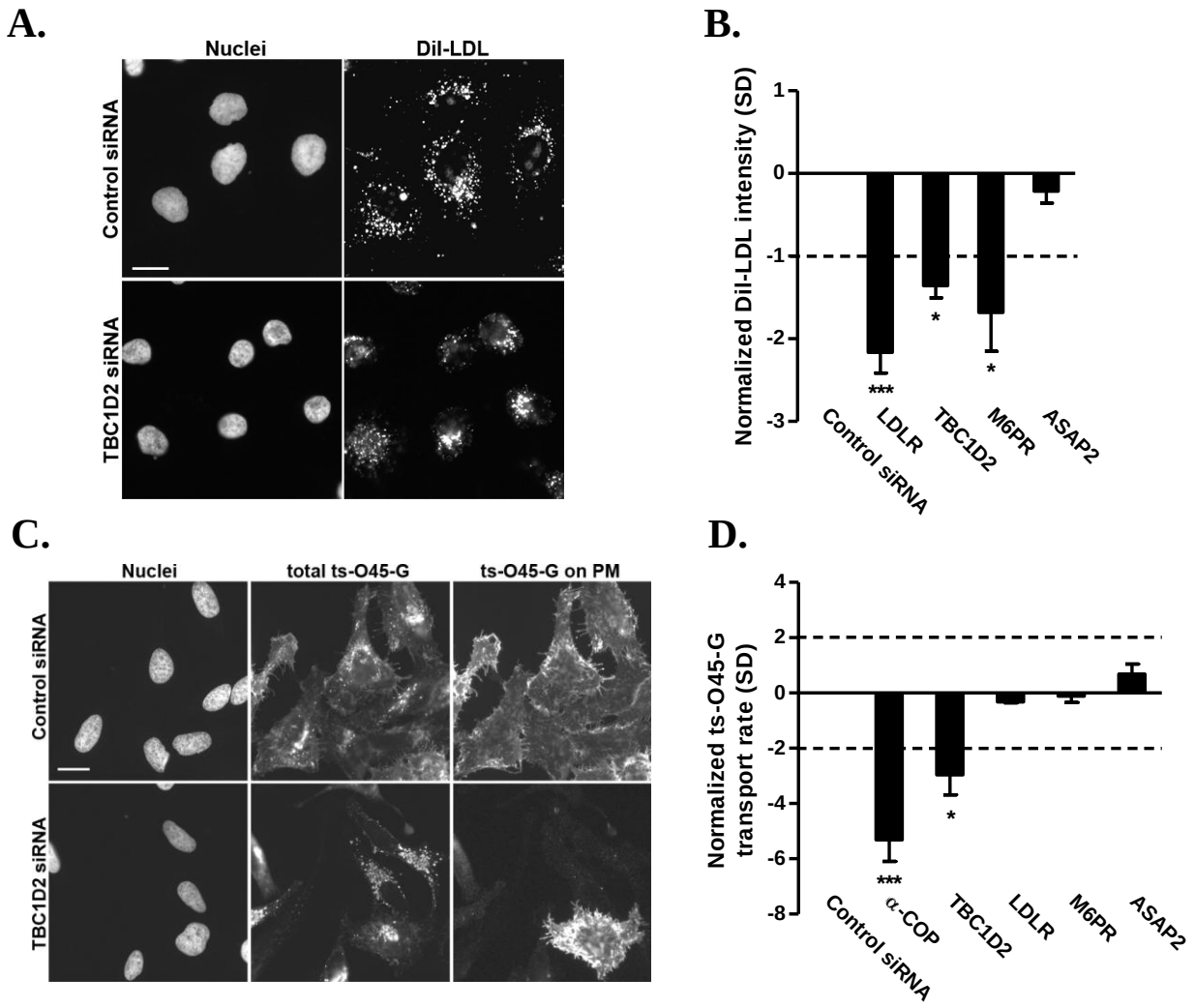

Figure R.13: Knockdown of potential *miR-17* targets inhibits DiI-LDL internalization and ts-O45-G transport. (**A**) Representative images of DiI-LDL internalization assay in HeLa cells transfected with control siRNA (upper row) or siRNA against *TBC1D2* (lower row). (**B**) Quantification of internalized DiI-LDL fluorescence intensity in cells transfected with indicated siRNAs on 8-well µ-slides. (**C**) Representative images of ts-O45-G transport assay in HeLa cells transfected as in (A). (**D**) Quantification of ts-O45-G transport rate in cells transfected with indicated siRNAs on 8-well µ-slides. Data of both assays were normalized to control siRNA samples as described in Methods. Results are represented as means of normalized DiI-LDL intensity values (B) or mean values of normalized ts-O45-G transport rates (D) from at least three independent experiments ($n \geq 3$) ± S.E.M. *, $p<0.05$; ***, $p<0.001$. Scale bars represent 20 µm. PM, the plasma membrane.

We next examined whether the *miR-17*-mediated changes in ts-O45-G trafficking rate are associated with downregulation of *TBC1D2*, *LDLR*, *M6PR* and *ASAP2*. We performed a ts-O45-G transport assay in cells transfected with siRNAs against each of these potential *miR-17* targets. Quantification of ts-O45-G transport assay revealed that RNAi of *TBC1D2* significantly inhibited

cargo trafficking 48h after transfection, whereas knockdown of other three genes had no significant effect (**Fig. R.13 C and D**). This experiment confirms an active regulatory role of TBC1D2 in ts-O45-G progression through the biosynthetic system, however, the siRNA-mediated RNAi resulted in an opposite cargo trafficking phenotype to the one observed upon overexpression of *miR-17*.

Together, these results confirmed that *TBC1D2*, *LDLR* and *M6PR* genes play an active role in membrane trafficking. Specifically, knockdown of these genes significantly reduced cellular DiI-LDL uptake, further suggesting that they may contribute to *miR-17*-mediated effect on endocytosis.

6.4.3. Validation of novel *miR-17* targets *TBC1D2* and *LDLR*

Previous studies have shown that TBC1D2 acts as GAP for RAB7, which is involved in late endocytic trafficking and lysosomal biogenesis (Bucci *et al*, 2000; Chavrier *et al*, 1990; Frasa *et al*, 2010). LDLR is a key player in maintaining balanced blood cholesterol level since it interacts with and internalizes LDL-cholesterol ester conjugates into cell via endocytosis machinery (Brown & Goldstein, 1986; Yamada *et al*, 1986). Moreover, numerous mutations in *LDLR* have been identified leading to familial hypercholesterolemia, a genetic disorder characterized by very high level of LDL conjugates in the plasma (Hobbs *et al*, 1992). Based on this knowledge, computational *miR-17* target prediction and our experimental data, we considered *TBC1D2* and *LDLR* as the most relevant genes that account for the *miR-17*-mediated effects on DiI-LDL internalization. To determine whether *miR-17* can directly interact with and repress *TBC1D2* and *LDLR* mRNAs via the predicted binding sites in their 3´UTRs, we constructed luciferase reporter vectors containing the *Renilla* luciferase gene fused to the full-length *TBC1D2* (~0.35kb) or *LDLR* (~2.5kb) 3´UTRs. Co-transfection of reporters with pre-miR-17 resulted in a significant reduction of luciferase activity compared to reporter vectors co-transfected with PNC. This indicates that *miR-17* inhibits *TBC1D2* and *LDLR* mRNA expression by binding directly to their 3´UTRs. Conversely, inhibition of *miR-17* by anti-miR-17 substantially increased luciferase expression from both *TBC1D2* and *LDLR* reporter vectors (**Fig. R.14 A and B**). Together, these results validate a functional interplay between *TBC1D2* and *LDLR* mRNAs and *miR-17*.

Since *TBC1D2* mRNA contains a single predicted binding site for *miR-17* in its 3´UTR, we next generated TBC1D2_Mut and TBC1D2_Del luciferase reporter vectors by mutating *miR-*

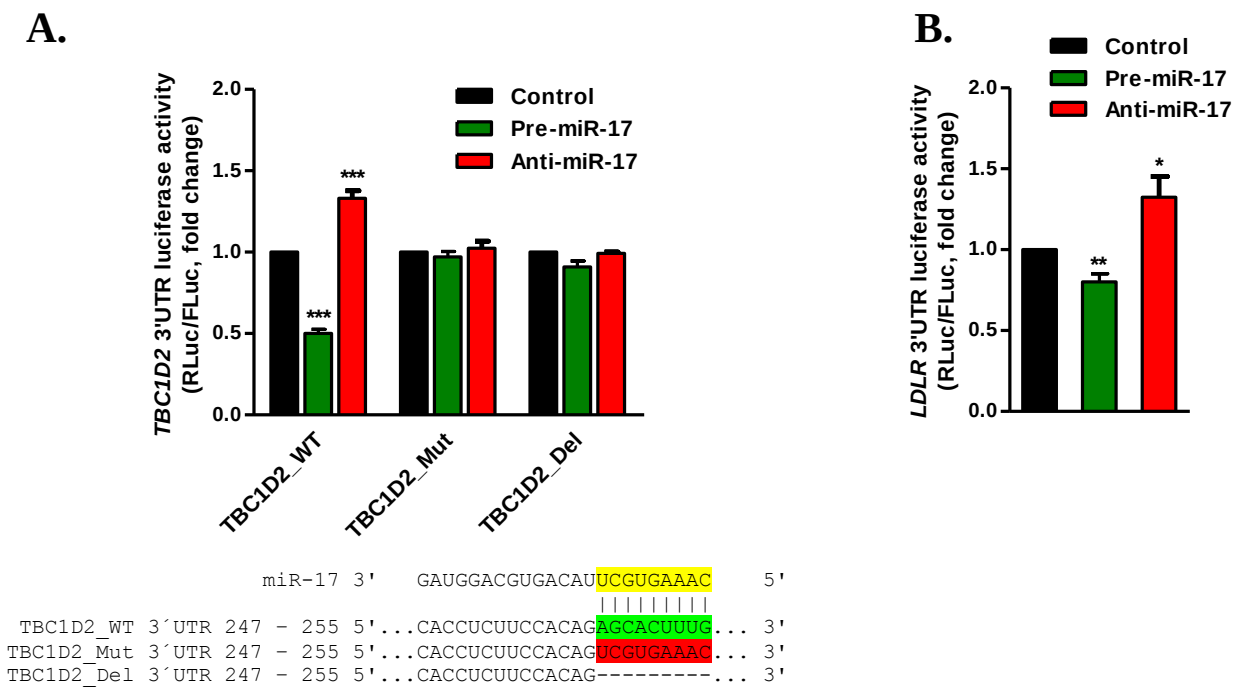

Figure R.14: *miR-17* binds directly to the 3´UTRs of *TBC1D2* and *LDLR* mRNAs. (**A and B**) *miR-17* binds to the 3'UTRs of *TBC1D2* and *LDLR* mRNAs, as determined by luciferase reporter assay. HeLa cells were co-transfected with *TBC1D2* (A) or *LDLR* (B) reporters and indicated oligonucleotides. Mutation (TBC1D2_Mut) or deletion (TBC1D2_Mut) of predicted *miR-17* binding site in the 3´UTR of *TBC1D2* rendered reporters inert to both overexpression and inhibition of *miR-17*. Luciferase activity was measured 24h following co-transfections. Controls indicate the luciferase expression in cells co-transfected with reporter vectors and PNC or ANC. Values represent mean fold changes of *Renilla* luciferase activity in relation to respective control from three experiments (n = 3) ± S.E.M.

17 binding site into anti-complementary sequence or deleting it, respectively (**Fig. R.14 A**). In contrast to the wild-type *TBC1D2* reporter (TBC1D2_WT), these specific mutations completely abolished the response of TBC1D2_Mut and TBC1D2_Del reporters to both overexpression and inhibition of *miR-17*, confirming a functionally active *miR-17* binding site in the 3´UTR of *TBC1D2* mRNA (**Fig. R.14 A**).

In a more biologically relevant experimental setup, we next assayed the potency of *miR-17* to modulate the levels of endogenous *TBC1D2* and *LDLR* mRNAs. Towards this, we performed a qRT-PCR analysis 12h, 24h and 48h after overexpression of *miR-17*. siRNAs targeting *TBC1D2* and *LDLR* mRNAs were used as positive controls. Consistent with microarray data, we observed that overexpression of *miR-17* decreased *TBC1D2* mRNA level around 50% compared to PNC at all three time points measured (**Fig. R.15 A**). Importantly, transfection with *TBC1D2* siRNA led to the same knockdown efficiency as *miR-17* overexpression. Analysis of *LDLR* mRNA revealed that transfection with pre-miR-17 also reduced *LDLR* mRNA level to the

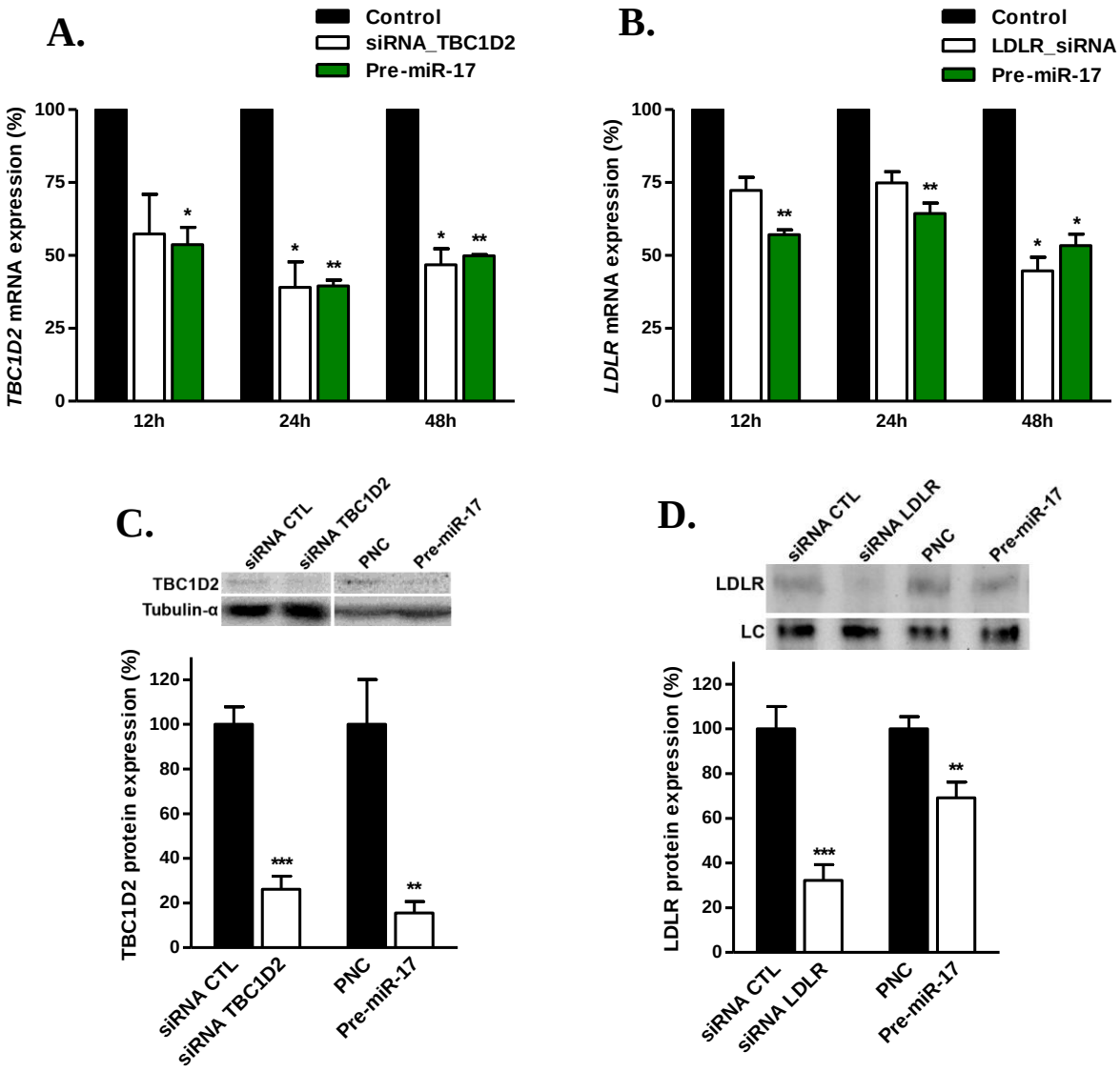

Figure R.15: *miR-17* inhibits the expression of *TBC1D2* and *LDLR* mRNAs and reduces protein levels. (A and B) Overexpression of *miR-17* decreases the expression levels of both *TBC1D2* (A) and *LDLR* (B) mRNAs as determined by qRT-PCR. Expression of *TBC1D2* and *LDLR* mRNAs was normalized against *GAPDH* mRNA level. Results are represented as mean mRNA expression values from two independent experiments (n = 2) ± S.E.M. **(C)** Western blot analysis of TBC1D2. Representative western blot of TBC1D2 (120kDa) and tubulin-α (55kDa) proteins in lysates of HeLa cells transfected with indicated oligonucleotides for 48h. TBC1D2 protein expression levels were normalized against tubulin-α, which served as a loading control in this experiment. **(D)** Western blot analysis of LDLR. Representative western blot of LDLR protein (130kDa) in lysates of HeLa cells transfected with indicated oligonucleotides. A cross-reacting band of the anti-LDLR antibody was used as loading control (LC, ~63kDa). Results are represented as normalized mean values of relative protein levels from at least three independent experiments (n ≥ 3) ± S.E.M. Relative expression levels of *TBC1D2* and *LDLR* mRNAs and proteins in siRNA- or pre-miR-17-transfected cells were normalized against the respective controls (*TBC1D2* and *LDLR* siRNAs to control siRNA, pre-miR-17 to PNC). *, $p<0.05$; **, $p<0.01$; ***, $p<0.001$.

same extent as *LDLR* siRNA (**Fig. R.15 B**). In line with observations that miRNAs predominantly induce target destabilization (Baek *et al*, 2008; Guo *et al*, 2010), our findings independently demonstrate that *miR-17* significantly reduces *TBC1D2* and *LDLR* mRNA levels.

Finally, we aimed to determine the extent to which expression of TBC1D2 and LDLR proteins is affected by overexpression of *miR-17*. Western blot analyses confirmed that both TBC1D2 and LDLR protein levels were significantly decreased 48h after transfection with pre-miR-17 (**Fig. R.15 C and D**). Like in the qRT-PCR experiments, siRNAs against *TBC1D2* and *LDLR* were used as positive controls. While *miR-17* reduced TBC1D2 level to the same extent as did specific *TBC1D2* siRNA (**Fig. R.15 C)**, overexpression of *miR-17* led to around 30% decrease of LDLR protein compared to around 60% reduction induced by *LDLR* siRNA (**Fig. R.15 D)**.

In summary, our combined results of luciferase reporters, mRNA and protein measurements validated that *TBC1D2* and *LDLR* are novel direct targets of *miR-17*. Furthermore, we confirmed the functionality of predicted *miR-17* binding sites in 3´UTRs of *TBC1D2* and *LDLR* mRNAs. We also demonstrated that single *miR-17* binding motif is necessary and sufficient to exert the miRNA-mediated regulation on *TBC1D2* mRNA. Finally, we showed that *miR-17*-mediated *TBC1D2* and *LDLR* gene silencing is significant on both mRNA and protein levels.

Conclusions: In order to identify potential targets of *miR-17*, we performed microarray-based gene expression profiling in cells transfected with pre-miR-17. Among downregulated, we found transcripts of *TBC1D2*, *LDLR*, *M6PR*, *ASAP2*, *RAB32* and *NKD2* genes. With the siRNA-mediated RNAi we demonstrated that single knockdowns of *TBC1D2*, *LDLR*, *M6PR* phenocopy *miR-17*-mediated effect on cellular DiI-LDL internalization. The results of luciferase reporter, qRT-PCR and western blot analyses confirmed that *TBC1D2* and *LDLR* are novel functional targets of *miR-17*. Further studies are needed to identify functionally relevant *miR-17* targets which are responsible for the miRNA-governed acceleration of ts-O45-G transport to the plasma membrane.

6.5. Time-resolved gene expression profiling upon expression of *miR-517a*

Members of the *miR-517* family, namely, *miR-517a*, *miR-517b* and *miR-517c*, were among the strongest ts-O45-G transport inhibitors in pre-miR library screening (**Table 1**). Moreover, biosynthetic transport phenotypes were associated with significant fragmentation of Golgi complex induced by all three family members (**Fig. 10**). Despite recently identified oncogenic role of *miR-517a* in progression of hepatocellular carcinoma (Toffanin *et al*, 2011), the functions of this miRNA family remain elusive. Previous studies have shown that *miR-517* family miRNAs are encoded in the largest human miRNA cluster *C19MC*; this cluster contains 46 primate-specific miRNA genes that ultimately yields up to 59 mature miRNAs (Borchert *et al*, 2006). *C19MC* cluster is mainly, if not exclusively, transcribed in undifferentiated tissues including placenta, human hematopoietic and embryonic stem cells (Bar *et al*, 2008; Laurent *et al*, 2008; Ren *et al*, 2009). Since all three *miR-517a*/*b*/*c* have identical seed sequence (5´-UGCACGA-3´) and were among the strongest effectors in our assays, we sought to investigate further this miRNA family. We selected *miR-517a* as representative member of the family on a basis of more pronounced phenotypic effects compared to other two miRNAs.

Similar to gene expression profiling with *miR-17*, we performed a time-resolved microarray analysis in order to identify potential *miR-517a* target genes that are functionally relevant to membrane trafficking. Total RNA was isolated from HeLa cells 12h, 24h and 48h after transfection with pre-miR-517a or PNC. Gene expression profiles were analysed on HumanHT-12 v4 BeadChip® arrays (Illumina) containing probes for 48 107 transcripts derived from RefSeq Release 38. The microarray data of the pre-miR-517a-transfected samples were compared to the PNC-transfected samples as decribed in Methods. In contrast to a relatively low number of *miR-17*-affected transcripts, we found that substantially more mRNAs were deregulated by *miR-517a* (**Table 7, Appendix IV**).

Table 7: Number of transcripts affected 12h, 24h and 48h after transfection with pre-miR-517a. Expression fold change cutoff values of -1.5 and 1.5 (in linear scale) corresponding to an adjusted p-value ≤ 0.01 were used as criteria to identify significantly downregulated and upregulated genes, respectively.

	Down-regulated	Up-regulated
12h	83	51
24h	360	379
48h	978	1111

We next aimed to determine how many affected genes have known functions in regulation of membrane trafficking. To this end, we first compiled a list of human genes that were directly annotated to the Gene Ontology (GO) terms of "Protein transport" (GO:0015031), "Endocytosis" (GO:0006897) and "Protein secretion" (GO:0009306) by two independent databases, namely, AmiGO and Ensembl. The list of 617 unique genes was then compared with genes affected upon expression of *miR-517a*. Comparative analysis revealed that 32 genes associated with membrane trafficking were significantly downregulated by *miR-517a* (**Appendix V A**). Interestingly, we found more (72) trafficking-related genes among upregulated by *miR-517a* (**Appendix V B**). The following computational miRNA target prediction analysis (MicroCosm Targets, Diana-microT and TargetScanHuman algorithms) indicated that among 32 downregulated genes, *AP1S2*, *ATG10*, *HRAS*, *INPPL1*, *NUPL2* and *LDLR* are potential direct targets of *miR-517a*. Among upregulated membrane trafficking-associated genes, only *GOLT1B* and *NUP35* were predicted as *miR-517a* targets. Strikingly, we have previously validated *LDLR* as a novel functional target of *miR-17*, suggesting an active post-transcriptional *LDLR* expression regulation by both *miR-17* and *miR-517a*.

Besides *LDLR*, integration of gene expression profiling data uncovered relatively few downregulated genes with direct functions in membrane trafficking (**Table 8**). For example, *AP1S2* encodes subunit sigma-2 of AP-1 adaptor complex, which is implicated in the formation of clathrin-coated vesicles at *trans*-Golgi network (TGN) and involved in TGN-to-endosome traffic (Robinson, 2004). Previous studies have reported that siRNA-mediated knockdown of *AP1S2* stimulates DiI-LDL uptake, but inhibits transferrin internalization in HeLa cells (Bartz *et al*, 2009), suggesting an active role of *miR-517a* also in endocytosis. The TGN-localized ADP-ribosylation factor (ARF3) is involved in the assembly of COPI and clathrin coat complexes onto budding vesicles, however, *ARF3* knockdown does not alter biosynthetic ts-O45-G transport to the plasma membrane and has no effect on the TGN morphology (Manolea *et al*, 2010; Volpicelli-Daley *et al*, 2005). Therefore, *miR-517a*-induced phenotypes are unlikely to be explained by direct targeting of *ARF3* mRNA. We also identified a group of poorly characterized Rab GTPase genes (*RAB26*, *RAB35*, *RAB40B* and *RAB40C*) that were significantly downregulated throughout the 48h expression profiling experiment.

Table 8: List of representative membrane trafficking-related genes that were downregulated in pre-miR-517a-transfected HeLa cells. Genes are listed alphabetically.

Number	Gene symbol	Fold-change			Predicted target?	Gene accession number
		12h	24h	48h		
1	AP1S2	-2.21	-2.31	-2.02	Yes	NM_003916.3
2	ARF3		-1.53			NM_001659.1
3	LDLR			-1.99	Yes	NM_000527.2
4	RAB26		-1.75	-2.98		NM_014353.4
5	RAB35	-1.74		-1.57		NM_006861.4
6	RAB40B	-1.95	-2.77	-2.95		NM_006822.1
7	RAB40C	-1.74	-1.53			NM_021168.2

Among upregulated membrane trafficking-related genes (**Table 9**), we found *COG3*, *COG5* and *COG6* genes encoding three subunits of the conserved oligomeric Golgi (COG) tethering complex that is essential for establishing and maintaining the normal structure and function of the Golgi apparatus (Ungar *et al*, 2002; Ungar *et al*, 2005). The transfection with pre-miR-517a also increased the expression of well-described genes like *ARF1*, *ARF4*, *ARFGAP1*, *ARFGAP3*, *COPE* that either play regulatory roles in the formation of protein transport vesicles on the Golgi membrane or encode structural components of these vesicles (Donaldson & Jackson, 2011; Hsu & Yang, 2009; Yang *et al*, 2002; Kartberg *et al*, 2010). YIP family member 5, (YIPF5, also known as YIP1A) co-localizes with COPII coatomer components SEC31A and SEC13 at ER exit sites (ERES). Moreover, overexpression of N terminus of YIPF5 blocks ER-Golgi transport of ts-O45-G and induces fragmentation of the Golgi complex (Stagg *et al*, 2006; Tang *et al*, 2001). Several genes of well-characterized Rab GTPases, including RAB5A that regulates early steps in endocytosis, RAB6A that acts on intra-Golgi transport, RAB8A that mediates anterograde transport from the TGN to the plasma membrane and RAB22 that controls bi-directional vesicular trafficking between the TGN and the early endosomes (Hutagalung & Novick, 2011) were among upregulated by *miR-517a*.

A number of recent bioinformatics studies have proposed the existence of mutual regulatory networks between miRNAs and transcription factors (TFs). The TFs seem to regulate miRNA, or to be regulated by the miRNA, forming a range of diverse feed-forward loops (Martinez & Walhout, 2009; Shalgi *et al*, 2007; Tran *et al*, 2010; Tu *et al*, 2009). Consistently, experimental evidence indicate that some transcription regulators, which are targets of miRNAs, can exert both positive and negative transcription regulation (van Rooij *et al*, 2007). Considering that the majority of membrane trafficking-related genes were upregulated only at 48h after transfection, we speculate that most of the functionally relevant genes to exert *miR-517a*-

mediated phenotypes are secondary targets of this miRNA. However, the structure of *miR-517a*-governed regulatory networks remains to be identified in future studies.

Table 9: List of representative membrane trafficking-related genes that were upregulated in pre-miR-517a-transfected HeLa cells. Genes are listed alphabetically.

Number	Gene symbol	Fold-change			Predicted target?	Gene accession number
		12h	24h	48h		
1	ARF1			1.87		NM_001024228.1
2	ARF4			2.71		NM_001660.2
3	ARFGAP1		2.11	3.43		NM_018209.2
4	ARFGAP3		1.62	2.06		NM_014570.3
5	COG3			2.04		NM_031431.2
6	COG5			2.17		NM_006348.2
7	COG6			2.22		NM_020751.1
8	COPE			1.62		NM_199442.1
9	RAB18			1.57		NM_021252.3
10	RAB22A		2.25	2.14		NM_020673.2
11	RAB32			1.74		NM_006834.2
12	RAB5A			1.54		NM_004162.3
13	RAB6A			1.83		NM_198896.1
14	RAB8B	2.21	2.26	2.81		NM_016530.2
15	SEC31A			2.02		NM_014933.2
16	YIPF5		1.77	2.32		NM_030799.6

Conclusions: In order to identify potential targets of *miR-517a*, we performed a microarray-based gene expression profiling in HeLa cells transfected with pre-miR-517a. Bioinformatics analysis of microarray data yielded a set of genes with previously described functions in membrane trafficking, however, their functional interactions with *miR-517a* remains to be identified in future studies.

6.6. Bioinformatics analysis of *miR-17* and *miR-517a* microarray data

The most compelling evidence that the downregulated transcripts are direct miRNA targets is the presence of miRNA binding sites in their 3´UTRs (Grimson *et al*, 2007; Lim *et al*, 2005). Therefore, we sought to investigate whether the transcripts downregulated upon overexpression of *miR-17* and *miR-517a* are enriched in the potential binding motifs for these miRNAs. In other words, this analysis addressed the question whether the downregulated transcripts are direct targets of the respective miRNA. For this purpose, we employed a Sylamer algorithm (van Dongen *et al*, 2008) to perform an unbiased analysis for overrepresented nucleotide motifs in 3´UTRs of the transcripts affected by *miR-17* or *miR-517a*. Sylamer

algorithm determines over- or underrepresented nucleotide motifs in a ranked transcript list and assigns the $\log_{10}$-transformed enrichment p-value to each of tested motifs (van Dongen *et al*, 2008). Therefore, prior to analysis, we ranked all transcripts analysed *miR-17* or *miR-517a* microarray experiments from the most downregulated to the most upregulated according to their expression fold change values. Using a word size of seven nucleotides, Sylamer identified significantly overrepresented motifs in both miRNA overexpression experiments at all three time points (**Fig. R.16**). For *miR-17* 12h experiment, the enrichment curve of seven nucleotides GCACUUU ($p<1 \times 10^{-27}$), which are complementary to the seed region of *miR-17* (positions 2-8), was peaking approximately at transcript 1 500 in the ranked list (**Fig. R.16 A**). This indicates that the set of approximately 1 500 most downregulated transcripts, located to the left of the significance peak, were significantly enriched for *miR-17* binding sites in relation to the remaining transcripts. In turn, this suggests that these transcripts are likely direct targets of *miR-17*. Consistent with observations by Grimson and colleagues (Grimson *et al*, 2007), the overrepressented motif corresponds to a canonical 7mer-m8 type of miRNA binding sites.

Analysis of *miR-517a* microarray data indicated three different heptamers with very similar enrichment patterns across all time points, especially at 12h (**Fig. R.16 D-F**). All three motifs contained the core hexamer (GCACGA) complementary to the seed sequence of *miR-517a*. Like in case of *miR-17*, the hexamer flanked by additional complementary nucleotide at its 5´ end (UGCACGA, 7mer-m8 type of binding site) was the most significantly overrepresented motif among the *miR-517a*-downregulated mRNAs. We also observed the enrichment of other two closely related heptamers GCACGAU (complementary to positions 1-7 of *miR-517a*) and GCACGAA (7mer-A1 type, hexamer seed match augmented by an A at target position 1). The enrichment of these two motifs indicates that nucleotides outside the minimal seed region (hexamer GCACGA) are less important for *miR-517a* to induce target degradation; the enrichment of single motif in *miR-17*-deregulated transcripts suggests that only the presence of this motif permits the destabilization of *miR-17*-bound transcripts. This observation might partially explain why *miR-517a* deregulates much more transcripts than *miR-17* when tranfected to cells.

In case when stringent expression change cutoff values are applied to select differently expressed transcripts, secondary miRNA-mediated effects are usually considered to occur later than 24h after transfection with exogenous miRNA (Tu *et al*, 2009). Consistently, our Sylamer analysis of *miR-17* and *miR-517a* microarray data resulted in a broader motif enrichment profiles 48h after transfection with respective pre-miRs (**Fig. R.16 C and F**) compared to the data

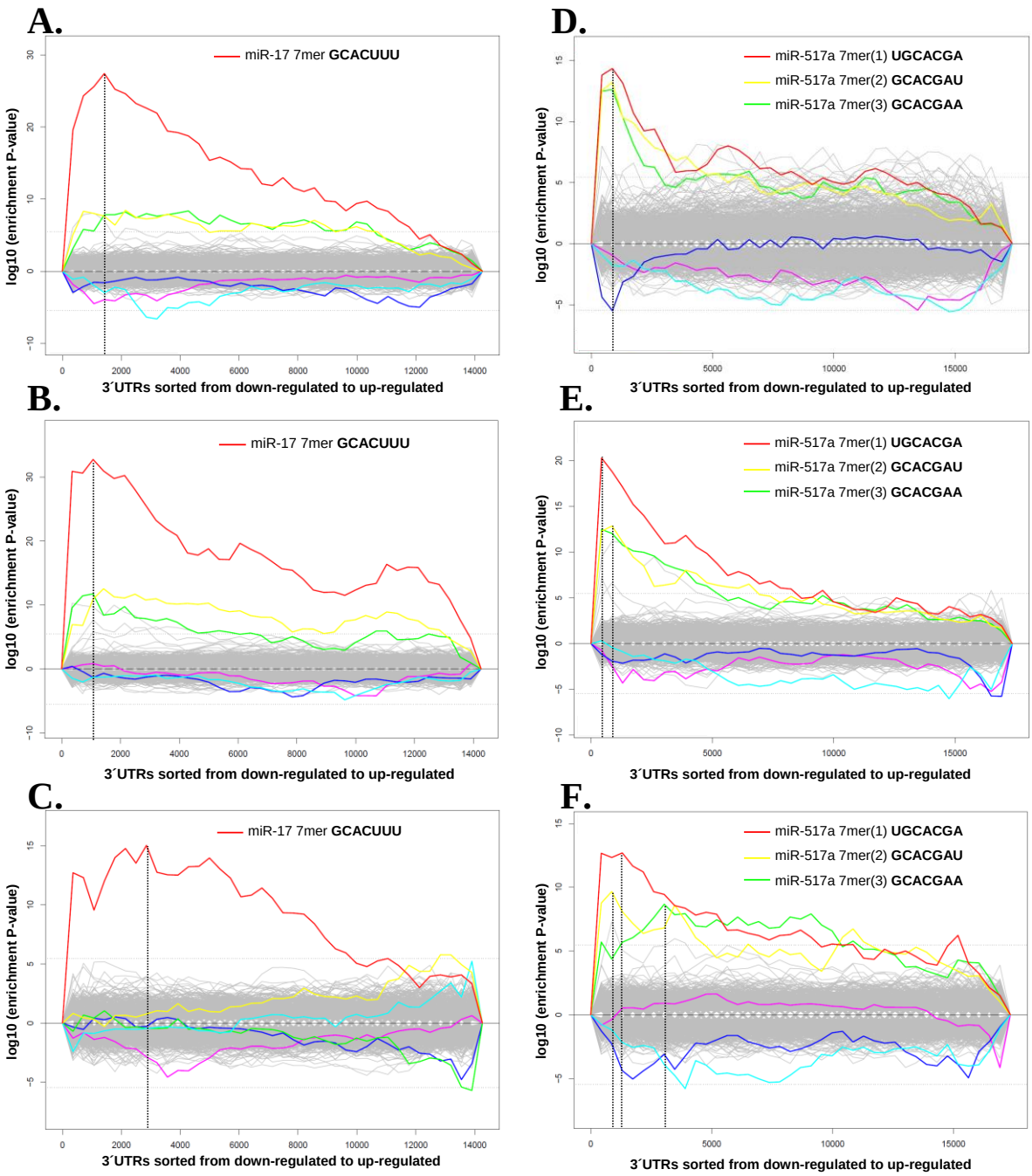

Figure R.16: Motif enrichment analysis of *miR-17* and *miR-517a* microarray data. (**A-C**) Motif enrichment landscape plots of *miR-17* microarray data 12h (**A**), 24h (**B**) and 48h (**C**) after transfection. (**D-F**) Motif enrichment landscape plots of *miR-517a* microarray data 12h (**D**), 24h (**E**) and 48h (**F**) after transfection. The *x* axes represent the sorted gene list from most downregulated (left) to most upregulated (right). Positive values on *y* axes indicate enrichment and negative values, depletion for each tested motif. The horizontal dotted lines indicate a multiple-testing *E*-value (Bonferroni-corrected) threshold of 0.01, whereas vertical dotted lines show significance peaks across the gene list for a given word. Coloured lines represent three most enriched and three most depleted motifs. Heptamers complementary to the seed regions of miRNAs of interest are represented in each plot. Significance peaks observed below *E*-value threshold are not considered as statistically significant.

from earlier time points. This type of motif enrichment profiles, peaking closer to the middle of the sorted transcript list, potentially represents situations when secondary miRNA targets compose a large fraction of the affected transcripts and thereby dilute the significance of motif enrichment (van Dongen *et al*, 2008).

To test this hypothesis with our microarray data, we selected sets of downregulated and upregulated transcripts with a fold change higher or equal to 1.5 at each time point and searched for *miR-17* and *miR-517a* binding sites in their 3´UTRs. Analysing *miR-17* microarray data, we found GCACUUU motif at least once in 76% of the 3´UTRs of the transcripts downregulated 12h after transfection. For comparison, the same heptamer was found only in 19% of all annotated human 3´UTRs (**Fig. R. 17 A and B**, background rate). In contrast to 12h time point, the frequency of *miR-17* binding sites in the 3´UTRs of transcripts downregulated at 48h was similar to the background rate. As anticipated, we found the intermediate frequency of GCACUUU heptamer at 24h time point (**Fig. R.17 A**). Analysis of the 3´UTRs of transcripts downregulated by *miR-517a* revealed similar trend of *miR-517a* binding site UGCACGA frequencies over the experimental period (**Fig. R.17 C**). Taken together, these results confirmed that the majority of the downregulated transcripts at early time points are most likely direct targets of *miR-17* or *miR-517a*.

We further searched the 5´UTRs and protein-coding sequences (CDS) of downregulated and the entire sequences of upregulated transcripts for heptamers complementary to the seeds of *miR-17* or *miR-517a*. Searching for *miR-17* or *miR-517a* seed-matched motifs in the 5´UTRs and in the CDS of downregulated transcripts did not yield any significant enrichment compared to the genome-wide frequency of these motifs (**Fig R.17 A and C**). These results are in line with the concept that metazoan miRNAs target 3´UTRs more frequently and more efficiently than other regions of transcripts (Lai, 2002; Lee *et al*, 1993; Lim *et al*, 2005). Sequence analysis of *miR-17*-upregulated transcripts revealed enrichment for the *miR-17* binding motif GCACUUU in the 3´UTRs. However, enrichment of this motif was much more pronounced in the downregulated transcripts (**Fig R.17 A and B**). Interestingly, the *miR-517a* binding motif UGCACGA was underrepresented in the CDS and the 3´UTRs of *miR-517a*-upregulated transcripts compared to the genome-wide frequency (**Fig R.17 D**). Although this finding further indicates that upregulated transcripts are likely indirect *miR-517a* targets, the miRNA-mediated regulatory networks that lead to increased gene expression remain to be elucidated. In summary, motif enrichment analysis confirmed that miRNAs, through direct interactions with their targets, act as predominantly negative post-transcriptional regulators of gene expression (Lai, 2002).

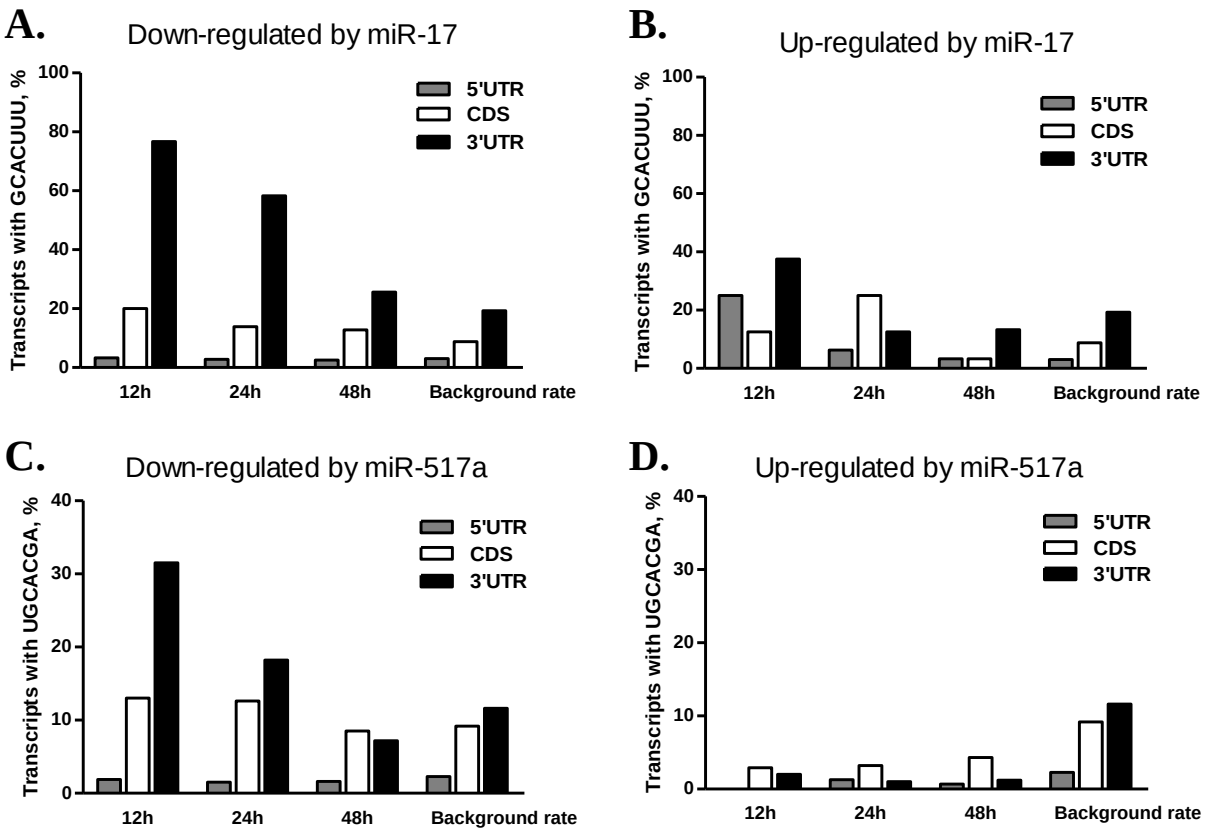

Figure R.17: Search of *miR-17* and *miR-517a* binding motifs in the sequences of transcripts affected by overexpression of the miRNAs. (**A, B**) Transcripts affected by overexpression of *miR-17* and (**C, D**) *miR-517a*. Only transcripts with an expression fold change higher or equal to 1.5 corresponding to an adjusted p-value ≤0.05 (*miR-17*) or ≤0.01 (*miR-517a*) and with annotated 3´UTR sequence were used for analysis. The most significantly enriched heptamers in Sylamer algorithm-based analysis (GCACUUU for *miR-17a* and UGCACGA for *miR-517a*; Fig. R.16) were used as search words. Transcripts with at least one word in a given region are represented as percentage in relation to all either downregulated (**A, C**) or upregulated (**B, D**) mRNAs at the indicated time points after transfection. Background rates were calculated by searching the given motifs within all annotated human 5´UTRs, coding sequences and 3´UTRs.

Computational miRNA target prediction is one of the most commonly used approaches for a rapid identification of potential miRNA targets. The main feature used in various prediction algorithms is the sequence alignment of the miRNA seed sequence to the 3´UTR of the transcript. Additionally, prediction specificity is increased using different combinations of other parameters, including evolutionary conservation, structural accessibility, nucleotide composition and location of the binding sites within the 3´UTR (Alexiou *et al*, 2009; Sethupathy *et al*, 2006). In order to evaluate the prediction quality of these algorithms, we selected three commonly used programs (MicroCosm Targets v5, Diana-microT v3.0 and TargetScanHuman release 5.2) and analyzed how many transcripts downregulated by *miR-17* or *miR-517a* are predicted as potential targets at

least by one of the mentioned programs. The analysis of microarray data showed that 58% of the transcripts, which are downregulated by fold change ≤ -1.5 12h after transfection, are predicted *miR-17* targets. For *miR-517a*, only 26% of the transcripts downregulated at 12h after transfection are predicted targets. Surprisingly, the simple search of miRNA binding motifs in the 3´UTRs of the downregulated transcripts indicated that 76% and 32% of the transcripts affected 12h after transfection are potential targets of *miR-17* and *miR-517a*, respectively (**Fig R.17 A and C**). These results indicate that the straightforward motif search outperforms more complex computational methods.

Conclusions: Applying global analysis of *miR-17* and *miR-517a* microarray data we showed that many transcripts are downregulated through direct miRNA:target interactions. On the other hand, upregulated transcripts are most likely indirect secondary targets of the investigated miRNAs. We also demonstrated that the searching of potential miRNA binding motif outperforms complex computational prediction programs and can be used as an alternative for a fast identification of putative miRNA targets.

7. DISCUSSION

The list of physiological and pathological processes where miRNAs play important regulatory roles is constantly growing. In this context, the area of membrane trafficking in eukaryotic cells has attracted little interest from the scientific miRNA community. To our knowledge, there are only three publications available that report the effects of *miR-375* (Poy *et al*, 2004), *miR-9* (Plaisance *et al*, 2006), *miR-124a* and *miR-96* (Lovis *et al*, 2008) on regulated insulin secretion in murine pancreatic β-cells. Moreover, Kanzaki and colleagues (Kanzaki *et al*, 2011) recently demonstrated that *miR-92a* regulates the expression of RAB14, which is involved in surfactant secretion in lung cells. These observations suggest that miRNAs might constitute a new regulatory level of complex membrane trafficking process. However, no large-scale studies to elucidate the effects of known miRNAs on membrane trafficking in human cells have been performed. In this study, we established an integrative platform of different experimental approaches that allowed us to identify miRNAs and their biologically relevant target genes involved in the regulation of membrane trafficking.

7.1. Proof of principle: functional activity of pre-miRs and anti-miRs

Effective and reliable approaches to modulate miRNA activity are crucial for understanding the biological importance of miRNAs. Generally, overexpression by introducing synthetic miRNAs (gain-of-function) and miRNA inhibition by antisense inhibitory oligonucleotides (loss-of-function) are the most straightforward and commonly used strategies for investigating miRNA functions. In this study, we first of all evaluated the potency of miRNA mimicking (pre-miRs) and antisense oligonucleotides (anti-miRs) to enhance or to inhibit the activity of specific miRNAs in cell cultures, respectively. Noteworthy, pre-miRs and anti-miRs are patent pending products of Ambion company and, therefore, the formulation of chemical modifications of these molecules is undisclosed. As previously showed by U. Neniškytė (previous member of Screening of Cellular Networks laboratory), synthetic pre-miRs and anti-miRs can be efficiently introduced into four adherent cell lines by using commercially available Lipofectamine 2000 transfection reagent. Furthermore, oligonucleotides could be successfully delivered by liquid-phase and solid-phase reverse transfections. The latter approach is of particular relevance in order to perform large-scale screenings of miRNA libraries (Erfle *et al*,

2007). In order to evaluate functionality of pre-miRs and anti-miRs, we selected three human miRNAs encoded by polycistronic *miR-17-92* cluster, namely *miR-17*, *miR-20a* and *miR-92a* (Tanzer & Stadler, 2004), and one unrelated – *miR-320a*. miRNA expression profiling by qRT-PCR showed that transfection with pre-miRs significantly increased the expression of respective miRNAs. These results were further confirmed by luciferase reporter assay. Except for *miR-92a*, we did not observe a significant reduction of miRNA levels in cells transfected with anti-miRs. Considering that inhibition of miRNA activity by anti-miRs is sometimes achieved without detectable miRNA degradation (Davis *et al*, 2009; Elmen *et al*, 2008), measuring miRNA level by qRT-PCR is not always a suitable method to assess inhibition. Moreover, Davis and colleagues (Davis *et al*, 2009) showed that some high affinity chemical modifications stabilize the anti-miR:miRNA complex and interfere with miRNA detection by qRT-PCR. Indeed, our results from the luciferase reporter assay showed that anti-miRs effectively inhibit the activity of endogenous miRNAs resulting in a relief of reporter gene suppression, which is reflected by increased luciferase protein expression.

Consistent with previous studies (Davis *et al*, 2006; Lennox & Behlke, 2010; Ovcharenko *et al*, 2007), we conclude that synthetic pre-miRs and anti-miRs are functional approaches, respectively, to efficiently enhance or inhibit the activity of endogenous miRNAs in cultured cells. We also show that pre-miRs are resistant to nuclease degradation up to 72h after transfection.

7.2. Members of the *miR-17* family are novel regulators of membrane trafficking

Biosynthetic trafficking and endocytic pathways are the major intracellular membrane trafficking routes in eukaryotic cells. To examine whether modulation of miRNA activity by pre-miRs or anti-miRs induces any detectable phenotypic changes in these pathways, we employed two well-established fluorescence-based assays. Changes in biosynthetic trafficking were measured by ts-O45-G protein transport assay (Starkuviene *et al*, 2004; Zilberstein *et al*, 1980), whereas efficiency of endocytosis was assayed by internalization of DiI-LDL ligand (Ghosh *et al*, 1994). The key feature of these assays is that, in combination with automated image acquisition and analysis, fluorescence intensity of ts-O45-G or Dil-LDL is measured at single cell level and, therefore, allows statistical data analysis.

miR-17-92 is one of the most extensively studied miRNA clusters in mammals. Aberrant expression of this cluster has been reported in numerous human malignancies (Coller *et al*, 2007;

Volinia *et al*, 2006), indicating that it is one of the most potent oncogenic clusters. According to their seed sequences, the six miRNAs encoded by *miR-17-92* cluster can be classified into four families. Thus, we selected *miR-17*, *miR-18a*, *miR-19a* and *miR-92a* as representative members of each seed family and performed membrane trafficking assays. Surprisingly, we observed that overexpression of *miR-17* significantly accelerated ts-O45-G transport rate and substantially reduced the amount of internalized DiI-LDL in HeLa cells. miRNAs with identical seed sequences have been predicted to modulate a highly overlapping set of target genes (Bartel, 2009; Lewis *et al*, 2005). Therefore, we hypothesized that other *miR-17* seed family members encoded by *miR-17-92* and its paralogous *miR-106a-363* and *miR-106b-25* clusters (Tanzer & Stadler, 2004) could modulate similar biological processes to the ones regulated by *miR-17*. Indeed, overexpression of *miR-20a*, *miR-20b* and *miR-93*, miRNAs that contain the same seed sequence as *miR-17*, accelerated ts-O45-G transport rate and reduced the cellular Dil-LDL uptake to a similar extent as *miR-17*. These findings validated our hypothesis suggesting that *miR-17* family members modulate a similar set of genes and the net outcome of this regulation is the enhanced biosynthetic ts-O45-G trafficking and the reduced internalization of DiI-LDL. In line with our results, previous studies have demonstrated functional redundancy of *miR-17* family members since they target common genes (Doebele *et al*, 2010; Wu *et al*, 2010) or regulate the same biological processes (Borgdorff *et al*, 2010). To our knowledge, this is the first experimental evidence demonstrating an active role of *miR-17* family members in regulation of membrane trafficking and, therefore, further expanding the functional repertoire of *miR-17-92* cluster.

In contrast to miRNA overexpression, we could not obtain biologically significant changes in biosynthetic trafficking or endocytosis upon inhibition of any tested miRNAs. Again, a possible explanation is that miRNAs sharing same seed sequence can be functionally redundant. This is exemplified by the lack of obvious phenotypes in *C. elegans* deficient for individual miRNAs whose functions are apparently compensated by other similar miRNAs (Miska *et al*, 2007). On the other hand, Brenner and colleagues (Brenner *et al*, 2010) were able to identify enhanced or synthetic phenotypes for most of the analyzed miRNAs in *alg-1* mutant nematodes with partially disabled miRNA silencing machinery and lower total miRNA activity. Another example of functional miRNA redundancy comes from mice deficient for *miR-106b-25* cluster. The function of this cluster was uncovered only in the context of *miR-17-92* deletion, suggesting that the loss of *miR-106b-25* is compensated by the paralogous miRNAs from *miR-17-92* cluster (Ventura *et al*, 2008). Moreover, functional redundancy of *miR-17* family members is supported by the fact that systematic inhibition of both *miR-17* and *miR-20a* induced stronger

effect on neovascularization than inhibition of *miR-20a* alone (Doebele *et al*, 2010). The results of our luciferase reporter assay indicate significant suppression of miRNA activity by different inhibition approaches. This could be explained by higher sensitivity of the artificial reporter to miRNA of interest in comparison to other similar miRNAs that are different in some nucleotides outside the seed region. Although further studies are needed, we believe that *miR-17* family members redundantly regulate a set of natural targets, which would explain the lack of significant phenotypes after inhibition of individual miRNAs. As mentioned before, this possibility has been supported by numerous experimental studies (Doebele *et al*, 2010; He *et al*, 2007; Uhlmann *et al*, 2010; Wu *et al*, 2010).

Taken together, we demonstrated for the first time a regulatory role of *miR-17* family miRNAs in biosynthetic trafficking and endocytosis, further indicating that miRNAs are actively involved in the control of membrane trafficking processes. Despite the lack of cellular phenotypes after inhibition of individual miRNAs, the overexpression of *miR-17* family miRNAs resulted in significant changes in biosynthetic ts-O45-G transport and internalization of extracellular Dil-LDL.

7.3. Large-scale screening identifies multiple miRNAs as regulators of biosynthetic trafficking

A number of miRNA-based screenings have been completed during the last 5 years. Surprisingly, in order to elucidate the biological roles of miRNAs, nearly all reported screenings used the gain-of-function approach. Overexpression of miRNAs often induces mutant phenotypes in a dominant fashion, and so they are potentially easier to evaluate compared to the ones caused by inhibition of miRNAs. Additionally, loss-of-function experiments are limited to the experimental system with endogenously expressed miRNAs of interest, whereas gain-of-function is in principle relevant to all tissue or cell types (Serva *et al*, 2011).

Based on successful proof of principle experiments, we designed a gain-of-function screening of 470 miRNAs to identify the ones that are involved in the regulation of biosynthetic ts-O45-G trafficking. Among 470 screened miRNAs, we identified 31 whose overexpression significantly inhibited ts-O45-G transport to the plasma membrane, whereas overexpression of other 13 miRNAs substantially accelerated cargo trafficking. In comparison to the relatively large number of miRNAs counted as primary hits in previously reported screenings (Ovcharenko *et al*,

2007; Sirotkin *et al*, 2009; Whittaker *et al*, 2010), we selected in total 44 miRNAs which represent less than 10% of all screened molecules, indicating stringent cutoff values. In line with the data from proof of principle experiments, we identified *miR-20b* as hit in library screening. The majority of arbitrarily selected inhibitory miRNAs (5 out of 6) was then confirmed in a small-scale experimental format using pre-miRs from a different batch, demonstrating the reproducibility of large-scale screening data. Among the inhibitory miRNAs we identified three poorly-characterized members of *miR-517* family, namely, *miR-517a*, *miR-517b* and *miR-517c*, which are mainly expressed in undifferentiated tissues (Ren *et al*, 2009). Recently, *miR-517a* has been identified as a novel oncogenic miRNA upregulated in human hepatocellular carcinoma samples (Toffanin *et al*, 2011). In contrast to previous finding in Huh7 cells (Toffanin *et al*, 2011), overexpression of *miR-517a* had no significant effect on HeLa cell growth, suggesting cell type-dependent function of the miRNA. Among ts-O45-G transport accelerators, we found *miR-34a* and *miR-34c*, members of *miR-34* family. All three family members (including *miR-34b*) are well-known tumor suppressors and their expression is transactivated by the transcription factor p53 (Chang *et al*, 2007; He *et al*, 2007). Ectopic expression of *miR-34* family miRNAs has been shown to cause cell-cycle arrest (Tarasov *et al*, 2007) or induce apoptosis (Raver-Shapira *et al*, 2007). Consistently, we found that overexpression of *miR-34a* significantly inhibited cell growth. None of *miR-517* and *miR-34* family members that affected ts-O45-G transport has been previously implicated in regulation of membrane trafficking. Furthermore, except for *miR-34a*, overexpression of these miRNAs had no significant effect on cell growth, indicating that observed changes in biosynthetic ts-O45-G transport was not caused by dysregulated cell proliferation (Misteli & Warren, 1995; Warren, 1993) or induced apoptosis (Nozawa *et al*, 2002). These representative examples demonstrate the potency of large-scale functional screening in identifying miRNAs with regulatory functions in biosynthetic trafficking.

The Golgi complex is a highly dynamic cellular structure responsible for modifying, sorting and packaging secretory proteins in mammalian cells. The functionality of the Golgi apparatus is closely related to its structure, and so any changes in structural integrity directly affect biosynthetic protein transport (Tamaki & Yamashina, 2002). Therefore, we developed a fully automated image analysis platform for quantification of Golgi complex integrity and investigated the effects of hit miRNAs on Golgi structure. Surprisingly, we observed that the inhibition of ts-O45-G transport by *miR-517a*, *miR-517b* and *miR-517c* is also associated with significant fragmentation of Golgi complex. Apart from *miR-517* family, we identified other four miRNAs (*miR-30b*, *miR-637*, *miR-432* and *miR-765*) that induced Golgi fragmentation by at least

1.75-fold compared to control, whereas *miR-382* caused condensation of the Golgi apparatus. All eight miRNAs identified as effectors of Golgi morphology inhibited ts-O45-G transport in the functional screening. Importantly, none of the miRNAs that accelerated protein transport had obvious effect on Golgi network, suggesting that other cellular organelles and/or Golgi morphology-independent regulatory mechanisms are involved in miRNA-mediated upregulation of biosynthetic protein transport.

In summary, through large-scale screening we identified 44 miRNAs regulating biosynthetic ts-O45-G trafficking. We also demonstrated that eight out of 31 inhibitory miRNAs significantly affect morphology of Golgi complex. The observed changes in Golgi structure suggest that functions of multiple targets that are deregulated by each of eight miRNAs converge on this organelle and potentially affect ts-O45-G transport in the Golgi complex.

7.4. Microarray-based expression profiling identifies miRNAs expressed in HeLa cells

Hundreds of miRNAs have been shown to be expressed in highly tissue specific patterns (Baskerville & Bartel, 2005; Landgraf *et al*, 2007). Therefore, the introduction of a miRNA that is not endogenously expressed would downregulate many transcripts that are not usually targeted in specific tissue under natural conditions. We speculated that the transfection with endogenously non-expressed miRNAs can induce stronger phenotypes compared to the overexpression of endogenous miRNAs. In agreement with this notion, our microarray-based miRNA expression profiling revealed that only 10 out of the 44 hit miRNAs from functional screening are endogenously expressed in HeLa cells. Even a smaller fraction of miRNAs was expressed if considering the Golgi effectors: we only detected the expression of *miR-30b*. Noteworthy, *miR-30b* were among the weakest hit miRNAs that inhibited ts-O45-G transport (-1.62 *Z*-scores) and the weakest inducer of Golgi fragmentation (1.78-fold) compared to other identified hit miRNAs. These findings validate our hypothesis and are in part supported by a report showing a strong correlation between miRNA and target mRNAs expression levels (Sood *et al*, 2006).

Several recent studies have reported aberrant cellular miRNA expression profiles following viral infection (Marquez *et al*, 2010; Triboulet *et al*, 2007; Wang *et al*, 2008). In parallel with the analysis of steady-state miRNA expression profiles, we examined how experimental conditions of ts-O45-G transport assay, which include incubation at 39.5°C and

adenoviral transduction (adenoviral vector encodes ts-O45-G), effect miRNA expression. We found that mere incubation at 39.5°C led to ~1.5-fold increase in global miRNA expression with *miR-1290* and *miR-1308* being most upregulated miRNAs. Although hyperthermia, in combination with adenoviral transduction, induced only a modest increase in global miRNA expression, the expression of poorly-characterized *miR-1290* and *miR-1308* remained significantly upregulated. The experimental settings we used did not allow to discern viral transduction-specific effects on cellular miRNA expression. However, constant upregulation of two specific miRNAs supports a previously suggested miRNA-specific response to temperature in mammals (Truettner *et al*, 2011).

Altogether, we detected 113 mature miRNAs expressed in HeLa cells under normal conditions. Integration of miRNA expression data revealed that the majority of miRNAs identified in our pre-miR library screening and Golgi complex integrity assay are not endogenously expressed. Furthermore, we identified temperature-dependent upregulation of *miR-1290* and *miR-1308*, providing an interesting basis for the follow-up studies to elucidate their upregulation mechanisms and potential effects on ts-O45-G transport.

7.5. Microarray-based identification of potential *miR-17* and *miR-517a* targets

As previously mentioned, several independent studies using different large-scale approaches have demonstrated that miRNA-mediated target mRNA destabilization, rather than translational repression, is the predominant mechanism for reduced protein levels (Baek *et al*, 2008; Guo *et al*, 2010; Hendrickson *et al*, 2009). These findings were at least partially anticipated considering that an early transcriptome profiling study revealed a large number of transcripts downregulated by ectopically introduced miRNAs (Lim *et al*, 2005). Based on these observations, we performed a time-resolved microarray-based mRNA expression profiling in order to identify biologically relevant targets of two miRNAs, *miR-17* and *miR-517a*. We selected *miR-17* as representative member of the *miR-17* family. *miR-517a* was chosen as representative member of the *miR-517* family because of its novelty and the magnitude of induced ts-O45-G transport inhibition and Golgi complex fragmentation. Noteworthy, our miRNA expression profiling experiment showed that *miR-17* is highly expressed, whereas members of the *miR-517* family are undetectable in HeLa cells.

Gene expression profiling identified 90 downregulated and 56 upregulated transcripts in the pre-miR-17-transfected cells throughout the 48h experiment. Surprisingly, we detected in

total 1 088 downregulated and 1 238 upregulated transcripts by enforced expression of *miR-517a*. The considerably higher number of transcripts affected by introduction of *miR-517a* compared to *miR-17* is in line with our previous speculation that many transcripts, which are not co-expressed in the same cell type with targeting miRNA, will be downregulated by introduction of the respective exogenous miRNA. One could argue that the majority of potential *miR-517a* targets identified by mRNA expression profiling are biologically irrelevant. However, Lim *et al*. showed that expression of tissue-specific miRNAs in HeLa cells shifts the entire gene expression pattern towards that tissue (Lim *et al*, 2005). Nevertheless, further studies are necessary to investigate whether it is valid for *miR-517a*, comparing our microarray data with mRNA expression profiles in cells that endogenously express *miR-517a*, for example, human embryonic stem cells (Bar *et al*, 2008).

Among *miR-17* downregulated transcripts, we identified six (*TBC1D2*, *LDLR*, *M6PR*, *ASAP2*, *RAB32* and *NKD2*) with described functions in membrane trafficking. Sequence analysis revealed that *TBC1D2*, *LDLR*, *M6PR*, *ASAP2* mRNAs have potential *miR-17* binding sites in their 3´UTRs or coding regions. Similar to our analysis, at least one of three miRNA target prediction tools (MicroCosm Targets v5, Diana-microT and TargetScanHuman) predicted *TBC1D2, LDLR and M6PR* as targets for *miR-17*. Further investigation of potential *miR-17* targets are discussed in the following section.

Comparative analysis of *miR-517a* microarray data with a set of 167 genes assigned to Gene Ontology terms “Protein transport”, “Endocytosis” and “Protein secretion” identified 32 and 72 membrane trafficking related genes downregulated and upregulated by *miR-517a*, respectively. Surprisingly, among downregulated transcripts we found *LDLR*, which was also validated as a novel *miR-17* target (discussed later). Although we did not confirm *LDLR* as a target of *miR-517a*, mRNA expression data suggest that this gene is potentially regulated by both *miR-17* and *miR-517a*. Analysis of other downregulated transcripts revealed a relatively few genes that exert *miR-517a*-mediated inhibition of ts-O45-G transport or Golgi complex fragmentation. One of these potential genes could be *ARF3*, however, Manolea and colleagues (Manolea *et al*, 2010) recently showed that *ARF3* knockdown does not interfere with biosynthetic ts-O45-G transport and has no effect on the *trans*-Golgi network. In contrast to downregulated, we found many upregulated genes with well-described functions in membrane trafficking. Such genes are *COG3*, *COG5* and *COG6* encoding different subunits of the conserved multisubunit tethering COG complex that is essential for COPI-mediated retrograde vesicle transport within the Golgi complex (Oka *et al*, 2004). Moreover, the COG complex has been shown to be

involved in Golgi-specific glycosylation process (Bruinsma *et al*, 2004) and maintenance of Golgi structure (Ungar *et al*, 2002; Ungar *et al*, 2005). Another example is *YIPF5* gene. Tang and colleagues demonstrated that overexpression of YIPF5 arrests ER-Golgi transport of ts-O45-G and induces Golgi complex fragmentation. It also co-localizes with COPII coatomer subunits SEC13 and SEC31A at ER exit sites (Tang *et al*, 2001). Importantly, *SEC31A* was also upregulated by *miR-517a*, indicating that this miRNA can potentially regulate different steps of ER-Golgi cargo transport. Besides well-described Rab genes (*RAB5A*, *RAB6A*, *RAB8A* and *RAB22*), we also detected upregulation of *RAB32*. In line with *miR-517a* effect, we recently demonstrated that knockdown of RAB32 results in acceleration of ts-O45-G transport to the plasma membrane (Sanchari Roy, personal communication). Despite experimental evidence that these genes can potentially play a role in *miR-517a*-mediated phenotypes, none of them is predicted to be target of *miR-517a*. Furthermore, all of them were upregulated and most of upregulation events were detected 48h after transfection, indicating that they are likely indirect *miR-517a* targets. Their upregulation might be induced through more complex *miR-517a*-governed secondary regulatory mechanisms, rather than by direct interactions with the miRNA (Martinez & Walhout, 2009; Shalgi *et al*, 2007; Tu *et al*, 2009).

Taken together, using time-resolved transcriptome profiling approach, in combination with bioinformatics analysis, we identified a set of membrane trafficking-related genes affected by transfection with pre-miR-17 or pre-miR-517a. While validation of novel *miR-17* targets is discussed in the following section, further investigation is necessary to elucidate *miR-517a*-mediated regulatory networks responsible for the upregulation of functionally relevant genes.

7.6. *miR-17* regulates membrane trafficking through novel targets *TBC1D2* and *LDLR*

As we demonstrated a novel function of *miR-17* in regulation of membrane trafficking, it is of great interest to identify the target genes that are responsible for the *miR-17*-mediated phenotypes in ts-O45-G transport and DiI-LDL internalization. Given the well-know *miR-17-92* functions in tumorigenesis (Olive *et al*, 2010; Xiang & Wu, 2010), most of the 33 to date experimentally validated *miR-17* targets are important cell cycle or apoptosis regulators (Hsu *et al*, 2011). In this study, integration of gene expression profiling data, transcript sequence analysis and computational target prediction indicated *TBC1D2*, *LDLR*, *M6PR* and *ASAP2* genes as

potential *miR-17* targets involved in the regulation of membrane trafficking. Among these genes, *TBC1D2* has been studied least. Recently, Armus, a highly homologous protein of TBC1D2 (TBC1D2 contains deletion of 11 amino acids compared to Armus), was shown to act as GTPase-activating protein (GAP) for RAB7 and to regulate ARF6-induced internalization of E-cadherin from keratinocyte cell-cell contacts (Frasa *et al*, 2010). LDLR is one of the most intensively studied proteins and functions as a major regulator of plasma LDL concentration (Yamada *et al*, 1986; Schneider, 1989). M6PR is required for the transport of lysosomal hydrolases from the TGN to pre-lysosomal compartments (Stein *et al*, 1987). ASAP2 functions as GAP for ARF1, ARF5 and ARF6 and thereby modules biosynthetic trafficking (Andreev *et al*, 1999).

To investigate whether *TBC1D2*, *LDLR*, *M6PR* and *ASAP2* genes are functionally relevant to the *miR-17*-mediated phenotypes, we downregulated them individually by siRNA-based RNAi and performed membrane trafficking assays. Apart from the anticipated effect of *LDLR* knockdown, RNAi of *TBC1D2* and *M6PR* led to the significantly reduced amount of internalized DiI-LDL and thereby phenocopied *miR-17*-mediated effect. The quantification of ts-O45-G trafficking assay showed that only the knockdown of *TBC1D2* significantly inhibited the cargo transport. Noteworthy, the transfection with siRNAs against *TBC1D2* resulted in an effect on ts-O45-G transport phenotype opposite to the one induced by overexpressed *miR-17*. This finding indicates that *TBC1D2* is important for cargo transport; however, it is not directly responsible for *miR-17*-regulated acceleration of ts-O45-G transport. Considering that *miR-17* has been shown to induce translational repression without detectable changes in transcript levels (Fontana *et al*, 2007; Hossain *et al*, 2006), we can not exclude that we could have missed some other biosynthetic trafficking-related targets by the gene expression profiling approach.

Since TBC1D2 is a GAP for RAB7, an essential regulator of late endocytic trafficking and lysosomal degradation (Bucci *et al*, 2000; Chavrier *et al*, 1990; Frasa *et al*, 2010), and LDLR is required for cellular LDL uptake (Brown & Goldstein, 1986), we considered *TBC1D2* and *LDLR* as the most potential genes to exert *miR-17* phenotype on DiI-LDL internalization. With the luciferase reporter assay we validated that *miR-17* directly regulates the expression of both *TBC1D2* and *LDLR* through binding to their 3´UTRs. Moreover, we showed that a single *miR-17* binding site in the 3´UTR of *TBC1D2* mRNA is functionally active and essential for the miRNA-mediated regulation. Finally, we demonstrated that overexpressed *miR-17* significantly decreased mRNA and protein levels of both investigated genes, further confirming that *TBC1D1* and *LDLR* are novel functional targets of this miRNA.

Internalized LDL-LDLR complex is dissociated in the RAB5-positive early endosomes and segregated components are directed towards two different endocytic pathways: (i) LDL proceeds through the endosomal pathway for subsequent degradation in lysosomes (Goldstein *et al*, 1985) and (ii) LDLR receptor is recycled back to the plasma membrane via the recycling pathway (Anderson *et al*, 1982). A recent fluorescence microscopy-based study has elegantly showed that the degradation of LDL occurs in the lysosome-associated membrane protein 1 (LAMP1)-positive late endosomes (Humphries *et al*, 2010). The formation of RAB7-positive late endosomes from RAB5-positive early endosomes requires the replacement of RAB5 with RAB7. This process, also known as Rab conversion, is mediated by the RAB5-recruited SAND-1-CCZ-1 complex, which acts as a guanine nucleotide exchange factor (GEF) for RAB7 (Kinchen & Ravichandran, 2010; Poteryaev *et al*, 2010). In this context, TBC1D2 GAP comes as a relevant regulator of early-to-late endosome maturation. Despite the fact that TBC1D2 was identified as GAP specific for RAB7, the experimental time settings (10min time point) of the biochemical GAP activity assay leaves the possibility that other fast-hydrolyzing Rabs, such as RAB5, are potential substrates for TBC1D2 (Frasa *et al*, 2010). Indeed, real-time measurement of GTP hydrolysis revealed that TBC-2 (*C. elegans* homolog of human TBC1D2) displays higher catalytic activity with *C. elegans* RAB-5 than with RAB-7 (Chotard *et al*, 2010). Moreover, studies in *C. elegans* demonstrated that TBC-2 co-localizes with RAB-7 on late endosomes and suggested that it inactivates RAB-5 during endosome maturation (Chotard *et al*, 2010).

Given that TBC1D2 might act as GAP for both RAB5 and RAB7 in human cells, we propose a potential mechanism via which TBC1D2 may regulate intracellular DiI-LDL trafficking. It is known that active RAB5 recruits its effector early endosome antigen 1 (EEA1) required for tethering and fusion of RAB5-positive endocytic vesicles to early endosomes (Simonsen *et al*, 1998; Stenmark *et al*, 1996). Importantly, the study by Haas *et al.* demonstrated that internalized EGF is retained in enlarged EEA1-positive structures in cells depleted for the RAB5-specific GAP RABGAP-5 (Haas *et al*, 2005). Consistently, the expression of constitutively active $RAB5_{Q79L}$ mutant has been showed to induce the formation of giant early endosomes with large amount of EEA1 (Lawe *et al*, 2002; Stenmark *et al*, 1994). Surprisingly, a recent study showed that $RAB5_{Q79L}$ recruits RAB7 and other late endosome markers to these enlarged endosomal structures (Wegner *et al*, 2010). Consistent with these findings, we observed that the knockdown of *TBC1D2* resulted in Dil-LDL accumulation in large juxtanuclear structures. Based on these observations, we propose that downregulation of TBC1D2 increases the activity of both RAB5 and RAB7 which leads to the loss of endosome functional identity. As

a result, this potentially compromises sorting of LDLR-LDL complex, recycling of LDLR back to the plasma membrane and subsequent endosomal trafficking of internalized LDL.

In conclusion, we identified and confirmed *TBC1D2* and *LDLR* as novel functional targets of *miR-17*. Although further studies are required to delineate TBC1D2 functions in endocytosis, our results revealed that *miR-17* is an important regulator of membrane trafficking and expanded the functional repertoire of the well-known oncogenic *miR-17-92* cluster.

7.7. Bioinformatics analysis of gene expression profiling data

Numerous large-scale studies have revealed that an individual miRNA can modulate the expression of many target mRNAs (Giraldez *et al*, 2006; Guo *et al*, 2010; Lim *et al*, 2005; Selbach *et al*, 2008). Consistently, by gene expression profiling experiments, we showed that overexpression of *miR-17* and *miR-517a* deregulates a large number of transcripts in HeLa cells. Although we also observed that many transcripts are upregulated by the investigated miRNAs, both transcriptome-wide miRNA binding site enrichment analysis and searching for specific *miR-17* or *miR-517a* binding motifs in affected transcripts indicated that only downregulated transcripts are potential direct targets of miRNAs (Lai, 2002). As anticipated, searching for binding motifs of a given miRNA demonstrated that most of the direct targets can be identified 12h after transfection; later they are increasingly masked by indirectly affected mRNAs.

Similar to the study that investigated the transcriptome of Huh7 cells stably expressing *miR-517a* (Toffanin *et al*, 2011), we found that upregulated transcripts represent more than half of affected mRNAs (1 238 upregulated versus 1 088 downregulated) in pre-miR-517a transfected HeLa cells. These observations suggest that *miR-517a* presumably modulates important transcription regulators leading to upregulation of numerous indirect targets. Although recently proposed mutual regulatory networks between miRNAs and transcription factors (Martinez & Walhout, 2009; Shalgi *et al*, 2007; Tu *et al*, 2009) support this possibility, further bioinformatics studies are needed in order to identify *miR-517a*-mediated gene activation mechanisms.

Identifying miRNA targets is essential for understanding miRNA functions. Various computational target prediction tools have been developed for rapid identification of potential miRNA targets (Alexiou *et al*, 2009). Usually, prediction algorithms are used in combination with other experimental approaches, for example, miRNA loss-of-function or gain-of-function experiments followed by transcriptome profiling. Intriguingly, we showed that simple search of miRNA binding site in the 3´UTRs of downregulated transcripts outperforms complex

computational methods used to identify potential *miR-17* and *miR-517a* targets from gene expression profiling data. The lower performance of computational prediction algorithms might be due to the fact that some of them use artificially designed miRNA:mRNA interactions to validate predicted sites (Maragkakis *et al*, 2009). Another possibility is that combining additional features such as site conservation, position in the 3´UTR, and UTR length are rather detrimental than advantageous, because they weakly correlate with the extent of target downregulation in some situations (Betel *et al*, 2010).

Altogether, we confirmed that the presence of miRNA seed binding site in the 3´UTRs of human mRNAs is an important determinant for functional miRNA:mRNA interaction. Additionally, we demonstrated that the sets of transcripts downregulated at early time points after transfection have substantially higher fractions of transcripts with potential miRNA binding sites in their 3´UTRs compared to the transcripts downregulated at late time points. Our results may also contribute to the development of more accurate miRNA target prediction tools.

7.8. Conclusions and future perspectives

The overall aim of this study was to identify miRNAs and their biologically relevant target genes involved in the regulation of membrane trafficking. To achieve this aim, we have established an integrative experimental platform that consists of (i) a screening module to identify miRNAs that affect membrane trafficking, (ii) a mRNA microarray module to identify potential miRNA target genes, (iii) a statistics and bioinformatics module for data analysis and integration and (iv) a target validation module to validate functional links between targets and miRNAs.

For this study, we successfully applied two quantitative fluorescence intensity-based functional assays that allowed us to detect miRNA-mediated changes in biosynthetic trafficking and endocytosis. As proof of principle, we showed for the first time that miRNAs belonging to the *miR-17* family are novel regulators of membrane trafficking in mammalian cells.

We next performed a gain-of-function large-scale screening and identified 44 miRNAs that affect the biosynthetic transport of ts-O45-G. The quantification of the Golgi complex integrity revealed that overexpression of eight identified hit miRNAs (*miR-30b*, *-382*, *-432*, *-517a*, *-517b*, *-517c*, *-637* and *-765*) significantly alters the Golgi morphology. The finding suggests that functions of multiple target genes modulated by each of these eight miRNAs converge on the Golgi complex and potentially regulate ts-O45-G transport at the level of this cellular organelle. Therefore, the functional miRNA screening, in combination with the Golgi

complex integrity assay, is an efficient strategy for identification of miRNAs that function as novel regulators of membrane trafficking.

Applying a genome-wide transcriptome profiling and bioinformatics, we identified numerous potential *miR-17* and *miR-517a* targets relevant to membrane trafficking. The results of follow-up detailed analysis validated *TBC1D2* and *LDLR* genes as novel functional *miR-17* targets and confirmed that they exert the *miR-17*-mediated regulation of endocytosis. Thus, our study revealed *miR-17* as a novel regulator of membrane trafficking and further expanded the functional repertoire of well-known oncogenic *miR-17-92* cluster. Further investigation is required to identify genes that play role in *miR-17*-mediated acceleration of ts-O45-G transport as well as to elucidate regulatory *miR-517a* networks that induce strong phenotypes observed in this study.

Considering that the number of known human miRNAs increased more than threefold (from 470 to 1527) during this project, the establishment of integrative experimental platform is of great importance for identification of other miRNAs and of their targets involved in the membrane trafficking process. The link between defects in membrane trafficking, tumorigenesis, various infectious and neurological diseases reflects the fundamental role of this cellular process. Such defects usually compromise sorting of internalized molecules, motility of vesicles along the cytoskeletal tracks or result in aberrant secretion of intracellular proteases and thereby facilitate invasive cell motility. In this context, the results of this study provide us new insight into miRNAs as potential therapeutic targets or agents for treatment of membrane trafficking-related diseases.

COLLABORATIONS

For this project we have established collaborations with:

- Dr. Ursula Rost and Prof. Dr. Ursula Kummer for bioinformatics analysis of mRNA microrray data (Modeling of Biological Processes, Institute of Zoology)

- Bettina Knapp and Dr. Lars Kaderali for statistical data analysis of functional miRNA assays and screening of large-scale pre-miR library (ViroQuant Research Group Modeling, BioQuant)

- Nina Beil, Jürgen Beneke, Dr. Jürgen Reymann and Dr. Holger Erfle for preparation of pre-miR library for high-throughput solid-phase transfection, automated image acquisition and analysis, and data storage (ViroQuant-CellNetworks RNAi Screening Facility, BioQuant)

- Jan-Philip Bergeest, Dr. Nathalie Harder, Dr. Petr Matula and Dr. Karl Rohr for automated analysis of Golgi complex and nuclear images (Biomedical Computer Vision, IPMB and DKFZ)

- Jessica Schilde and M.D. Heiko Runz for DiI-LDL internalization experiments

- Dr. Vladimir Kuryshev for bioinformatics analysis of genes involved in biosynthetic cargo trafficking and endocytosis (Data Integration and Knowledge Management, EMBL, BioQuant)

APPENDIXES

Appendix I: Accession numbers and IDs of 470 mature human miRNAs in Pre-miR™ miRNA Precursor Library. Library contains all human miRNAs annotated in miRBase v9.2. *Z*-scores of ts-O45-G trafficking rate changes and standard errors of the mean (S.E.M.) induced by overexpression of each miRNA are given. The median cargo transport rate is adjusted to *Z*-score of 0. The functional screen was performed in HeLa cells in 96-well µ-plate experimental format.

Accesion number in miRBase v9.2	miRNA ID	*Z*-score	S.E.M.
MIMAT0000062	let-7a	0.16	0.12
MIMAT0000063	let-7b	-0.18	0.25
MIMAT0000064	let-7c	-0.07	0.11
MIMAT0000065	let-7d	0.18	0.16
MIMAT0000066	let-7e	-0.44	0.35
MIMAT0000067	let-7f	0.03	0.17
MIMAT0000414	let-7g	0.06	0.21
MIMAT0000415	let-7i	0.31	0.18
MIMAT0000416	miR-1	-0.53	0.17
MIMAT0000098	miR-100	-0.82	0.32
MIMAT0000099	miR-101	1.18	0.01
MIMAT0000101	miR-103	0.22	0.26
MIMAT0000102	miR-105	0.88	0.09
MIMAT0000103	miR-106a	1.46	0.09
MIMAT0000680	miR-106b	1.44	0.13
MIMAT0000104	miR-107	-0.35	0.25
MIMAT0000253	miR-10a	0.09	0.08
MIMAT0000254	miR-10b	0.31	0.15
MIMAT0000422	miR-124a	-1.71	0.18
MIMAT0000443	miR-125a	-2.06	0.34
MIMAT0000423	miR-125b	-1.66	0.12
MIMAT0000445	miR-126	-0.19	0.38
MIMAT0000444	miR-126*	1.01	0.13
MIMAT0000446	miR-127	-0.62	0.16
MIMAT0000424	miR-128a	-0.65	0.09
MIMAT0000676	miR-128b	3.06	0.11
MIMAT0000242	miR-129	-0.18	0.32
MIMAT0000425	miR-130a	-1.28	0.19
MIMAT0000691	miR-130b	-0.97	0.08
MIMAT0000426	miR-132	1.37	0.19
MIMAT0000427	miR-133a	-0.62	0.09
MIMAT0000770	miR-133b	-0.97	0.17
MIMAT0000447	miR-134	-0.14	0.21
MIMAT0000428	miR-135a	-0.58	0.30
MIMAT0000758	miR-135b	-0.64	0.05
MIMAT0000448	miR-136	0.47	0.12
MIMAT0000429	miR-137	0.86	0.24
MIMAT0000430	miR-138	0.33	0.04
MIMAT0000250	miR-139	0.49	0.20
MIMAT0000431	miR-140	-1.36	0.09
MIMAT0000432	miR-141	0.39	0.25
MIMAT0000434	miR-142-3p	0.71	0.18
MIMAT0000433	miR-142-5p	0.61	0.37
MIMAT0000435	miR-143	0.43	0.27
MIMAT0000436	miR-144	0.63	0.10

Accesion number in miRBase v9.2	miRNA ID	*Z*-score	S.E.M.
MIMAT0000437	miR-145	-0.63	0.53
MIMAT0000449	miR-146a	1.20	0.49
MIMAT0002809	miR-146b	0.51	0.24
MIMAT0000251	miR-147	-0.73	0.23
MIMAT0000243	miR-148a	0.43	0.10
MIMAT0000759	miR-148b	0.07	0.40
MIMAT0000450	miR-149	-0.06	0.13
MIMAT0000451	miR-150	0.48	0.46
MIMAT0000757	miR-151	-0.12	0.13
MIMAT0000438	miR-152	1.16	0.24
MIMAT0000439	miR-153	0.15	0.25
MIMAT0000452	miR-154	1.81	0.18
MIMAT0000453	miR-154*	1.68	0.49
MIMAT0000646	miR-155	0.64	0.44
MIMAT0000068	miR-15a	0.38	0.05
MIMAT0000417	miR-15b	-0.20	0.24
MIMAT0000069	miR-16	0.49	0.39
MIMAT0000071	miR-17-3p	-0.07	0.04
MIMAT0000070	miR-17-5p	0.97	0.10
MIMAT0000256	miR-181a	1.23	0.09
MIMAT0000270	miR-181a*	-0.28	0.11
MIMAT0000257	miR-181b	-0.30	0.06
MIMAT0000258	miR-181c	-0.61	0.11
MIMAT0002821	miR-181d	-1.05	0.16
MIMAT0000259	miR-182	-1.73	0.12
MIMAT0000260	miR-182*	-0.49	0.28
MIMAT0000261	miR-183	-0.12	0.28
MIMAT0000454	miR-184	-0.68	0.33
MIMAT0000455	miR-185	0.92	0.33
MIMAT0000456	miR-186	-0.06	0.19
MIMAT0000262	miR-187	0.06	0.15
MIMAT0000457	miR-188	-0.03	0.15
MIMAT0000079	miR-189	-0.26	0.26
MIMAT0000072	miR-18a	-0.30	0.02
MIMAT0002891	miR-18a*	-0.51	0.09
MIMAT0001412	miR-18b	0.44	0.18
MIMAT0000458	miR-190	-0.16	0.65
MIMAT0000440	miR-191	-1.27	0.43
MIMAT0001618	miR-191*	-0.36	0.29
MIMAT0000222	miR-192	1.01	0.08
MIMAT0000459	miR-193a	0.16	0.26
MIMAT0002819	miR-193b	-0.14	0.43
MIMAT0000460	miR-194	0.52	0.18
MIMAT0000461	miR-195	-1.20	0.29
MIMAT0000226	miR-196a	0.95	0.18

Accesion number in miRBase v9.2	miRNA ID	*Z*-score	S.E.M.
MIMAT0001080	miR-196b	-1.55	0.53
MIMAT0000227	miR-197	2.01	0.25
MIMAT0000228	miR-198	0.18	0.31
MIMAT0000231	miR-199a	0.18	0.31
MIMAT0000232	miR-199a*	0.64	0.11
MIMAT0000263	miR-199b	0.02	0.13
MIMAT0000073	miR-19a	-1.34	0.41
MIMAT0000074	miR-19b	-2.59	0.91
MIMAT0000682	miR-200a	0.96	0.28
MIMAT0001620	miR-200a*	-0.10	0.47
MIMAT0000318	miR-200b	-1.04	0.29
MIMAT0000617	miR-200c	-0.99	0.26
MIMAT0002811	miR-202	0.10	0.26
MIMAT0002810	miR-202*	0.01	0.27
MIMAT0000264	miR-203	-0.27	0.27
MIMAT0000265	miR-204	-0.43	0.28
MIMAT0000266	miR-205	0.78	0.03
MIMAT0000462	miR-206	-1.54	0.18
MIMAT0000241	miR-208	0.49	0.05
MIMAT0000075	miR-20a	0.49	0.10
MIMAT0001413	miR-20b	1.65	0.22
MIMAT0000076	miR-21	-0.02	0.39
MIMAT0000267	miR-210	-2.42	0.28
MIMAT0000268	miR-211	-0.20	0.10
MIMAT0000269	miR-212	0.76	0.16
MIMAT0000271	miR-214	-0.20	0.18
MIMAT0000272	miR-215	0.09	0.16
MIMAT0000273	miR-216	0.37	0.29
MIMAT0000274	miR-217	0.45	0.44
MIMAT0000275	miR-218	-2.43	0.24
MIMAT0000276	miR-219	-0.42	0.25
MIMAT0000077	miR-22	0.00	0.04
MIMAT0000277	miR-220	-0.27	0.20
MIMAT0000278	miR-221	-0.09	0.18
MIMAT0000279	miR-222	0.53	0.08
MIMAT0000280	miR-223	1.09	0.13
MIMAT0000281	miR-224	-0.42	0.33
MIMAT0000078	miR-23a	0.52	0.10
MIMAT0000418	miR-23b	0.70	0.15
MIMAT0000080	miR-24	-0.28	0.39
MIMAT0000081	miR-25	0.87	0.14
MIMAT0000082	miR-26a	-1.33	0.32
MIMAT0000083	miR-26b	-0.78	0.39
MIMAT0000084	miR-27a	0.40	0.18
MIMAT0000419	miR-27b	0.45	0.15
MIMAT0000085	miR-28	-1.25	0.22
MIMAT0000690	miR-296	0.60	0.33
MIMAT0004450	miR-297	1.62	1.02
MIMAT0000687	miR-299-3p	-1.35	0.29
MIMAT0002890	miR-299-5p	1.03	0.59
MIMAT0000086	miR-29a	1.22	0.61
MIMAT0000100	miR-29b	0.93	0.47
MIMAT0000681	miR-29c	2.07	0.10
MIMAT0000688	miR-301	-0.33	0.38
MIMAT0000684	miR-302a	-0.12	0.38
MIMAT0000683	miR-302a*	-0.04	0.14

Accesion number in miRBase v9.2	miRNA ID	*Z*-score	S.E.M.
MIMAT0000715	miR-302b	0.16	0.03
MIMAT0000714	miR-302b*	-0.40	0.33
MIMAT0000717	miR-302c	0.80	0.19
MIMAT0000716	miR-302c*	0.45	0.11
MIMAT0000718	miR-302d	0.52	0.31
MIMAT0000088	miR-30a-3p	-1.29	0.92
MIMAT0000087	miR-30a-5p	-0.66	0.27
MIMAT0000420	miR-30b	-1.62	0.26
MIMAT0000244	miR-30c	-1.14	0.11
MIMAT0000245	miR-30d	0.22	0.19
MIMAT0000693	miR-30e-3p	-0.02	0.17
MIMAT0000692	miR-30e-5p	-1.47	0.17
MIMAT0000089	miR-31	0.62	0.11
MIMAT0000090	miR-32	-0.28	0.23
MIMAT0000510	miR-320	-0.05	0.46
MIMAT0000755	miR-323	-0.06	0.20
MIMAT0000762	miR-324-3p	-0.29	0.34
MIMAT0000761	miR-324-5p	0.95	0.15
MIMAT0000771	miR-325	-1.29	0.10
MIMAT0000756	miR-326	-0.23	0.38
MIMAT0000752	miR-328	0.14	0.53
MIMAT0001629	miR-329	-1.45	0.10
MIMAT0000091	miR-33	0.52	0.29
MIMAT0000751	miR-330	1.22	0.18
MIMAT0000760	miR-331	-0.01	0.37
MIMAT0000765	miR-335	0.47	0.05
MIMAT0000754	miR-337	-0.05	0.13
MIMAT0000763	miR-338	0.28	0.18
MIMAT0000764	miR-339	0.18	0.05
MIMAT0003301	miR-33b	1.18	0.40
MIMAT0000750	miR-340	0.97	0.19
MIMAT0000753	miR-342	0.28	0.28
MIMAT0000772	miR-345	0.45	0.29
MIMAT0000773	miR-346	-1.89	0.30
MIMAT0000255	miR-34a	1.61	0.24
MIMAT0000685	miR-34b	0.26	0.28
MIMAT0000686	miR-34c	2.17	0.33
MIMAT0000703	miR-361	-1.01	0.62
MIMAT0000705	miR-362	-0.45	0.44
MIMAT0000707	miR-363	-0.23	0.28
MIMAT0003385	miR-363*	-0.43	0.14
MIMAT0000710	miR-365	-2.04	0.07
MIMAT0000719	miR-367	0.76	0.34
MIMAT0000720	miR-368	0.44	0.17
MIMAT0000721	miR-369-3p	-0.04	0.43
MIMAT0001621	miR-369-5p	0.49	0.26
MIMAT0000722	miR-370	0.47	0.28
MIMAT0000723	miR-371	-0.74	0.51
MIMAT0000724	miR-372	0.67	0.31
MIMAT0000726	miR-373	0.75	0.06
MIMAT0000725	miR-373*	-0.13	0.11
MIMAT0000727	miR-374	0.96	0.22
MIMAT0000728	miR-375	0.47	0.44
MIMAT0000729	miR-376a	1.32	0.38
MIMAT0003386	miR-376a*	1.42	0.10
MIMAT0002172	miR-376b	1.12	0.16

Accesion number in miRBase v9.2	miRNA ID	*Z*-score	S.E.M.
MIMAT0000730	miR-377	0.27	0.36
MIMAT0000731	miR-378	-0.51	0.24
MIMAT0000733	miR-379	1.16	0.16
MIMAT0000735	miR-380-3p	-0.11	0.24
MIMAT0000734	miR-380-5p	1.22	0.39
MIMAT0000736	miR-381	-0.28	0.04
MIMAT0000737	miR-382	-1.90	0.19
MIMAT0000738	miR-383	0.64	0.29
MIMAT0001075	miR-384	0.32	0.23
MIMAT0001639	miR-409-3p	-0.35	0.22
MIMAT0001638	miR-409-5p	1.00	0.16
MIMAT0002171	miR-410	-0.50	0.05
MIMAT0003329	miR-411	0.15	0.38
MIMAT0002170	miR-412	-0.32	0.11
MIMAT0003339	miR-421	-0.01	0.24
MIMAT0001339	miR-422a	-0.24	0.32
MIMAT0000732	miR-422b	-0.23	0.16
MIMAT0001340	miR-423	-0.01	0.37
MIMAT0001341	miR-424	-0.14	0.18
MIMAT0001343	miR-425-3p	1.10	0.13
MIMAT0003393	miR-425-5p	-0.46	0.19
MIMAT0001536	miR-429	-0.66	0.19
MIMAT0001625	miR-431	1.02	0.18
MIMAT0002814	miR-432	-1.58	0.38
MIMAT0002815	miR-432*	-0.03	0.34
MIMAT0001627	miR-433	0.70	0.16
MIMAT0001532	miR-448	0.75	0.13
MIMAT0001541	miR-449	0.08	0.12
MIMAT0003327	miR-449b	-0.03	0.41
MIMAT0001545	miR-450	-0.13	0.13
MIMAT0001631	miR-451	0.61	0.30
MIMAT0001635	miR-452	-0.55	0.36
MIMAT0001636	miR-452*	-2.31	0.32
MIMAT0001630	miR-453	0.50	0.42
MIMAT0003885	miR-454-3p	-0.70	0.31
MIMAT0003884	miR-454-5p	-0.83	0.41
MIMAT0003150	miR-455	-0.99	0.26
MIMAT0002173	miR-483	-1.62	0.57
MIMAT0002174	miR-484	-1.54	0.27
MIMAT0002176	miR-485-3p	1.07	0.37
MIMAT0002175	miR-485-5p	-0.11	1.02
MIMAT0002177	miR-486	-0.61	0.73
MIMAT0002178	miR-487a	0.42	0.12
MIMAT0003180	miR-487b	0.44	0.58
MIMAT0002804	miR-488	1.54	0.16
MIMAT0002805	miR-489	1.68	0.41
MIMAT0002806	miR-490	0.41	0.21
MIMAT0002807	miR-491	0.32	0.41
MIMAT0002812	miR-492	0.39	0.20
MIMAT0003161	miR-493-3p	0.31	0.18
MIMAT0002813	miR-493-5p	0.16	0.24
MIMAT0002816	miR-494	-0.26	0.07
MIMAT0002817	miR-495	0.43	0.13
MIMAT0002818	miR-496	0.53	0.05
MIMAT0002820	miR-497	-0.20	0.06
MIMAT0002824	miR-498	0.54	0.12

Accesion number in miRBase v9.2	miRNA ID	*Z*-score	S.E.M.
MIMAT0002870	miR-499	0.32	0.12
MIMAT0002871	miR-500	-0.34	0.35
MIMAT0002872	miR-501	0.15	0.26
MIMAT0002873	miR-502	0.24	0.19
MIMAT0002874	miR-503	-0.56	0.36
MIMAT0002875	miR-504	0.39	0.07
MIMAT0002876	miR-505	-0.16	0.05
MIMAT0002878	miR-506	0.29	0.19
MIMAT0002879	miR-507	0.44	0.25
MIMAT0002880	miR-508	0.02	0.09
MIMAT0002881	miR-509	0.34	0.18
MIMAT0002882	miR-510	0.37	0.32
MIMAT0002808	miR-511	-1.41	0.67
MIMAT0002823	miR-512-3p	0.56	0.05
MIMAT0002822	miR-512-5p	0.63	0.37
MIMAT0002877	miR-513	-0.32	0.18
MIMAT0002883	miR-514	0.39	0.02
MIMAT0002827	miR-515-3p	-0.21	0.24
MIMAT0002826	miR-515-5p	0.16	0.18
MIMAT0002860	miR-516-3p	0.36	0.18
MIMAT0002859	miR-516-5p	0.34	0.37
MIMAT0002851	miR-517*	-0.12	0.24
MIMAT0002852	miR-517a	-3.70	0.76
MIMAT0002857	miR-517b	-3.16	0.22
MIMAT0002866	miR-517c	-1.86	0.48
MIMAT0002863	miR-518a	0.44	0.02
MIMAT0002844	miR-518b	0.38	0.10
MIMAT0002848	miR-518c	-0.09	0.34
MIMAT0002847	miR-518c*	-1.13	0.06
MIMAT0002864	miR-518d	-0.01	0.20
MIMAT0002861	miR-518e	0.73	0.10
MIMAT0002842	miR-518f	0.31	0.06
MIMAT0002841	miR-518f*	0.20	0.04
MIMAT0002869	miR-519a	0.14	0.04
MIMAT0002837	miR-519b	-0.01	0.35
MIMAT0002832	miR-519c	-0.34	0.21
MIMAT0002853	miR-519d	0.36	0.49
MIMAT0002829	miR-519e	0.73	0.19
MIMAT0002828	miR-519e*	0.25	0.14
MIMAT0002834	miR-520a	0.76	0.08
MIMAT0002833	miR-520a*	0.12	0.39
MIMAT0002843	miR-520b	0.20	0.29
MIMAT0002846	miR-520c	-0.16	0.23
MIMAT0002856	miR-520d	0.17	0.11
MIMAT0002855	miR-520d*	0.23	0.17
MIMAT0002825	miR-520e	0.27	0.05
MIMAT0002830	miR-520f	-0.48	0.07
MIMAT0002858	miR-520g	1.05	0.28
MIMAT0002867	miR-520h	1.28	0.29
MIMAT0002854	miR-521	-0.34	0.28
MIMAT0002868	miR-522	0.05	0.31
MIMAT0002840	miR-523	-1.29	0.24
MIMAT0002850	miR-524	-0.79	0.18
MIMAT0002849	miR-524*	0.88	0.53
MIMAT0002838	miR-525	0.40	0.23
MIMAT0002839	miR-525*	-0.36	0.09

Accesion number in miRBase v9.2	miRNA ID	*Z*-score	S.E.M.
MIMAT0002845	miR-526a	0.12	0.32
MIMAT0002835	miR-526b	0.35	0.14
MIMAT0002836	miR-526b*	0.22	0.35
MIMAT0002831	miR-526c	-0.07	0.24
MIMAT0002862	miR-527	0.41	0.45
MIMAT0002888	miR-532	-4.14	0.61
MIMAT0003163	miR-539	-0.16	0.44
MIMAT0003389	miR-542-3p	1.30	0.48
MIMAT0003340	miR-542-5p	-1.15	0.41
MIMAT0003164	miR-544	0.69	0.15
MIMAT0003165	miR-545	0.06	0.61
MIMAT0003251	miR-548a	-0.25	0.62
MIMAT0003254	miR-548b	0.46	0.08
MIMAT0003285	miR-548c	0.48	0.38
MIMAT0003323	miR-548d	-0.03	0.42
MIMAT0003333	miR-549	-0.41	0.56
MIMAT0003257	miR-550	0.05	0.37
MIMAT0003214	miR-551a	0.13	0.17
MIMAT0003233	miR-551b	-0.53	0.02
MIMAT0003215	miR-552	0.97	0.28
MIMAT0003216	miR-553	-1.55	0.33
MIMAT0003217	miR-554	-0.26	0.21
MIMAT0003219	miR-555	-1.21	0.23
MIMAT0003220	miR-556	-0.62	0.22
MIMAT0003221	miR-557	0.19	0.33
MIMAT0003222	miR-558	0.57	0.26
MIMAT0003223	miR-559	0.75	0.30
MIMAT0003224	miR-560	0.48	0.27
MIMAT0003225	miR-561	0.36	0.66
MIMAT0003226	miR-562	-0.19	0.67
MIMAT0003227	miR-563	0.90	0.70
MIMAT0003228	miR-564	-0.21	0.55
MIMAT0003229	miR-565	-0.80	0.10
MIMAT0003230	miR-566	-0.33	0.21
MIMAT0003231	miR-567	-0.65	0.48
MIMAT0003232	miR-568	-0.20	0.22
MIMAT0003234	miR-569	-0.50	0.20
MIMAT0003235	miR-570	-0.22	0.51
MIMAT0003236	miR-571	-0.38	0.27
MIMAT0003237	miR-572	-0.25	0.17
MIMAT0003238	miR-573	0.49	0.38
MIMAT0003239	miR-574	-1.65	0.35
MIMAT0003240	miR-575	0.34	0.20
MIMAT0003241	miR-576	0.26	0.44
MIMAT0003242	miR-577	0.24	0.22
MIMAT0003243	miR-578	0.08	0.60
MIMAT0003244	miR-579	-0.72	0.34
MIMAT0003245	miR-580	0.12	0.32
MIMAT0003246	miR-581	-0.01	0.32
MIMAT0003247	miR-582	0.11	0.97
MIMAT0003248	miR-583	0.70	0.35
MIMAT0003249	miR-584	-0.55	0.33
MIMAT0003250	miR-585	-1.00	0.66
MIMAT0003252	miR-586	1.20	0.49
MIMAT0003253	miR-587	0.72	0.10
MIMAT0003255	miR-588	-0.14	0.61

Accesion number in miRBase v9.2	miRNA ID	*Z*-score	S.E.M.
MIMAT0003256	miR-589	1.24	0.10
MIMAT0003258	miR-590	0.70	0.61
MIMAT0003259	miR-591	-0.57	0.46
MIMAT0003260	miR-592	0.67	0.35
MIMAT0003261	miR-593	-0.18	0.60
MIMAT0003263	miR-595	1.68	0.14
MIMAT0003264	miR-596	-1.03	0.04
MIMAT0003265	miR-597	0.56	0.19
MIMAT0003266	miR-598	0.09	0.23
MIMAT0003267	miR-599	0.25	0.91
MIMAT0003268	miR-600	-0.11	0.86
MIMAT0003269	miR-601	0.26	0.29
MIMAT0003270	miR-602	-0.52	0.28
MIMAT0003271	miR-603	1.19	0.18
MIMAT0003272	miR-604	-1.67	0.97
MIMAT0003273	miR-605	-0.20	0.48
MIMAT0003274	miR-606	0.78	0.31
MIMAT0003275	miR-607	0.45	0.20
MIMAT0003276	miR-608	-2.35	0.43
MIMAT0003277	miR-609	0.29	0.37
MIMAT0003278	miR-610	0.26	0.27
MIMAT0003279	miR-611	0.40	0.28
MIMAT0003280	miR-612	0.26	0.07
MIMAT0003281	miR-613	-1.18	0.11
MIMAT0003282	miR-614	-0.52	0.37
MIMAT0003283	miR-615	-0.42	0.18
MIMAT0003284	miR-616	0.05	0.16
MIMAT0003286	miR-617	-0.52	0.23
MIMAT0003287	miR-618	0.33	0.09
MIMAT0003288	miR-619	0.05	0.11
MIMAT0003289	miR-620	0.41	0.04
MIMAT0003290	miR-621	0.61	0.79
MIMAT0003291	miR-622	0.69	0.27
MIMAT0003292	miR-623	0.07	0.31
MIMAT0003293	miR-624	0.63	0.23
MIMAT0003294	miR-625	-0.83	0.18
MIMAT0003295	miR-626	-0.06	0.13
MIMAT0003296	miR-627	0.29	0.14
MIMAT0003297	miR-628	0.34	0.42
MIMAT0003298	miR-629	0.58	0.33
MIMAT0003299	miR-630	1.56	0.20
MIMAT0003300	miR-631	-0.41	0.41
MIMAT0003302	miR-632	0.45	0.21
MIMAT0003303	miR-633	0.25	0.07
MIMAT0003304	miR-634	-0.45	0.22
MIMAT0003305	miR-635	0.56	0.22
MIMAT0003306	miR-636	-0.51	0.10
MIMAT0003307	miR-637	-3.20	0.14
MIMAT0003308	miR-638	0.03	0.09
MIMAT0003309	miR-639	-0.34	0.26
MIMAT0003310	miR-640	0.36	0.18
MIMAT0003311	miR-641	0.96	0.19
MIMAT0003312	miR-642	0.49	0.08
MIMAT0003313	miR-643	0.21	0.29
MIMAT0003314	miR-644	0.56	0.42
MIMAT0003315	miR-645	1.03	0.28

Accesion number in miRBase v9.2	miRNA ID	*Z*-score	S.E.M.
MIMAT0003316	miR-646	-0.53	1.20
MIMAT0003317	miR-647	-2.15	0.12
MIMAT0003318	miR-648	0.51	0.49
MIMAT0003319	miR-649	0.07	0.19
MIMAT0003320	miR-650	0.33	0.28
MIMAT0003321	miR-651	0.45	0.49
MIMAT0003322	miR-652	-0.43	0.09
MIMAT0003328	miR-653	0.94	0.37
MIMAT0003330	miR-654	-2.54	0.79
MIMAT0003331	miR-655	0.80	0.06
MIMAT0003332	miR-656	0.50	0.05
MIMAT0003335	miR-657	0.42	0.10
MIMAT0003336	miR-658	0.12	0.28
MIMAT0003337	miR-659	0.17	0.12
MIMAT0003338	miR-660	-0.01	0.66
MIMAT0003324	miR-661	-0.69	0.29
MIMAT0003325	miR-662	-0.63	0.56
MIMAT0003326	miR-663	-1.83	0.37
MIMAT0003881	miR-668	-1.46	0.12
MIMAT0003880	miR-671	-0.61	0.33
MIMAT0004284	miR-675	-1.11	0.26
MIMAT0000252	miR-7	-0.11	0.08

Accesion number in miRBase v9.2	miRNA ID	*Z*-score	S.E.M.
MIMAT0003879	miR-758	-0.35	0.50
MIMAT0003945	miR-765	-2.09	0.52
MIMAT0003888	miR-766	-0.11	0.76
MIMAT0003883	miR-767-3p	-0.38	0.22
MIMAT0003882	miR-767-5p	-0.01	0.20
MIMAT0003947	miR-768-3p	-0.08	0.10
MIMAT0003946	miR-768-5p	-0.20	0.21
MIMAT0003887	miR-769-3p	0.01	0.17
MIMAT0003886	miR-769-5p	-1.28	0.71
MIMAT0003948	miR-770-5p	0.55	0.41
MIMAT0004209	miR-801	-1.12	0.39
MIMAT0004185	miR-802	-0.05	0.17
MIMAT0000441	miR-9	0.17	0.44
MIMAT0000442	miR-9*	0.14	0.71
MIMAT0000092	miR-92	-0.12	0.32
MIMAT0003218	miR-92b	0.00	0.37
MIMAT0000093	miR-93	0.12	0.21
MIMAT0000094	miR-95	0.23	0.37
MIMAT0000095	miR-96	-1.67	0.19
MIMAT0000096	miR-98	-0.68	0.06
MIMAT0000097	miR-99a	-0.09	0.46
MIMAT0000689	miR-99b	-0.46	0.24

Appendix II: Accession numbers and IDs of 113 mature human miRNAs that were detected in HeLa cells by expression profiling analysis. Microarrays were designed for profiling all miRNAs annotated in miRBase v14. Median-normalized expression levels (in linear scale) and standard errors of the mean (S.E.M.) are given. The median signal intensity of each microarray is adjusted to "1".

Accesion number in miRBase v14	miRNA ID	Expression level	S.E.M
MIMAT0000062	let-7a	97.68	4.15
MIMAT0000063	let-7b	57.19	1.18
MIMAT0000064	let-7c	16.45	0.62
MIMAT0000065	let-7d	11.27	0.52
MIMAT0000066	let-7e	12.00	0.29
MIMAT0000067	let-7f	68.45	3.18
MIMAT0000414	let-7g	17.72	0.89
MIMAT0000415	let-7i	76.44	2.89
MIMAT0000098	miR-100	8.85	0.27
MIMAT0000099	miR-101	2.04	0.17
MIMAT0000101	miR-103	8.27	0.34
MIMAT0000680	miR-106b	13.65	0.89
MIMAT0000104	miR-107	8.86	0.51
MIMAT0005865	miR-1202	1.66	0.09
MIMAT0005898	miR-1246	8.63	0.16
MIMAT0000443	miR-125a-	4.05	0.09
MIMAT0000423	miR-125b	21.14	0.92
MIMAT0005911	miR-1260	44.10	3.29
MIMAT0005927	miR-1274a	23.88	1.68
MIMAT0005938	miR-1274b	153.88	10.82
MIMAT0005946	miR-1280	3.02	0.19

Accesion number in miRBase v14	miRNA ID	Expression level	S.E.M
MIMAT0005880	miR-1290	1.17	0.05
MIMAT0005893	miR-1305	1.22	0.07
MIMAT0005947	miR-1308	1.17	0.09
MIMAT0000425	miR-130a	10.14	0.48
MIMAT0000691	miR-130b	2.42	0.09
MIMAT0000448	miR-136	3.25	0.21
MIMAT0000431	miR-140-5p	2.66	0.18
MIMAT0000759	miR-148b	1.34	0.10
MIMAT0000757	miR-151-3p	1.68	0.06
MIMAT0004697	miR-151-5p	6.89	0.21
MIMAT0000068	miR-15a	18.68	1.09
MIMAT0000417	miR-15b	44.05	1.55
MIMAT0000069	miR-16	36.33	1.58
MIMAT0000070	miR-17	22.06	1.11
MIMAT0000071	miR-17*	4.91	0.26
MIMAT0000256	miR-181a	5.05	0.23
MIMAT0000257	miR-181b	3.07	0.14
MIMAT0000455	miR-185	1.26	0.07
MIMAT0000072	miR-18a	3.56	0.23
MIMAT0001412	miR-18b	1.22	0.08
MIMAT0007892	miR-1915	1.81	0.13

Accesion number in miRBase v14	miRNA ID	Expression level	S.E.M
MIMAT0000459	miR-193a-	5.41	0.37
MIMAT0002819	miR-193b	14.62	0.79
MIMAT0000226	miR-196a	6.49	0.32
MIMAT0001080	miR-196b	1.64	0.07
MIMAT0000227	miR-197	1.41	0.06
MIMAT0009449	miR-1974	812.96	56.92
MIMAT0009454	miR-1979	1.87	0.12
MIMAT0000073	miR-19a	26.34	1.62
MIMAT0000074	miR-19b	62.64	3.42
MIMAT0000075	miR-20a	50.29	1.91
MIMAT0001413	miR-20b	9.21	0.57
MIMAT0000076	miR-21	1082.09	45.52
MIMAT0004494	miR-21*	3.17	0.20
MIMAT0000077	miR-22	36.57	1.54
MIMAT0000278	miR-221	3.25	0.24
MIMAT0000281	miR-224	8.29	0.54
MIMAT0000078	miR-23a	85.07	5.22
MIMAT0000418	miR-23b	21.34	1.17
MIMAT0000080	miR-24	59.26	3.31
MIMAT0000081	miR-25	7.80	0.26
MIMAT0000082	miR-26a	3.13	0.20
MIMAT0000083	miR-26b	2.95	0.15
MIMAT0000084	miR-27a	114.31	6.11
MIMAT0000419	miR-27b	33.99	1.67
MIMAT0000085	miR-28-5p	2.11	0.14
MIMAT0000086	miR-29a	16.87	0.91
MIMAT0000100	miR-29b	14.17	0.88
MIMAT0000681	miR-29c	2.15	0.14
MIMAT0000688	miR-301a	4.29	0.21
MIMAT0000087	miR-30a	16.33	0.94
MIMAT0000088	miR-30a*	4.02	0.22
MIMAT0000420	miR-30b	5.49	0.35
MIMAT0000244	miR-30c	8.58	0.23
MIMAT0000245	miR-30d	3.17	0.12
MIMAT0000692	miR-30e	1.96	0.16
MIMAT0000693	miR-30e*	1.30	0.06

Accesion number in miRBase v14	miRNA ID	Expression level	S.E.M
MIMAT0000089	miR-31	7.76	0.67
MIMAT0004504	miR-31*	11.31	0.61
MIMAT0000510	miR-320a	2.26	0.11
MIMAT0005792	miR-320b	5.95	0.28
MIMAT0005793	miR-320c	6.14	0.33
MIMAT0006764	miR-320d	9.12	0.37
MIMAT0000762	miR-324-3p	4.39	0.29
MIMAT0000761	miR-324-5p	2.51	0.08
MIMAT0000760	miR-331-3p	3.59	0.19
MIMAT0000091	miR-33a	1.84	0.16
MIMAT0000753	miR-342-3p	1.35	0.04
MIMAT0000255	miR-34a	9.06	0.49
MIMAT0000703	miR-361-5p	2.85	0.11
MIMAT0000710	miR-365	7.90	0.87
MIMAT0000727	miR-374a	2.51	0.18
MIMAT0000720	miR-376c	1.84	0.09
MIMAT0000730	miR-377	1.62	0.09
MIMAT0001341	miR-424	4.25	0.19
MIMAT0003393	miR-425	1.71	0.10
MIMAT0001635	miR-452	1.10	0.06
MIMAT0004784	miR-455-3p	2.23	0.10
MIMAT0003233	miR-551b	2.14	0.12
MIMAT0003239	miR-574-3p	3.14	0.22
MIMAT0004795	miR-574-5p	2.40	0.14
MIMAT0003247	miR-582-5p	4.43	0.22
MIMAT0003258	miR-590-5p	3.11	0.14
MIMAT0004814	miR-654-3p	1.24	0.09
MIMAT0005954	miR-720	491.34	17.46
MIMAT0004906	miR-886-3p	33.14	2.64
MIMAT0000092	miR-92a	15.84	0.80
MIMAT0000093	miR-93	8.24	0.51
MIMAT0000095	miR-96	4.71	0.21
MIMAT0000096	miR-98	2.49	0.14
MIMAT0000097	miR-99a	6.52	0.29
MIMAT0000689	miR-99b	2.25	0.10

Appendix III: Genes affected by overexpression of *miR-17*. An expression change cutoff values of -1.5 and 1.5 (in linear scale) corresponding to an adjusted p-value ≤ 0.05 were used as criteria to identify significantly downregulated and upregulated genes, respectively. Genes are listed from the most to the least affected according to the time point at which individual gene was identified as significantly deregulated for the first time. "Yes" indicates that gene is a predicted target of *miR-17* by at least one of the three computational prediction programs (MicroCosm Targets v5, Diana-microT v3.0, TargetScanHuman release 5.2).

(**A**) Genes downregulated by overexpressed *miR-17*

Number	Gene symbol	Expression change			Predicted target?	Gene accession number
		12h	24h	48h		
1	TGFBR2	-2.00	-1.90		Yes	NM_001024847.1
2	DAZAP2	-1.92	-1.87		Yes	NM_014764.2
3	MICA	-1.85	-1.71	-1.58	Yes	NM_000247.1
4	TBC1D2	-1.78	-1.95	-1.52	Yes	NM_018421.2

Number	Gene symbol	Expression change			Predicted target?	Gene accession number
		12h	24h	48h		
5	NKIRAS1	-1.75	-1.62		Yes	NM_020345.3
6	SQSTM1	-1.72	-1.67		Yes	NM_003900.3
7	NETO2	-1.72				NM_018092.3
8	HDHD1A	-1.69	-1.93			NM_012080.3
9	FLJ31438	-1.69				NM_152385.1
10	JAK1	-1.65	-2.00		Yes	NM_002227.1
11	CYBRD1	-1.63			Yes	NM_024843.2
12	IL6	-1.63	-2.12	-3.49		NM_000600.1
13	TMEM64	-1.61			Yes	NM_001008495.2
14	RNH1	-1.60	-2.01	-1.56	Yes	NM_203385.1
15	FYCO1	-1.60	-1.68	-1.52	Yes	NM_024513.1
16	TNFRSF21	-1.59			Yes	NM_014452.3
17	FAM79A	-1.59	-1.64			NM_182752.3
18	TMEM9B	-1.58	-1.57			NM_020644.1
19	MKRN1	-1.57			Yes	NM_013446.2
20	FASTK	-1.57			Yes	NM_033015.2
21	C2ORF29	-1.57				NM_017546.3
22	ASAP2	-1.56	-1.65			NM_003887.1
23	C21ORF25	-1.55	-1.61	-1.53	Yes	NM_199050.1
24	NLRP8	-1.55				NM_176811.2
25	SLC28A1	-1.54				NM_201651.1
26	KATNAL1	-1.54				NM_032116.3
27	FNBP1L	-1.53			Yes	NM_017737.3
28	KIF23	-1.53			Yes	NM_004856.4
29	PNKD	-1.53	-1.56			NM_022572.2
30	IRAK2	-1.53	-1.55	-1.87		NM_001570.3
31	PSCD1	-1.53				NM_017456.2
32	FBXO18	-1.52			Yes	NM_032807.3
33	ZFP91	-1.52			Yes	NM_053023.2
34	TNFRSF10B	-1.51			Yes	NM_003842.3
35	LIMA1	-1.51			Yes	NM_016357.3
36	LOC205251	-1.50	-1.68			NM_174925.1
37	C9ORF152		-1.87	-1.51		NM_001012993.1
38	MT2A		-1.78			NM_005953.2
39	FAM18B		-1.74			NM_016078.3
40	DNAJB6		-1.72			NM_005494.2
41	TNFAIP1		-1.71		Yes	NM_021137.3
42	EGR1		-1.69			NM_001964.2
43	FAM46C		-1.65		Yes	NM_017709.2
44	ETS2		-1.64			NM_005239.4
45	DNAJC12		-1.59	-1.54		NM_021800.2
46	MRPL24		-1.59		Yes	NM_024540.2
47	OBFC2A		-1.59		Yes	NM_022837.1
48	CYR61		-1.58	-1.91		NM_001554.3
49	WDR4		-1.57			NM_018669.4
50	BIRC3		-1.54	-1.68		NM_001165.3
51	M6PR		-1.53		Yes	NM_002355.2
52	WBSCR22		-1.53		Yes	NM_017528.2
53	DCPS		-1.52			NM_014026.3
54	C9ORF40		-1.52		Yes	NM_017998.1
55	PFKP		-1.52		Yes	NM_002627.3
56	CASP1		-1.52			NM_033294.2
57	MT1A		-1.51			NM_005946.2
58	RAB32		-1.51			NM_006834.2
59	EPAS1		-1.50			NM_001430.3
60	KRT17			-2.11		NM_000422.1
61	C1QTNF1			-1.97		NM_198594.1

Number	Gene symbol	Expression change			Predicted target?	Gene accession number
		12h	24h	48h		
62	C8ORF4			-1.93		NM_020130.2
63	CCL20			-1.92		NM_004591.1
64	S100P			-1.91		NM_005980.2
65	SLC16A6			-1.86		NM_004694.2
66	HSF2BP			-1.79		NM_007031.1
67	MMP12			-1.74		NM_002426.2
68	TMEM16B			-1.74		NM_020373.1
69	TESC			-1.69	Yes	NM_017899.1
70	WDR69			-1.66		NM_178821.1
71	IL32			-1.64		NM_001012633.1
72	CA9			-1.64		NM_001216.1
73	LDLR			-1.64	Yes	NM_000527.2
74	RGS2			-1.61		NM_002923.1
75	CXCR7			-1.61		NM_001047841.1
76	NKD2			-1.61		NM_033120.2
77	GDF15			-1.59		NM_004864.1
78	CMKOR1			-1.57		NM_020311.1
79	WDR54			-1.57		NM_032118.2
80	AOX1			-1.55		NM_001159.3
81	CTGF			-1.53		NM_001901.2
82	SRGN			-1.53		NM_002727.2
83	ADAM9			-1.52	Yes	NM_003816.2
84	PITPNC1			-1.52		NM_181671.1
85	SERPINB8			-1.52		NM_001031848.1
86	C1S			-1.51		NM_001734.2
87	MUC1			-1.51		NM_001018021.1
88	TFPI			-1.51		NM_001032281.1
89	KRT16			-1.51		NM_005557.2
90	GNS			-1.51	Yes	NM_002076.2

(**B**) Genes upregulated by overexpressed *miR-17*

Number	Gene symbol	Expression change			Predicted target?	Gene accession number
		12h	24h	48h		
1	BAT2D1	1.70	1.52			NM_015172.2
2	PPIF	1.63				NM_005729.3
3	ICMT	1.62			Yes	NM_012405.2
4	LOC285636	1.57	1.66			NM_175921.4
5	PMM2	1.57	1.58			NM_000303.1
6	ETF1	1.53			Yes	NM_004730.1
7	TSC22D3	1.53	1.75			NM_004089.3
8	TMEM41A	1.52			Yes	NM_080652.2
9	UBE2O	1.51				NM_022066.2
10	B4GALT4	1.50				NM_003778.3
11	ARID3A		1.69			NM_005224.1
12	SNRPC		1.66	1.60		NM_003093.1
13	DDAH1		1.62			NM_012137.2
14	GNB1		1.62			NM_002074.2
15	SLC35A1		1.61			NM_006416.2
16	PPM1B		1.60			NM_177968.2
17	PSAT1		1.58		Yes	NM_021154.3
18	EML4		1.56			NM_019063.2
19	TRIM2		1.56			NM_015271.2
20	ARID5B		1.55			NM_032199.1
21	SLC11A2		1.55			NM_000617.1

Number	Gene symbol	Expression change			Predicted target?	Gene accession number
		12h	24h	48h		
22	PLCXD1		1.54		Yes	NM_018390.1
23	CITED2		1.54			NM_006079.3
24	ARPC4		1.54			NM_001024960.1
25	TAC3			3.75		NM_001006667.1
26	ACTA2			2.01		NM_001613.1
27	KRT86			1.95		NM_002284.3
28	KRTHB1			1.89		NM_002281.2
29	OLFML1			1.86		NM_198474.2
30	ALDH1A3			1.86		NM_000693.1
31	SLC1A3			1.85		NM_004172.3
32	CLCA2			1.84		NM_006536.4
33	S100A4			1.77		NM_002961.2
34	CRYAB			1.77		NM_001885.1
35	SPINK4			1.77		NM_014471.1
36	SNCG			1.64		NM_003087.1
37	KRT8			1.63		NM_002273.2
38	TNFSF9			1.62		NM_003811.2
39	ZNF467			1.62		NM_207336.1
40	LOC91461			1.61		NM_138370.1
41	ENO3			1.60		NM_001976.2
42	VAV3			1.60		NM_006113.4
43	MGP			1.59		NM_000900.2
44	SUSD2			1.58		NM_019601.3
45	SLC12A3			1.55		NM_000339.1
46	PPFIBP2			1.55		NM_003621.1
47	FGFR3			1.55		NM_000142.2
48	RPESP			1.53		NM_153225.2
49	STEAP4			1.53		NM_024636.1
50	GPR37			1.53		NM_005302.2
51	TST			1.52		NM_003312.4
52	SCNN1A			1.51		NM_001038.4
53	VAMP5			1.51		NM_006634.2
54	GAS1			1.51		NM_002048.1
55	REEP6			1.51		NM_138393.1
56	CRIP1			1.50		NM_001311.3

Appendix IV: Genes affected by *miR-517a*. An expression change cutoff values of -1.5 and 1.5 (in linear scale) corresponding to an adjusted p-value ≤ 0.01 were used as criteria to identify significantly downregulated and upregulated genes, respectively. Genes are listed from the most to the least affected according to the time point at which individual gene was identified as significantly deregulated for the first time. "Yes" indicates that gene is a predicted target of *miR-517a* by at least one of the three computational prediction programs (MicroCosm Targets v5, Diana-microT v3.0, TargetScanHuman release 5.2).

(A) Genes downregulated by *miR-517a*

Number	Gene symbol	Fold change			Predicted target?	Gene accession number
		12h	24h	48h		
1	EPDR1	-3.26	-6.06	-5.21		NM_017549.3
2	STUB1	-3.13	-4.03	-3.90		NM_005861.2
3	TNIP1	-2.73	-2.50	-1.91	Yes	NM_006058.3
4	DBN1	-2.64	-2.45	-2.13	Yes	NM_004395.2
5	CARM1	-2.61	-3.68	-3.84		NM_199141.1
6	TOMM5	-2.58	-3.93	-4.59		NM_001001790.2
7	TMEM30A	-2.51	-2.15	-1.96		NM_018247.2

Number	Gene symbol	Fold change			Predicted target?	Gene accession number
		12h	24h	48h		
8	PDXP	-2.49	-3.52	-3.89		NM_020315.4
9	SLC7A5	-2.45	-2.73	-2.42		NM_003486.5
10	LOC390298	-2.45	-3.41	-2.56		XR_019644.1
11	CDKN1C	-2.45	-3.46	-3.03	Yes	NM_000076.1
12	NCLN	-2.44	-2.46	-1.82		NM_020170.3
13	NFIA	-2.40	-2.65	-3.03		NM_005595.1
14	ELFN2	-2.40	-2.02	-2.27	Yes	NM_052906.3

Number	Gene symbol	Fold change			Predicted target?	Gene accession number
		12h	24h	48h		
15	AKIRIN1	-2.30	-1.95	-2.26	Yes	NM_024595.1
16	PTGES	-2.25	-1.57		Yes	NM_004878.3
17	TIMM17B	-2.24	-3.10	-2.37	Yes	NM_005834.1
18	CERK	-2.23	-2.58	-2.45		NM_022766.4
19	AP1S2	-2.21	-2.31	-2.02		NM_003916.3
20	CABLES1	-2.18	-3.04	-2.45		NM_138375.1
21	SLC3A2	-2.05	-1.91	-1.54		NM_001013251.1
22	LOC730455	-2.03	-3.68	-3.34		XM_001125904.1
23	PACS1	-2.01	-2.64	-2.36		NM_018026.2
24	LOC100134182	-2.00		-1.53		XM_001715185.1
25	KATNAL1	-1.99	-1.87	-1.67		NM_001014380.1
26	NFIC	-1.97	-1.72	-1.95		NM_205843.1
27	RAB40B	-1.95	-2.77	-2.95		NM_006822.1
28	CDK2AP1	-1.93	-2.46	-1.98	Yes	NM_004642.2
29	NTAN1	-1.93	-3.35	-3.36		NM_173474.2
30	TSKU	-1.93	-1.57			NM_015516.3
31	WDR45L	-1.92	-2.06	-1.77	Yes	NM_019613.2
32	CDS2	-1.92	-2.63	-2.51		NM_003818.2
33	MAPK6	-1.91	-2.03			NM_002748.2
34	EFHD2	-1.90	-2.50	-1.89		NM_024329.4
35	FAM189B	-1.90	-3.00	-3.13		NM_006589.2
36	CHRAC1	-1.89	-2.01	-1.97		NM_017444.3
37	STK39	-1.83	-1.58	-1.72		NM_013233.2
38	HYAL1	-1.82	-2.20	-2.04		NM_153282.1
39	CBX6	-1.82	-1.97	-1.96		NM_014292.3
40	UBR7	-1.81	-2.33	-2.57		NM_001100417.1
41	TMEM87A	-1.81				NM_015497.2
42	ADAM9	-1.80	-2.39	-2.59		NM_003816.2
43	ASB13	-1.80	-1.88	-1.60		NM_024701.2
44	FOXJ3	-1.80	-2.14	-1.78	Yes	NM_014947.3
45	ETNK1	-1.79	-1.91	-1.53		NM_018638.4
46	CTBP1	-1.79	-1.77	-1.81		NM_001328.2
47	SEPHS1	-1.78	-2.20	-2.54	Yes	NM_012247.3
48	CSNK2A2	-1.78	-1.87	-1.80		NM_001896.2
49	NUPL2	-1.78	-1.56	-1.79	Yes	NM_007342.1
50	ARCN1	-1.76	-1.71		Yes	NM_001655.3
51	CEP55	-1.75	-1.89	-3.58		NM_018131.3
52	CSK	-1.74	-1.85	-1.54		NM_004383.1
53	C5ORF46	-1.74	-2.16	-3.39		NM_206966.2
54	LOC100129828	-1.74	-1.77	-2.14		XM_001724980.1
55	GRAMD1A	-1.74	-1.71	-1.81	Yes	NM_020895.2
56	RAB35	-1.74		-1.57		NM_006861.4
57	RAB40C	-1.74	-1.53			NM_021168.2
58	SLC6A9	-1.73	-1.62		Yes	NM_001024845.1
59	TOB1	-1.72	-1.69	-1.88		NM_005749.2
60	METRNL	-1.72				XM_941466.2
61	AES	-1.72	-2.99	-2.94		NM_001130.5
62	USP1	-1.72	-2.02	-2.40	Yes	NM_001017416.1
63	C22ORF9	-1.71		-1.77		NM_015264.1
64	YDJC	-1.70	-2.35	-2.51		NM_001017964.1
65	RPS23	-1.70	-1.72	-1.85		
66	C12ORF49	-1.70	-1.94	-1.88	Yes	NM_024738.1
67	TRAK1	-1.69				NM_014965.2
68	DVL3	-1.69	-1.73	-1.83		NM_004423.3
69	DOK4	-1.68	-1.99	-2.36		NM_018110.2
70	MRRF	-1.68	-2.59	-2.56	Yes	NM_199177.1
71	NFIB	-1.68	-1.91	-2.77	Yes	NM_005596.2

Number	Gene symbol	Fold change			Predicted target?	Gene accession number
		12h	24h	48h		
72	CCNK	-1.67	-1.59		Yes	NM_003858.3
73	LRSAM1	-1.67	-1.59			NM_138361.3
74	TSPYL6	-1.67				NM_001003937.2
75	LYSMD2	-1.66	-2.11	-2.20		NM_153374.1
76	PLAGL2	-1.64	-1.77	-1.99		NM_002657.2
77	PSMF1	-1.64	-2.52	-2.75		NM_178579.1
78	ZFAND6	-1.64	-1.77	-1.82		NM_019006.2
79	FGFRL1	-1.64	-1.98	-1.98		NM_021923.3
80	C20ORF11	-1.62	-1.95	-1.71		NM_017896.2
81	TMEM203	-1.62	-2.01	-2.22		NM_053045.1
82	C17ORF49	-1.62	-2.01	-2.33	Yes	NM_174893.1
83	SMYD3	-1.58	-1.87	-1.51	Yes	NM_022743.1
84	EPDR1		-6.06	-5.21		NM_017549.2
85	LOC392437		-3.04	-1.95		XR_037197.1
86	LPL		-2.75	-4.42		NM_000237.1
87	UBP1		-2.45	-2.24		NM_014517.2
88	ANKRD29		-2.36	-2.50		NM_173505.2
89	VTI1B		-2.35	-2.15		NM_006370.1
90	PANX2		-2.31			NM_052839.2
91	GINS2		-2.31	-3.67		NM_016095.1
92	RRP1B		-2.21	-2.07		NM_015056.1
93	REEP5		-2.21	-2.06		NM_005669.3
94	CDCA7L		-2.21	-2.27		NM_018719.2
95	C4orf34		-2.20		Yes	NM_174921.1
96	CMBL		-2.18	-1.84		NM_138809.2
97	LOC440731		-2.14	-2.42		XM_933693.1
98	TMEM109		-2.11	-2.12		NM_024092.1
99	CAP2		-2.10	-1.87	Yes	NM_006366.2
100	SLC25A23		-2.08	-2.41		NM_024103.2
101	JPH1		-2.08	-2.12		NM_020647.2
102	DYM		-2.06		Yes	NM_017653.2
103	GOLSYN		-2.06	-2.35		NM_017786.2
104	SRM		-2.06	-1.58		NM_003132.2
105	MUTED		-2.04	-1.99		NM_201280.1
106	RPS6KA4		-2.01	-1.62		NM_003942.2
107	KIAA1671		-2.01	-1.92		XM_371461.4
108	C1orf43		-2.00	-1.59		NM_015449.1
109	ZDHHC4		-2.00	-1.92		NM_018106.3
110	FAM3A		-2.00	-2.08		NM_021806.1
111	DCAF6		-1.99	-2.05		NM_018442.2
112	ABHD14B		-1.97	-1.67		
113	WSB2		-1.96	-1.52		NM_018639.3
114	RPLP1		-1.96	-2.89		NM_001003.2
115	LOC728640		-1.95			XR_015400.1
116	FREQ		-1.94			NM_014286.2
117	NA		-1.93	-3.56		Hs.370359
118	CYBASC3		-1.92	-1.54		NM_153611.3
119	ARL5A		-1.92	-1.57		NM_012097.2
120	SFRS1		-1.91	-1.93	Yes	NM_006924.3
121	RAC1		-1.91	-4.11		NM_018890.2
122	USP13		-1.91	-2.67		NM_003940.1
123	SDCBP		-1.90			NM_001007067.1
124	HOXA10		-1.90	-1.99		NM_153715.1
125	MYC		-1.89	-2.04	Yes	NM_002467.3
126	RUNX3		-1.89	-1.52		NM_004350.1
127	LOC652685		-1.88			XM_942289.1
128	PHF13		-1.87	-1.68	Yes	NM_153812.1

Number	Gene symbol	Fold change			Predicted target?	Gene accession number
		12h	24h	48h		
129	TERF2		-1.87	-1.95		NM_005652.2
130	KIF26A		-1.87			NM_015656.1
131	TLN2		-1.87		Yes	NM_015059.1
132	FAM171A1		-1.87	-1.79		NM_001010924.1
133	MARCKSL1		-1.86	-3.01		NM_023009.4
134	B4GALT2		-1.85	-1.71		NM_001005417.1
135	RIPK2		-1.84			NM_003821.4
136	TNFRSF11B		-1.84	-3.80		NM_002546.2
137	TCEAL1		-1.83	-1.85		NM_001006639.1
138	SMU1		-1.82	-1.74		NM_018225.1
139	SEPT11		-1.82	-2.36		NM_018243.2
140	LOC647349		-1.82			NM_001284.2
141	HOXC4		-1.82			NM_153633.1
142	PARVB		-1.81	-1.83		NM_013327.3
143	MGAT4B		-1.81	-1.52		
144	AGPAT3		-1.80			NM_020132.3
145	LOC652233		-1.80	-2.62		XM_941627.1
146	TMEM111		-1.80	-1.59	Yes	NM_018447.1
147	GOLGA8A		-1.80	-1.81		NM_181077.2
148	LUZP1		-1.79	-1.72		NM_033631.2
149	PPP6C		-1.79	-1.74		NM_002721.3
150	PLEKHA9		-1.78	-1.51		NM_015899.1
151	LOC653383		-1.78	-1.69		XM_927177.1
152	IRAK1		-1.78	-2.20	Yes	NM_001025243.1
153	LYRM7		-1.77	-2.33		NM_181705.2
154	BCAP31		-1.77	-1.75		NM_005745.6
155	C6orf211		-1.77	-1.54		NM_024573.1
156	PSME4		-1.76			NM_014614.1
157	ABCD1		-1.76	-1.82		NM_000033.2
158	EXOSC6		-1.76	-1.83		NM_058219.2
159	PRUNE		-1.76	-1.67		NM_021222.1
160	EI24		-1.75	-1.61		NM_004879.3
161	TYSND1		-1.75	-3.11		NM_173555.1
162	RAB26		-1.75	-2.98		NM_014353.4
163	PABPC1L		-1.75	-1.99		XM_001722078.1
164	KIF3B		-1.75	-1.66		NM_004798.2
165	C8orf33		-1.75	-1.93		NM_023080.1
166	LOC100134361		-1.75	-2.39		XM_001726827.1
167	LOC283267		-1.75	-1.69		NR_015451.1
168	CCNE1		-1.75	-1.89		NM_001238.1
169	ALDH3A2		-1.74	-2.11		NM_001031806.1
170	FANCE		-1.74			NM_021922.2
171	FBXL16		-1.74			NM_153350.2
172	IGF2R		-1.73			NM_000876.1
173	PREPL		-1.73	-1.87		NM_006036.2
174	TMEM5		-1.73	-2.42		NM_014254.1
175	FLJ20674		-1.72	-2.02		NM_019086.2
176	YAP1		-1.72	-1.71		NM_006106.2
177	GDE1		-1.72	-1.70		NM_016641.3
178	ELL2		-1.72			NM_012081.3
179	CAMKK2		-1.71			NM_172215.1
180	ALG3		-1.71	-1.62		NM_001006940.1
181	CPSF4		-1.71	-1.89		NM_006693.1
182	POLR1D		-1.71	-2.31		NM_015972.1
183	EIF2C2		-1.71			NM_012154.2
184	ATG10		-1.70	-1.65		NM_031482.3
185	ICAM2		-1.70			NM_000873.2

Number	Gene symbol	Fold change			Predicted target?	Gene accession number
		12h	24h	48h		
186	WNT5A		-1.69	-2.39		NM_003392.3
187	SNORD83B		-1.69	-1.94		NR_000028.1
188	OLR1		-1.69			NM_002543.2
189	PRMT6		-1.68	-1.60		NM_018137.1
190	C17orf85		-1.68	-1.56		NM_018553.1
191	HIST2H2AA4		-1.68	-2.98		NM_001040874.1
192	ECEL1		-1.68	-2.13		NM_004826.1
193	CCNJL		-1.68	-1.50		NM_024565.5
194	JAG2		-1.68			NM_002226.3
195	LOC389816		-1.68	-2.17		NM_001013653.1
196	TTYH3		-1.67			NM_025250.2
197	FBXO9		-1.67		Yes	NM_033480.1
198	LOC645781		-1.67			XM_933141.1
199	FAM133B		-1.67	-1.98		NM_152789.2
200	ALCAM		-1.67			NM_001627.2
201	ARMC1		-1.66	-2.03		NM_018120.3
202	STX11		-1.66			NM_003764.2
203	DHX40		-1.66			NM_024612.3
204	RBPMS2		-1.66	-1.75		NM_194272.1
205	IFIT2		-1.66	-1.54		NM_001547.3
206	KCTD12		-1.66	-1.85		NM_138444.2
207	HPD		-1.66	-3.05		NM_002150.2
208	TAF6		-1.66			NM_139122.1
209	ATF1		-1.65	-1.91		NM_005171.2
210	OBFC2A		-1.65	-1.53		NM_022837.1
211	TMEM201		-1.65	-2.01		NM_001010866.1
212	FNBP1		-1.65			NM_015033.2
213	POLDIP2		-1.65	-1.83		NM_015584.2
214	MAT2B		-1.65	-1.71		NM_182796.1
215	URM1		-1.64			NM_030914.1
216	C12orf65		-1.64	-1.60	Yes	NM_152269.1
217	SNX5		-1.64	-1.89		NM_152227.1
218	STAC2		-1.64	-1.71		NM_198993.2
219	CTSZ		-1.64	-2.06	Yes	NM_001336.2
220	PLD6		-1.64			NM_178836.2
221	E2F2		-1.64	-1.93		NM_004091.2
222	UROS		-1.64	-1.96		NM_000375.1
223	LOC100129673		-1.64	-3.61		XM_001715544.1
224	RYBP		-1.63	-1.99	Yes	NM_012234.3
225	ZNF783		-1.63			NM_001004302.2
226	TTLL12		-1.63	-2.00		NM_015140.2
227	AP3S1		-1.63			NM_001002924.1
228	RPP25		-1.63	-1.59		NM_017793.1
229	PVT1		-1.63	-2.14		XM_944465.1
230	SLC6A10P		-1.62			NM_198857.1
231	PLCD3		-1.62			NM_133373.2
232	OPN3		-1.62	-2.05		NM_001030012.1
233	MANSC1		-1.62	-1.70		NM_018050.2
234	B3GALT6		-1.62			NM_080605.2
235	RAPGEF2		-1.62	-1.56		NM_014247.2
236	ACAA1		-1.62		Yes	NM_001607.2
237	LOC389641		-1.62	-1.68		XM_374260.3
238	KIAA0101		-1.62	-3.00		NM_014736.4
239	GOLGA8B		-1.62	-1.71		NM_001023567.2
240	PDSS1		-1.62	-1.95		NM_014317.3
241	OSBPL5		-1.62			NM_020896.2
242	IFITM1		-1.62	-2.08	Yes	NM_003641.2

Number	Gene symbol	Fold change			Predicted target?	Gene accession number
		12h	24h	48h		
243	SQRDL		-1.61			NM_021199.2
244	TMEM150A		-1.61			NM_001031738.1
245	MORF4L1		-1.61	-1.59		NM_006791.2
246	NBEAL2		-1.61	-1.67		XM_941211.1
247	LOC644033		-1.61	-1.93		XM_927280.1
248	SNHG9		-1.61	-2.80		NR_003142.2
249	LRRC26		-1.61	-2.11		XM_939320.1
250	LOC653308		-1.61			XM_928675.1
251	CDS1		-1.61			NM_001263.2
252	SMG7		-1.61	-1.84	Yes	NM_014837.3
253	EIF2S3		-1.60			NM_001415.2
254	BOLA1		-1.60	-1.85		NM_016074.1
255	FANCG		-1.60	-2.63		NM_004629.1
256	C3orf72		-1.60	-1.66		XM_376269.2
257	SEC11A		-1.60	-1.51		NM_014300.2
258	CXCR4		-1.60			NM_003467.2
259	CSRP2BP		-1.60	-1.64		NM_020536.2
260	HMOX1		-1.60			NM_002133.1
261	ZNF581		-1.60			NM_016535.3
262	POLR2D		-1.60			NM_004805.2
263	HIST2H2AA3		-1.60	-3.00		NM_003516.2
264	UHRF1BP1		-1.59			NM_017754.3
265	LOC728715		-1.59	-1.94		XM_931759.1
266	LOC100129866		-1.59	-1.53		XR_037532.1
267	STOM		-1.59	-1.50		NM_004099.4
268	FAM119B		-1.59	-1.55		NM_206914.1
269	LOC286208		-1.59	-1.55		XM_379668.3
270	ELAC2		-1.58	-2.17		
271	RFNG		-1.58		Yes	NM_002917.1
272	MGST1		-1.58		Yes	NM_145792.1
273	C1orf107		-1.58			NM_014388.5
274	TXNRD1		-1.58			NM_182743.1
275	CTSC		-1.58			NM_001814.2
276	LOC440927		-1.58	-1.68		XM_944816.1
277	C9orf46		-1.57			NM_018465.1
278	CNN2		-1.57	-2.33		NM_201277.1
279	LOC729887		-1.57	-2.36		XR_040891.1
280	JDP2		-1.57			NM_130469.2
281	FLJ11235		-1.57	-1.75		XR_000626.1
282	DAB2		-1.57	-1.62		NM_001343.1
283	CPNE8		-1.57	-1.85		NM_153634.2
284	LOC648526		-1.56	-1.64		XM_937579.1
285	LOC90624		-1.56	-1.64		NM_181705.1
286	ZIC2		-1.56	-1.66		NM_007129.2
287	HIST2H2AC		-1.56	-3.25		NM_003517.2
288	MEIS2		-1.56	-1.85		NM_020149.2
289	FLJ20021		-1.56			XM_028217.4
290	MCOLN2		-1.55	-1.95		NM_153259.2
291	CPA4		-1.55	-1.94		NM_016352.2
292	LOC100129028		-1.55	-1.88		XM_001722134.1
293	SLC6A8		-1.55			NM_005629.1
294	CCDC92		-1.55	-1.53		NM_025140.1
295	PGAM5		-1.55	-1.80		XM_942043.1
296	CLIC4		-1.55			NM_013943.1
297	SNORA10		-1.55	-1.90		NR_002327.1
298	LOC407835		-1.55			NR_002144.1
299	WRB		-1.55	-1.84		NM_004627.2

Number	Gene symbol	Fold change			Predicted target?	Gene accession number
		12h	24h	48h		
300	ILF3		-1.55	-1.66		NM_004516.2
301	GJC2		-1.55			NM_020435.2
302	RPL17		-1.55			NM_000985.2
303	HSPB3		-1.54	-2.33		NM_006308.1
304	GRPEL1		-1.54	-1.95		NM_025196.2
305	CNRIP1		-1.54	-1.74		NM_015463.2
306	HDAC4		-1.54			NM_006037.2
307	F12		-1.54			NM_000505.2
308	RNF41		-1.54			NM_194359.1
309	PKP3		-1.54			NM_007183.2
310	ACY1		-1.54			NM_000666.1
311	TRIM23		-1.54			NM_001656.3
312	TMEM64		-1.54			NM_001008495.2
313	DNAJB4		-1.54			NM_007034.3
314	ADCY9		-1.54			NM_001116.2
315	ANKRD10		-1.53			NM_017664.2
316	RRM2		-1.53	-2.06		NM_001034.1
317	DUS3L		-1.53	-1.60		NM_020175.1
318	EMR2		-1.53	-1.53		NM_152916.1
319	SULT1A3		-1.53		Yes	NM_001017389.1
320	SNHG4		-1.53	-3.16		NM_199189.1
321	TTC9C		-1.53	-1.53	Yes	NM_173810.3
322	ARF3		-1.53			NM_001659.1
323	LOC401397		-1.53			Hs.117929
324	KITLG		-1.53	-1.54		NM_000899.3
325	TEAD4		-1.53	-1.95		NM_201441.1
326	LOC645236		-1.53	-1.62		XM_928275.1
327	TCEA3		-1.53	-2.31		NM_003196.1
328	FKBP4		-1.53	-1.97		NM_002014.2
329	FAR2		-1.53			NM_018099.3
330	BLCAP		-1.53			NM_006698.2
331	MT1E		-1.52			NM_175617.3
332	CDC42SE2		-1.52			NM_001038702.1
333	KIF1C		-1.52	-1.61		NM_006612.3
334	ATN1		-1.52	-1.97		NM_001007026.1
335	TXNDC15		-1.52			NM_024715.2
336	MYO9B		-1.52			NM_004145.2
337	GLS		-1.52			NM_014905.2
338	KCTD14		-1.52	-1.55		NM_023930.2
339	BFAR		-1.52			
340	ITGA2		-1.52			NM_002203.2
341	UBAP2		-1.52		Yes	NM_018449.2
342	FOXC1		-1.52			NM_001453.1
343	INPPL1		-1.52		Yes	NM_001567.2
344	ITPRIPL2		-1.51	-1.93		XM_943094.1
345	RALGAPA1		-1.51	-1.91		NM_194301.2
346	PDPR		-1.51			NM_017990.3
347	ZNF514		-1.51			NM_032788.1
348	FJX1		-1.51	-2.26		NM_014344.2
349	PPL		-1.51	-2.22		NM_002705.3
350	VAMP2		-1.51	-1.99		NM_014232.1
351	C5orf25		-1.51	-1.77		NM_198567.1
352	YWHAZ		-1.51	-1.75		NM_003406.2
353	LOC340274		-1.51			XR_017256.2
354	SLC25A19		-1.51	-1.79	Yes	
355	NARS2		-1.51	-1.54		NM_024678.3
356	HNRNPU		-1.51	-2.38	Yes	NM_031844.2

Number	Gene symbol	Fold change			Predicted target?	Gene accession number
		12h	24h	48h		
357	SACS		-1.51			NM_014363.3
358	NCRNA00152		-1.51	-1.80		NR_024204.1
359	ANAPC7		-1.51			NM_016238.1
360	DLX1		-1.51	-1.50		NM_178120.3
361	PRKAR1B		-1.50			NM_002735.1
362	SLC25A40		-1.50			NM_018843.2
363	MGC61598		-1.50	-1.99		XM_939432.1
364	PTGFRN		-1.50	-2.02		NM_020440.2
365	C13orf25		-1.50	-2.08		XM_931068.1
366	SEMA4D		-1.50	-1.62		NM_006378.2
367	DIP2A		-1.50			NM_015151.2
368	PEX5		-1.50			NM_000319.3
369	CCL2			-3.07		NM_002982.3
370	PLAC8			-2.90		NM_016619.1
371	H2AFJ			-2.84		NM_177925.2
372	AOX1			-2.81		NM_001159.3
373	MATR3			-2.70		NM_199189.1
374	LOC440957			-2.68		NM_001124767.1
375	TNS3			-2.64		NM_022748.10
376	NMU			-2.64		NM_006681.1
377	HIST2H4A			-2.59		NM_003548.2
378	EBPL			-2.58		NM_032565.2
379	C18orf56			-2.53		NM_001012716.1
380	PRR11			-2.46		NM_018304.2
381	CD83			-2.44	Yes	NM_004233.3
382	CRB1			-2.40		NM_201253.1
383	SNORD80			-2.40		NR_003940.1
384	HIST3H2A			-2.40		NM_033445.2
385	MOSC1			-2.39	Yes	NM_022746.2
386	PEG10			-2.37		NM_001040152.1
387	MAPKAP1			-2.36		NM_001006618.1
388	NUSAP1			-2.35		NM_018454.5
389	RPL39L			-2.34		NM_052969.1
390	FAM179A			-2.31		NM_199280.2
391	HIST1H2AC			-2.28		NM_003512.3
392	STMN1			-2.27		NM_203401.1
393	ACYP1			-2.27		NM_001107.3
394	TMOD1			-2.27		NM_003275.2
395	FOXM1			-2.25		NM_021953.2
396	MYLIP			-2.23		NM_013262.3
397	DHFR			-2.23	Yes	NM_000791.3
398	DHRS11			-2.21		NM_024308.3
399	IFIT1			-2.20		NM_001548.3
400	AFAP1			-2.20	Yes	NM_021638.4
401	AGMAT			-2.20		NM_024758.3
402	FBL			-2.20		NM_001436.2
403	NME1			-2.18		NM_198175.1
404	HIST1H1C			-2.18		NM_005319.3
405	ADCY3			-2.17		NM_004036.3
406	AGAP3			-2.17		NM_001042535.1
407	SCARA3			-2.17		NM_016240.2
408	CENPA			-2.15		NM_001042426.1
409	ZNF548			-2.14		NM_152909.2
410	KIF11			-2.14		NM_004523.2
411	CRISPLD2			-2.14		NM_031476.2
412	CSTF3			-2.12		NM_001033506.1
413	LARP6			-2.12	Yes	NM_197958.1

Number	Gene symbol	Fold change			Predicted target?	Gene accession number
		12h	24h	48h		
414	FAM81A			-2.12		NM_152450.2
415	CENPM			-2.11		NM_001002876.1
416	CDC2			-2.10		NM_001786.2
417	CALML4			-2.09		NM_001031733.1
418	COBL			-2.08		NM_015198.2
419	SKP2			-2.08		NM_005983.2
420	TPR			-2.08		NM_003292.2
421	FERMT2			-2.07		NM_006832.1
422	C7orf11			-2.07		NM_138701.1
423	LOC729217			-2.07		XR_015614.2
424	ID1			-2.07		NM_181353.1
425	EXO1			-2.06		NM_006027.3
426	TACSTD1			-2.06		NM_002354.1
427	HIST1H2BG			-2.05	Yes	NM_003518.3
428	BOP1			-2.05		NM_015201.3
429	TTF2			-2.05		NM_003594.3
430	HIST2H4B			-2.04		NM_001034077.4
431	TUBD1			-2.04		NM_016261.2
432	SFRS7			-2.03		NM_001031684.1
433	ASF1B			-2.03		NM_018154.2
434	PARD6A			-2.03		NM_001037281.1
435	SNHG3-RCC1			-2.03		NM_001048197.1
436	COQ2			-2.03	Yes	NM_015697.6
437	RAD51C			-2.03		NM_002876.2
438	ADAMTS8			-2.03		NM_007037.3
439	TPM2			-2.02		NM_003289.3
440	CENPK			-2.01		NM_022145.3
441	SPC24			-2.01		NM_182513.1
442	C9orf103			-2.01		NM_001001551.1
443	ASPM			-2.01		NM_018136.3
444	NR2F1			-2.01		NM_005654.4
445	OLFM1			-2.01		NM_006334.3
446	AGBL5			-2.00		NM_001035507.2
447	FARP1			-2.00		NM_005766.2
448	DIS3L			-2.00		NM_133375.2
449	ALDH5A1			-1.99		NM_001080.3
450	LDLR			-1.99		NM_000527.2
451	LHX2			-1.99		NM_004789.3
452	C21orf58			-1.98		NM_199071.2
453	CTDSPL2			-1.97		NM_016396.2
454	PNN			-1.97		NM_002687.3
455	HIST1H3G			-1.96		NM_003534.2
456	RNU1G2			-1.95		NR_004426.1
457	SNRPD3			-1.95		NM_004175.3
458	LOC388564			-1.95		XM_498725.3
459	DIO2			-1.95		NM_001007023.2
460	SLC1A3			-1.95		NM_004172.3
461	PDE7B			-1.94		NM_018945.3
462	IGSF10			-1.94		NM_178822.3
463	GTSE1			-1.94		NM_016426.4
464	FUBP1			-1.94		NM_003902.3
465	FAH			-1.94		NM_000137.1
466	SERPINI1			-1.93		NM_005025.3
467	UNG			-1.93		NM_003362.2
468	MCM10			-1.93		NM_018518.3
469	PHF19			-1.93		NM_001009936.1
470	LOC387841			-1.92		XM_932678.1

Number	Gene symbol	Fold change			Predicted target?	Gene accession number
		12h	24h	48h		
471	PIF1			-1.92		NM_025049.2
472	WNT10B			-1.91		NM_003394.2
473	RPL8			-1.91		NM_033301.1
474	APOA1BP			-1.91		NM_144772.1
475	TACC3			-1.91		NM_006342.1
476	C21orf34			-1.91		NM_001005734.1
477	FLJ35934			-1.91		NM_207453.1
478	LOC731049			-1.91		XM_001129232.1
479	MYO5C			-1.91		NM_018728.2
480	OGG1			-1.91		NM_002542.4
481	FAM72D			-1.90		NM_207418.2
482	LOC644254			-1.90		XM_932079.1
483	SLC16A10			-1.90		NM_018593.3
484	MND1			-1.90		NM_032117.2
485	METTL7A			-1.89		NM_014033.3
486	TRIM7			-1.89		NM_033342.2
487	C20orf72			-1.89		NM_052865.2
488	LOC652235			-1.89		XM_941629.1
489	NCRNA00085			-1.89		NR_024330.1
490	PSRC1			-1.89		NM_001032290.1
491	KRT13			-1.88		NM_002274.3
492	SNCA			-1.88		NM_007308.1
493	SNORD36A			-1.88		NR_002448.1
494	CHAF1B			-1.88		NM_005441.2
495	AGXT2L1			-1.88		NM_031279.2
496	PAFAH1B3			-1.87		NM_002573.2
497	AK2			-1.87		NM_001625.2
498	SLC27A2			-1.87		NM_003645.2
499	HIST2H2AB			-1.87		NM_175065.2
500	RNU1-5			-1.87		NR_004400.1
501	DDX54			-1.87		NM_024072.3
502	PPIL5			-1.87	Yes	NM_203467.1
503	ZNF787			-1.87		NM_001002836.2
504	RNF212			-1.87		NM_194439.1
505	GCHFR			-1.87		NM_005258.2
506	CCNB1			-1.87		NM_031966.2
507	FAM133A			-1.87		NM_173698.1
508	LOC100130506			-1.86		XM_001724500.1
509	LOC730101			-1.86		NR_024403.1
510	LMNB1			-1.86		NM_005573.2
511	GPATCH4			-1.85		NM_182679.1
512	TMEM56			-1.85		NM_152487.1
513	NRG4			-1.85		NM_138573.2
514	SLC27A5			-1.85		NM_012254.1
515	BCAT2			-1.85		NM_001190.2
516	VAMP1			-1.85		NM_199245.1
517	EFHD1			-1.85		NM_025202.2
518	TRAP1			-1.85		NM_016292.1
519	CDCA3			-1.84		NM_031299.3
520	CHAC2			-1.84		NM_001008708.1
521	RDM1			-1.83		NM_001034836.1
522	CAMK1D			-1.83		NM_153498.2
523	LOC143543			-1.83		NR_002197.1
524	LOC100133328			-1.83		XR_038620.1
525	C11orf83			-1.83		NM_001085372.1
526	DPM3			-1.83		NM_153741.1
527	ATRIP			-1.83		NM_032166.2

Number	Gene symbol	Fold change			Predicted target?	Gene accession number
		12h	24h	48h		
528	GSTM1			-1.83		NM_000561.2
529	C6orf176			-1.83		XR_017929.2
530	KIF2C			-1.82		NM_006845.2
531	MCM3APAS			-1.82		NR_002776.1
532	LOC401152			-1.82		NM_001001701.1
533	CXorf61			-1.82		NM_001017978.1
534	RAD51AP1			-1.82		NM_006479.3
535	NMB			-1.82		NM_021077.3
536	HIST1H2AG			-1.82		NM_021064.3
537	LOC100130921			-1.82		XM_001723862.1
538	LOC541471			-1.82		XR_001013.1
539	PDE8B			-1.81		NM_001029851.1
540	C1orf135			-1.81		NM_024037.1
541	KIAA0114			-1.81		NR_024031.1
542	HIST2H2BE			-1.80		NM_003528.2
543	NUP62CL			-1.80		NM_017681.1
544	TROAP			-1.80		NM_005480.2
545	C19orf48			-1.80		NM_199250.1
546	ANKRD32			-1.80		NM_032290.2
547	CDK6			-1.80		NM_001259.5
548	LOC653610			-1.80		XM_928387.1
549	PAK2			-1.80		XM_001126110.1
550	LOC93622			-1.79		XR_017952.1
551	ZDHHC3			-1.79		NM_016598.1
552	LYAR			-1.79		NM_017816.1
553	NR2C2AP			-1.79		NM_176880.4
554	TUB			-1.79		NM_177972.1
555	BZW2			-1.79		NM_014038.1
556	IMPDH2			-1.78		NM_000884.2
557	LOC645726			-1.78		XR_018230.2
558	MSH5			-1.78		NM_172166.2
559	C9orf140			-1.78		NM_178448.2
560	HAUS4			-1.78		NM_017815.1
561	SMOC1			-1.78		NM_001034852.1
562	SRRM4			-1.78		NM_194286.2
563	LOC653820			-1.78		XM_930579.2
564	MEGF9			-1.78		NM_001080497.1
565	LXN			-1.77		NM_020169.2
566	POLA1			-1.77		NM_016937.2
567	PRDX3			-1.77		NM_006793.2
568	BRCA1			-1.77		NM_007299.2
569	ANXA2			-1.77		NM_001002857.1
570	DSCC1			-1.77		NM_024094.1
571	ZNF556			-1.77		NM_024967.1
572	DCTPP1			-1.77		NM_024096.1
573	CENPF			-1.77		NM_016343.3
574	PLCXD1			-1.76		NM_018390.2
575	LOC346887			-1.76		XM_943533.1
576	ASB9			-1.76		NM_024087.1
577	RFK			-1.76		NM_018339.3
578	INPP5E			-1.76		NM_019892.3
579	GPR37			-1.75		NM_005302.2
580	LOC651816			-1.75		XM_941060.1
581	RAD54L			-1.75	Yes	NM_003579.2
582	UGT8			-1.75		NM_003360.2
583	SMC2			-1.75		NM_001042550.1
584	IL17RB			-1.75		NM_018725.3

Number	Gene symbol	Fold change			Predicted target?	Gene accession number
		12h	24h	48h		
585	CDC45L			-1.75		NM_003504.3
586	KRT18P13			-1.75		XM_001726959.1
587	NGEF			-1.75	Yes	NM_019850.1
588	HIST1H2BD			-1.74		NM_138720.1
589	PDE12			-1.74		NM_177966.4
590	C1orf86			-1.74		NM_182533.1
591	HPDL			-1.74		NM_032756.2
592	IMPA2			-1.74		NM_014214.1
593	VAV3			-1.74		NM_006113.4
594	MESP1			-1.74		NM_018670.2
595	PTP4A1			-1.74		NM_003463.3
596	PUS7			-1.74		NM_019042.3
597	DFFA			-1.74		NM_004401.2
598	RACGAP1			-1.73		NM_013277.2
599	PRMT3			-1.73		NM_005788.1
600	CDCA7			-1.73		NM_031942.4
601	HSPC111			-1.73		NM_016391.3
602	EPCAM			-1.73		NM_002354.2
603	MRI1			-1.73		NM_001031727.2
604	RNU1-3			-1.73		NR_004408.1
605	SUV39H1			-1.72		NM_003173.2
606	HIST1H3H			-1.72		NM_003536.2
607	C5orf36			-1.72		NM_173665.1
608	HN1			-1.72	Yes	NM_016185.2
609	KDELC2			-1.72		NM_153705.4
610	DUT			-1.72		NM_001025248.1
611	KIF15			-1.72		NM_020242.1
612	SLC16A14			-1.72		NM_152527.3
613	TMEM106C			-1.72		NM_024056.2
614	RCCD1			-1.72		NM_001017919.1
615	KIAA1688			-1.72		NM_025251.1
616	CHCHD7			-1.72		NM_001011671.1
617	BICD2			-1.72		NM_001003800.1
618	APOBEC3B			-1.71		NM_004900.3
619	C7orf55			-1.71		NM_197964.3
620	HSDL2			-1.71	Yes	NM_032303.3
621	ABL1			-1.71		NM_007313.2
622	MNS1			-1.71		NM_018365.1
623	OSR2			-1.71		XM_001126824.1
624	SSBP3			-1.71		NM_018070.3
625	RBM4			-1.71	Yes	NM_002896.2
626	LOC727761			-1.71		XM_001126211.1
627	NHP2			-1.71		NM_001034833.1
628	LOC100128191			-1.71		XM_001718586.1
629	LSM5			-1.71		NM_012322.1
630	IL7R			-1.71		XM_937367.1
631	DBNDD1			-1.71		NM_001042610.1
632	ADD3			-1.71		NM_016824.3
633	NR4A2			-1.71		NM_006186.2
634	C15orf23			-1.71		NM_033286.2
635	ZWINT			-1.71		NM_001005413.1
636	CCDC34			-1.70		NM_030771.1
637	IFI44			-1.70		NM_006417.3
638	H1FX			-1.70		NM_006026.2
639	HIST1H3F			-1.70		NM_021018.2
640	MGC3731			-1.69		NM_024313.1
641	ADAP2			-1.69		NM_018404.2

Number	Gene symbol	Fold change			Predicted target?	Gene accession number
		12h	24h	48h		
642	MKI67			-1.69		NM_002417.3
643	C5orf34			-1.69		NM_198566.1
644	ESPL1			-1.69		NM_012291.4
645	ANLN			-1.69		NM_018685.2
646	GSTT2			-1.69		NM_000854.2
647	NCAPG			-1.69		NM_022346.3
648	RAVER2			-1.69		NM_018211.2
649	FAM107B			-1.69		NM_031453.2
650	ABCA7			-1.69		NM_019112.3
651	NOP56			-1.69		NM_006392.2
652	C13orf3			-1.69		NM_145061.3
653	OIP5			-1.69		NM_007280.1
654	C16orf53			-1.69		NM_024516.2
655	CSE1L			-1.69	Yes	NM_177436.1
656	TMEM47			-1.69		NM_031442.2
657	PTBP2			-1.69		NM_021190.1
658	FHL1			-1.69		NM_001449.3
659	FBXO43			-1.68		NM_001029860.2
660	ZNF207			-1.68		NM_001032293.2
661	THOP1			-1.68		NM_003249.3
662	DCXR			-1.68		NM_016286.2
663	LOC442727			-1.68		XR_017503.2
664	NRM			-1.68		NM_007243.1
665	PTCD1			-1.68		NM_015545.2
666	ETS2			-1.68		NM_005239.4
667	URB2			-1.68		NM_014777.2
668	RNU11			-1.68		NR_004407.1
669	CCNF			-1.68		NM_001761.1
670	NOTCH2NL			-1.68		NM_203458.3
671	FAM86A			-1.68		NM_201598.1
672	NTHL1			-1.68		NM_002528.4
673	PSMG4			-1.68		NM_001128591.1
674	LOC650029			-1.68		XM_941861.1
675	SLC25A15			-1.68		NM_014252.1
676	LOC100131735			-1.68		XR_038716.1
677	CDC25B			-1.68		NM_004358.3
678	CCNO			-1.68		NM_021147.3
679	CCDC74B			-1.68		NM_207310.1
680	PPA2			-1.68		NM_176866.2
681	MGP			-1.68		NM_000900.2
682	KLHDC8B			-1.67		NM_173546.1
683	DHRS4			-1.67		NM_021004.2
684	BCL7C			-1.67		NM_004765.2
685	ABCB10			-1.67		NM_012089.1
686	NUDT3			-1.67	Yes	NM_006703.2
687	SHROOM3			-1.67		NM_020859.3
688	LOC100128221			-1.67		XM_001713928.1
689	UHRF1			-1.67		NM_001048201.1
690	CCDC14			-1.67		NM_022757.3
691	LOC729421			-1.67		XM_001133682.1
692	PMS2L4			-1.67		NR_022007.1
693	CTSL2			-1.67	Yes	NM_001333.2
694	CENPE			-1.67		NM_001813.2
695	CCDC152			-1.66		NM_001134848.1
696	C17orf90			-1.66		NM_001039842.1
697	C12orf24			-1.66		NM_013300.1
698	HIST1H4K			-1.66		

Number	Gene symbol	Fold change			Predicted target?	Gene accession number
		12h	24h	48h		
699	ERCC1			-1.66		NM_001983.2
700	MXD3			-1.66		NM_031300.2
701	C17orf89			-1.66		NM_001086521.1
702	TAP2			-1.66		NM_000544.3
703	MCM3			-1.66		NM_002388.3
704	PMS2			-1.66		NR_003085.1
705	C16orf59			-1.66		NM_025108.2
706	PLK4			-1.66		NM_014264.3
707	LOC399959			-1.66		NR_024430.1
708	RFXAP			-1.66		NM_000538.2
709	BUB1B			-1.66		NM_001211.4
710	KIF18A			-1.66		NM_031217.2
711	PLK1			-1.66		NM_005030.3
712	LOC345041			-1.66		XR_038458.1
713	PDDC1			-1.66		NM_182612.1
714	CTNNAL1			-1.65		NM_003798.1
715	ATOH8			-1.65		NM_032827.4
716	FBXO5			-1.65		NM_012177.2
717	CNKSR3			-1.65		NM_173515.2
718	RFWD3			-1.65		NM_018124.3
719	LOC100133747			-1.65		XM_001719129.1
720	SURF2			-1.65		NM_017503.2
721	AMOT			-1.65		NM_133265.2
722	C12orf48			-1.65		NM_017915.2
723	RFC1			-1.65		NM_002913.3
724	RFC3			-1.65		NM_002915.3
725	CMTM4			-1.65		NM_181521.2
726	ACOT4			-1.65		NM_152331.2
727	LOC643918			-1.65		XM_933328.1
728	SAC3D1			-1.65		NM_013299.3
729	NCAPG2			-1.65		NM_017760.5
730	POLR1E			-1.65		NM_022490.1
731	C21orf51			-1.65		NM_001042401.1
732	FANCI			-1.65		NM_018193.2
733	RRP1			-1.64		NM_003683.5
734	ZNF121			-1.64		NM_001008727.1
735	CHAF1A			-1.64		NM_005483.2
736	BTF3			-1.64		NM_001037637.1
737	RNU1F1			-1.64		NR_004402.1
738	LOC100128266			-1.64		XR_037888.1
739	ISL1			-1.64	Yes	NM_002202.1
740	LOC100131609			-1.64		XR_038433.1
741	NICN1			-1.64		NM_032316.3
742	TGIF2			-1.64		NM_021809.5
743	BARD1			-1.64	Yes	NM_000465.1
744	dJ222E13.2			-1.64		NR_002184.1
745	ADRA2A			-1.64		NM_000681.2
746	PSMB10			-1.64		NM_002801.2
747	ASTE1			-1.64		NM_014065.2
748	SHQ1			-1.64		NM_018130.2
749	PA2G4			-1.64		NM_006191.2
750	FABP5L2			-1.63		XM_001134012.2
751	WDR4			-1.63	Yes	NM_033661.3
752	ZBTB22			-1.63		NM_005453.3
753	BID			-1.63		NM_197966.1
754	TMX4			-1.63		NM_021156.2
755	PALM2			-1.63		NM_001037293.1

Number	Gene symbol	Fold change			Predicted target?	Gene accession number
		12h	24h	48h		
756	UCP2			-1.62		NM_003355.2
757	NSBP1			-1.62		NM_030763.1
758	CCDC88C			-1.62		NM_001080414.2
759	EFCAB4A			-1.62		NM_173584.3
760	LAMA3			-1.62		NM_198129.1
761	DAZAP1			-1.62		NM_170711.1
762	ZNF789			-1.62		NM_213603.2
763	TRIM5			-1.62		NM_033093.1
764	C10orf2			-1.62		NM_021830.3
765	ACN9			-1.62		NM_020186.1
766	RBM12B			-1.62		NM_203390.2
767	TUBGCP4			-1.62		NM_014444.2
768	NAAA			-1.62		NM_014435.3
769	MAST4			-1.62		NM_198828.2
770	NUFIP1			-1.62		NM_012345.1
771	SNAPC5			-1.62		NM_006049.2
772	C14orf167			-1.62		NR_023921.1
773	RBMX			-1.62		NM_002139.2
774	CENPQ			-1.61		NM_018132.3
775	SNHG6			-1.61		NR_002599.1
776	MGC27348			-1.61		XM_171158.5
777	C9orf10OS			-1.61		NM_198841.1
778	LRP3			-1.61		NM_002333.1
779	RANBP1			-1.61		NM_002882.2
780	TOMM40			-1.61		NM_006114.1
781	SYT15			-1.61		NM_181519.2
782	MTCP1			-1.61		NM_014221.3
783	APEX1			-1.61		NM_080649.1
784	HADH			-1.61		NM_005327.2
785	NME4			-1.61		NM_005009.2
786	TRAFD1			-1.61		NM_006700.1
787	SCG2			-1.61		NM_003469.3
788	DEPDC1B			-1.61		NM_018369.1
789	LRRN2			-1.61		NM_201630.1
790	GEMIN4			-1.61		NM_015721.2
791	STXBP6			-1.61		NM_014178.6
792	LGSN			-1.61		NM_016571.1
793	HNRNPA1			-1.61		NM_031157.2
794	MORC2			-1.60		NM_014941.1
795	LSMD1			-1.60		NM_032356.3
796	CHDH			-1.60		NM_018397.3
797	LOC643287			-1.60		XM_928075.2
798	SLC29A1			-1.60		NM_001078174.1
799	WEE1			-1.60	Yes	NM_003390.2
800	THUMPD2			-1.60		NM_025264.3
801	GTPBP6			-1.60		NM_012227.1
802	LOC728572			-1.60		XR_039595.1
803	SGOL2			-1.60		NM_152524.3
804	KIF23			-1.60		NM_138555.1
805	LOC440498			-1.60		XM_938817.2
806	DLEU1			-1.60		NR_002605.1
807	TAOK1			-1.60		NM_020791.1
808	RFX7			-1.60		NM_022841.5
809	WASPIP			-1.60		NM_003387.3
810	CCDC47			-1.60		NM_020198.1
811	SKA2			-1.60		NM_182620.3
812	BUB1			-1.60		NM_004336.2

Number	Gene symbol	Fold change			Predicted target?	Gene accession number
		12h	24h	48h		
813	SERBP1			-1.59		NM_001018069.1
814	ADAMTS1			-1.59		NM_006988.3
815	LOC646993			-1.59		XM_001717725.1
816	ATOX1			-1.59		NM_004045.3
817	CCDC85B			-1.59		NM_006848.2
818	RTN4IP1			-1.59		NM_032730.4
819	ECHDC2			-1.59		NM_018281.2
820	KRT19			-1.59		NM_002276.3
821	ARHGAP23			-1.59		XM_290799.7
822	SETMAR			-1.59		NM_006515.1
823	C15orf38			-1.59		NM_182616.1
824	SNORD87			-1.59		NR_002598.1
825	FAM165B			-1.59		NM_058182.4
826	LOC400304			-1.59		XM_375152.3
827	RPL36			-1.59		NM_015414.2
828	ZWILCH			-1.59		NM_017975.3
829	CIAO1			-1.59		NM_004804.2
830	CDK2			-1.59		NM_001798.2
831	HMGA1			-1.59		NM_145899.1
832	C12orf30			-1.59		NM_024953.2
833	PODXL2			-1.59		NM_015720.1
834	C9orf142			-1.59		NM_183241.1
835	KCNIP3			-1.59	Yes	NM_013434.4
836	SHMT1			-1.59		NM_004169.3
837	BTBD3			-1.59		NM_014962.2
838	NFX1			-1.59		NM_002504.3
839	H2AFY			-1.59		NM_138609.2
840	SHRM			-1.59		NM_020859.1
841	SLC44A2			-1.59		NM_020428.2
842	LOC728006			-1.59		XM_001128698.1
843	LOC282997			-1.58		XR_041083.1
844	LOC100132774			-1.58		XM_001725935.1
845	BRI3BP			-1.58		XM_941876.1
846	SNORD104			-1.58		NR_004380.1
847	CCNG1			-1.58		NM_199246.1
848	RNU1A3			-1.58		NR_004430.1
849	FAM38B			-1.58		NM_022068.1
850	RANBP3			-1.58		NM_007320.1
851	SLC43A3			-1.58		NM_017611.2
852	GRB14			-1.58		NM_004490.2
853	MCM7			-1.58		NM_005916.3
854	REPIN1			-1.57		NM_014374.1
855	TCF3			-1.57		NM_003200.1
856	LOC286467			-1.57		XR_015266.1
857	NPR3			-1.57		NM_000908.2
858	SDCCAG3			-1.57		NM_001039708.1
859	KAT2A			-1.57		NM_021078.2
860	FEN1			-1.57		NM_004111.4
861	FERMT1			-1.57		NM_017671.4
862	SP110			-1.57		NM_004510.2
863	TMEM80			-1.57		
864	FLJ40504			-1.57		NM_173624.1
865	LOC641746			-1.57		XR_036993.1
866	SMC4			-1.57		NM_001002800.1
867	NT5C3L			-1.57		NM_052935.2
868	CCNB2			-1.57		NM_004701.2
869	UBE2C			-1.57		NM_181803.1

Number	Gene symbol	Fold change			Predicted target?	Gene accession number
		12h	24h	48h		
870	ADAL			-1.57		NM_001012969.1
871	MDC1			-1.57		NM_014641.1
872	NUDCD2			-1.57		NM_145266.4
873	LOC729057			-1.57		XR_042044.1
874	NFYC			-1.57	Yes	NM_014223.2
875	C3orf26			-1.57		NM_032359.2
876	MANEAL			-1.57		NM_001031740.1
877	CDC25A			-1.57		NM_001789.2
878	IQCC			-1.56		NM_018134.1
879	TMEM14B			-1.56		NM_030969.2
880	POLR3G			-1.56		NM_006467.2
881	FOXRED2			-1.56		NM_024955.4
882	CDCA5			-1.56		NM_080668.2
883	DLGAP5			-1.56		NM_014750.3
884	BIVM			-1.56		NM_017693.2
885	PDCD2			-1.56		NM_144781.1
886	TMEM149			-1.56		NM_024660.2
887	C16orf13			-1.56		NM_001040161.1
888	LOC728408			-1.56		XR_039142.1
889	RBBP7			-1.56		NM_002893.2
890	LOC730323			-1.56		XM_001722097.1
891	WNT7B			-1.56		NM_058238.1
892	FAM64A			-1.56		NM_019013.1
893	KIF22			-1.56		NM_007317.1
894	ARL17P1			-1.56		NM_016632.1
895	SAMD1			-1.56		NM_138352.1
896	LOC339290			-1.56		NR_015389.1
897	PTGES2			-1.56		NM_198938.1
898	NOP2			-1.56		NM_006170.2
899	TSTD1			-1.56		NM_001113206.1
900	ADCK2			-1.56		NM_052853.3
901	LOC644029			-1.56		XR_017397.1
902	PKN3			-1.56		NM_013355.3
903	LOC391532			-1.56		XR_017653.1
904	MTHFD1			-1.56		NM_005956.2
905	GXYLT2			-1.56		NM_001080393.1
906	TUBG1			-1.56		NM_001070.3
907	TAF7L			-1.56		NM_024885.2
908	DR1			-1.56		NM_001938.2
909	ZNF274			-1.55		NM_016324.2
910	ARL17B			-1.55		NM_001103154.1
911	PEMT			-1.55		NM_148172.1
912	PTMA			-1.55		NM_001099285.1
913	EPHX1			-1.55		NM_000120.2
914	XPO5			-1.55		NM_020750.1
915	PPP2R3B			-1.55		NM_013239.3
916	RUSC1			-1.55		NM_014328.2
917	UBA52			-1.55		NM_003333.3
918	UBXN2B			-1.55		NM_001077619.1
919	KIAA1618			-1.55		NM_020954.2
920	RPL14			-1.55		NM_001034996.1
921	LOC652837			-1.55		XM_942529.1
922	LOC391019			-1.55		XR_019605.1
923	TATDN2			-1.55		NM_014760.2
924	C13orf37			-1.55		NM_001071775.2
925	LOC100129585			-1.55		XM_001720509.1
926	MACROD1			-1.55		NM_014067.2

Number	Gene symbol	Fold change			Predicted target?	Gene accession number
		12h	24h	48h		
927	ABCF2			-1.55		NM_005692.3
928	LOC642934			-1.55		XM_942991.2
929	RNFT2			-1.55		NM_032814.3
930	LOC400986			-1.55		XM_001126815.1
931	BLM			-1.55		NM_000057.2
932	SKAP2			-1.55		NM_003930.3
933	CDKN3			-1.55		NM_005192.2
934	KLC1			-1.55		NM_005552.4
935	SSBP4			-1.55		NM_032627.2
936	FAM104A			-1.55		NM_032837.1
937	HCP5			-1.55		NM_006674.2
938	LOC100130009			-1.55		XM_001720338.1
939	DHX34			-1.55		NM_014681.4
940	GPD2			-1.55		NM_001083112.1
941	LOC649841			-1.54		XM_938906.2
942	CENPN			-1.54		NM_018455.3
943	B3GALNT1			-1.54		NM_033168.2
944	HRAS			-1.54	Yes	NM_005343.2
945	KIAA1644			-1.54		XM_936510.2
946	AMFR			-1.54		NM_001144.4
947	HIST1H2BH			-1.54		NM_003524.2
948	BAZ1A			-1.54		NM_182648.1
949	KRT86			-1.54		NM_002284.3
950	TOP2A			-1.54		NM_001067.2
951	SLC47A1			-1.54		NM_018242.2
952	RBMS1			-1.54		NM_002897.3
953	RPS7			-1.54		NM_001011.3
954	LOC100133923			-1.54		XM_001714921.1
955	LOC645691			-1.54		XM_928701.3
956	CD320			-1.54		NM_016579.2
957	LOC100129267			-1.54		XR_037397.1
958	TOE1			-1.54		NM_025077.2
959	CKB			-1.54		NM_001823.3
960	MCM5			-1.54		NM_006739.3
961	TMEM133			-1.54		NM_032021.2
962	SNORD96A			-1.54		NR_002592.1
963	RAD54B			-1.54		NM_012415.2
964	REXO4			-1.54		NM_020385.2
965	C9orf100			-1.54		NM_032818.1
966	HIST1H2BJ			-1.54		NM_021058.3
967	H1F0			-1.54		NM_005318.2
968	NPM3			-1.54		NM_006993.1
969	LRRCC1			-1.54		NM_033402.3
970	HMG20B			-1.54		NM_006339.1
971	LRRC14			-1.54		NM_014665.1
972	HIST1H4C			-1.54		NM_003542.3
973	LOC100134648			-1.53		XM_001724681.1
974	ACAT1			-1.53		NM_000019.2
975	SIGMAR1			-1.53		NM_005866.2
976	SELENBP1			-1.53		NM_003944.2
977	C6orf167			-1.53		NM_198468.2
978	RAP1GDS1			-1.53		NM_021159.3
979	CDC42EP3			-1.53		NM_006449.3
980	KRT18P17			-1.53		XR_037953.1
981	MPRIP			-1.53		NM_015134.2
982	CCDC97			-1.53		NM_052848.1
983	ZBTB47			-1.53		NM_145166.2

Number	Gene symbol	Fold change			Predicted target?	Gene accession number
		12h	24h	48h		
984	NRGN			-1.53		NM_006176.1
985	MCM4			-1.53		NM_182746.1
986	OBFC1			-1.53		NM_024928.3
987	RFX5			-1.53		NM_001025603.1
988	NME3			-1.53	Yes	NM_002513.2
989	CDC25C			-1.53		NM_001790.3
990	GCSH			-1.53		NM_004483.3
991	TPX2			-1.53		NM_012112.4
992	FABP5			-1.53		NM_001444.1
993	EXOSC9			-1.53		NM_001034194.1
994	CYTSB			-1.53		NM_001033553.1
995	GRHPR			-1.53		NM_012203.1
996	LOC646044			-1.53		XR_037328.1
997	COBRA1			-1.53		NM_015456.2
998	CCNE2			-1.53		NM_057735.1
999	OXA1L			-1.53		NM_005015.1
1000	ABHD15			-1.52		NM_198147.1
1001	KIF20A			-1.52		NM_005733.1
1002	C1QBP			-1.52		NM_001212.3
1003	C2orf68			-1.52		NM_001013649.3
1004	SLC16A9			-1.52		NM_194298.1
1005	CTAG2			-1.52		NM_020994.2
1006	PRC1			-1.52		NM_199413.1
1007	POLQ			-1.52		NM_199420.3
1008	AURKB			-1.52		NM_004217.2
1009	GINS4			-1.52		NM_032336.1
1010	GEMIN6			-1.52		NM_024775.9
1011	MSX1			-1.52		NM_002448.3
1012	DDX39			-1.52	Yes	NM_005804.2
1013	NEK2			-1.52		NM_002497.2
1014	WDR51A			-1.52		NM_015426.2
1015	MKRN3			-1.52		NM_005664.3
1016	AIF1L			-1.52		NM_031426.2
1017	FAM83D			-1.52	Yes	NM_030919.2
1018	SNORD15B			-1.52		NR_000025.1
1019	LOC648164			-1.52		XM_936503.1
1020	TRIM28			-1.52		NM_005762.2
1021	PRTFDC1			-1.52		NM_020200.5
1022	ZNF32			-1.52		NM_006973.2
1023	HIST1H2AE			-1.52		NM_021052.2
1024	PEBP1			-1.52		NM_002567.2
1025	POLD1			-1.52	Yes	NM_002691.1
1026	PARP1			-1.52		NM_001618.2
1027	CISD1			-1.52		NM_018464.2
1028	KIAA1545			-1.52		XM_495939.3
1029	PABPC1			-1.52		NM_002568.3
1030	CNOT7			-1.52		NM_013354.5
1031	C11orf58			-1.52		NM_001142705.1
1032	NEFH			-1.52	Yes	NM_021076.2
1033	PYCARD			-1.52		NM_013258.3
1034	TMEM160			-1.52		NM_017854.1
1035	CCDC77			-1.52		NM_032358.2
1036	KIAA0495			-1.52		NM_207306.1
1037	EML3			-1.52		NM_153265.2
1038	MRPS27			-1.51		NM_015084.1
1039	LSM2			-1.51		NM_021177.3
1040	FBXL20			-1.51		NM_032875.1

Number	Gene symbol	Fold change			Predicted target?	Gene accession number
		12h	24h	48h		
1041	C3orf31			-1.51		NM_138807.2
1042	GPC4			-1.51		NM_001448.2
1043	ZNF302			-1.51		NM_018443.2
1044	LOC643995			-1.51		XM_934410.1
1045	TMSB15A			-1.51		NM_021992.2
1046	DTL			-1.51		NM_016448.1
1047	LOC728153			-1.51		XM_001128002.1
1048	AADAT			-1.51		NM_182662.1
1049	LOC100128060			-1.51		XM_001723512.1
1050	MTA2			-1.51		NM_004739.2
1051	ZHX1			-1.51		NM_007222.3
1052	SRPK1			-1.51		NM_003137.3
1053	UCK2			-1.51		NM_012474.3
1054	AKR1C2			-1.51	Yes	NM_001354.4
1055	PXMP2			-1.51		NM_018663.1
1056	GPN3			-1.51		NM_016301.2
1057	C9orf40			-1.51		NM_017998.1
1058	C10orf54			-1.51		NM_022153.1
1059	CENPO			-1.51		NM_024322.1
1060	RALBP1			-1.51		NM_006788.3
1061	NHP2L1			-1.51		NM_005008.2
1062	SNORD99			-1.51		NR_003077.1
1063	LOC440145			-1.51		NM_001071775.1
1064	C4orf32			-1.51		NM_152400.1

Number	Gene symbol	Fold change			Predicted target?	Gene accession number
		12h	24h	48h		
1065	MRPL40			-1.51		NM_003776.2
1066	SYCE1L			-1.51		NM_001129979.1
1067	DDX12			-1.51		XM_931833.1
1068	PMS2L5			-1.51		NM_174930.2
1069	SLC2A4RG			-1.51		NM_020062.3
1070	ZNF462			-1.51		NM_021224.4
1071	SMYD2			-1.51		NM_020197.1
1072	C17orf58			-1.51		NM_181656.3
1073	SNORD65			-1.50		NR_003054.1
1074	TMEM97			-1.50		NM_014573.2
1075	SPTAN1			-1.50		NM_003127.1
1076	GBAS			-1.50		NM_001483.1
1077	MRPL24			-1.50		NM_145729.1
1078	XRCC3			-1.50		NM_001100118.1
1079	BCOR			-1.50	Yes	NM_020926.2
1080	FLJ35776			-1.50		NR_024101.1
1081	IREB2			-1.50		NM_004136.2
1082	C6orf155			-1.50		NM_024882.1
1083	LOC728312			-1.50		XR_042333.1
1084	AMD1			-1.50		NM_001033059.1
1085	KLF10			-1.50		NM_005655.1
1086	C5orf21			-1.50		NM_032042.3
1087	GNG11			-1.50		NM_004126.3
1088	ZNF580			-1.50		NM_016202.2

(**B**) Genes upregulated by *miR-517a*

Number	Gene symbol	Fold change			Predicted target?	Gene accession number
		12h	24h	48h		
1	DDAH1	2.75	3.46	1.80		NM_012137.2
2	TMEM189-UBE2V1	2.53	2.90	2.45		NM_003349.4
3	RDX	2.51	3.04	2.61		NM_002906.3
4	RAB8B	2.21	2.26	2.81		NM_016530.2
5	IDI1	2.18	2.74			NM_004508.2
6	RAB11FIP1	2.16	3.08	3.00		NM_001002814.1
7	ERLIN2	2.13	3.08	3.02		NM_007175.5
8	SLC35A1	2.10	1.78	2.03		NM_006416.3
9	SYPL1	2.10	1.65	1.82		NM_182715.1
10	ARL8B	2.02	2.20	3.90		NM_018184.2
11	PKIA	2.01	1.99	2.54		NM_006823.2
12	TMEM2	2.00	3.03	2.86		NM_013390.1
13	FGF2	1.98	1.70	2.95		NM_002006.4
14	INSIG1	1.94	1.97	1.65		NM_198336.1
15	C5ORF51	1.93	2.43	3.54		NM_175921.4
16	NUP35	1.91	1.92	1.88	Yes	NM_138285.3
17	PFTK1	1.87		1.54	Yes	NM_012395.2
18	BTG3	1.85	2.03	2.27	Yes	NM_006806.3
19	FAM116A	1.85	2.75	2.12		XM_001132771.1
20	HMGCR	1.83	1.66			NM_000859.1
21	ERLIN1	1.82	2.23	2.06		NM_006459.2
22	RBM12	1.82	2.00			NM_006047.4
23	SNRPC	1.81	3.28	2.96		NM_003093.1
24	HMGCS1	1.81	1.51			NM_002130.6
25	LOC730052	1.80	2.72	2.45		XR_038933.1

Number	Gene symbol	Fold change			Predicted target?	Gene accession number
		12h	24h	48h		
26	HNRNPR	1.78				NM_005826.3
27	PPIF	1.77	1.58	1.83		NM_005729.3
28	TMTC3	1.77				NM_181783.2
29	SLC4A7	1.75	1.74			NM_003615.3
30	PPM1B	1.74	1.91	1.77		NM_177968.2
31	NPTN	1.74	2.53	2.32		NM_012428.2
32	RAP1B	1.73	2.14	2.67		NM_015646.4
33	HS.21177	1.72				AJ420516
34	EIF2A	1.72	2.07	2.03		NM_032025.3
35	UBLCP1	1.71	2.15	1.99		NM_145049.1
36	IRF2BP2	1.71	1.93	2.30		NM_182972.2
37	IL8	1.70	1.89	5.35		NM_000584.2
38	SRI	1.69	2.20	1.54		NM_198901.1
39	HS.127310	1.68				AL137257
40	HNRPR	1.67	1.81			NM_005826.2
41	CTNNB1	1.66	1.76	1.93		NM_001098209.1
42	GXYLT1	1.66				NM_001099650.1
43	SH3RF1	1.65	1.58			NM_020870.3
44	SEC24A	1.65	1.95	2.69		NM_021982.1
45	RP2	1.65	1.89	1.91		NM_006915.1
46	FAS	1.65				NM_152877.1
47	ST5	1.64				NM_213618.1
48	CYBRD1	1.64	1.72	2.54		NM_024843.2
49	STBD1	1.63				NM_003943.2
50	MBNL1	1.62				NM_207295.1
51	ZFYVE20	1.60	1.85	1.66		NM_022340.2

Number	Gene symbol	Fold change			Predicted target?	Gene accession number
		12h	24h	48h		
52	DDAH1		3.46	1.80		NM_012137.2
53	COMMD10		3.17	2.66		NM_016144.2
54	LOC100129566		3.06	3.10		XM_001718519.1
55	ACTC1		2.94			NM_005159.3
56	PMM2		2.83	3.40		NM_000303.1
57	FSTL1		2.67	2.52		NM_007085.3
58	RDH11		2.57	2.03		NM_016026.2
59	WIPI1		2.44	8.40		NM_017983.3
60	C12orf23		2.35	2.63		NM_152261.1
61	SEC24D		2.34	2.71		NM_014822.1
62	IL11		2.34	4.38		NM_000641.2
63	NXNL2		2.33	2.08		NM_145283.1
64	TNFSF9		2.32	3.14		NM_003811.2
65	RAB22A		2.25	2.14		NM_020673.2
66	SPOCD1		2.23	2.83		NM_144569.3
67	TUBB3		2.22	2.06		NM_006086.2
68	CAV2		2.21			NM_001233.3
69	STK38L		2.20	1.56		NM_015000.1
70	KIAA0367		2.17	2.06		NM_015225.1
71	TGM2		2.14	2.55		NM_004613.2
72	C14orf45		2.14	4.18		
73	ACSS2		2.14	1.61		NM_001076552.1
74	NT5E		2.13	5.70		NM_002526.1
75	SERPINE1		2.12	4.41	Yes	NM_000602.1
76	LOC158160		2.10			NM_001031744.1
77	TMEM154		2.10	3.75		NM_152680.1
78	LARP6		2.08	3.71	Yes	NM_018357.2
79	SRA1		2.08	3.42		NM_001035235.2
80	HSPA5		2.06	2.27		NM_005347.2
81	MEX3B		2.06			NM_032246.3
82	TMEM181		2.05	2.62		XM_941693.1
83	LOC648742		2.05	2.70		XM_001714210.1
84	EIF2S1		2.01	1.58		NM_004094.4
85	TPST1		2.01	2.15		NM_003596.2
86	H3F3B		2.01	1.50		NM_005324.3
87	IKBIP		1.99	2.20		NM_153687.2
88	UBE2V1		1.99	1.53		NM_001032288.1
89	ARPC4		1.98	2.51		NM_001024960.1
90	KIAA0494		1.98	2.44		NM_014774.1
91	OPTN		1.97	2.71		NM_001008213.1
92	CPOX		1.97	1.58		NM_000097.4
93	MTAP		1.97			NM_002451.3
94	GPR180		1.97	2.38		NM_180989.3
95	RAP1BL		1.97	2.28		NM_001089704.3
96	PCSK9		1.96			NM_174936.2
97	IDH1		1.96	2.54		NM_005896.2
98	PRRC1		1.95	2.11		NM_130809.2
99	LOC650517		1.95	2.03		XM_496202.2
100	LPIN1		1.93			NM_145693.1
101	LOC653631		1.92	2.20		XM_930476.1
102	SLC39A14		1.91	2.50		NM_015359.1
103	CD70		1.91	2.78		NM_001252.2
104	PDGFRL		1.91	3.03		NM_006207.1
105	XBP1		1.90	2.64		NM_005080.2
106	SC4MOL		1.90	1.54		NM_006745.3
107	ATPAF1		1.89			NM_001042546.1
108	SLCO1B3		1.88	2.51		NM_019844.1

Number	Gene symbol	Fold change			Predicted target?	Gene accession number
		12h	24h	48h		
109	PNMA1		1.88			NM_006029.4
110	FAM69A		1.87	1.69		NM_001006605.3
111	SELT		1.87			NM_016275.3
112	FAM114A1		1.85	2.14		NM_138389.1
113	GLIPR1		1.85	1.86		NM_006851.1
114	SNAI2		1.85	2.55		NM_003068.3
115	NEDD4		1.85	2.12		NM_198400.1
116	PLA2G3		1.83			NM_015715.2
117	LOC645313		1.83	1.57		XR_017585.2
118	MAP1LC3B		1.83	2.82		NM_022818.3
119	CCPG1		1.83	3.56		NM_004748.3
120	YWHAG		1.83	1.67		NM_012479.2
121	AIDA		1.83	2.89		NM_022831.2
122	PDGFRB		1.83	2.27		NM_002609.3
123	TRIM2		1.82	2.49		NM_015271.2
124	PDIA5		1.82	4.07		NM_006810.1
125	C14orf32		1.81	1.77		NM_144578.2
126	ETF1		1.80	1.60		NM_004730.1
127	VKORC1L1		1.80	1.75		NM_173517.3
128	GFPT2		1.80	1.72	Yes	NM_005110.1
129	B4GALT4		1.80	2.42		NM_003778.3
130	CDK2AP2		1.79	2.98		NM_005851.3
131	GABPB1		1.78			NM_181427.3
132	FAM3C		1.77	1.57		NM_014888.1
133	INO80C		1.77	1.82		NM_194281.2
134	ARHGAP19		1.77			NM_032900.4
135	SLCO2A1		1.77	1.95		NM_005630.1
136	ITGA6		1.77	1.80		NM_000210.2
137	GABPB2		1.77			NM_181427.2
138	C17orf91		1.77	2.27		NM_001001870.1
139	YIPF5		1.77	2.32		NM_030799.6
140	APPL2		1.76		Yes	NM_018171.2
141	UCN2		1.76	2.90		NM_033199.3
142	ICMT		1.76	1.72		NM_012405.2
143	POFUT2		1.76	3.41		NM_133635.3
144	DNAJC25		1.76	2.35		NM_001015882.1
145	MVK		1.75			NM_000431.1
146	NARF		1.75	1.69		NM_001038618.1
147	TMED7		1.75	1.80		NM_181836.3
148	LOC402232		1.75			XM_499226.2
149	KDELR2		1.75	3.10		NM_006854.2
150	FECH		1.75			NM_000140.2
151	RTCD1		1.74	1.99		NM_003729.1
152	BMPR2		1.74	2.00		NM_001204.5
153	MOBKL2B		1.74			NM_024761.3
154	RCE1		1.74			NM_001032279.1
155	DCP2		1.74	1.76		NM_152624.4
156	SCD		1.74			NM_005063.4
157	LIPG		1.74	1.72		NM_006033.2
158	SUGT1		1.74			NM_006704.2
159	GNA13		1.74	2.25		NM_006572.3
160	DRAM1		1.74	3.43		NM_018370.1
161	TXNDC5		1.74	2.43		NM_022085.3
162	USP47		1.74			NM_017944.3
163	CACHD1		1.73	2.21		NM_020925.1
164	C20orf20		1.73	1.68		NM_018270.3
165	GPX8		1.72	2.74		NM_001008397.2

Number	Gene symbol	Fold change			Predicted target?	Gene accession number
		12h	24h	48h		
166	ARFGAP1		1.72	3.43		NM_175609.1
167	GBP1		1.72			NM_002053.1
168	DEDD2		1.72	2.02		NM_133328.2
169	KDELR3		1.72	4.42		NM_016657.1
170	ACLY		1.72	1.74		NM_198830.1
171	SOX9		1.72			NM_000346.2
172	DNAJB11		1.71	2.04		NM_016306.4
173	C12orf31		1.70	1.83		NM_032338.2
174	COPS8		1.69	1.66		NM_198189.2
175	SLC11A2		1.69	2.08		NM_000617.1
176	IGFBP3		1.69	1.97		NM_001013398.1
177	PGM3		1.69	3.15		NM_015599.1
178	KRT17P3		1.69	1.95		XR_015626.2
179	FRMD6		1.69	2.58		NM_152330.3
180	LSS		1.68	1.59		NM_002340.3
181	ALDH9A1		1.68	1.59		NM_000696.2
182	MED8		1.68	2.12		NM_001001651.1
183	GFM1		1.68	1.52		NM_024996.5
184	KLHL13		1.68			NM_033495.2
185	SLC26A2		1.68	2.20		NM_000112.2
186	C10orf75		1.68			XR_041972.1
187	ASF1A		1.68			NM_014034.1
188	FURIN		1.68	2.06		NM_002569.2
189	JUN		1.68	2.39		NM_002228.3
190	CUL4B		1.67	1.89		NM_001079872.1
191	SEMA4F		1.66	2.36	Yes	NM_004263.2
192	GNB1		1.66	1.77		NM_002074.2
193	ERI1		1.66			NM_153332.3
194	HDAC1		1.66	1.50		NM_004964.2
195	C2orf30		1.66	2.08		NM_015701.2
196	IVNS1ABP		1.66	1.60		NM_006469.4
197	NDUFA6		1.66		Yes	NM_002490.3
198	PJA2		1.65	2.05		NM_014819.2
199	GPR1		1.65	2.32		NM_005279.2
200	TNFRSF12A		1.65	2.13		NM_016639.1
201	ITFG2		1.65	1.67		NM_018463.2
202	ING3		1.65	1.75		NM_198267.1
203	ASPH		1.65	1.93		NM_032468.2
204	FDFT1		1.65			NM_004462.3
205	FDPS		1.64			NM_002004.2
206	AURKA		1.64			NM_198434.1
207	ACBD3		1.64	2.70		NM_022735.3
208	ROD1		1.64	1.71		NM_005156.4
209	SLC2A6		1.64	1.82		NM_017585.2
210	MAP1B		1.64	1.52		NM_032010.1
211	TMEM231		1.64			NM_001077419.1
212	TMEM39A		1.64	2.19		NM_018266.1
213	CAB39		1.63	1.70		NM_016289.2
214	CRIPT		1.63	1.69		NM_014171.3
215	CYB5R4		1.63	1.65		NM_016230.2
216	ARFGAP3		1.62	2.06		NM_014570.3
217	DUSP5		1.62	3.18		NM_004419.3
218	IPO11		1.62			NM_016338.3
219	WDR25		1.62	2.58		NM_024515.3
220	MCFD2		1.62	1.91		NM_139279.3
221	RBM7		1.62			NM_016090.2
222	ANXA7		1.62	1.74		NM_004034.1

Number	Gene symbol	Fold change			Predicted target?	Gene accession number
		12h	24h	48h		
223	SLC35B3		1.62	1.82		NM_015948.2
224	ZFAND2A		1.62	1.95		NM_182491.1
225	ZYX		1.62		Yes	NM_003461.4
226	TNFAIP8		1.62	1.89		NM_001077654.1
227	ANKRD1		1.62	2.03		NM_014391.2
228	MORN4		1.61	2.17		NM_178832.2
229	TSPAN13		1.61	3.08		NM_014399.3
230	ULK1		1.61	2.89		XM_942125.1
231	NRBF2		1.61	1.72		NM_030759.3
232	MGC18216		1.61	1.80		XM_927732.1
233	RNF14		1.61	2.21		NM_004290.3
234	LSM14A		1.61			NM_015578.1
235	DHCR7		1.61	1.51	Yes	NM_001360.2
236	CYP51A1		1.61			NM_000786.2
237	PTPRR		1.61	2.41		NM_002849.2
238	EML1		1.61			NM_004434.2
239	SLC35B4		1.61	1.87		NM_032826.3
240	TMEM45A		1.61	4.06		NM_018004.1
241	LOC731999		1.61	1.62		XM_942260.1
242	KLHL2		1.61	1.65		NM_007246.2
243	LOC649679		1.60			XM_945045.1
244	DNAJC15		1.60	1.55		NM_013238.2
245	P2RX1		1.60	1.89		NM_002558.2
246	TRIM29		1.60	2.38		NM_058193.1
247	LEPRE1		1.60	2.58	Yes	NM_022356.2
248	DNAJB9		1.60	4.00		NM_012328.1
249	TRIOBP		1.60	1.64		NM_138632.1
250	INTS2		1.60			NM_020748.1
251	FADS1		1.60			NM_013402.3
252	HACL1		1.60	1.51		NM_012260.1
253	PROSC		1.60			NM_007198.2
254	SAR1A		1.60	1.95		NM_020150.3
255	SERP1		1.60	1.92		NM_014445.2
256	ARL6IP1		1.60			NM_015161.1
257	SYVN1		1.60	2.41		NM_032431.2
258	PDGFC		1.59			NM_016205.1
259	PCNP		1.59	1.53		NM_020357.1
260	SPINK5L3		1.59			XM_376433.2
261	CDKN2B		1.59			NM_078487.2
262	GPN1		1.59			NM_007266.1
263	C5orf15		1.59	1.94		NM_020199.1
264	RAN		1.59			NM_006325.2
265	ZNF365		1.59	1.80		NM_014951.1
266	ZBTB9		1.59			NM_152735.3
267	ITGA5		1.59	2.98		NM_002205.2
268	ATG4A		1.59	1.74		NM_178270.1
269	EPHB2		1.59			NM_004442.6
270	LRRC1		1.59	1.85		NM_018214.3
271	LOX		1.59	2.37		NM_002317.3
272	MVD		1.59			NM_002461.1
273	FOXP1		1.58	1.73		NM_032682.4
274	FHL2		1.58			NM_001450.3
275	YPEL5		1.58	3.22		NM_016061.1
276	KLF9		1.58	2.42		NM_001206.2
277	C10orf88		1.58			NM_024942.1
278	VLDLR		1.58	3.23		NM_001018056.1
279	RRBP1		1.57	2.17		NM_001042576.1

Number	Gene symbol	Fold change			Predicted target?	Gene accession number
		12h	24h	48h		
280	ACTA2		1.57	3.14		NM_001613.1
281	PBK		1.57			NM_018492.2
282	ARID3A		1.57	1.87		NM_005224.1
283	TM4SF1		1.57	1.64		NM_014220.2
284	GEM		1.57	1.60		NM_181702.1
285	MCEE		1.57	1.62		NM_032601.2
286	LSM8		1.57			NM_016200.2
287	RER1		1.57	1.51		NM_007033.3
288	PDCD4		1.57			NM_145341.2
289	C6orf62		1.57	1.66		NM_030939.3
290	GDF15		1.57	7.46		NM_004864.1
291	KAT2B		1.57			NM_003884.4
292	TIMP3		1.57	1.53		NM_000362.4
293	LOC652846		1.57	2.19		XM_942545.1
294	STAG2		1.56			NM_006603.3
295	KRT16		1.56	1.93		NM_005557.2
296	MED31		1.56			NM_016060.2
297	ADAM17		1.56	1.72		NM_003183.4
298	TMEM41B		1.56			NM_015012.1
299	STAT3		1.56	1.89		NM_139276.2
300	ID2		1.56			NM_002166.4
301	CALD1		1.56	1.57		NM_004342.5
302	C9orf123		1.56			NM_033428.1
303	XRCC4		1.56			NM_022406.1
304	ANKRD13C		1.56	1.80		NM_030816.2
305	NPC1		1.56	2.23		NM_000271.1
306	USO1		1.56	1.96		NM_003715.1
307	MAPK1		1.56	2.31		NM_138957.2
308	ALDOC		1.56	2.23		NM_005165.2
309	ZC3H14		1.56			NM_024824.3
310	ARNT		1.56			NM_178426.1
311	RWDD2A		1.56	1.64		NM_033411.2
312	LOC652175		1.56			XM_941526.1
313	CCDC99		1.56			NM_017785.2
314	SERF2		1.55	2.38		NM_001018108.2
315	SLC7A1		1.55	1.66		NM_003045.3
316	FNDC3B		1.55	1.90		NM_022763.3
317	HCCS		1.55	1.89		NM_005333.2
318	TROVE2		1.55			NM_001042369.1
319	METAP2		1.55			NM_006838.2
320	LOC440093		1.55	1.55		NM_001013699.1
321	RGL1		1.55			NM_015149.2
322	MRPS36		1.55			NM_033281.5
323	RCAN1		1.55	1.75		NM_203418.1
324	CXorf26		1.54	1.52		NM_016500.3
325	RELL1		1.54	1.60		NM_001085400.1
326	HNRNPH3		1.54			NM_012207.2
327	TRA1P2		1.54	1.65		XR_000203.3
328	LOC729372		1.54			XM_001720639.1
329	SERPINH1		1.54	2.48		NM_001235.2
330	CRELD2		1.54	2.54		NM_024324.2
331	SMAD7		1.54			NM_005904.2
332	LOC285550		1.54			XR_001250.1
333	HIF1A		1.54			NM_001530.2
334	AKAP12		1.54			NM_005100.2
335	BAT2D1		1.54	2.01		NM_015172.2
336	ISCU		1.54	2.27	Yes	NM_014301.2

Number	Gene symbol	Fold change			Predicted target?	Gene accession number
		12h	24h	48h		
337	DOCK11		1.53			NM_144658.2
338	PMEPA1		1.53	1.62		NM_199169.1
339	WAC		1.53			NM_100486.1
340	PELI2		1.53	2.01		NM_021255.1
341	HNRNPM		1.53			NM_031203.2
342	KPNA2		1.53			NM_002266.2
343	UBE2Q2		1.53	1.68		NM_173469.1
344	CDA		1.53	3.19		NM_001785.1
345	DUSP12		1.53	1.59		NM_007240.1
346	MRS2		1.53			NM_020662.1
347	UBE2E3		1.53	1.51		XM_944996.1
348	SQLE		1.52			NM_003129.3
349	FHL3		1.52			NM_004468.3
350	SPAG1		1.52		Yes	NM_003114.3
351	LOC400759		1.52			XR_000992.1
352	NA		1.52	3.49		Hs.194225
353	LOC283050		1.52	2.09		XM_944265.1
354	IFNE		1.52			NM_176891.4
355	CAPZA1		1.52			NM_006135.1
356	SLITRK5		1.52			NM_015567.1
357	LOC100131261		1.52			XM_001723141.1
358	CKAP2		1.52			NM_018204.2
359	DCBLD1		1.52	2.02		NM_173674.1
360	ENAH		1.52			NM_018212.4
361	SEC13		1.52	2.69		NM_001136232.1
362	NEDD9		1.52			NM_006403.2
363	KIAA1539		1.52	2.58		NM_025182.2
364	PRKCB1		1.52			NM_002738.5
365	TPM4		1.51			NM_003290.1
366	EPS8		1.51	1.61		NM_004447.4
367	SLC7A6		1.51			NM_001076785.1
368	FLJ22447		1.51	1.95		XM_379075.3
369	ANXA10		1.51	2.52	Yes	NM_007193.3
370	LPAR1		1.51	1.84		NM_001401.3
371	NSDHL		1.51			NM_015922.1
372	POPDC3		1.51			NM_022361.3
373	PMM1		1.51			NM_002676.1
374	CD47		1.51			NM_001025080.1
375	LAMP2		1.51	2.06		NM_013995.1
376	EML4		1.51			NM_019063.2
377	DMBT1		1.51	1.94		NM_017579.1
378	TNFRSF10B		1.51	2.53		NM_003842.3
379	HERPUD1		1.51	4.76		NM_001010990.1
380	PJA1		1.51	2.08		NM_001032396.1
381	ARMCX3		1.51	2.25		NM_177947.2
382	MIR21		1.51	1.69		NR_029493.1
383	B9D2		1.51			NM_030578.2
384	LRIG1		1.51	2.26		NM_015541.2
385	RNF19A		1.50			NM_015435.3
386	RHOBTB1		1.50			NM_198225.1
387	HSD17B7P2		1.50			NM_182829.1
388	LOC650132		1.50			XM_939218.1
389	FAM36A		1.50			NM_198076.4
390	CSGALNACT1		1.50			NM_018371.3
391	DDIT3			5.24		NM_004083.4
392	GCNT3			4.53		NM_004751.1
393	ETV5			4.29		NM_004454.1

Number	Gene symbol	Fold change			Predicted target?	Gene accession number
		12h	24h	48h		
394	BEX2			3.96		NM_032621.2
395	TNFRSF14			3.86		NM_003820.2
396	INHBE			3.66		NM_031479.3
397	LRRC32			3.53		NM_005512.1
398	TOM1			3.33		NM_005488.1
399	ASNS			3.25		NM_133436.1
400	STC2			3.16		NM_003714.2
401	TSPAN10			3.13		NM_031945.3
402	P4HA2			3.06		NM_001017973.1
403	KCNK6			3.01		NM_004823.1
404	SLC35A2			3.00		NM_001032289.1
405	NTN4			2.94		NM_021229.3
406	ABCA1			2.92		NM_005502.2
407	PTGS2			2.91		NM_000963.1
408	VEGFC			2.91		NM_005429.2
409	TMEM50B			2.88		NM_006134.5
410	ARHGEF4			2.88		NM_015320.2
411	CD68			2.86		NM_001251.1
412	CRELD1			2.84		NM_001031717.2
413	UBAP2L			2.83	Yes	NM_014847.2
414	RNY1			2.82		NR_004391.1
415	LOXL4			2.80		NM_032211.6
416	SPINK1			2.76		NM_003122.2
417	RABAC1			2.74		NM_006423.1
418	ARF4			2.71		NM_001660.2
419	MFGE8			2.71		NM_005928.1
420	DNAJB6			2.71		NM_058246.3
421	IER3			2.70		NM_003897.3
422	RSPO3			2.70	Yes	NM_032784.3
423	SLC10A7			2.69		NM_001029998.2
424	SELM			2.69		NM_080430.2
425	SLC22A18			2.66		NM_002555.3
426	CTH			2.65		NM_153742.3
427	NDRG4			2.64		NM_022910.1
428	ENO2			2.63		NM_001975.2
429	C15orf48			2.63		NM_032413.2
430	KLHL24			2.63		NM_017644.3
431	ADM2			2.61		NM_024866.4
432	ARMCX1			2.61		NM_016608.1
433	STAT2			2.60		NM_005419.2
434	CREB5			2.56		NM_182898.2
435	OKL38			2.55		NM_013370.2
436	UAP1L1			2.53		NM_207309.1
437	HK2			2.53		NM_000189.4
438	LAMB3			2.51		NM_000228.2
439	CDRT4			2.49		NM_173622.3
440	SLC39A11			2.48		NM_139177.2
441	HS1BP3			2.47		NM_022460.3
442	WARS			2.47		NM_173701.1
443	NOV			2.46		NM_002514.2
444	DUSP10			2.46		NM_144729.1
445	DKK3			2.46		NM_013253.4
446	GPR137B			2.45		NM_003272.1
447	LOC387763			2.45		XM_941665.2
448	SLC33A1			2.45		NM_004733.2
449	NDRG1			2.45		NM_006096.2
450	CLDN1			2.43		NM_021101.3

Number	Gene symbol	Fold change			Predicted target?	Gene accession number
		12h	24h	48h		
451	ANXA8			2.42		NM_001630.1
452	TIMP4			2.39		NM_003256.2
453	GMPPB			2.38		NM_021971.1
454	RNF145			2.37		NM_144726.1
455	ABTB1			2.37		NM_032548.2
456	PRKCDBP			2.37		NM_145040.2
457	ANTXR2			2.36		NM_058172.3
458	CFB			2.36		NM_001710.4
459	YIF1A			2.36		NM_020470.1
460	GPRC5C			2.36		NM_018653.3
461	P4HA1			2.35		NM_000917.2
462	BCAT1			2.35		NM_005504.4
463	PCSK1			2.33		NM_000439.3
464	PPP1R15A			2.33		NM_014330.2
465	IGFBP6			2.32		NM_002178.2
466	ZMAT3			2.30		NM_152240.1
467	ALDH1L2			2.29		XM_927536.1
468	CTHRC1			2.28		NM_138455.2
469	SEMA4B			2.28		NM_198925.1
470	COPB2			2.27		NM_004766.1
471	YPEL3			2.27		NM_031477.4
472	HYOU1			2.27		NM_006389.2
473	C5orf41			2.27		NM_153607.1
474	GMPPA			2.27		NM_205847.1
475	PCK2			2.26		NM_004563.2
476	YIPF2			2.26		NM_024029.3
477	MOGS			2.26		NM_006302.2
478	TMBIM1			2.26		NM_022152.4
479	EPPB9			2.25		NM_015681.2
480	SLC37A3			2.24		NM_032295.2
481	CTSD			2.23		NM_001909.3
482	CHAC1			2.23		NM_024111.2
483	FAM102A			2.23		NM_001035254.1
484	COG6			2.22		NM_020751.1
485	ETS1			2.22		NM_005238.2
486	FAM113B			2.20		NM_138371.1
487	SEC61A1			2.20		NM_013336.3
488	TMEM214			2.20		NM_017727.4
489	SLC12A8			2.20		NM_024628.4
490	RHOQ			2.20		NM_012249.3
491	C19orf4			2.20		NM_012109.1
492	ASS1			2.19		NM_000050.4
493	C3orf52			2.19		NM_024616.1
494	RBKS			2.18		NM_022128.1
495	TRIB3			2.17		NM_021158.3
496	PTK6			2.17		NM_005975.2
497	COG5			2.17		NM_006348.2
498	PFKFB4			2.17		NM_004567.2
499	PTGES			2.16	Yes	NM_004878.3
500	SRGN			2.15		NM_002727.2
501	MAGED2			2.15		NM_201222.1
502	CTSL1			2.15		NM_001912.3
503	PRKAG2			2.14		NM_024429.1
504	MLPH			2.14		NM_001042467.1
505	PELO			2.14		NM_015946.4
506	DGKA			2.14		NM_201554.1
507	CLDN12			2.12		NM_012129.2

Number	Gene symbol	Fold change			Predicted target?	Gene accession number
		12h	24h	48h		
508	VEGFA			2.12		NM_003376.4
509	RNMT			2.12	Yes	NM_003799.1
510	SLC1A1			2.11		NM_004170.4
511	LOC344887			2.11		XR_038616.1
512	RRAGB			2.11		NM_006064.3
513	SIRPA			2.10		NM_001040023.1
514	FNIP1			2.09		NM_001008738.2
515	TBC1D2			2.09		NM_018421.2
516	TMED9			2.09		NM_017510.4
517	PPAPDC1B			2.09		NM_032483.2
518	GMPR2			2.09		NM_001002000.1
519	PLAUR			2.08		NM_001005376.1
520	BNIP3L			2.08		
521	PIP4K2C			2.08		NM_024779.3
522	FICD			2.08		NM_007076.2
523	NCF2			2.07		NM_000433.2
524	SEMA3B			2.07		NM_001005914.1
525	STYXL1			2.07		NM_016086.2
526	ITGB3			2.07		NM_000212.2
527	FAP			2.07		NM_004460.2
528	MICAL1			2.07		NM_022765.2
529	TP53INP1			2.06		NM_033285.2
530	IFT20			2.06		NM_174887.2
531	SEL1L3			2.06		NM_015187.3
532	VAMP5			2.06		NM_006634.2
533	EEF1A1			2.05		NM_001402.5
534	PHLDA1			2.05		NM_007350.3
535	B9D1			2.05		NM_015681.3
536	MYLK			2.05		NM_053032.2
537	COG3			2.04		NM_031431.2
538	GABARAPL1			2.04		NM_031412.2
539	ORAI3			2.04		NM_152288.1
540	OAT			2.04		NM_000274.1
541	PDIA3P			2.03		NR_002305.1
542	SLC35E1			2.03		NM_024881.4
543	S100P			2.02		NM_005980.2
544	RIT1			2.02		NM_006912.4
545	CHN2			2.02		NM_004067.2
546	LOC339192			2.02		XM_001726300.1
547	SEC31A			2.02		NM_014933.2
548	CD55			2.01		NM_000574.2
549	C6orf223			2.01		NM_153246.3
550	YIPF1			2.01		NM_018982.3
551	RNASE4			2.01		NM_194431.1
552	YIPF3			2.01		NM_015388.2
553	DOM3Z			2.01	Yes	NM_005510.3
554	WISP2			2.00		NM_003881.2
555	NPAS2			2.00		NM_002518.3
556	BBS9			1.99		NM_001033604.1
557	MCOLN1			1.99		NM_020533.1
558	SSR1			1.99		NM_003144.2
559	GOLT1B			1.99	Yes	NM_016072.3
560	LOC729768			1.98		XR_016076.2
561	MEG3			1.98		NR_002766.1
562	ACTG2			1.98		NM_001615.3
563	CLIP4			1.97		NM_024692.3
564	NGF			1.97		NM_002506.2

Number	Gene symbol	Fold change			Predicted target?	Gene accession number
		12h	24h	48h		
565	KRT80			1.97		NM_182507.2
566	ABHD3			1.97		NM_138340.3
567	SERPINB5			1.97		NM_002639.3
568	CDKN1A			1.97		NM_000389.2
569	SCYL1			1.97		NM_020680.3
570	HHAT			1.97		NM_018194.2
571	SCYL1BP1			1.97		NM_152281.1
572	RAB11FIP5			1.97		NM_015470.2
573	SH2D5			1.96		XM_375698.3
574	PID1			1.96		NM_017933.3
575	LACTB			1.96		NM_032857.2
576	GOLGA5			1.96		NM_005113.2
577	LOC493869			1.96		NM_001008397.1
578	CMAS			1.96		NM_018686.3
579	TPP1			1.96		NM_000391.3
580	LOC400750			1.95		XR_039444.1
581	GADD45A			1.95		NM_001924.2
582	ABLIM3			1.95		NM_014945.2
583	THSD4			1.95		NM_024817.1
584	UGDH			1.95		NM_003359.2
585	C16orf45			1.95		NM_033201.1
586	PAPSS2			1.95		NM_004670.3
587	RPL34			1.95		NM_000995.2
588	TMEM97			1.95		NM_014573.2
589	DPY19L3			1.95		NM_207325.1
590	GPT2			1.95		NM_133443.1
591	OTUD1			1.95		XM_001134465.1
592	TAGLN			1.95		NM_003186.3
593	UGCG			1.95		NM_003358.1
594	LEPREL2			1.95		NM_014262.2
595	LOC648399			1.95		XM_937448.1
596	CANX			1.94		NM_001746.3
597	GALNT10			1.94		NM_017540.3
598	COPB1			1.94		NM_016451.3
599	PLEKHM1			1.94		XM_001128220.1
600	C9orf169			1.94		NM_199001.1
601	SURF4			1.93		NM_033161.2
602	DNER			1.93		NM_139072.3
603	DHDDS			1.93		NM_024887.2
604	SELS			1.93		NM_018445.4
605	C1orf85			1.93		NM_144580.1
606	SDF2L1			1.93		NM_022044.2
607	STX5			1.93		NM_003164.3
608	WDSUB1			1.93		NM_152528.1
609	PTPRF			1.93		NM_002840.3
610	GCNT2			1.92		NM_001491.2
611	CATSPER1			1.92		NM_053054.2
612	USP36			1.92		NM_025090.2
613	KLF4			1.92		NM_004235.3
614	SERPINB8			1.91		NM_002640.3
615	SARS			1.91		NM_006513.2
616	UBC			1.91		NM_021009.3
617	PYCR1			1.91		NM_153824.1
618	C9orf119			1.91		NM_001040011.1
619	STS-1			1.91		NM_032873.3
620	IL32			1.91		NM_001012636.1
621	PLAU			1.91		NM_002658.2

Number	Gene symbol	Fold change			Predicted target?	Gene accession number
		12h	24h	48h		
622	CPZ			1.91		NM_001014447.1
623	ANKRD33			1.91		NM_182608.2
624	F3			1.90		NM_001993.2
625	ATF4			1.90		NM_182810.1
626	CYB561			1.90		NM_001017917.1
627	GPR175			1.90		NM_016372.1
628	IFNGR1			1.90		NM_000416.1
629	CALU			1.90		NM_001219.2
630	PPPDE1			1.90		NM_016076.3
631	LGALS8			1.89		NM_006499.3
632	IL6			1.89		NM_000600.1
633	LOC730996			1.89		XM_001128017.1
634	RPS29			1.89		NM_001030001.1
635	ATXN1			1.89		NM_000332.2
636	FAM134B			1.89		NM_001034850.1
637	COPG			1.88	Yes	NM_016128.3
638	WBP5			1.87		NM_001006612.1
639	TPRG1L			1.87		NM_182752.3
640	ALS2			1.87		NM_020919.2
641	COPA			1.87		NM_004371.3
642	CNN1			1.87		NM_001299.4
643	SRP54			1.87		NM_003136.2
644	ARF1			1.87		NM_001024228.1
645	PIM1			1.87		NM_002648.2
646	LOC401805			1.87		XR_038835.1
647	SPAG9			1.86		NM_172345.1
648	LOC392871			1.86		XR_018049.2
649	HSPA13			1.86		NM_006948.4
650	BIRC2			1.86		NM_001166.3
651	CAPRIN2			1.86		NM_001002259.1
652	NUDT18			1.86		NM_024815.3
653	SLC30A5			1.86		NM_022902.2
654	TPMT			1.85		NM_000367.2
655	C20orf100			1.85		NM_032883.1
656	SDSL			1.85		NM_138432.2
657	BHLHB2			1.85		NM_003670.1
658	QPRT			1.85		NM_014298.3
659	DOCK2			1.85	Yes	NM_004946.1
660	KRT81			1.85		NM_002281.2
661	PEPD			1.85		NM_000285.2
662	CTNS			1.85		NM_004937.2
663	PHTF1			1.85		NM_006608.1
664	PTPRE			1.85		NM_130435.2
665	UFC1			1.84		NM_016406.1
666	IRS2			1.84		NM_003749.2
667	PDE2A			1.84		NM_002599.1
668	RUNX2			1.84		NM_001024630.2
669	ATG2A			1.84		NM_015104.1
670	SLC7A11			1.83		NM_014331.3
671	C7orf10			1.83		NM_024728.1
672	KCNMB1			1.83		NM_004137.2
673	LPPR2			1.83		NM_022737.1
674	TNFRSF25			1.83		NM_148973.1
675	BTBD7			1.83		NM_001002860.2
676	LOC100128077			1.83		XM_001721943.1
677	ETV4			1.83		NM_001986.1
678	SLC2A1			1.83		NM_006516.1

Number	Gene symbol	Fold change			Predicted target?	Gene accession number
		12h	24h	48h		
679	GOLGB1			1.83		NM_004487.3
680	JUB			1.83		NM_198086.1
681	CDCP1			1.83		NM_022842.3
682	RAB6A			1.83		NM_198896.1
683	DKK1			1.83		NM_012242.2
684	MTMR2			1.82		NM_201281.1
685	CHPF			1.82		NM_024536.4
686	NAGK			1.82		NM_017567.2
687	PNPLA8			1.82		NM_015723.2
688	IFRD1			1.82		NM_001550.2
689	SSR2			1.82		XM_945430.1
690	LMAN2			1.82		NM_006816.1
691	RRAGC			1.82		NM_022157.2
692	NEU1			1.82		NM_000434.2
693	TCP11L2			1.82		NM_152772.1
694	ARMET			1.82		NM_006010.2
695	SLC25A46			1.82		NM_138773.1
696	TRPC4AP			1.82		NM_015638.2
697	C6orf85			1.82		NM_021945.4
698	PTRH1			1.82		NM_001002913.1
699	LOC284988			1.82		XR_017252.1
700	RIOK3			1.81		NM_003831.3
701	SLC25A20			1.81		NM_000387.3
702	PHLDA3			1.81	Yes	NM_012396.3
703	LCN2			1.81		NM_005564.3
704	UFM1			1.81		NM_016617.1
705	INSIG2			1.80		NM_016133.2
706	TCEAL8			1.80		NM_153333.2
707	NUPR1			1.80		NM_001042483.1
708	ECM2			1.80		NM_001393.2
709	SLC38A2			1.80		NM_018976.3
710	RND3			1.80		NM_005168.3
711	ANGPTL4			1.80		NM_139314.1
712	MAP2K1			1.80		NM_002755.2
713	EPHA2			1.80		NM_004431.2
714	FKBP10			1.80		NM_021939.2
715	EPOR			1.80		NM_000121.2
716	SLC38A10			1.80		NM_138570.2
717	MUC1			1.80		NM_001044390.1
718	EIF2AK3			1.80		NM_004836.4
719	DKFZp451A211			1.80		NM_001003399.1
720	MBNL2			1.80		NM_207304.1
721	STMN3			1.80		NM_015894.2
722	RSL24D1			1.79		NM_016304.2
723	STX3			1.79		NM_004177.3
724	TMEM151A			1.79		NM_153266.2
725	C12orf57			1.79		NM_138425.2
726	AGPAT9			1.79		NM_032717.3
727	DNAJB2			1.79		NM_006736.5
728	CYB5R1			1.78		NM_016243.2
729	LMAN1			1.78		NM_005570.2
730	RHOU			1.78		NM_021205.4
731	COQ10B			1.78		NM_025147.3
732	DUSP4			1.78		NM_001394.5
733	LOC730820			1.78		XM_001127763.1
734	SYT11			1.78		NM_152280.2
735	GARS			1.78		NM_002047.2

Number	Gene symbol	Fold change			Predicted target?	Gene accession number
		12h	24h	48h		
736	FAM18B			1.78		NM_016078.4
737	NAGLU			1.78		NM_000263.3
738	TNC			1.78		NM_002160.2
739	C6orf1			1.78		NM_001008704.1
740	JUP			1.78		NM_021991.1
741	FOXQ1			1.78		NM_033260.3
742	MYL9			1.78		NM_006097.3
743	PDXDC1			1.78		NM_015027.2
744	CALCOCO1			1.78		NM_020898.1
745	BCL2L1			1.78		NM_138578.1
746	RENBP			1.77		NM_002910.4
747	TRIP11			1.77		NM_004239.1
748	ERRFI1			1.77		NM_018948.2
749	SMPDL3A			1.77		NM_006714.2
750	NME7			1.77		NM_013330.3
751	CPEB4			1.77		NM_030627.1
752	LIPA			1.77		NM_000235.2
753	LAT			1.77		NM_001014987.1
754	HMGCL			1.77		NM_000191.2
755	DAP			1.77		NM_004394.1
756	TGDS			1.77		NM_014305.2
757	COL4A1			1.77		NM_001845.4
758	CEBPG			1.77		NM_001806.2
759	OCIAD2			1.76		NM_001014446.1
760	CYFIP2			1.76		NM_014376.2
761	LIF			1.76		NM_002309.2
762	C8orf83			1.76		NR_015339.1
763	COL15A1			1.76		NM_001855.3
764	HBP1			1.76		NM_012257.3
765	C1S			1.76		NM_001734.2
766	ISG20L1			1.76		NM_022767.2
767	LOC401317			1.76		XM_379479.3
768	MOBKL2C			1.76		NM_145279.4
769	SEPX1			1.76		NM_016332.2
770	NAMPT			1.76		NM_005746.2
771	GRN			1.76		NM_002087.2
772	GALNT12			1.75		NM_024642.3
773	MAMLD1			1.75		NM_005491.2
774	KLHL30			1.75		NM_198582.2
775	UNC84B			1.75		NM_015374.1
776	WDR45			1.75		NM_007075.3
777	RRAGD			1.75		NM_021244.3
778	AUH			1.75		NM_001698.1
779	KIAA0251			1.75		XM_001125924.1
780	ECE1			1.75		NM_001397.1
781	ORMDL3			1.75		NM_139280.1
782	HPS3			1.75		NM_032383.3
783	TWF2			1.75		NM_007284.3
784	PARP3			1.75		NM_005485.3
785	TBC1D8B			1.75		NM_017752.2
786	IL1A			1.75		NM_000575.3
787	CHIC2			1.75		NM_012110.2
788	CGNL1			1.75		NM_032866.3
789	DNAJC10			1.75		NM_018981.1
790	CDH13			1.75		NM_001257.3
791	CLCN7			1.75		NM_001287.3
792	SUMF1			1.74		NM_182760.2

Number	Gene symbol	Fold change			Predicted target?	Gene accession number
		12h	24h	48h		
793	POL3S			1.74		NM_001039503.2
794	CCRK			1.74		NM_012119.3
795	VAT1			1.74		NM_006373.3
796	PDIA4			1.74		NM_004911.3
797	FBXL13			1.74		NM_145032.2
798	RAB32			1.74		NM_006834.2
799	MBD1			1.74		NM_015845.2
800	CALCOCO2			1.74		NM_005831.3
801	PPP2R5B			1.74		NM_006244.2
802	HK1			1.74		NM_033500.1
803	LOC653994			1.73		XM_944439.2
804	ZNF622			1.73		NM_033414.2
805	IL24			1.73		NM_006850.2
806	COMMD3			1.73		NM_012071.2
807	FLJ20254			1.73		NM_017727.3
808	GNPDA1			1.73		NM_005471.3
809	TICAM2			1.72		NM_021649.3
810	MTMR10			1.72		NM_017762.2
811	B3GNT5			1.72		NM_032047.4
812	MBTPS1			1.72		NM_003791.2
813	SH3BGRL3			1.72		NM_031286.3
814	PSCA			1.72		NM_005672.3
815	GALK2			1.72		NM_002044.2
816	GOLGA2			1.72		NM_004486.4
817	CLDN23			1.72		NM_194284.2
818	C10orf118			1.72		NM_018017.2
819	FUCA1			1.72		NM_000147.3
820	CD24			1.72		NM_013230.2
821	MARS			1.72		NM_004990.2
822	THBS3			1.72		NM_007112.3
823	RNF13			1.72		NM_183381.1
824	KIAA0913			1.72		NM_015037.2
825	AKAP13			1.72		NM_007200.3
826	EXT1			1.71		NM_000127.2
827	STK19			1.71	Yes	NM_004197.1
828	CAPN7			1.71		NM_014296.2
829	DERL2			1.71		NM_016041.3
830	LOC143666			1.71		XM_001127524.1
831	C10orf11			1.71		NM_032024.3
832	BMP1			1.71		NM_006129.2
833	C7orf23			1.71		NM_024315.2
834	ALDH18A1			1.71		NM_002860.3
835	MLEC			1.71		NM_014730.2
836	OSMR			1.71		NM_003999.1
837	YIPF6			1.71		NM_173834.2
838	CCND1			1.71		NM_053056.2
839	LOC390557			1.71		XM_001726973.1
840	CMPK1			1.71		NM_016308.1
841	KRT17			1.71		NM_000422.1
842	OSBPL9			1.71		NM_148906.1
843	PHGDH			1.70		NM_006623.2
844	GBA			1.70		NM_001005742.1
845	ZMIZ1			1.70		NM_020338.2
846	C15orf39			1.70		NM_015492.4
847	HSDL1			1.70		NM_031463.3
848	CCDC90B			1.70		NM_021825.3
849	PPIB			1.70		NM_000942.4

Number	Gene symbol	Fold change			Predicted target?	Gene accession number
		12h	24h	48h		
850	LOC340274			1.70		XR_017256.2
851	TBX3			1.70		NM_005996.3
852	ITPRIP			1.69		NM_033397.2
853	BAX			1.69		NM_138765.2
854	GOSR2			1.69		NM_004287.3
855	SLC31A2			1.69		NM_001860.2
856	TBC1D20			1.69		NM_144628.2
857	SDC4			1.69		NM_002999.2
858	BAD			1.69		NM_004322.2
859	FTH1			1.69		NM_002032.2
860	CDH2			1.69		NM_001792.2
861	PNKD			1.69		NM_022572.2
862	SULF2			1.69		NM_018837.2
863	PSG4			1.69		NM_002780.3
864	MTHFD2			1.69		NM_006636.3
865	CD276			1.69		NM_001024736.1
866	SECISBP2			1.69		NM_024077.3
867	SPTLC1			1.68	Yes	NM_178324.1
868	FAM55C			1.68		NM_145037.1
869	BRI3P1			1.68		XR_015539.2
870	WSB1			1.68		NM_134264.2
871	LOC645638			1.68		XR_040455.1
872	MAPK13			1.68		NM_002754.3
873	ZBTB43			1.68		NM_014007.2
874	ECM1			1.68		NM_022664.1
875	KIAA0363			1.68		XM_001133202.1
876	CDH15			1.68		NM_004933.2
877	IRF9			1.68		NM_006084.4
878	FVT1			1.68		NM_002035.1
879	FMNL2			1.68		NM_052905.3
880	SLC35C1			1.68		NM_018389.3
881	NFIL3			1.68		NM_005384.2
882	PCTP			1.68		NM_021213.1
883	TMF1			1.68		NM_007114.2
884	UNC50			1.68		NM_014044.4
885	SIL1			1.68		NM_001037633.1
886	SLC31A1			1.68		NM_001859.2
887	CD59			1.68		NM_203331.1
888	LOC729779			1.68		XR_019592.2
889	PARP4			1.68		NM_006437.3
890	ALDH2			1.67		NM_000690.2
891	LAMA1			1.67		NM_005559.2
892	PLOD1			1.67		NM_000302.2
893	ASAP2			1.67		NM_003887.2
894	CHPF2			1.67		NM_019015.1
895	IL18BP			1.67		NM_173042.2
896	C9orf21			1.67		NM_153698.1
897	LOC100132564			1.67		XM_001713808.1
898	TMEM59			1.66		NM_004872.3
899	CGB5			1.66		NM_033043.1
900	CHKA			1.66		NM_212469.1
901	B3GNT6			1.66		NM_006876.1
902	SLC36A1			1.66		NM_078483.2
903	HSPBAP1			1.66		NM_024610.4
904	LOC441711			1.66		XR_037852.1
905	GNPTAB			1.66		NM_024312.3
906	COL4A2			1.66		NM_001846.2

Number	Gene symbol	Fold change			Predicted target?	Gene accession number
		12h	24h	48h		
907	APBB3			1.66		NM_133172.2
908	ARHGEF18			1.66		NM_015318.2
909	ANKRA2			1.66		NM_023039.2
910	EDEM1			1.66		NM_014674.1
911	PSPH			1.66		NM_004577.3
912	HM13			1.66		NM_178580.1
913	CYP4V2			1.66		NM_207352.2
914	SESN1			1.66		NM_014454.1
915	TIMP2			1.66		NM_003255.4
916	SEC61G			1.65		NM_014302.3
917	UBR4			1.65		NM_020765.2
918	SLC35C2			1.65		NM_173073.2
919	SPINK6			1.65		NM_205841.2
920	EBI3			1.65		NM_005755.2
921	FOXD1			1.65		NM_004472.2
922	SLC2A5			1.65		NM_003039.1
923	ZFPL1			1.65		NM_006782.3
924	ATP6V0E1			1.65		NM_003945.3
925	ZNF697			1.65		NM_001080470.1
926	TBC1D7			1.65		NM_016495.2
927	AARS			1.65		NM_001605.2
928	COL7A1			1.65		NM_000094.2
929	TTC3			1.65		NM_003316.3
930	PPT2			1.65		NM_138717.1
931	DCUN1D3			1.65		NM_173475.1
932	STARD3NL			1.65		NM_032016.2
933	PRDX5			1.65		NM_181652.1
934	PPP1CB			1.65	Yes	NM_206876.1
935	LPIN2			1.65		NM_014646.2
936	OSTCL			1.64		NM_145303.3
937	MANBA			1.64		NM_005908.3
938	FLNB			1.64		NM_001457.1
939	NECAP2			1.64		NM_018090.3
940	RGS20			1.64		NM_170587.1
941	CSPG4			1.64		NM_001897.4
942	TERF1			1.64		NM_017489.1
943	VPS18			1.64		NM_020857.2
944	C19orf10			1.64		NM_019107.3
945	LOC644496			1.64		XR_039005.1
946	RETSAT			1.64		NM_017750.2
947	GPX7			1.64		NM_015696.3
948	ATXN2L			1.64		XM_939199.1
949	IFI16			1.64		NM_005531.1
950	TAX1BP3			1.64		NM_014604.2
951	PSAT1			1.64		NM_021154.3
952	KDSR			1.64		NM_002035.2
953	OSBPL2			1.64		NM_144498.1
954	CHMP2B			1.64		NM_014043.2
955	CGB1			1.64		NM_033377.1
956	COL4A3BP			1.64		NM_005713.1
957	CD82			1.64		NM_001024844.1
958	TFG			1.63		NM_001007565.1
959	CCDC50			1.63	Yes	NM_174908.2
960	NPC2			1.63		NM_006432.3
961	COL5A1			1.63		NM_000093.3
962	CLIC3			1.63		NM_004669.2
963	FAM98A			1.63		NM_015475.3

Number	Gene symbol	Fold change			Predicted target?	Gene accession number
		12h	24h	48h		
964	SND1			1.63		NM_014390.2
965	DTWD1			1.63		NM_020234.4
966	KIAA1715			1.63		NM_030650.1
967	CKAP4			1.63		NM_006825.2
968	LOC646567			1.63		XM_929503.2
969	B4GALNT1			1.63		NM_001478.3
970	ZNF295			1.62		NM_001098402.1
971	ANKDD1A			1.62		NM_182703.3
972	APCDD1L			1.62		NM_153360.1
973	CHST15			1.62		NM_015892.2
974	TLE1			1.62		NM_005077.3
975	GLT8D1			1.62		NM_018446.2
976	GRAMD4			1.62		NM_015124.2
977	TPBG			1.62		NM_006670.3
978	SPSB1			1.62		NM_025106.2
979	NUB1			1.62		NM_016118.3
980	C10orf58			1.62		NM_032333.4
981	COPE			1.62		NM_199442.1
982	MAGED4B			1.62	Yes	NM_030801.2
983	LRP1			1.62		NM_002332.2
984	SH3RF2			1.62		NM_152550.2
985	F2RL1			1.62		NM_005242.3
986	VASN			1.62		NM_138440.2
987	JMY			1.62		NM_152405.3
988	ULBP2			1.62		NM_025217.2
989	JMJD1A			1.62		NM_018433.3
990	DUSP11			1.62		NM_003584.1
991	MATN2			1.62		NM_002380.3
992	TRIO			1.61		NM_007118.2
993	TPD52			1.61		NM_005079.2
994	C12orf5			1.61		NM_020375.2
995	IQGAP1			1.61		NM_003870.3
996	GAB2			1.61		NM_080491.1
997	TESK2			1.61		NM_007170.2
998	ADORA2B			1.61		NM_000676.2
999	TANC2			1.61		NM_025185.3
1000	TOX2			1.61		NM_001098797.1
1001	RRM2B			1.61		NM_015713.3
1002	TINAGL1			1.61		NM_022164.1
1003	ABHD10			1.61		NM_018394.1
1004	RINT1			1.61		NM_021930.4
1005	TP53BP1			1.61		NM_005657.1
1006	ERMAP			1.61		NM_001017922.1
1007	LOC653566			1.61		XM_934796.2
1008	C1orf54			1.61		NM_024579.2
1009	TMEM144			1.61		NM_018342.3
1010	PTDSS2			1.61		NM_030783.1
1011	REPS2			1.61		NM_004726.2
1012	C1orf56			1.61		NM_017860.3
1013	TPCN2			1.61		NM_139075.2
1014	ARFGEF1			1.61		NM_006421.3
1015	DIRC2			1.60		NM_032839.1
1016	TCEAL3			1.60		NM_001006933.1
1017	SYNC1			1.60		NM_030786.1
1018	TTPAL			1.60		NM_001039199.1
1019	MACF1			1.60		NM_012090.3
1020	ARID5B			1.60		NM_032199.1

Number	Gene symbol	Fold change			Predicted target?	Gene accession number
		12h	24h	48h		
1021	DCBLD2			1.60		NM_080927.3
1022	SRPR			1.60		NM_003139.2
1023	PLDN			1.60		NM_012388.2
1024	CYB561D2			1.60		NM_007022.3
1025	ENC1			1.60		NM_003633.1
1026	LRRC59			1.60		NM_018509.2
1027	TMEM131			1.60		NM_015348.1
1028	AMDHD2			1.60		NM_015944.2
1029	EXOC2			1.60		NM_018303.4
1030	SYNGR3			1.60		NM_004209.4
1031	NFKB2			1.60		NM_001077493.1
1032	KIAA0194			1.60		XM_001714730.1
1033	LINGO2			1.59		NM_152570.1
1034	NGRN			1.59		NM_016645.2
1035	WASF2			1.59		NM_006990.2
1036	GCGR			1.59		NM_000160.2
1037	ERP29			1.59		NM_006817.3
1038	LOC730278			1.59		XM_001126471.1
1039	RPS27L			1.59		NM_015920.3
1040	ACYP2			1.59		NM_138448.2
1041	WBP2			1.59		NM_012478.3
1042	GLG1			1.59		NM_012201.4
1043	CLIP2			1.59		NM_032421.2
1044	RALA			1.59		NM_005402.2
1045	TBL2			1.59		NM_012453.2
1046	CYLN2			1.59		NM_032421.1
1047	TMEM184B			1.59		NM_012264.3
1048	KLF6			1.59		NM_001300.4
1049	P8			1.59		NM_012385.1
1050	TMEM22			1.59		NM_001097599.1
1051	ARMCX2			1.58		NM_177949.1
1052	CARS			1.58		NM_001014438.1
1053	ERCC5			1.58		NM_000123.2
1054	YIF1B			1.58		NM_001031731.1
1055	WDR26			1.58		NM_025160.4
1056	OSTC			1.57		NM_021227.2
1057	DNASE2			1.57		NM_001375.2
1058	MBP			1.57		NM_001025100.1
1059	ATM			1.57		NM_000051.3
1060	PKIB			1.57		NM_032471.4
1061	SPIRE1			1.57		NM_020148.2
1062	BET1			1.57		NM_005868.4
1063	ATP6V0D1			1.57		NM_004691.4
1064	RAB18			1.57		NM_021252.3
1065	SERPINE2			1.57		NM_006216.2
1066	ADM			1.57		NM_001124.1
1067	SELI			1.57		NM_033505.2
1068	NHLRC3			1.57		NM_001017370.1
1069	CCDC28A			1.57		NM_015439.2
1070	EVI5L			1.57		NM_145245.2
1071	GBE1			1.57		NM_000158.2
1072	MAFB			1.57		NM_005461.3
1073	LOC100132394			1.57		XM_001713809.1
1074	AHCYL1			1.57		NM_006621.4
1075	HSPC171			1.56		NM_014187.2
1076	EBI2			1.56		NM_004951.3
1077	RP11-529I10.4			1.56		NM_015448.1

Number	Gene symbol	Fold change			Predicted target?	Gene accession number
		12h	24h	48h		
1078	C2orf43			1.56		NM_021925.2
1079	BECN1			1.56		NM_003766.2
1080	LOC652968			1.56		NM_001037666.1
1081	CHURC1			1.56		NM_145165.2
1082	IRS1			1.56		NM_005544.1
1083	BAG1			1.56		NM_004323.4
1084	TMTC1			1.56		NM_175861.2
1085	LOC646463			1.56		XM_001130106.1
1086	FAM70B			1.56		XM_001130122.1
1087	PTGS1			1.56		NM_080591.1
1088	ASB1			1.56		NM_016114.3
1089	THUMPD1			1.56		NM_017736.3
1090	MAMDC4			1.56		NM_206920.2
1091	LGALS1			1.56		NM_002305.3
1092	TRIM25			1.56		NM_005082.4
1093	HRASLS3			1.56		NM_007069.2
1094	TOM1L2			1.56		NM_001082968.1
1095	HERC3			1.56		NM_014606.1
1096	ATP6V1E1			1.56		NM_001039367.1
1097	TIPARP			1.56		NM_015508.3
1098	ATP8B2			1.56		NM_020452.2
1099	DACT1			1.56		NM_016651.4
1100	GGT1			1.56		NM_005265.2
1101	SRPK2			1.56		NM_182691.1
1102	GPX1			1.56		NM_201397.1
1103	UBE2H			1.56		NM_003344.2
1104	SLC15A4			1.55		NM_145648.1
1105	SYNJ2			1.55		NM_003898.2
1106	TES			1.55		NM_152829.1
1107	LOC731007			1.55		XM_001132080.1
1108	PICALM			1.55		NM_007166.2
1109	C12orf44			1.55		NM_001098673.1
1110	FOXO1			1.55		NM_002015.3
1111	ADAMTSL5			1.55		NM_213604.1
1112	GSTO1			1.55		NM_004832.1
1113	TM9SF1			1.55		NM_006405.5
1114	RCN3			1.55		NM_020650.2
1115	ABHD5			1.55		NM_016006.3
1116	OSBP			1.55		NM_002556.2
1117	TMED2			1.55		NM_006815.3
1118	ZHX2			1.55		NM_014943.3
1119	CD63			1.55		NM_001040034.1
1120	FST			1.55		NM_013409.1
1121	ANXA5			1.55		NM_001154.2
1122	XPR1			1.55		NM_004736.2
1123	CTSB			1.55		NM_147780.2
1124	HSP90B1			1.55		NM_003299.1
1125	CHST7			1.55		NM_019886.2
1126	SFXN3			1.55		NM_030971.3
1127	OSBP2			1.55		NM_030758.3
1128	TM9SF4			1.55		NM_014742.2
1129	LTBP2			1.55		NM_000428.2
1130	SENP2			1.55		NM_021627.2
1131	PKD2			1.54		NM_000297.2
1132	APH1B			1.54		NM_031301.2
1133	IGFL1			1.54		NM_198541.1
1134	CBLB			1.54		NM_170662.3

Number	Gene symbol	Fold change			Predicted target?	Gene accession number
		12h	24h	48h		
1135	P2RY2			1.54		NM_002564.2
1136	BDNF			1.54		NM_001709.3
1137	RNF160			1.54		NM_015565.1
1138	ARL1			1.54		NM_001177.3
1139	NISCH			1.54		NM_007184.3
1140	EXOSC1			1.54		XM_001131367.1
1141	MED23			1.54		NM_004830.2
1142	PSG5			1.54		NM_002781.2
1143	SLC22A15			1.54		NM_018420.1
1144	LOC338758			1.54		XM_931359.2
1145	C19orf63			1.54		NM_175063.4
1146	MIA3			1.54		NM_198551.2
1147	RAB5A			1.54		NM_004162.3
1148	RAC2			1.54		NM_002872.3
1149	C3			1.54		NM_000064.1
1150	CMTM3			1.53		NM_144601.2
1151	BRI3			1.53		NM_015379.3
1152	NOTCH3			1.53		NM_000435.1
1153	LOC730358			1.53		
1154	AHNAK			1.53		NM_001620.1
1155	OSTM1			1.53		NM_014028.3
1156	KDELR1			1.53		NM_006801.2
1157	FAM50A			1.53	Yes	NM_004699.1
1158	STAM2			1.53		NM_005843.3
1159	IER5L			1.53		NM_203434.2
1160	FKBP14			1.53		NM_017946.2
1161	SLC41A2			1.53		NM_032148.2
1162	CDC42EP2			1.53		NM_006779.2
1163	RNF146			1.53		NM_030963.2
1164	SQSTM1			1.53		NM_003900.3
1165	KLHL21			1.53		NM_014851.2
1166	GGTLC2			1.53		NM_199127.1
1167	ABHD4			1.53		NM_022060.2
1168	TMEM106B			1.53		NM_018374.2
1169	FKBP2			1.52		NM_004470.2
1170	CENTB2			1.52		NM_012287.3
1171	IBTK			1.52		NM_015525.2
1172	SAR1B			1.52	Yes	NM_001033503.1
1173	OSBPL7			1.52		NM_145798.2
1174	GK			1.52		NM_203391.1
1175	CORO1C			1.52		NM_014325.2
1176	C1R			1.52		NM_001733.4
1177	WTAP			1.52		NM_152858.1
1178	C2orf29			1.52		NM_017546.3
1179	C9orf150			1.52		NM_203403.1
1180	FOSL1			1.52		NM_005438.2
1181	USP4			1.52		NM_003363.2
1182	TMEM55A			1.52		NM_018710.1
1183	IL13RA1			1.52		NM_001560.2
1184	TGFA			1.52		NM_003236.1
1185	SEC63			1.52		NM_007214.3
1186	CD58			1.52		NM_001779.1
1187	CXCL2			1.52		NM_002089.3
1188	ABLIM2			1.52		NM_032432.3
1189	GGT2			1.52		XM_001129425.1
1190	GGPS1			1.52		NM_001037277.1
1191	DDEF2			1.52		NM_003887.1

Number	Gene symbol	Fold change			Predicted target?	Gene accession number
		12h	24h	48h		
1192	TAF9L			1.52		NM_015975.3
1193	MGAT1			1.52		NM_002406.2
1194	SLC22A23			1.52		NM_015482.1
1195	CA12			1.51		NM_001218.3
1196	SEC16A			1.51		NM_014866.1
1197	ATP6AP1			1.51		NM_001183.4
1198	PSMD9			1.51		NM_002813.4
1199	HSPA12A			1.51		NM_025015.2
1200	MAP4K2			1.51		NM_004579.2
1201	SAT1			1.51		NM_002970.1
1202	NUCB2			1.51		NM_005013.2
1203	LOC653354			1.51		XM_927053.2
1204	LAMC1			1.51		NM_002293.2
1205	GORASP2			1.51		NM_015530.3
1206	SLC30A1			1.51		NM_021194.2
1207	FOXO3			1.51		NM_201559.2
1208	PRKAR1A			1.51		NM_002734.3
1209	ASAH1			1.51		NM_177924.2
1210	C16orf7			1.51		NM_004913.2
1211	HINT3			1.51		NM_138571.4
1212	TMED3			1.51		NM_007364.2
1213	LMBRD1			1.51		NM_018368.2
1214	FNDC3A			1.51		NM_001079673.1
1215	LIMS2			1.51		NM_017980.3

Number	Gene symbol	Fold change			Predicted target?	Gene accession number
		12h	24h	48h		
1216	NUAK1			1.51		NM_014840.2
1217	A2LD1			1.51		NM_033110.1
1218	LFNG			1.51		NM_001040167.1
1219	ZDHHC13			1.51		NM_001001483.1
1220	CIB1			1.51		NM_006384.2
1221	PINK1			1.51		NM_032409.2
1222	C1orf128			1.51		NM_020362.3
1223	TBC1D23			1.51		NM_018309.1
1224	SCPEP1			1.51		NM_021626.1
1225	C5orf28			1.51		NM_022483.3
1226	LZTFL1			1.51		NM_020347.2
1227	ADAM19			1.50		NM_033274.2
1228	S100A11			1.50		NM_005620.1
1229	ENTPD7			1.50		NM_020354.2
1230	DFFB			1.50		NM_004402.2
1231	CIR1			1.50		NM_004882.3
1232	ARMCX5			1.50		NM_022838.2
1233	DNAJC1			1.50		NM_022365.3
1234	TGIF1			1.50		NM_170695.2
1235	ASB3			1.50		NM_145863.1
1236	LOC650128			1.50		XM_945833.1
1237	SRPRB			1.50		NM_021203.2
1238	HIPK2			1.50		NM_022740.2

Appendix V: Membrane trafficking-related genes affected in pre-miR-517a-transfected HeLa cells. Genes are listed alphabetically.

(**A**) Membrane trafficking-related genes downregulated by *miR-517a*.

Number	Gene symbol	Expression change			Predicted target?	Gene accession number
		12h	24h	48h		
1	ABL1			-1.71		NM_007313.2
2	AGAP3			-2.17		NM_001042535.1
3	AP1S2	-2.21	-2.31	-2.02	Yes	NM_003916.3
4	AP3S1		-1.63			NM_001002924.1
5	ARF3		-1.53			NM_001659.1
6	ARL17B			-1.55		NM_001103154.1
7	ATG10		-1.70	-1.65	Yes	NM_031482.3
8	CENPF			-1.77		NM_016343.3
9	FNBP1		-1.65			NM_015033.2
10	HRAS			-1.54	Yes	NM_005343.2
11	INPPL1		-1.52		Yes	NM_001567.2
12	KIF18A			-1.66		NM_031217.2
13	KIF20A			-1.52		NM_005733.1
14	LDLR			-1.99	Yes	NM_000527.2
15	LRSAM1	-1.67	-1.59			NM_138361.3
16	NME1			-2.18		NM_198175.1
17	NUP62CL			-1.80		NM_017681.1
18	NUPL2	-1.78	-1.56	-1.79	Yes	NM_007342.1
19	PEX5		-1.50			NM_000319.3
20	RAB26		-1.75	-2.98		NM_014353.4
21	RAB35	-1.74		-1.57		NM_006861.4
22	RAB40B	-1.95	-2.77	-2.95		NM_006822.1
23	RAB40C	-1.74	-1.53			NM_021168.2

Number	Gene symbol	Expression change			Predicted target?	Gene accession number
		12h	24h	48h		
24	RAC1		-1.91	-4.11		NM_018890.2
25	RANBP3			-1.58		NM_007320.1
26	SCG2			-1.61		NM_003469.3
27	SELENBP1			-1.53		NM_003944.2
28	SNX5		-1.64	-1.89		NM_152227.1
29	TAP2			-1.66		NM_000544.3
30	TOMM40			-1.61		NM_006114.1
31	TPR			-2.08		NM_003292.2
32	TRIM23		-1.54			NM_001656.3

(B) Membrane trafficking-related genes upregulated by *miR-517a*.

Number	Gene symbol	Expression change			Predicted target?	Gene accession number
		12h	24h	48h		
1	ARF1			1.87		NM_001024228.1
2	ARF4			2.71		NM_001660.2
3	ARFGAP1		2.11	3.43		NM_018209.2
4	ARFGAP3		1.62	2.06		NM_014570.3
5	ARL1			1.54		NM_001177.3
6	ARL8B	2.02	2.20	3.90		NM_018184.2
7	ATG4A		1.59	1.74		NM_178270.1
8	BET1			1.57		NM_005868.4
9	CANX			1.94		NM_001746.3
10	CHMP2B			1.64		NM_014043.2
11	COG3			2.04		NM_031431.2
12	COG5			2.17		NM_006348.2
13	COG6			2.22		NM_020751.1
14	COPE			1.62		NM_199442.1
15	DMBT1		1.51	1.94		NM_017579.1
16	DNER			1.93		NM_139072.3
17	ERP29			1.59		NM_006817.3
18	EXOC2			1.60		NM_018303.4
19	GEM		1.57	1.60		NM_181702.1
20	GNPTAB			1.66		NM_024312.3
21	GOLT1B			1.99	Yes	NM_016072.3
22	GOSR2			1.63		NM_001012511.1
23	HSP90B1			1.55		NM_003299.1
24	KDELR3		1.84	4.42		NM_016657.1
25	LMAN1			1.78		NM_005570.2
26	LMAN2			1.82		NM_006816.1
27	LTBP2			1.55		NM_000428.2
28	MAMDC4			1.56		NM_206920.2
29	MCFD2		1.62	1.91		NM_139279.3
30	MIA3			1.54		NM_198551.2
31	NECAP2			1.64		NM_018090.3
32	NUP35	2.08	2.43	1.88	Yes	NM_138285.3
33	PDIA4			1.74		NM_004911.3
34	RAB11FIP1	2.16	3.08	3.00		NM_001002814.1
35	RAB11FIP5			1.97		NM_015470.2
36	RAB18			1.57		NM_021252.3
37	RAB22A		2.25	2.14		NM_020673.2
38	RAB32			1.74		NM_006834.2
39	RAB5A			1.54		NM_004162.3
40	RAB6A			1.83		NM_198896.1
41	RAB8B	2.21	2.26	2.81		NM_016530.2

Number	Gene symbol	Expression change			Predicted target?	Gene accession number
		12h	24h	48h		
42	RAC2			1.54		NM_002872.3
43	RALA			1.59		NM_005402.2
44	RAN		1.59			NM_006325.2
45	RAP1B	1.73	2.14	2.67		NM_015646.4
46	RHOBTB1		1.50			NM_198225.1
47	RHOQ			2.20		NM_012249.3
48	RHOU			1.78		NM_021205.4
49	RINT1			1.61		NM_021930.4
50	RIT1			2.02		NM_006912.4
51	RND3			1.80		NM_005168.3
52	RRBP1		1.57	2.17		NM_001042576.1
53	SEC16A			1.51		NM_014866.1
54	SEC31A			2.02		NM_014933.2
55	SEC61A1			2.20		NM_013336.3
56	SEC61G			1.65		NM_014302.3
57	SEC63			1.52		NM_007214.3
58	SENP2			1.55		NM_021627.2
59	SERP1		1.60	1.92		NM_014445.3
60	SLC15A4			1.55		NM_145648.1
61	TM9SF1			1.55		NM_006405.5
62	TMED2			1.55		NM_006815.3
63	TMED3			1.51		NM_007364.2
64	TOM1			3.33		NM_005488.1
65	UNC50			1.68		NM_014044.4
66	VLDLR		1.58	3.23		NM_001018056.1
67	VPS18			1.64		NM_020857.2
68	WASF2			1.59		NM_006990.2
69	YIF1A			2.36		NM_020470.1
70	YIPF5		1.77	2.32		NM_030799.6
71	ZFYVE20	1.60	1.85	1.66		NM_022340.2
72	ZMAT3			2.30		NM_152240.1

REFERENCES

Abbott AL, Alvarez-Saavedra E, Miska EA, Lau NC, Bartel DP, Horvitz HR, Ambros V (2005) **The let-7 MicroRNA family members mir-48, mir-84, and mir-241 function together to regulate developmental timing in Caenorhabditis elegans**. Dev Cell 9: 403-414

Abramoff MD, Magalhaes PJ, Rams SJ (2004) **Image Processing with ImageJ**. Biophotonics International 11: 36-42

Alexiou P, Maragkakis M, Papadopoulos GL, Reczko M, Hatzigeorgiou AG (2009) **Lost in translation: an assessment and perspective for computational microRNA target identification**. Bioinformatics 25: 3049-3055

Allan BB, Moyer BD, Balch WE (2000) **Rab1 recruitment of p115 into a cis-SNARE complex: programming budding COPII vesicles for fusion**. Science 289: 444-448

Alto NM, Soderling J, Scott JD (2002) **Rab32 is an A-kinase anchoring protein and participates in mitochondrial dynamics**. J Cell Biol 158: 659-668

Andag U, Neumann T, Schmitt HD (2001) **The coatomer-interacting protein Dsl1p is required for Golgi-to-endoplasmic reticulum retrieval in yeast**. J Biol Chem 276: 39150-39160

Anderson RG, Brown MS, Beisiegel U, Goldstein JL (1982) **Surface distribution and recycling of the low density lipoprotein receptor as visualized with antireceptor antibodies**. J Cell Biol 93: 523-531

Andreev J, Simon JP, Sabatini DD, Kam J, Plowman G, Randazzo PA, Schlessinger J (1999) **Identification of a new Pyk2 target protein with Arf-GAP activity**. Mol Cell Biol 19: 2338-2350

Andres DA, Seabra MC, Brown MS, Armstrong SA, Smeland TE, Cremers FP, Goldstein JL (1993) **cDNA cloning of component A of Rab geranylgeranyl transferase and demonstration of its role as a Rab escort protein**. Cell 73: 1091-1099

Antonny B, Beraud-Dufour S, Chardin P, Chabre M (1997) **N-terminal hydrophobic residues of the G-protein ADP-ribosylation factor-1 insert into membrane phospholipids upon GDP to GTP exchange**. Biochemistry 36: 4675-4684

Appenzeller-Herzog C, Hauri HP (2006) **The ER-Golgi intermediate compartment (ERGIC): in search of its identity and function**. J Cell Sci 119: 2173-2183

Arnaoutova I, Jackson CL, Al-Awar OS, Donaldson JG, Loh YP (2003) **Recycling of Raft-associated prohormone sorting receptor carboxypeptidase E requires interaction with ARF6**. Mol Biol Cell 14: 4448-4457

Baek D, Villen J, Shin C, Camargo FD, Gygi SP, Bartel DP (2008) **The impact of microRNAs on protein output**. Nature 455: 64-71

Bagga S, Bracht J, Hunter S, Massirer K, Holtz J, Eachus R, Pasquinelli AE (2005) **Regulation by let-7 and lin-4 miRNAs results in target mRNA degradation**. Cell 122: 553-563

Bannykh SI, Nishimura N, Balch WE (1998) **Getting into the Golgi**. Trends Cell Biol 8: 21-25

Bar M, Wyman SK, Fritz BR, Qi J, Garg KS, Parkin RK, Kroh EM, Bendoraite A, Mitchell PS, Nelson AM, Ruzzo WL, Ware C, Radich JP, Gentleman R, Ruohola-Baker H, Tewari M (2008) **MicroRNA discovery and profiling in human embryonic stem cells by deep sequencing of small RNA libraries**. Stem Cells 26: 2496-2505

Barlowe C (2002) **COPII-dependent transport from the endoplasmic reticulum**. Curr Opin Cell Biol 14: 417-422

Baroukh N, Ravier MA, Loder MK, Hill EV, Bounacer A, Scharfmann R, Rutter GA, Van Obberghen E (2007) **MicroRNA-124a regulates Foxa2 expression and intracellular signaling in pancreatic beta-cell lines**. J Biol Chem 282: 19575-19588

Bartel DP (2009) **MicroRNAs: target recognition and regulatory functions**. Cell 136: 215-233

Bartz F, Kern L, Erz D, Zhu M, Gilbert D, Meinhof T, Wirkner U, Erfle H, Muckenthaler M, Pepperkok R, Runz H (2009) **Identification of cholesterol-regulating genes by targeted RNAi screening**. Cell Metab 10: 63-75

Baskerville S, Bartel DP (2005) **Microarray profiling of microRNAs reveals frequent coexpression with neighboring miRNAs and host genes**. Rna 11: 241-247

Behm-Ansmant I, Rehwinkel J, Doerks T, Stark A, Bork P, Izaurralde E (2006) **mRNA degradation by miRNAs and GW182 requires both CCR4:NOT deadenylase and DCP1:DCP2 decapping complexes**. Genes Dev 20: 1885-1898

Berezikov E, Chung WJ, Willis J, Cuppen E, Lai EC (2007) **Mammalian mirtron genes**. Mol Cell 28: 328-336

Bernards A (2003) **GAPs galore! A survey of putative Ras superfamily GTPase activating proteins in man and Drosophila**. Biochim Biophys Acta 1603: 47-82

Bernstein E, Kim SY, Carmell MA, Murchison EP, Alcorn H, Li MZ, Mills AA, Elledge SJ, Anderson KV, Hannon GJ (2003) **Dicer is essential for mouse development**. Nat Genet 35: 215-217

Betel D, Koppal A, Agius P, Sander C, Leslie C (2010) **Comprehensive modeling of microRNA targets predicts functional non-conserved and non-canonical sites**. Genome Biol 11: R90
Bielli A, Haney CJ, Gabreski G, Watkins SC, Bannykh SI, Aridor M (2005) **Regulation of Sar1 NH2 terminus by GTP binding and hydrolysis promotes membrane deformation to control COPII vesicle fission**. J Cell Biol 171: 919-924
Block MR, Glick BS, Wilcox CA, Wieland FT, Rothman JE (1988) **Purification of an N-ethylmaleimide-sensitive protein catalyzing vesicular transport**. Proc Natl Acad Sci U S A 85: 7852-7856
Boehm M, Aguilar RC, Bonifacino JS (2001) **Functional and physical interactions of the adaptor protein complex AP-4 with ADP-ribosylation factors (ARFs)**. Embo J 20: 6265-6276
Bonifacino JS, Glick BS (2004) **The mechanisms of vesicle budding and fusion**. Cell 116: 153-166
Bonifacino JS, Rojas R (2006) **Retrograde transport from endosomes to the trans-Golgi network**. Nat Rev Mol Cell Biol 7: 568-579
Borchert GM, Lanier W, Davidson BL (2006) **RNA polymerase III transcribes human microRNAs**. Nat Struct Mol Biol 13: 1097-1101
Borgdorff V, Lleonart ME, Bishop CL, Fessart D, Bergin AH, Overhoff MG, Beach DH (2010) **Multiple microRNAs rescue from Ras-induced senescence by inhibiting p21(Waf1/Cip1)**. Oncogene 29: 2262-2271
Bortolin-Cavaille ML, Dance M, Weber M, Cavaille J (2009) **C19MC microRNAs are processed from introns of large Pol-II, non-protein-coding transcripts**. Nucleic Acids Res 37: 3464-3473
Bossard C, Bresson D, Polishchuk RS, Malhotra V (2007) **Dimeric PKD regulates membrane fission to form transport carriers at the TGN**. J Cell Biol 179: 1123-1131
Boucrot E, Saffarian S, Zhang R, Kirchhausen T (2010) **Roles of AP-2 in clathrin-mediated endocytosis**. PLoS One 5: e10597
Braulke T, Bonifacino JS (2009) **Sorting of lysosomal proteins**. Biochim Biophys Acta 1793: 605-614
Brennecke J, Hipfner DR, Stark A, Russell RB, Cohen SM (2003) **bantam encodes a developmentally regulated microRNA that controls cell proliferation and regulates the proapoptotic gene hid in Drosophila**. Cell 113: 25-36
Brenner JL, Jasiewicz KL, Fahley AF, Kemp BJ, Abbott AL (2010) **Loss of individual microRNAs causes mutant phenotypes in sensitized genetic backgrounds in C. elegans**. Curr Biol 20: 1321-1325
Brocker C, Engelbrecht-Vandre S, Ungermann C (2010) **Multisubunit tethering complexes and their role in membrane fusion**. Curr Biol 20: R943-952
Brown MS, Goldstein JL (1986) **A receptor-mediated pathway for cholesterol homeostasis**. Science 232: 34-47
Bruinsma P, Spelbrink RG, Nothwehr SF (2004) **Retrograde transport of the mannosyltransferase Och1p to the early Golgi requires a component of the COG transport complex**. J Biol Chem 279: 39814-39823
Bucci C, Thomsen P, Nicoziani P, McCarthy J, van Deurs B (2000) **Rab7: a key to lysosome biogenesis**. Mol Biol Cell 11: 467-480
Burgoyne RD, Morgan A (2003) **Secretory granule exocytosis**. Physiol Rev 83: 581-632
Cai H, Yu S, Menon S, Cai Y, Lazarova D, Fu C, Reinisch K, Hay JC, Ferro-Novick S (2007) **TRAPPI tethers COPII vesicles by binding the coat subunit Sec23**. Nature 445: 941-944
Cai X, Hagedorn CH, Cullen BR (2004) **Human microRNAs are processed from capped, polyadenylated transcripts that can also function as mRNAs**. Rna 10: 1957-1966
Cai X, Schafer A, Lu S, Bilello JP, Desrosiers RC, Edwards R, Raab-Traub N, Cullen BR (2006) **Epstein-Barr virus microRNAs are evolutionarily conserved and differentially expressed**. PLoS Pathog 2: e23
Carroll KS, Hanna J, Simon I, Krise J, Barbero P, Pfeffer SR (2001) **Role of Rab9 GTPase in facilitating receptor recruitment by TIP47**. Science 292: 1373-1376
Carthew RW, Sontheimer EJ (2009) **Origins and Mechanisms of miRNAs and siRNAs**. Cell 136: 642-655
Chalfie M, Horvitz HR, Sulston JE (1981) **Mutations that lead to reiterations in the cell lineages of C. elegans**. Cell 24: 59-69
Chan JA, Krichevsky AM, Kosik KS (2005) **MicroRNA-21 is an antiapoptotic factor in human glioblastoma cells**. Cancer Res 65: 6029-6033
Chang TC, Yu D, Lee YS, Wentzel EA, Arking DE, West KM, Dang CV, Thomas-Tikhonenko A, Mendell JT (2008) **Widespread microRNA repression by Myc contributes to tumorigenesis**. Nat Genet 40: 43-50
Chang TC, Wentzel EA, Kent OA, Ramachandran K, Mullendore M, Lee KH, Feldmann G, Yamakuchi M, Ferlito M, Lowenstein CJ, Arking DE, Beer MA, Maitra A, Mendell JT (2007) **Transactivation of miR-34a by p53 broadly influences gene expression and promotes apoptosis**. Mol Cell 26: 745-752
Chapman RE, Munro S (1994) **Retrieval of TGN proteins from the cell surface requires endosomal acidification**. Embo J 13: 2305-2312
Chavrier P, Parton RG, Hauri HP, Simons K, Zerial M (1990) **Localization of low molecular weight GTP binding proteins to exocytic and endocytic compartments**. Cell 62: 317-329

Cheloufi S, Dos Santos CO, Chong MM, Hannon GJ (2010) **A dicer-independent miRNA biogenesis pathway that requires Ago catalysis**. Nature 465: 584-589
Chen C, Ridzon DA, Broomer AJ, Zhou Z, Lee DH, Nguyen JT, Barbisin M, Xu NL, Mahuvakar VR, Andersen MR, Lao KQ, Livak KJ, Guegler KJ (2005) **Real-time quantification of microRNAs by stem-loop RT-PCR**. Nucleic Acids Res 33: e179
Chen CZ, Li L, Lodish HF, Bartel DP (2004) **MicroRNAs modulate hematopoietic lineage differentiation**. Science 303: 83-86
Chen YJ, Stevens TH (1996) **The VPS8 gene is required for localization and trafficking of the CPY sorting receptor in Saccharomyces cerevisiae**. Eur J Cell Biol 70: 289-297
Chen J, Lozach J, Garcia EW, Barnes B, Luo S, Mikoulitch I, Zhou L, Schroth G, Fan JB (2008) **Highly sensitive and specific microRNA expression profiling using BeadArray technology**. Nucleic Acids Res 36: e87
Chendrimada TP, Gregory RI, Kumaraswamy E, Norman J, Cooch N, Nishikura K, Shiekhattar R (2005) **TRBP recruits the Dicer complex to Ago2 for microRNA processing and gene silencing**. Nature 436: 740-744
Cheng AM, Byrom MW, Shelton J, Ford LP (2005) **Antisense inhibition of human miRNAs and indications for an involvement of miRNA in cell growth and apoptosis**. Nucleic Acids Res 33: 1290-1297
Chiang HR, Schoenfeld LW, Ruby JG, Auyeung VC, Spies N, Baek D, Johnston WK, Russ C, Luo S, Babiarz JE, Blelloch R, Schroth GP, Nusbaum C, Bartel DP (2010) **Mammalian microRNAs: experimental evaluation of novel and previously annotated genes**. Genes Dev 24: 992-1009
Chotard L, Mishra AK, Sylvain MA, Tuck S, Lambright DG, Rocheleau CE (2010) **TBC-2 regulates RAB-5/RAB-7-mediated endosomal trafficking in Caenorhabditis elegans**. Mol Biol Cell 21: 2285-2296
Christoforidis S, McBride HM, Burgoyne RD, Zerial M (1999) **The Rab5 effector EEA1 is a core component of endosome docking**. Nature 397: 621-625
Cifuentes D, Xue H, Taylor DW, Patnode H, Mishima Y, Cheloufi S, Ma E, Mane S, Hannon GJ, Lawson ND, Wolfe SA, Giraldez AJ (2010) **A novel miRNA processing pathway independent of Dicer requires Argonaute2 catalytic activity**. Science 328: 1694-1698
Cimmino A, Calin GA, Fabbri M, Iorio MV, Ferracin M, Shimizu M, Wojcik SE, Aqeilan RI, Zupo S, Dono M, Rassenti L, Alder H, Volinia S, Liu CG, Kipps TJ, Negrini M, Croce CM (2005) **miR-15 and miR-16 induce apoptosis by targeting BCL2**. Proc Natl Acad Sci U S A 102: 13944-13949
Claude A, Zhao BP, Kuziemsky CE, Dahan S, Berger SJ, Yan JP, Armold AD, Sullivan EM, Melancon P (1999) **GBF1: A novel Golgi-associated BFA-resistant guanine nucleotide exchange factor that displays specificity for ADP-ribosylation factor 5**. J Cell Biol 146: 71-84
Clavel F, Charneau P (1994) **Fusion from without directed by human immunodeficiency virus particles**. J Virol 68: 1179-1185
Cloonan N, Brown MK, Steptoe AL, Wani S, Chan WL, Forrest AR, Kolle G, Gabrielli B, Grimmond SM (2008) **The miR-17-5p microRNA is a key regulator of the G1/S phase cell cycle transition**. Genome Biol 9: R127
Cole KA, Attiyeh EF, Mosse YP, Laquaglia MJ, Diskin SJ, Brodeur GM, Maris JM (2008) **A functional screen identifies miR-34a as a candidate neuroblastoma tumor suppressor gene**. Mol Cancer Res 6: 735-742
Cole MD, McMahon SB (1999) **The Myc oncoprotein: a critical evaluation of transactivation and target gene regulation**. Oncogene 18: 2916-2924
Coller HA, Forman JJ, Legesse-Miller A (2007) **"Myc'ed messages": myc induces transcription of E2F1 while inhibiting its translation via a microRNA polycistron**. PLoS Genet 3: e146
Collins KM, Thorngren NL, Fratti RA, Wickner WT (2005) **Sec17p and HOPS, in distinct SNARE complexes, mediate SNARE complex disruption or assembly for fusion**. Embo J 24: 1775-1786
Coppola T, Frantz C, Perret-Menoud V, Gattesco S, Hirling H, Regazzi R (2002) **Pancreatic beta-cell protein granuphilin binds Rab3 and Munc-18 and controls exocytosis**. Mol Biol Cell 13: 1906-1915
Corcoran DL, Pandit KV, Gordon B, Bhattacharjee A, Kaminski N, Benos PV (2009) **Features of mammalian microRNA promoters emerge from polymerase II chromatin immunoprecipitation data**. PLoS One 4: e5279
Cosson P, Amherdt M, Rothman JE, Orci L (2002) **A resident Golgi protein is excluded from peri-Golgi vesicles in NRK cells**. Proc Natl Acad Sci U S A 99: 12831-12834
Croce CM (2009) **Causes and consequences of microRNA dysregulation in cancer**. Nat Rev Genet 10: 704-714
D'Souza-Schorey C, Chavrier P (2006) **ARF proteins: roles in membrane traffic and beyond**. Nat Rev Mol Cell Biol 7: 347-358
D'Souza-Schorey C, Li G, Colombo MI, Stahl PD (1995) **A regulatory role for ARF6 in receptor-mediated endocytosis**. Science 267: 1175-1178
Davis BN, Hata A (2009) **Regulation of MicroRNA Biogenesis: A miRiad of mechanisms**. Cell Commun Signal 7: 18

Davis BN, Hilyard AC, Nguyen PH, Lagna G, Hata A (2010) **Smad proteins bind a conserved RNA sequence to promote microRNA maturation by Drosha**. Mol Cell 39: 373-384
Davis S, Lollo B, Freier S, Esau C (2006) **Improved targeting of miRNA with antisense oligonucleotides**. Nucleic Acids Res 34: 2294-2304
Davis S, Propp S, Freier SM, Jones LE, Serra MJ, Kinberger G, Bhat B, Swayze EE, Bennett CF, Esau C (2009) **Potent inhibition of microRNA in vivo without degradation**. Nucleic Acids Res 37: 70-77
De Matteis MA, Luini A (2011) **Mendelian disorders of membrane trafficking**. N Engl J Med 365: 927-938
Denli AM, Tops BB, Plasterk RH, Ketting RF, Hannon GJ (2004) **Processing of primary microRNAs by the Microprocessor complex**. Nature 432: 231-235
Desnoyers L, Anant JS, Seabra MC (1996) **Geranylgeranylation of Rab proteins**. Biochem Soc Trans 24: 699-703
Dews M, Homayouni A, Yu D, Murphy D, Sevignani C, Wentzel E, Furth EE, Lee WM, Enders GH, Mendell JT, Thomas-Tikhonenko A (2006) **Augmentation of tumor angiogenesis by a Myc-activated microRNA cluster**. Nat Genet 38: 1060-1065
Diaz E, Pfeffer SR (1998) **TIP47: a cargo selection device for mannose 6-phosphate receptor trafficking**. Cell 93: 433-443
Didiano D, Hobert O (2006) **Perfect seed pairing is not a generally reliable predictor for miRNA-target interactions**. Nat Struct Mol Biol 13: 849-851
Diederichs S, Haber DA (2007) **Dual role for argonautes in microRNA processing and posttranscriptional regulation of microRNA expression**. Cell 131: 1097-1108
Ding XC, Grosshans H (2009) **Repression of C. elegans microRNA targets at the initiation level of translation requires GW182 proteins**. Embo J 28: 213-222
Doebele C, Bonauer A, Fischer A, Scholz A, Reiss Y, Urbich C, Hofmann WK, Zeiher AM, Dimmeler S (2010) **Members of the microRNA-17-92 cluster exhibit a cell-intrinsic antiangiogenic function in endothelial cells**. Blood 115: 4944-4950
Doherty GJ, McMahon HT (2009) **Mechanisms of endocytosis**. Annu Rev Biochem 78: 857-902
Donaldson JG (2003) **Multiple roles for Arf6: sorting, structuring, and signaling at the plasma membrane**. J Biol Chem 278: 41573-41576
Donaldson JG, Jackson CL (2011) **ARF family G proteins and their regulators: roles in membrane transport, development and disease**. Nat Rev Mol Cell Biol 12: 362-375
Donaldson JG, Lippincott-Schwartz J (2000) **Sorting and signaling at the Golgi complex**. Cell 101: 693-696
Du L, Schageman JJ, Subauste MC, Saber B, Hammond SM, Prudkin L, Wistuba, II, Ji L, Roth JA, Minna JD, Pertsemlidis A (2009) **miR-93, miR-98, and miR-197 regulate expression of tumor suppressor gene FUS1**. Mol Cancer Res 7: 1234-1243
Echard A, Jollivet F, Martinez O, Lacapere JJ, Rousselet A, Janoueix-Lerosey I, Goud B (1998) **Interaction of a Golgi-associated kinesin-like protein with Rab6**. Science 279: 580-585
Elcheva I, Goswami S, Noubissi FK, Spiegelman VS (2009) **CRD-BP protects the coding region of betaTrCP1 mRNA from miR-183-mediated degradation**. Mol Cell 35: 240-246
Ellgaard L, Helenius A (2003) **Quality control in the endoplasmic reticulum**. Nat Rev Mol Cell Biol 4: 181-191
Elmen J, Lindow M, Schutz S, Lawrence M, Petri A, Obad S, Lindholm M, Hedtjarn M, Hansen HF, Berger U, Gullans S, Kearney P, Sarnow P, Straarup EM, Kauppinen S (2008) **LNA-mediated microRNA silencing in non-human primates**. Nature 452: 896-899
Erfle H, Neumann B, Liebel U, Rogers P, Held M, Walter T, Ellenberg J, Pepperkok R (2007) **Reverse transfection on cell arrays for high content screening microscopy**. Nat Protoc 2: 392-399
Erfle H, Neumann B, Rogers P, Bulkescher J, Ellenberg J, Pepperkok R (2008) **Work flow for multiplexing siRNA assays by solid-phase reverse transfection in multiwell plates**. J Biomol Screen 13: 575-580
Erfle H, Simpson JC, Bastiaens PI, Pepperkok R (2004) **siRNA cell arrays for high-content screening microscopy**. Biotechniques 37: 454-458, 460, 462
Esau C, Davis S, Murray SF, Yu XX, Pandey SK, Pear M, Watts L, Booten SL, Graham M, McKay R, Subramaniam A, Propp S, Lollo BA, Freier S, Bennett CF, Bhanot S, Monia BP (2006) **miR-122 regulation of lipid metabolism revealed by in vivo antisense targeting**. Cell Metab 3: 87-98
Esau CC (2008) **Inhibition of microRNA with antisense oligonucleotides**. Methods 44: 55-60
Eulalio A, Huntzinger E, Izaurralde E (2008) **GW182 interaction with Argonaute is essential for miRNA-mediated translational repression and mRNA decay**. Nat Struct Mol Biol 15: 346-353
Fang Z, Rajewsky N (2011) **The impact of miRNA target sites in coding sequences and in 3'UTRs**. PLoS One 6: e18067
Felder S, Miller K, Moehren G, Ullrich A, Schlessinger J, Hopkins CR (1990) **Kinase activity controls the sorting of the epidermal growth factor receptor within the multivesicular body**. Cell 61: 623-634

Fontana L, Fiori ME, Albini S, Cifaldi L, Giovinazzi S, Forloni M, Boldrini R, Donfrancesco A, Federici V, Giacomini P, Peschle C, Fruci D (2008) **Antagomir-17-5p abolishes the growth of therapy-resistant neuroblastoma through p21 and BIM**. PLoS One 3: e2236

Fontana L, Pelosi E, Greco P, Racanicchi S, Testa U, Liuzzi F, Croce CM, Brunetti E, Grignani F, Peschle C (2007) **MicroRNAs 17-5p-20a-106a control monocytopoiesis through AML1 targeting and M-CSF receptor upregulation**. Nat Cell Biol 9: 775-787

Frasa MA, Maximiano FC, Smolarczyk K, Francis RE, Betson ME, Lozano E, Goldenring J, Seabra MC, Rak A, Ahmadian MR, Braga VM (2010) **Armus is a Rac1 effector that inactivates Rab7 and regulates E-cadherin degradation**. Curr Biol 20: 198-208

Friedman RC, Farh KK, Burge CB, Bartel DP (2009) **Most mammalian mRNAs are conserved targets of microRNAs**. Genome Res 19: 92-105

Fu M, Wang C, Li Z, Sakamaki T, Pestell RG (2004) **Minireview: Cyclin D1: normal and abnormal functions**. Endocrinology 145: 5439-5447

Fukuda M (2011) **TBC proteins: GAPs for mammalian small GTPase Rab?** Biosci Rep 31: 159-168

Fukuda T, Yamagata K, Fujiyama S, Matsumoto T, Koshida I, Yoshimura K, Mihara M, Naitou M, Endoh H, Nakamura T, Akimoto C, Yamamoto Y, Katagiri T, Foulds C, Takezawa S, Kitagawa H, Takeyama K, O'Malley BW, Kato S (2007) **DEAD-box RNA helicase subunits of the Drosha complex are required for processing of rRNA and a subset of microRNAs**. Nat Cell Biol 9: 604-611

Garzon R, Fabbri M, Cimmino A, Calin GA, Croce CM (2006) **MicroRNA expression and function in cancer**. Trends Mol Med 12: 580-587

Gerich B, Orci L, Tschochner H, Lottspeich F, Ravazzola M, Amherdt M, Wieland F, Harter C (1995) **Non-clathrin-coat protein alpha is a conserved subunit of coatomer and in Saccharomyces cerevisiae is essential for growth**. Proc Natl Acad Sci U S A 92: 3229-3233

Ghosh RN, Gelman DL, Maxfield FR (1994) **Quantification of low density lipoprotein and transferrin endocytic sorting HEp2 cells using confocal microscopy**. J Cell Sci 107 (Pt 8): 2177-2189

Gilbert DF, Meinhof T, Pepperkok R, Runz H (2009) **DetecTiff: a novel image analysis routine for high-content screening microscopy**. J Biomol Screen 14: 944-955

Gilchrist A, Au CE, Hiding J, Bell AW, Fernandez-Rodriguez J, Lesimple S, Nagaya H, Roy L, Gosline SJ, Hallett M, Paiement J, Kearney RE, Nilsson T, Bergeron JJ (2006) **Quantitative proteomics analysis of the secretory pathway**. Cell 127: 1265-1281

Gillingham AK, Munro S (2007) **The small G proteins of the Arf family and their regulators**. Annu Rev Cell Dev Biol 23: 579-611

Giraldez AJ, Cinalli RM, Glasner ME, Enright AJ, Thomson JM, Baskerville S, Hammond SM, Bartel DP, Schier AF (2005) **MicroRNAs regulate brain morphogenesis in zebrafish**. Science 308: 833-838

Giraldez AJ, Mishima Y, Rihel J, Grocock RJ, Van Dongen S, Inoue K, Enright AJ, Schier AF (2006) **Zebrafish MiR-430 promotes deadenylation and clearance of maternal mRNAs**. Science 312: 75-79

Glick BS, Nakano A (2009) **Membrane traffic within the Golgi apparatus**. Annu Rev Cell Dev Biol 25: 113-132

Goldstein JL, Brown MS, Anderson RG, Russell DW, Schneider WJ (1985) **Receptor-mediated endocytosis: concepts emerging from the LDL receptor system**. Annu Rev Cell Biol 1: 1-39

Gou D, Mishra A, Weng T, Su L, Chintagari NR, Wang Z, Zhang H, Gao L, Wang P, Stricker HM, Liu L (2008) **Annexin A2 interactions with Rab14 in alveolar type II cells**. J Biol Chem 283: 13156-13164

Gregory RI, Chendrimada TP, Cooch N, Shiekhattar R (2005) **Human RISC couples microRNA biogenesis and posttranscriptional gene silencing**. Cell 123: 631-640

Gregory RI, Yan KP, Amuthan G, Chendrimada T, Doratotaj B, Cooch N, Shiekhattar R (2004) **The Microprocessor complex mediates the genesis of microRNAs**. Nature 432: 235-240

Griffiths-Jones S, Saini HK, van Dongen S, Enright AJ (2008) **miRBase: tools for microRNA genomics**. Nucleic Acids Res 36: D154-158

Grimson A, Farh KK, Johnston WK, Garrett-Engele P, Lim LP, Bartel DP (2007) **MicroRNA targeting specificity in mammals: determinants beyond seed pairing**. Mol Cell 27: 91-105

Grishok A, Pasquinelli AE, Conte D, Li N, Parrish S, Ha I, Baillie DL, Fire A, Ruvkun G, Mello CC (2001) **Genes and mechanisms related to RNA interference regulate expression of the small temporal RNAs that control C. elegans developmental timing**. Cell 106: 23-34

Guay C, Roggli E, Nesca V, Jacovetti C, Regazzi R (2011) **Diabetes mellitus, a microRNA-related disease?** Transl Res 157: 253-264

Guo H, Ingolia NT, Weissman JS, Bartel DP (2010) **Mammalian microRNAs predominantly act to decrease target mRNA levels**. Nature 466: 835-840

Haas AK, Fuchs E, Kopajtich R, Barr FA (2005) **A GTPase-activating protein controls Rab5 function in endocytic trafficking**. Nat Cell Biol 7: 887-893

Hayashita Y, Osada H, Tatematsu Y, Yamada H, Yanagisawa K, Tomida S, Yatabe Y, Kawahara K, Sekido Y, Takahashi T (2005) **A polycistronic microRNA cluster, miR-17-92, is overexpressed in human lung cancers and enhances cell proliferation**. Cancer Res 65: 9628-9632

Hales CM, Vaerman JP, Goldenring JR (2002) **Rab11 family interacting protein 2 associates with Myosin Vb and regulates plasma membrane recycling**. J Biol Chem 277: 50415-50421

Hammell CM, Karp X, Ambros V (2009) **A feedback circuit involving let-7-family miRNAs and DAF-12 integrates environmental signals and developmental timing in Caenorhabditis elegans**. Proc Natl Acad Sci U S A 106: 18668-18673

Han J, Lee Y, Yeom KH, Kim YK, Jin H, Kim VN (2004) **The Drosha-DGCR8 complex in primary microRNA processing**. Genes Dev 18: 3016-3027

Han J, Lee Y, Yeom KH, Nam JW, Heo I, Rhee JK, Sohn SY, Cho Y, Zhang BT, Kim VN (2006) **Molecular basis for the recognition of primary microRNAs by the Drosha-DGCR8 complex**. Cell 125: 887-901

Hanina SA, Mifsud W, Down TA, Hayashi K, O'Carroll D, Lao K, Miska EA, Surani MA (2010) **Genome-wide identification of targets and function of individual MicroRNAs in mouse embryonic stem cells**. PLoS Genet 6: e1001163

Harder N, Eils R, Rohr K (2008) **Automated classification of mitotic phenotypes of human cells using fluorescent proteins**. Methods Cell Biol 85: 539-554

Hata A, Davis BN (2011) **Regulation of pri-miRNA Processing Through Smads**. Adv Exp Med Biol 700: 15-27

Haucke V (2005) **Phosphoinositide regulation of clathrin-mediated endocytosis**. Biochem Soc Trans 33: 1285-1289

He L, He X, Lim LP, de Stanchina E, Xuan Z, Liang Y, Xue W, Zender L, Magnus J, Ridzon D, Jackson AL, Linsley PS, Chen C, Lowe SW, Cleary MA, Hannon GJ (2007) **A microRNA component of the p53 tumour suppressor network**. Nature 447: 1130-1134

He L, Thomson JM, Hemann MT, Hernando-Monge E, Mu D, Goodson S, Powers S, Cordon-Cardo C, Lowe SW, Hannon GJ, Hammond SM (2005) **A microRNA polycistron as a potential human oncogene**. Nature 435: 828-833

Hendrickson DG, Hogan DJ, McCullough HL, Myers JW, Herschlag D, Ferrell JE, Brown PO (2009) **Concordant regulation of translation and mRNA abundance for hundreds of targets of a human microRNA**. PLoS Biol 7: e1000238

Henke JI, Goergen D, Zheng J, Song Y, Schuttler CG, Fehr C, Junemann C, Niepmann M (2008) **microRNA-122 stimulates translation of hepatitis C virus RNA**. Embo J 27: 3300-3310

Henne WM, Boucrot E, Meinecke M, Evergren E, Vallis Y, Mittal R, McMahon HT (2010) **FCHo proteins are nucleators of clathrin-mediated endocytosis**. Science 328: 1281-1284

Hicke L, Yoshihisa T, Schekman R (1992) **Sec23p and a novel 105-kDa protein function as a multimeric complex to promote vesicle budding and protein transport from the endoplasmic reticulum**. Mol Biol Cell 3: 667-676

Hille-Rehfeld A (1995) **Mannose 6-phosphate receptors in sorting and transport of lysosomal enzymes**. Biochim Biophys Acta 1241: 177-194

Hinske LC, Galante PA, Kuo WP, Ohno-Machado L (2010) **A potential role for intragenic miRNAs on their hosts' interactome**. BMC Genomics 11: 533

Hobbs HH, Brown MS, Goldstein JL (1992) **Molecular genetics of the LDL receptor gene in familial hypercholesterolemia**. Hum Mutat 1: 445-466

Honda A, Al-Awar OS, Hay JC, Donaldson JG (2005) **Targeting of Arf-1 to the early Golgi by membrin, an ER-Golgi SNARE**. J Cell Biol 168: 1039-1051

Hossain A, Kuo MT, Saunders GF (2006) **Mir-17-5p regulates breast cancer cell proliferation by inhibiting translation of AIB1 mRNA**. Mol Cell Biol 26: 8191-8201

Hsu SD, Lin FM, Wu WY, Liang C, Huang WC, Chan WL, Tsai WT, Chen GZ, Lee CJ, Chiu CM, Chien CH, Wu MC, Huang CY, Tsou AP, Huang HD (2011) **miRTarBase: a database curates experimentally validated microRNA-target interactions**. Nucleic Acids Res 39: D163-169

Hsu VW, Yang JS (2009) **Mechanisms of COPI vesicle formation**. FEBS Lett 583: 3758-3763

Huang F, Khvorova A, Marshall W, Sorkin A (2004) **Analysis of clathrin-mediated endocytosis of epidermal growth factor receptor by RNA interference**. J Biol Chem 279: 16657-16661

Huang Q, Gumireddy K, Schrier M, le Sage C, Nagel R, Nair S, Egan DA, Li A, Huang G, Klein-Szanto AJ, Gimotty PA, Katsaros D, Coukos G, Zhang L, Pure E, Agami R (2008) **The microRNAs miR-373 and miR-520c promote tumour invasion and metastasis**. Nat Cell Biol 10: 202-210

Huang X, Ding L, Bennewith KL, Tong RT, Welford SM, Ang KK, Story M, Le QT, Giaccia AJ (2009) **Hypoxia-inducible mir-210 regulates normoxic gene expression involved in tumor initiation**. Mol Cell 35: 856-867

Humphries WHt, Fay NC, Payne CK (2010) **Intracellular degradation of low-density lipoprotein probed with two-color fluorescence microscopy**. Integr Biol (Camb) 2: 536-544
Huntzinger E, Izaurralde E (2011) **Gene silencing by microRNAs: contributions of translational repression and mRNA decay**. Nat Rev Genet 12: 99-110
Hutagalung AH, Novick PJ (2011) **Role of Rab GTPases in membrane traffic and cell physiology**. Physiol Rev 91: 119-149
Hutvagner G, Simard MJ, Mello CC, Zamore PD (2004) **Sequence-specific inhibition of small RNA function**. PLoS Biol 2: E98
Jackson CL, Casanova JE (2000) **Turning on ARF: the Sec7 family of guanine-nucleotide-exchange factors**. Trends Cell Biol 10: 60-67
Jahn R, Scheller RH (2006) **SNAREs--engines for membrane fusion**. Nat Rev Mol Cell Biol 7: 631-643
Jay C, Nemunaitis J, Chen P, Fulgham P, Tong AW (2007) **miRNA profiling for diagnosis and prognosis of human cancer**. DNA Cell Biol 26: 293-300
Johnson CD, Esquela-Kerscher A, Stefani G, Byrom M, Kelnar K, Ovcharenko D, Wilson M, Wang X, Shelton J, Shingara J, Chin L, Brown D, Slack FJ (2007) **The let-7 microRNA represses cell proliferation pathways in human cells**. Cancer Res 67: 7713-7722
Johnston RJ, Hobert O (2003) **A microRNA controlling left/right neuronal asymmetry in Caenorhabditis elegans**. Nature 426: 845-849
Jones S, Newman C, Liu F, Segev N (2000) **The TRAPP complex is a nucleotide exchanger for Ypt1 and Ypt31/32**. Mol Biol Cell 11: 4403-4411
Jopling CL, Yi M, Lancaster AM, Lemon SM, Sarnow P (2005) **Modulation of hepatitis C virus RNA abundance by a liver-specific MicroRNA**. Science 309: 1577-1581
Kahn RA, Cherfils J, Elias M, Lovering RC, Munro S, Schurmann A (2006) **Nomenclature for the human Arf family of GTP-binding proteins: ARF, ARL, and SAR proteins**. J Cell Biol 172: 645-650
Kanzaki H, Ito S, Hanafusa H, Jitsumori Y, Tamaru S, Shimizu K, Ouchida M (2011) **Identification of direct targets for the miR-17-92 cluster by proteomic analysis**. Proteomics 11: 3531-3539
Kapp LD, Lorsch JR (2004) **The molecular mechanics of eukaryotic translation**. Annu Rev Biochem 73: 657-704
Kartberg F, Asp L, Dejgaard SY, Smedh M, Fernandez-Rodriguez J, Nilsson T, Presley JF (2010) **ARFGAP2 and ARFGAP3 are essential for COPI coat assembly on the Golgi membrane of living cells**. J Biol Chem 285: 36709-36720
Katzmann DJ, Odorizzi G, Emr SD (2002) **Receptor downregulation and multivesicular-body sorting**. Nat Rev Mol Cell Biol 3: 893-905
Kawahara Y, Zinshteyn B, Chendrimada TP, Shiekhattar R, Nishikura K (2007) **RNA editing of the microRNA-151 precursor blocks cleavage by the Dicer-TRBP complex**. EMBO Rep 8: 763-769
Khvorova A, Reynolds A, Jayasena SD (2003) **Functional siRNAs and miRNAs exhibit strand bias**. Cell 115: 209-216
Kinch LN, Grishin NV (2009) **The human Ago2 MC region does not contain an eIF4E-like mRNA cap binding motif**. Biol Direct 4: 2
Kinchen JM, Ravichandran KS (2010) **Identification of two evolutionarily conserved genes regulating processing of engulfed apoptotic cells**. Nature 464: 778-782
Kiriakidou M, Tan GS, Lamprinaki S, De Planell-Saguer M, Nelson PT, Mourelatos Z (2007) **An mRNA m7G cap binding-like motif within human Ago2 represses translation**. Cell 129: 1141-1151
Kirkham M, Parton RG (2005) **Clathrin-independent endocytosis: new insights into caveolae and non-caveolar lipid raft carriers**. Biochim Biophys Acta 1746: 349-363
Kleizen B, Braakman I (2004) **Protein folding and quality control in the endoplasmic reticulum**. Curr Opin Cell Biol 16: 343-349
Kondo A, Hashimoto S, Yano H, Nagayama K, Mazaki Y, Sabe H (2000) **A new paxillin-binding protein, PAG3/Papalpha/KIAA0400, bearing an ADP-ribosylation factor GTPase-activating protein activity, is involved in paxillin recruitment to focal adhesions and cell migration**. Mol Biol Cell 11: 1315-1327
Krauss M, Kinuta M, Wenk MR, De Camilli P, Takei K, Haucke V (2003) **ARF6 stimulates clathrin/AP-2 recruitment to synaptic membranes by activating phosphatidylinositol phosphate kinase type Igamma**. J Cell Biol 162: 113-124
Krol J, Loedige I, Filipowicz W (2010) **The widespread regulation of microRNA biogenesis, function and decay**. Nat Rev Genet 11: 597-610
Krutzfeldt J, Kuwajima S, Braich R, Rajeev KG, Pena J, Tuschl T, Manoharan M, Stoffel M (2007) **Specificity, duplex degradation and subcellular localization of antagomirs**. Nucleic Acids Res 35: 2885-2892
Krutzfeldt J, Rajewsky N, Braich R, Rajeev KG, Tuschl T, Manoharan M, Stoffel M (2005) **Silencing of microRNAs in vivo with 'antagomirs'**. Nature 438: 685-689

Kuehn MJ, Herrmann JM, Schekman R (1998) **COPII-cargo interactions direct protein sorting into ER-derived transport vesicles**. Nature 391: 187-190
Laemmli UK (1970) **Cleavage of structural proteins during the assembly of the head of bacteriophage T4**. Nature 227: 680-685
Lagos-Quintana M, Rauhut R, Lendeckel W, Tuschl T (2001) **Identification of novel genes coding for small expressed RNAs**. Science 294: 853-858
Lai EC (2002) **Micro RNAs are complementary to 3' UTR sequence motifs that mediate negative post-transcriptional regulation**. Nat Genet 30: 363-364
Lai EC, Tam B, Rubin GM (2005) **Pervasive regulation of Drosophila Notch target genes by GY-box-, Brd-box-, and K-box-class microRNAs**. Genes Dev 19: 1067-1080
Lam LT, Lu X, Zhang H, Lesniewski RR, Rosenberg SH, Semizarov D (2010) **A microRNA screen to identify modulators of sensitivity to BCL2 inhibitor ABT-263 (Navitoclax)**. Mol Cancer Ther
Landgraf P, Rusu M, Sheridan R, Sewer A, Iovino N, Aravin A, Pfeffer S, Rice A, Kamphorst AO, Landthaler M, Lin C, Socci ND, Hermida L, Fulci V, Chiaretti S, Foa R, Schliwka J, Fuchs U, Novosel A, Muller RU, et al (2007) **A mammalian microRNA expression atlas based on small RNA library sequencing**. Cell 129: 1401-1414
Lau NC, Lim LP, Weinstein EG, Bartel DP (2001) **An abundant class of tiny RNAs with probable regulatory roles in Caenorhabditis elegans**. Science 294: 858-862
Laurent LC, Chen J, Ulitsky I, Mueller FJ, Lu C, Shamir R, Fan JB, Loring JF (2008) **Comprehensive microRNA profiling reveals a unique human embryonic stem cell signature dominated by a single seed sequence**. Stem Cells 26: 1506-1516
Lawe DC, Chawla A, Merithew E, Dumas J, Carrington W, Fogarty K, Lifshitz L, Tuft R, Lambright D, Corvera S (2002) **Sequential roles for phosphatidylinositol 3-phosphate and Rab5 in tethering and fusion of early endosomes via their interaction with EEA1**. J Biol Chem 277: 8611-8617
le Sage C, Nagel R, Egan DA, Schrier M, Mesman E, Mangiola A, Anile C, Maira G, Mercatelli N, Ciafre SA, Farace MG, Agami R (2007) **Regulation of the p27(Kip1) tumor suppressor by miR-221 and miR-222 promotes cancer cell proliferation**. Embo J 26: 3699-3708
Lee I, Ajay SS, Yook JI, Kim HS, Hong SH, Kim NH, Dhanasekaran SM, Chinnaiyan A, Athey BD (2009) **New class of microRNA targets containing simultaneous 5'-UTR and 3'-UTR interaction sites**. Genome Res
Lee Y, Ahn C, Han J, Choi H, Kim J, Yim J, Lee J, Provost P, Radmark O, Kim S, Kim VN (2003) **The nuclear RNase III Drosha initiates microRNA processing**. Nature 425: 415-419
Lee Y, Hur I, Park SY, Kim YK, Suh MR, Kim VN (2006) **The role of PACT in the RNA silencing pathway**. Embo J 25: 522-532
Lee Y, Kim M, Han J, Yeom KH, Lee S, Baek SH, Kim VN (2004) **MicroRNA genes are transcribed by RNA polymerase II**. Embo J 23: 4051-4060
Lee RC, Ambros V (2001) **An extensive class of small RNAs in Caenorhabditis elegans**. Science 294: 862-864
Lee RC, Feinbaum RL, Ambros V (1993) **The C. elegans heterochronic gene lin-4 encodes small RNAs with antisense complementarity to lin-14**. Cell 75: 843-854
Lee SY, Yang JS, Hong W, Premont RT, Hsu VW (2005) **ARFGAP1 plays a central role in coupling COPI cargo sorting with vesicle formation**. J Cell Biol 168: 281-290
Lennox KA, Behlke MA (2010) **A direct comparison of anti-microRNA oligonucleotide potency**. Pharm Res 27: 1788-1799
Letourneur F, Gaynor EC, Hennecke S, Demolliere C, Duden R, Emr SD, Riezman H, Cosson P (1994) **Coatomer is essential for retrieval of dilysine-tagged proteins to the endoplasmic reticulum**. Cell 79: 1199-1207
Lewis BP, Burge CB, Bartel DP (2005) **Conserved seed pairing, often flanked by adenosines, indicates that thousands of human genes are microRNA targets**. Cell 120: 15-20
Li C, Hao M, Cao Z, Ding W, Graves-Deal R, Hu J, Piston DW, Coffey RJ (2007) **Naked2 acts as a cargo recognition and targeting protein to ensure proper delivery and fusion of TGF-alpha containing exocytic vesicles at the lower lateral membrane of polarized MDCK cells**. Mol Biol Cell 18: 3081-3093
Li Y, Xu X, Liang Y, Liu S, Xiao H, Li F, Cheng H, Fu Z (2010) **miR-375 enhances palmitate-induced lipoapoptosis in insulin-secreting NIT-1 cells by repressing myotrophin (V1) protein expression**. Int J Clin Exp Pathol 3: 254-264
Li M, Jones-Rhoades MW, Lau NC, Bartel DP, Rougvie AE (2005) **Regulatory mutations of mir-48, a C. elegans let-7 family MicroRNA, cause developmental timing defects**. Dev Cell 9: 415-422
Lightfoot HL, Bugaut A, Armisen J, Lehrbach NJ, Miska EA, Balasubramanian S (2011) **A LIN28-Dependent Structural Change in pre-let-7g Directly Inhibits Dicer Processing**. Biochemistry
Lim LP, Lau NC, Garrett-Engele P, Grimson A, Schelter JM, Castle J, Bartel DP, Linsley PS, Johnson JM (2005) **Microarray analysis shows that some microRNAs downregulate large numbers of target mRNAs**. Nature 433: 769-773

Lin WC, Lin FT, Nevins JR (2001) **Selective induction of E2F1 in response to DNA damage, mediated by ATM-dependent phosphorylation**. Genes Dev 15: 1833-1844
Lippincott-Schwartz J, Cole NB, Donaldson JG (1998) **Building a secretory apparatus: role of ARF1/COPI in Golgi biogenesis and maintenance**. Histochem Cell Biol 109: 449-462
Liu J, Rivas FV, Wohlschlegel J, Yates JR, 3rd, Parker R, Hannon GJ (2005) **A role for the P-body component GW182 in microRNA function**. Nat Cell Biol 7: 1261-1266
Livak KJ, Schmittgen TD (2001) **Analysis of relative gene expression data using real-time quantitative PCR and the 2(-Delta Delta C(T)) Method**. Methods 25: 402-408
Lynam-Lennon N, Maher SG, Reynolds JV (2009) **The roles of microRNA in cancer and apoptosis**. Biol Rev Camb Philos Soc 84: 55-71
Lytle JR, Yario TA, Steitz JA (2007) **Target mRNAs are repressed as efficiently by microRNA-binding sites in the 5' UTR as in the 3' UTR**. Proc Natl Acad Sci U S A 104: 9667-9672
Llave C, Xie Z, Kasschau KD, Carrington JC (2002) **Cleavage of Scarecrow-like mRNA targets directed by a class of Arabidopsis miRNA**. Science 297: 2053-2056
Lombardi D, Soldati T, Riederer MA, Goda Y, Zerial M, Pfeffer SR (1993) **Rab9 functions in transport between late endosomes and the trans Golgi network**. Embo J 12: 677-682
Lovis P, Gattesco S, Regazzi R (2008) **Regulation of the expression of components of the exocytotic machinery of insulin-secreting cells by microRNAs**. Biol Chem 389: 305-312
Lu Y, Thomson JM, Wong HY, Hammond SM, Hogan BL (2007) **Transgenic over-expression of the microRNA miR-17-92 cluster promotes proliferation and inhibits differentiation of lung epithelial progenitor cells**. Dev Biol 310: 442-453
Lu J, Getz G, Miska EA, Alvarez-Saavedra E, Lamb J, Peck D, Sweet-Cordero A, Ebert BL, Mak RH, Ferrando AA, Downing JR, Jacks T, Horvitz HR, Golub TR (2005) **MicroRNA expression profiles classify human cancers**. Nature 435: 834-838
Mallard F, Antony C, Tenza D, Salamero J, Goud B, Johannes L (1998) **Direct pathway from early/recycling endosomes to the Golgi apparatus revealed through the study of shiga toxin B-fragment transport**. J Cell Biol 143: 973-990
Mallet WG, Maxfield FR (1999) **Chimeric forms of furin and TGN38 are transported with the plasma membrane in the trans-Golgi network via distinct endosomal pathways**. J Cell Biol 146: 345-359
Maniataki E, Mourelatos Z (2005) **A human, ATP-independent, RISC assembly machine fueled by pre-miRNA**. Genes Dev 19: 2979-2990
Manolea F, Chun J, Chen DW, Clarke I, Summerfeldt N, Dacks JB, Melancon P (2010) **Arf3 is activated uniquely at the trans-Golgi network by brefeldin A-inhibited guanine nucleotide exchange factors**. Mol Biol Cell 21: 1836-1849
Maragkakis M, Reczko M, Simossis VA, Alexiou P, Papadopoulos GL, Dalamagas T, Giannopoulos G, Goumas G, Koukis E, Kourtis K, Vergoulis T, Koziris N, Sellis T, Tsanakas P, Hatzigeorgiou AG (2009) **DIANA-microT web server: elucidating microRNA functions through target prediction**. Nucleic Acids Res 37: W273-276
Markgraf DF, Ahnert F, Arlt H, Mari M, Peplowska K, Epp N, Griffith J, Reggiori F, Ungermann C (2009) **The CORVET subunit Vps8 cooperates with the Rab5 homolog Vps21 to induce clustering of late endosomal compartments**. Mol Biol Cell 20: 5276-5289
Marquez RT, Bandyopadhyay S, Wendlandt EB, Keck K, Hoffer BA, Icardi MS, Christensen RN, Schmidt WN, McCaffrey AP (2010) **Correlation between microRNA expression levels and clinical parameters associated with chronic hepatitis C viral infection in humans**. Lab Invest 90: 1727-1736
Martinez-Menarguez JA, Prekeris R, Oorschot VM, Scheller R, Slot JW, Geuze HJ, Klumperman J (2001) **Peri-Golgi vesicles contain retrograde but not anterograde proteins consistent with the cisternal progression model of intra-Golgi transport**. J Cell Biol 155: 1213-1224
Martinez NJ, Walhout AJ (2009) **The interplay between transcription factors and microRNAs in genome-scale regulatory networks**. Bioessays 31: 435-445
Matsui Y, Kikuchi A, Araki S, Hata Y, Kondo J, Teranishi Y, Takai Y (1990) **Molecular cloning and characterization of a novel type of regulatory protein (GDI) for smg p25A, a ras p21-like GTP-binding protein**. Mol Cell Biol 10: 4116-4122
Matsumoto M, Miki T, Shibasaki T, Kawaguchi M, Shinozaki H, Nio J, Saraya A, Koseki H, Miyazaki M, Iwanaga T, Seino S (2004) **Noc2 is essential in normal regulation of exocytosis in endocrine and exocrine cells**. Proc Natl Acad Sci U S A 101: 8313-8318
Matula P, Kumar A, Worz I, Erfle H, Bartenschlager R, Eils R, Rohr K (2009) **Single-cell-based image analysis of high-throughput cell array screens for quantification of viral infection**. Cytometry A 75: 309-318
Maxfield FR, McGraw TE (2004) **Endocytic recycling**. Nat Rev Mol Cell Biol 5: 121-132

McBride HM, Rybin V, Murphy C, Giner A, Teasdale R, Zerial M (1999) **Oligomeric complexes link Rab5 effectors with NSF and drive membrane fusion via interactions between EEA1 and syntaxin 13**. Cell 98: 377-386
Meister G, Landthaler M, Dorsett Y, Tuschl T (2004) **Sequence-specific inhibition of microRNA- and siRNA-induced RNA silencing**. Rna 10: 544-550
Meister G, Landthaler M, Peters L, Chen PY, Urlaub H, Luhrmann R, Tuschl T (2005) **Identification of novel argonaute-associated proteins**. Curr Biol 15: 2149-2155
Miaczynska M, Zerial M (2002) **Mosaic organization of the endocytic pathway**. Exp Cell Res 272: 8-14
Miki H, Miura K, Takenawa T (1996) **N-WASP, a novel actin-depolymerizing protein, regulates the cortical cytoskeletal rearrangement in a PIP2-dependent manner downstream of tyrosine kinases**. Embo J 15: 5326-5335
Miska EA, Alvarez-Saavedra E, Abbott AL, Lau NC, Hellman AB, McGonagle SM, Bartel DP, Ambros VR, Horvitz HR (2007) **Most Caenorhabditis elegans microRNAs are individually not essential for development or viability**. PLoS Genet 3: e215
Misteli T, Warren G (1995) **Mitotic disassembly of the Golgi apparatus in vivo**. J Cell Sci 108 (Pt 7): 2715-2727
Moyer BD, Allan BB, Balch WE (2001) **Rab1 interaction with a GM130 effector complex regulates COPII vesicle cis--Golgi tethering**. Traffic 2: 268-276
Molnar A, Schwach F, Studholme DJ, Thuenemann EC, Baulcombe DC (2007) **miRNAs control gene expression in the single-cell alga Chlamydomonas reinhardtii**. Nature 447: 1126-1129
Mortensen RD, Serra M, Steitz JA, Vasudevan S (2011) **Posttranscriptional activation of gene expression in Xenopus laevis oocytes by microRNA-protein complexes (microRNPs)**. Proc Natl Acad Sci U S A 108: 8281-8286
Mu P, Han YC, Betel D, Yao E, Squatrito M, Ogrodowski P, de Stanchina E, D'Andrea A, Sander C, Ventura A (2009) **Genetic dissection of the miR-17~92 cluster of microRNAs in Myc-induced B-cell lymphomas**. Genes Dev 23: 2806-2811
Nagel R, Clijsters L, Agami R (2009) **The miRNA-192/194 cluster regulates the Period gene family and the circadian clock**. Febs J 276: 5447-5455
Nakamura N, Hirata A, Ohsumi Y, Wada Y (1997a) **Vam2/Vps41p and Vam6/Vps39p are components of a protein complex on the vacuolar membranes and involved in the vacuolar assembly in the yeast Saccharomyces cerevisiae**. J Biol Chem 272: 11344-11349
Nakamura N, Lowe M, Levine TP, Rabouille C, Warren G (1997b) **The vesicle docking protein p115 binds GM130, a cis-Golgi matrix protein, in a mitotically regulated manner**. Cell 89: 445-455
Nakano A, Brada D, Schekman R (1988) **A membrane glycoprotein, Sec12p, required for protein transport from the endoplasmic reticulum to the Golgi apparatus in yeast**. J Cell Biol 107: 851-863
Nakano A, Muramatsu M (1989) **A novel GTP-binding protein, Sar1p, is involved in transport from the endoplasmic reticulum to the Golgi apparatus**. J Cell Biol 109: 2677-2691
Nelson DS, Alvarez C, Gao YS, Garcia-Mata R, Fialkowski E, Sztul E (1998) **The membrane transport factor TAP/p115 cycles between the Golgi and earlier secretory compartments and contains distinct domains required for its localization and function**. J Cell Biol 143: 319-331
Neumann B, Held M, Liebel U, Erfle H, Rogers P, Pepperkok R, Ellenberg J (2006) **High-throughput RNAi screening by time-lapse imaging of live human cells**. Nat Methods 3: 385-390
Nielsen E, Severin F, Backer JM, Hyman AA, Zerial M (1999) **Rab5 regulates motility of early endosomes on microtubules**. Nat Cell Biol 1: 376-382
Nimmo RA, Slack FJ (2009) **An elegant miRror: microRNAs in stem cells, developmental timing and cancer**. Chromosoma 118: 405-418
Nottrott S, Simard MJ, Richter JD (2006) **Human let-7a miRNA blocks protein production on actively translating polyribosomes**. Nat Struct Mol Biol 13: 1108-1114
Nozawa K, Casiano CA, Hamel JC, Molinaro C, Fritzler MJ, Chan EK (2002) **Fragmentation of Golgi complex and Golgi autoantigens during apoptosis and necrosis**. Arthritis Res 4: R3
O'Donnell KA, Wentzel EA, Zeller KI, Dang CV, Mendell JT (2005) **c-Myc-regulated microRNAs modulate E2F1 expression**. Nature 435: 839-843
Obernosterer G, Leuschner PJ, Alenius M, Martinez J (2006) **Post-transcriptional regulation of microRNA expression**. Rna 12: 1161-1167
Ohno H (2006) **Clathrin-associated adaptor protein complexes**. J Cell Sci 119: 3719-3721
Oka T, Ungar D, Hughson FM, Krieger M (2004) **The COG and COPI complexes interact to control the abundance of GEARs, a subset of Golgi integral membrane proteins**. Mol Biol Cell 15: 2423-2435
Okamura K, Hagen JW, Duan H, Tyler DM, Lai EC (2007) **The mirtron pathway generates microRNA-class regulatory RNAs in Drosophila**. Cell 130: 89-100

Olive V, Bennett MJ, Walker JC, Ma C, Jiang I, Cordon-Cardo C, Li QJ, Lowe SW, Hannon GJ, He L (2009) **miR-19 is a key oncogenic component of mir-17-92**. Genes Dev 23: 2839-2849
Olive V, Jiang I, He L (2010) **mir-17-92, a cluster of miRNAs in the midst of the cancer network**. Int J Biochem Cell Biol
Olsen PH, Ambros V (1999) **The lin-4 regulatory RNA controls developmental timing in Caenorhabditis elegans by blocking LIN-14 protein synthesis after the initiation of translation**. Dev Biol 216: 671-680
Ooi CE, Dell'Angelica EC, Bonifacino JS (1998) **ADP-Ribosylation factor 1 (ARF1) regulates recruitment of the AP-3 adaptor complex to membranes**. J Cell Biol 142: 391-402
Orci L, Stamnes M, Ravazzola M, Amherdt M, Perrelet A, Sollner TH, Rothman JE (1997) **Bidirectional transport by distinct populations of COPI-coated vesicles**. Cell 90: 335-349
Orcl L, Palmer DJ, Amherdt M, Rothman JE (1993) **Coated vesicle assembly in the Golgi requires only coatomer and ARF proteins from the cytosol**. Nature 364: 732-734
Orom UA, Kauppinen S, Lund AH (2006) **LNA-modified oligonucleotides mediate specific inhibition of microRNA function**. Gene 372: 137-141
Orom UA, Nielsen FC, Lund AH (2008) **MicroRNA-10a binds the 5'UTR of ribosomal protein mRNAs and enhances their translation**. Mol Cell 30: 460-471
Ota A, Tagawa H, Karnan S, Tsuzuki S, Karpas A, Kira S, Yoshida Y, Seto M (2004) **Identification and characterization of a novel gene, C13orf25, as a target for 13q31-q32 amplification in malignant lymphoma**. Cancer Res 64: 3087-3095
Ovcharenko D, Kelnar K, Johnson C, Leng N, Brown D (2007) **Genome-scale microRNA and small interfering RNA screens identify small RNA modulators of TRAIL-induced apoptosis pathway**. Cancer Res 67: 10782-10788
Paleotti O, Macia E, Luton F, Klein S, Partisani M, Chardin P, Kirchhausen T, Franco M (2005) **The small G-protein Arf6GTP recruits the AP-2 adaptor complex to membranes**. J Biol Chem 280: 21661-21666
Park JE, Heo I, Tian Y, Simanshu DK, Chang H, Jee D, Patel DJ, Kim VN (2011) **Dicer recognizes the 5' end of RNA for efficient and accurate processing**. Nature 475: 201-205
Park SY, Lee JH, Ha M, Nam JW, Kim VN (2009) **miR-29 miRNAs activate p53 by targeting p85 alpha and CDC42**. Nat Struct Mol Biol 16: 23-29
Parker R, Song H (2004) **The enzymes and control of eukaryotic mRNA turnover**. Nat Struct Mol Biol 11: 121-127
Parlati F, Varlamov O, Paz K, McNew JA, Hurtado D, Sollner TH, Rothman JE (2002) **Distinct SNARE complexes mediating membrane fusion in Golgi transport based on combinatorial specificity**. Proc Natl Acad Sci U S A 99: 5424-5429
Pasquinelli AE, Reinhart BJ, Slack F, Martindale MQ, Kuroda MI, Maller B, Hayward DC, Ball EE, Degnan B, Muller P, Spring J, Srinivasan A, Fishman M, Finnerty J, Corbo J, Levine M, Leahy P, Davidson E, Ruvkun G (2000) **Conservation of the sequence and temporal expression of let-7 heterochronic regulatory RNA**. Nature 408: 86-89
Pavelka M, Ellinger A, Debbage P, Loewe C, Vetterlein M, Roth J (1998) **Endocytic routes to the Golgi apparatus**. Histochem Cell Biol 109: 555-570
Pavelka M, Neumuller J, Ellinger A (2008) **Retrograde traffic in the biosynthetic-secretory route**. Histochem Cell Biol 129: 277-288
Peng R, Gallwitz D (2002) **Sly1 protein bound to Golgi syntaxin Sed5p allows assembly and contributes to specificity of SNARE fusion complexes**. J Cell Biol 157: 645-655
Pepperkok R, Ellenberg J (2006) **High-throughput fluorescence microscopy for systems biology**. Nat Rev Mol Cell Biol 7: 690-696
Pereira-Leal JB, Seabra MC (2001) **Evolution of the Rab family of small GTP-binding proteins**. J Mol Biol 313: 889-901
Petersen CP, Bordeleau ME, Pelletier J, Sharp PA (2006) **Short RNAs repress translation after initiation in mammalian cells**. Mol Cell 21: 533-542
Pfeffer S (2005) **A model for Rab GTPase localization**. Biochem Soc Trans 33: 627-630
Piao X, Zhang X, Wu L, Belasco JG (2010) **CCR4-NOT deadenylates mRNA associated with RNA-induced silencing complexes in human cells**. Mol Cell Biol 30: 1486-1494
Pillai RS, Artus CG, Filipowicz W (2004) **Tethering of human Ago proteins to mRNA mimics the miRNA-mediated repression of protein synthesis**. Rna 10: 1518-1525
Pillai RS, Bhattacharyya SN, Artus CG, Zoller T, Cougot N, Basyuk E, Bertrand E, Filipowicz W (2005) **Inhibition of translational initiation by Let-7 MicroRNA in human cells**. Science 309: 1573-1576
Plaisance V, Abderrahmani A, Perret-Menoud V, Jacquemin P, Lemaigre F, Regazzi R (2006) **MicroRNA-9 controls the expression of Granuphilin/Slp4 and the secretory response of insulin-producing cells**. J Biol Chem 281: 26932-26942

Poy MN, Eliasson L, Krutzfeldt J, Kuwajima S, Ma X, Macdonald PE, Pfeffer S, Tuschl T, Rajewsky N, Rorsman P, Stoffel M (2004) **A pancreatic islet-specific microRNA regulates insulin secretion**. Nature 432: 226-230
Poteryaev D, Datta S, Ackema K, Zerial M, Spang A (2010) **Identification of the switch in early-to-late endosome transition**. Cell 141: 497-508
Puthenveedu MA, Linstedt AD (2004) **Gene replacement reveals that p115/SNARE interactions are essential for Golgi biogenesis**. Proc Natl Acad Sci U S A 101: 1253-1256
Rabouille C, Hui N, Hunte F, Kieckbusch R, Berger EG, Warren G, Nilsson T (1995) **Mapping the distribution of Golgi enzymes involved in the construction of complex oligosaccharides**. J Cell Sci 108 (Pt 4): 1617-1627
Radhakrishna H, Klausner RD, Donaldson JG (1996) **Aluminum fluoride stimulates surface protrusions in cells overexpressing the ARF6 GTPase**. J Cell Biol 134: 935-947
Randazzo PA, Hirsch DS (2004) **Arf GAPs: multifunctional proteins that regulate membrane traffic and actin remodelling**. Cell Signal 16: 401-413
Raver-Shapira N, Marciano E, Meiri E, Spector Y, Rosenfeld N, Moskovits N, Bentwich Z, Oren M (2007) **Transcriptional activation of miR-34a contributes to p53-mediated apoptosis**. Mol Cell 26: 731-743
Reinhart BJ, Slack FJ, Basson M, Pasquinelli AE, Bettinger JC, Rougvie AE, Horvitz HR, Ruvkun G (2000) **The 21-nucleotide let-7 RNA regulates developmental timing in Caenorhabditis elegans**. Nature 403: 901-906
Ren J, Jin P, Wang E, Marincola FM, Stroncek DF (2009) **MicroRNA and gene expression patterns in the differentiation of human embryonic stem cells**. J Transl Med 7: 20
Rhoades MW, Reinhart BJ, Lim LP, Burge CB, Bartel B, Bartel DP (2002) **Prediction of plant microRNA targets**. Cell 110: 513-520
Rieber N, Knapp B, Eils R, Kaderali L (2009) **RNAither, an automated pipeline for the statistical analysis of high-throughput RNAi screens**. Bioinformatics 25: 678-679
Rink J, Ghigo E, Kalaidzidis Y, Zerial M (2005) **Rab conversion as a mechanism of progression from early to late endosomes**. Cell 122: 735-749
Rybak A, Fuchs H, Smirnova L, Brandt C, Pohl EE, Nitsch R, Wulczyn FG (2008) **A feedback loop comprising lin-28 and let-7 controls pre-let-7 maturation during neural stem-cell commitment**. Nat Cell Biol 10: 987-993
Robinson MS (2004) **Adaptable adaptors for coated vesicles**. Trends Cell Biol 14: 167-174
Rodriguez-Boulan E, Musch A (2005) **Protein sorting in the Golgi complex: shifting paradigms**. Biochim Biophys Acta 1744: 455-464
Rothman JE (1994) **Mechanisms of intracellular protein transport**. Nature 372: 55-63
Rougvie AE, Ambros V (1995) **The heterochronic gene lin-29 encodes a zinc finger protein that controls a terminal differentiation event in Caenorhabditis elegans**. Development 121: 2491-2500
Ruby JG, Jan CH, Bartel DP (2007) **Intronic microRNA precursors that bypass Drosha processing**. Nature 448: 83-86
Sacher R, Stergiou L, Pelkmans L (2008) **Lessons from genetics: interpreting complex phenotypes in RNAi screens**. Curr Opin Cell Biol 20: 483-489
Saini HK, Griffiths-Jones S, Enright AJ (2007) **Genomic analysis of human microRNA transcripts**. Proc Natl Acad Sci U S A 104: 17719-17724
Salzman DW, Shubert-Coleman J, Furneaux H (2007) **P68 RNA helicase unwinds the human let-7 microRNA precursor duplex and is required for let-7-directed silencing of gene expression**. J Biol Chem 282: 32773-32779
Scales SJ, Pepperkok R, Kreis TE (1997) **Visualization of ER-to-Golgi transport in living cells reveals a sequential mode of action for COPII and COPI**. Cell 90: 1137-1148
Schaar DG, Medina DJ, Moore DF, Strair RK, Ting Y (2009) **miR-320 targets transferrin receptor 1 (CD71) and inhibits cell proliferation**. Exp Hematol 37: 245-255
Schanen BC, Li X (2011) **Transcriptional regulation of mammalian miRNA genes**. Genomics 97: 1-6
Schlossman DM, Schmid SL, Braell WA, Rothman JE (1984) **An enzyme that removes clathrin coats: purification of an uncoating ATPase**. J Cell Biol 99: 723-733
Schneider WJ (1989) **The low density lipoprotein receptor**. Biochim Biophys Acta 988: 303-317
Schrag JD, Procopio DO, Cygler M, Thomas DY, Bergeron JJ (2003) **Lectin control of protein folding and sorting in the secretory pathway**. Trends Biochem Sci 28: 49-57
Schratt GM, Tuebing F, Nigh EA, Kane CG, Sabatini ME, Kiebler M, Greenberg ME (2006) **A brain-specific microRNA regulates dendritic spine development**. Nature 439: 283-289
Schroeder A, Mueller O, Stocker S, Salowsky R, Leiber M, Gassmann M, Lightfoot S, Menzel W, Granzow M, Ragg T (2006) **The RIN: an RNA integrity number for assigning integrity values to RNA measurements**. BMC Mol Biol 7: 3

Schwab R, Palatnik JF, Riester M, Schommer C, Schmid M, Weigel D (2005) **Specific effects of microRNAs on the plant transcriptome**. Dev Cell 8: 517-527

Scott BL, Van Komen JS, Irshad H, Liu S, Wilson KA, McNew JA (2004) **Sec1p directly stimulates SNARE-mediated membrane fusion in vitro**. J Cell Biol 167: 75-85

Seggerson K, Tang L, Moss EG (2002) **Two genetic circuits repress the Caenorhabditis elegans heterochronic gene lin-28 after translation initiation**. Dev Biol 243: 215-225

Selbach M, Schwanhausser B, Thierfelder N, Fang Z, Khanin R, Rajewsky N (2008) **Widespread changes in protein synthesis induced by microRNAs**. Nature 455: 58-63

Semerdjieva S, Shortt B, Maxwell E, Singh S, Fonarev P, Hansen J, Schiavo G, Grant BD, Smythe E (2008) **Coordinated regulation of AP2 uncoating from clathrin-coated vesicles by rab5 and hRME-6**. J Cell Biol 183: 499-511

Serva A, Claas C, Starkuviene V (2011) **A Potential of microRNAs for High-Content Screening**. J Nucleic Acids 2011: 870903

Sethupathy P, Megraw M, Hatzigeorgiou AG (2006) **A guide through present computational approaches for the identification of mammalian microRNA targets**. Nat Methods 3: 881-886

Shalgi R, Lieber D, Oren M, Pilpel Y (2007) **Global and local architecture of the mammalian microRNA-transcription factor regulatory network**. PLoS Comput Biol 3: e131

Shen J, Tareste DC, Paumet F, Rothman JE, Melia TJ (2007) **Selective activation of cognate SNAREpins by Sec1/Munc18 proteins**. Cell 128: 183-195

Shen X, Xu KF, Fan Q, Pacheco-Rodriguez G, Moss J, Vaughan M (2006) **Association of brefeldin A-inhibited guanine nucleotide-exchange protein 2 (BIG2) with recycling endosomes during transferrin uptake**. Proc Natl Acad Sci U S A 103: 2635-2640

Shiba T, Kawasaki M, Takatsu H, Nogi T, Matsugaki N, Igarashi N, Suzuki M, Kato R, Nakayama K, Wakatsuki S (2003) **Molecular mechanism of membrane recruitment of GGA by ARF in lysosomal protein transport**. Nat Struct Biol 10: 386-393

Shin HW, Hayashi M, Christoforidis S, Lacas-Gervais S, Hoepfner S, Wenk MR, Modregger J, Uttenweiler-Joseph S, Wilm M, Nystuen A, Frankel WN, Solimena M, De Camilli P, Zerial M (2005) **An enzymatic cascade of Rab5 effectors regulates phosphoinositide turnover in the endocytic pathway**. J Cell Biol 170: 607-618

Shorter J, Beard MB, Seemann J, Dirac-Svejstrup AB, Warren G (2002) **Sequential tethering of Golgins and catalysis of SNAREpin assembly by the vesicle-tethering protein p115**. J Cell Biol 157: 45-62

Siegel G, Obernosterer G, Fiore R, Oehmen M, Bicker S, Christensen M, Khudayberdiev S, Leuschner PF, Busch CJ, Kane C, Hubel K, Dekker F, Hedberg C, Rengarajan B, Drepper C, Waldmann H, Kauppinen S, Greenberg ME, Draguhn A, Rehmsmeier M, et al (2009) **A functional screen implicates microRNA-138-dependent regulation of the depalmitoylation enzyme APT1 in dendritic spine morphogenesis**. Nat Cell Biol 11: 705-716

Simonsen A, Lippe R, Christoforidis S, Gaullier JM, Brech A, Callaghan J, Toh BH, Murphy C, Zerial M, Stenmark H (1998) **EEA1 links PI(3)K function to Rab5 regulation of endosome fusion**. Nature 394: 494-498

Siniossoglou S, Pelham HR (2001) **An effector of Ypt6p binds the SNARE Tlg1p and mediates selective fusion of vesicles with late Golgi membranes**. Embo J 20: 5991-5998

Siomi H, Siomi MC (2010) **Posttranscriptional regulation of microRNA biogenesis in animals**. Mol Cell 38: 323-332

Sirotkin AV, Laukova M, Ovcharenko D, Brenaut P, Mlyncek M (2010) **Identification of microRNAs controlling human ovarian cell proliferation and apoptosis**. J Cell Physiol 223: 49-56

Sirotkin AV, Ovcharenko D, Grossmann R, Laukova M, Mlyncek M (2009) **Identification of microRNAs controlling human ovarian cell steroidogenesis via a genome-scale screen**. J Cell Physiol 219: 415-420

Sitia R, Braakman I (2003) **Quality control in the endoplasmic reticulum protein factory**. Nature 426: 891-894

Sivars U, Aivazian D, Pfeffer SR (2003) **Yip3 catalyses the dissociation of endosomal Rab-GDI complexes**. Nature 425: 856-859

Sylvestre Y, De Guire V, Querido E, Mukhopadhyay UK, Bourdeau V, Major F, Ferbeyre G, Chartrand P (2007) **An E2F/miR-20a autoregulatory feedback loop**. J Biol Chem 282: 2135-2143

Soille P (2004) **Morphological Image Analysis: Principles and Applications**. 2nd ed. Berlin, Germany: Springer

Soldati T, Shapiro AD, Svejstrup AB, Pfeffer SR (1994) **Membrane targeting of the small GTPase Rab9 is accompanied by nucleotide exchange**. Nature 369: 76-78

Sood P, Krek A, Zavolan M, Macino G, Rajewsky N (2006) **Cell-type-specific signatures of microRNAs on target mRNA expression**. Proc Natl Acad Sci U S A 103: 2746-2751

Souret FF, Kastenmayer JP, Green PJ (2004) **AtXRN4 degrades mRNA in Arabidopsis and its substrates include selected miRNA targets**. Mol Cell 15: 173-183

Stagg SM, Gurkan C, Fowler DM, LaPointe P, Foss TR, Potter CS, Carragher B, Balch WE (2006) **Structure of the Sec13/31 COPII coat cage**. Nature 439: 234-238
Stamnes MA, Rothman JE (1993) **The binding of AP-1 clathrin adaptor particles to Golgi membranes requires ADP-ribosylation factor, a small GTP-binding protein**. Cell 73: 999-1005
Starkuviene V, Liebel U, Simpson JC, Erfle H, Poustka A, Wiemann S, Pepperkok R (2004) **High-content screening microscopy identifies novel proteins with a putative role in secretory membrane traffic**. Genome Res 14: 1948-1956
Starkuviene V, Pepperkok R (2007) **The potential of high-content high-throughput microscopy in drug discovery**. Br J Pharmacol 152: 62-71
Stein M, Zijderhand-Bleekemolen JE, Geuze H, Hasilik A, von Figura K (1987) **Mr 46,000 mannose 6-phosphate specific receptor: its role in targeting of lysosomal enzymes**. Embo J 6: 2677-2681
Stenmark H (2009) **Rab GTPases as coordinators of vesicle traffic**. Nat Rev Mol Cell Biol 10: 513-525
Stenmark H, Aasland R, Toh BH, D'Arrigo A (1996) **Endosomal localization of the autoantigen EEA1 is mediated by a zinc-binding FYVE finger**. J Biol Chem 271: 24048-24054
Stenmark H, Parton RG, Steele-Mortimer O, Lutcke A, Gruenberg J, Zerial M (1994) **Inhibition of rab5 GTPase activity stimulates membrane fusion in endocytosis**. Embo J 13: 1287-1296
Stephens DJ (2003) **De novo formation, fusion and fission of mammalian COPII-coated endoplasmic reticulum exit sites**. EMBO Rep 4: 210-217
Stimpson HE, Toret CP, Cheng AT, Pauly BS, Drubin DG (2009) **Early-arriving Syp1p and Ede1p function in endocytic site placement and formation in budding yeast**. Mol Biol Cell 20: 4640-4651
Strom M, Vollmer P, Tan TJ, Gallwitz D (1993) **A yeast GTPase-activating protein that interacts specifically with a member of the Ypt/Rab family**. Nature 361: 736-739
Subramanian S, Woolford CA, Jones EW (2004) **The Sec1/Munc18 protein, Vps33p, functions at the endosome and the vacuole of Saccharomyces cerevisiae**. Mol Biol Cell 15: 2593-2605
Suzuki HI, Miyazono K (2010) **Emerging complexity of microRNA generation cascades**. J Biochem 149: 15-25
Sweitzer SM, Hinshaw JE (1998) **Dynamin undergoes a GTP-dependent conformational change causing vesiculation**. Cell 93: 1021-1029
Szittya G, Silhavy D, Molnar A, Havelda Z, Lovas A, Lakatos L, Banfalvi Z, Burgyan J (2003) **Low temperature inhibits RNA silencing-mediated defence by the control of siRNA generation**. Embo J 22: 633-640
Tagawa H, Karube K, Tsuzuki S, Ohshima K, Seto M (2007) **Synergistic action of the microRNA-17 polycistron and Myc in aggressive cancer development**. Cancer Sci 98: 1482-1490
Tamaki H, Yamashina S (2002) **Structural integrity of the Golgi stack is essential for normal secretory functions of rat parotid acinar cells: effects of brefeldin A and okadaic acid**. J Histochem Cytochem 50: 1611-1623
Tan LP, Seinen E, Duns G, de Jong D, Sibon OC, Poppema S, Kroesen BJ, Kok K, van den Berg A (2009) **A high throughput experimental approach to identify miRNA targets in human cells**. Nucleic Acids Res 37: e137
Tang BL, Ong YS, Huang B, Wei S, Wong ET, Qi R, Horstmann H, Hong W (2001) **A membrane protein enriched in endoplasmic reticulum exit sites interacts with COPII**. J Biol Chem 276: 40008-40017
Tanzer A, Stadler PF (2004) **Molecular evolution of a microRNA cluster**. J Mol Biol 339: 327-335
Taoka M, Ichimura T, Wakamiya-Tsuruta A, Kubota Y, Araki T, Obinata T, Isobe T (2003) **V-1, a protein expressed transiently during murine cerebellar development, regulates actin polymerization via interaction with capping protein**. J Biol Chem 278: 5864-5870
Tarasov V, Jung P, Verdoodt B, Lodygin D, Epanchintsev A, Menssen A, Meister G, Hermeking H (2007) **Differential regulation of microRNAs by p53 revealed by massively parallel sequencing: miR-34a is a p53 target that induces apoptosis and G1-arrest**. Cell Cycle 6: 1586-1593
Tennessen JM, Thummel CS (2008) **Developmental timing: let-7 function conserved through evolution**. Curr Biol 18: R707-708
Thermann R, Hentze MW (2007) **Drosophila miR2 induces pseudo-polysomes and inhibits translation initiation**. Nature 447: 875-878
Tian S, Huang S, Wu S, Guo W, Li J, He X (2010) **MicroRNA-1285 inhibits the expression of p53 by directly targeting its 3' untranslated region**. Biochem Biophys Res Commun 396: 435-439
Toffanin S, Hoshida Y, Lachenmayer A, Villanueva A, Cabellos L, Minguez B, Savic R, Ward SC, Thung S, Chiang DY, Alsinet C, Tovar V, Roayaie S, Schwartz M, Bruix J, Waxman S, Friedman SL, Golub T, Mazzaferro V, Llovet JM (2011) **MicroRNA-Based Classification of Hepatocellular Carcinoma and Oncogenic Role of miR-517a**. Gastroenterology 140: 1618-1628 e1616
Tran DH, Satou K, Ho TB, Pham TH (2010) **Computational discovery of miR-TF regulatory modules in human genome**. Bioinformation 4: 371-377

Traub LM (2005) **Common principles in clathrin-mediated sorting at the Golgi and the plasma membrane**. Biochim Biophys Acta 1744: 415-437
Triboulet R, Mari B, Lin YL, Chable-Bessia C, Bennasser Y, Lebrigand K, Cardinaud B, Maurin T, Barbry P, Baillat V, Reynes J, Corbeau P, Jeang KT, Benkirane M (2007) **Suppression of microRNA-silencing pathway by HIV-1 during virus replication**. Science 315: 1579-1582
Truettner JS, Alonso OF, Bramlett HM, Dietrich WD (2011) **Therapeutic hypothermia alters microRNA responses to traumatic brain injury in rats**. J Cereb Blood Flow Metab 31: 1897-1907
Tsuchida A, Ohno S, Wu W, Borjigin N, Fujita K, Aoki T, Ueda S, Takanashi M, Kuroda M (2011) **miR-92 is a key oncogenic component of the miR-17-92 cluster in colon cancer**. Cancer Sci
Tu K, Yu H, Hua YJ, Li YY, Liu L, Xie L, Li YX (2009) **Combinatorial network of primary and secondary microRNA-driven regulatory mechanisms**. Nucleic Acids Res
Uhlmann S, Zhang JD, Schwager A, Mannsperger H, Riazalhosseini Y, Burmester S, Ward A, Korf U, Wiemann S, Sahin O (2010) **miR-200bc/429 cluster targets PLCgamma1 and differentially regulates proliferation and EGF-driven invasion than miR-200a/141 in breast cancer**. Oncogene 29: 4297-4306
Ullrich O, Horiuchi H, Bucci C, Zerial M (1994) **Membrane association of Rab5 mediated by GDP-dissociation inhibitor and accompanied by GDP/GTP exchange**. Nature 368: 157-160
Ungar D, Oka T, Brittle EE, Vasile E, Lupashin VV, Chatterton JE, Heuser JE, Krieger M, Waters MG (2002) **Characterization of a mammalian Golgi-localized protein complex, COG, that is required for normal Golgi morphology and function**. J Cell Biol 157: 405-415
Ungar D, Oka T, Vasile E, Krieger M, Hughson FM (2005) **Subunit architecture of the conserved oligomeric Golgi complex**. J Biol Chem 280: 32729-32735
Ungewickell E, Ungewickell H, Holstein SE, Lindner R, Prasad K, Barouch W, Martin B, Greene LE, Eisenberg E (1995) **Role of auxilin in uncoating clathrin-coated vesicles**. Nature 378: 632-635
van Dongen S, Abreu-Goodger C, Enright AJ (2008) **Detecting microRNA binding and siRNA off-target effects from expression data**. Nat Methods 5: 1023-1025
van Rooij E, Sutherland LB, Qi X, Richardson JA, Hill J, Olson EN (2007) **Control of stress-dependent cardiac growth and gene expression by a microRNA**. Science 316: 575-579
Vasudevan S, Tong Y, Steitz JA (2007) **Switching from repression to activation: microRNAs can up-regulate translation**. Science 318: 1931-1934
Vasudevan S, Tong Y, Steitz JA (2008) **Cell-cycle control of microRNA-mediated translation regulation**. Cell Cycle 7: 1545-1549
Vella MC, Choi EY, Lin SY, Reinert K, Slack FJ (2004) **The C. elegans microRNA let-7 binds to imperfect let-7 complementary sites from the lin-41 3'UTR**. Genes Dev 18: 132-137
Ventura A, Young AG, Winslow MM, Lintault L, Meissner A, Erkeland SJ, Newman J, Bronson RT, Crowley D, Stone JR, Jaenisch R, Sharp PA, Jacks T (2008) **Targeted deletion reveals essential and overlapping functions of the miR-17 through 92 family of miRNA clusters**. Cell 132: 875-886
Volinia S, Calin GA, Liu CG, Ambs S, Cimmino A, Petrocca F, Visone R, Iorio M, Roldo C, Ferracin M, Prueitt RL, Yanaihara N, Lanza G, Scarpa A, Vecchione A, Negrini M, Harris CC, Croce CM (2006) **A microRNA expression signature of human solid tumors defines cancer gene targets**. Proc Natl Acad Sci U S A 103: 2257-2261
Volpicelli-Daley LA, Li Y, Zhang CJ, Kahn RA (2005) **Isoform-selective effects of the depletion of ADP-ribosylation factors 1-5 on membrane traffic**. Mol Biol Cell 16: 4495-4508
Voorhoeve PM, le Sage C, Schrier M, Gillis AJ, Stoop H, Nagel R, Liu YP, van Duijse J, Drost J, Griekspoor A, Zlotorynski E, Yabuta N, De Vita G, Nojima H, Looijenga LH, Agami R (2006) **A genetic screen implicates miRNA-372 and miRNA-373 as oncogenes in testicular germ cell tumors**. Cell 124: 1169-1181
Wakiyama M, Takimoto K, Ohara O, Yokoyama S (2007) **Let-7 microRNA-mediated mRNA deadenylation and translational repression in a mammalian cell-free system**. Genes Dev 21: 1857-1862
Wang B, Love TM, Call ME, Doench JG, Novina CD (2006) **Recapitulation of short RNA-directed translational gene silencing in vitro**. Mol Cell 22: 553-560
Wang FZ, Weber F, Croce C, Liu CG, Liao X, Pellett PE (2008) **Human cytomegalovirus infection alters the expression of cellular microRNA species that affect its replication**. J Virol 82: 9065-9074
Warren G (1993) **Membrane partitioning during cell division**. Annu Rev Biochem 62: 323-348
Wasmeier C, Romao M, Plowright L, Bennett DC, Raposo G, Seabra MC (2006) **Rab38 and Rab32 control post-Golgi trafficking of melanogenic enzymes**. J Cell Biol 175: 271-281
Weber T, Zemelman BV, McNew JA, Westermann B, Gmachl M, Parlati F, Sollner TH, Rothman JE (1998) **SNAREpins: minimal machinery for membrane fusion**. Cell 92: 759-772

Wegner CS, Malerod L, Pedersen NM, Progida C, Bakke O, Stenmark H, Brech A (2010) **Ultrastructural characterization of giant endosomes induced by GTPase-deficient Rab5**. Histochem Cell Biol 133: 41-55

Weide T, Bayer M, Koster M, Siebrasse JP, Peters R, Barnekow A (2001) **The Golgi matrix protein GM130: a specific interacting partner of the small GTPase rab1b**. EMBO Rep 2: 336-341

Weinmann L, Hock J, Ivacevic T, Ohrt T, Mutze J, Schwille P, Kremmer E, Benes V, Urlaub H, Meister G (2009) **Importin 8 is a gene silencing factor that targets argonaute proteins to distinct mRNAs**. Cell 136: 496-507

Wenk MR, De Camilli P (2004) **Protein-lipid interactions and phosphoinositide metabolism in membrane traffic: insights from vesicle recycling in nerve terminals**. Proc Natl Acad Sci U S A 101: 8262-8269

Whittaker R, Loy PA, Sisman E, Suyama E, Aza-Blanc P, Ingermanson RS, Price JH, McDonough PM (2010) **Identification of MicroRNAs that control lipid droplet formation and growth in hepatocytes via high-content screening**. J Biomol Screen 15: 798-805

Wiederkehr A, De Craene JO, Ferro-Novick S, Novick P (2004) **Functional specialization within a vesicle tethering complex: bypass of a subset of exocyst deletion mutants by Sec1p or Sec4p**. J Cell Biol 167: 875-887

Wightman B, Ha I, Ruvkun G (1993) **Posttranscriptional regulation of the heterochronic gene lin-14 by lin-4 mediates temporal pattern formation in C. elegans**. Cell 75: 855-862

Woods K, Thomson JM, Hammond SM (2007) **Direct regulation of an oncogenic micro-RNA cluster by E2F transcription factors**. J Biol Chem 282: 2130-2134

Wu S, Huang S, Ding J, Zhao Y, Liang L, Liu T, Zhan R, He X (2010) **Multiple microRNAs modulate p21Cip1/Waf1 expression by directly targeting its 3' untranslated region**. Oncogene 29: 2302-2308

Wu W, Sun M, Zou GM, Chen J (2007) **MicroRNA and cancer: Current status and prospective**. Int J Cancer 120: 953-960

Xiang J, Wu J (2010) **Feud or Friend? The Role of the miR-17-92 Cluster in Tumorigenesis**. Curr Genomics 11: 129-135

Xiao C, Rajewsky K (2009) **MicroRNA control in the immune system: basic principles**. Cell 136: 26-36

Xiao C, Srinivasan L, Calado DP, Patterson HC, Zhang B, Wang J, Henderson JM, Kutok JL, Rajewsky K (2008) **Lymphoproliferative disease and autoimmunity in mice with increased miR-17-92 expression in lymphocytes**. Nat Immunol 9: 405-414

Xu Y, Li F, Zhang B, Zhang K, Zhang F, Huang X, Sun N, Ren Y, Sui M, Liu P (2010) **MicroRNAs and target site screening reveals a pre-microRNA-30e variant associated with schizophrenia**. Schizophr Res 119: 219-227

Xu S, Witmer PD, Lumayag S, Kovacs B, Valle D (2007) **MicroRNA (miRNA) transcriptome of mouse retina and identification of a sensory organ-specific miRNA cluster**. J Biol Chem 282: 25053-25066

Yamada N, Shames DM, Stoudemire JB, Havel RJ (1986) **Metabolism of lipoproteins containing apolipoprotein B-100 in blood plasma of rabbits: heterogeneity related to the presence of apolipoprotein E**. Proc Natl Acad Sci U S A 83: 3479-3483

Yamakuni T, Yamamoto T, Ishida Y, Yamamoto H, Song SY, Adachi E, Hiwatashi Y, Ohizumi Y (2002) **V-1, a catecholamine biosynthesis regulatory protein, positively controls catecholamine secretion in PC12D cells**. FEBS Lett 530: 94-98

Yang JS, Lee SY, Gao M, Bourgoin S, Randazzo PA, Premont RT, Hsu VW (2002) **ARFGAP1 promotes the formation of COPI vesicles, suggesting function as a component of the coat**. J Cell Biol 159: 69-78

Yang JS, Phillips MD, Betel D, Mu P, Ventura A, Siepel AC, Chen KC, Lai EC (2011) **Widespread regulatory activity of vertebrate microRNA* species**. Rna 17: 312-326

Yang W, Chendrimada TP, Wang Q, Higuchi M, Seeburg PH, Shiekhattar R, Nishikura K (2006) **Modulation of microRNA processing and expression through RNA editing by ADAR deaminases**. Nat Struct Mol Biol 13: 13-21

Yekta S, Shih IH, Bartel DP (2004) **MicroRNA-directed cleavage of HOXB8 mRNA**. Science 304: 594-596

Yi R, Qin Y, Macara IG, Cullen BR (2003) **Exportin-5 mediates the nuclear export of pre-microRNAs and short hairpin RNAs**. Genes Dev 17: 3011-3016

Yi Z, Yokota H, Torii S, Aoki T, Hosaka M, Zhao S, Takata K, Takeuchi T, Izumi T (2002) **The Rab27a/granuphilin complex regulates the exocytosis of insulin-containing dense-core granules**. Mol Cell Biol 22: 1858-1867

Yu Z, Wang C, Wang M, Li Z, Casimiro MC, Liu M, Wu K, Whittle J, Ju X, Hyslop T, McCue P, Pestell RG (2008) **A cyclin D1/microRNA 17/20 regulatory feedback loop in control of breast cancer cell proliferation**. J Cell Biol 182: 509-517

Yuan X, Liu C, Yang P, He S, Liao Q, Kang S, Zhao Y (2009) **Clustered microRNAs' coordination in regulating protein-protein interaction network**. BMC Syst Biol 3: 65

Zack GW, Rogers WE, Latt SA (1977) **Automatic measurement of sister chromatid exchange frequency**. J Histochem Cytochem 25: 741-753

Zhang X, Yu H, Lou JR, Zheng J, Zhu H, Popescu NI, Lupu F, Lind SE, Ding WQ (2011) **MicroRNA-19 (miR-19) regulates tissue factor expression in breast cancer cells**. J Biol Chem 286: 1429-1435

Zhao L, Helms JB, Brugger B, Harter C, Martoglio B, Graf R, Brunner J, Wieland FT (1997) **Direct and GTP-dependent interaction of ADP ribosylation factor 1 with coatomer subunit beta**. Proc Natl Acad Sci U S A 94: 4418-4423

Zhao L, Helms JB, Brunner J, Wieland FT (1999) **GTP-dependent binding of ADP-ribosylation factor to coatomer in close proximity to the binding site for dilysine retrieval motifs and p23**. J Biol Chem 274: 14198-14203

Zhu C, Bossy-Wetzel E, Jiang W (2005) **Recruitment of MKLP1 to the spindle midzone/midbody by INCENP is essential for midbody formation and completion of cytokinesis in human cells**. Biochem J 389: 373-381

Zilberstein A, Snider MD, Porter M, Lodish HF (1980) **Mutants of vesicular stomatitis virus blocked at different stages in maturation of the viral glycoprotein**. Cell 21: 417-427